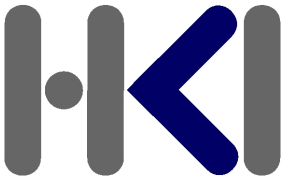

Individual-based Modeling and Predictive Simulation of Fungal Infection Dynamics

Dissertation
zur Erlangung des akademischen Grades
doctor rerum naturalium (Dr. rer. nat.)

vorgelegt dem Rat der
Biologisch-Pharmazeutischen Fakultät der
Friedrich-Schiller-Universität Jena

von Johannes Pollmächer
geb. am 15.12.1984 in Eilenburg

Gutachter:

1. Prof. Dr. Marc Thilo Figge (Hans-Knöll-Institut Jena)
2. Prof. Dr. Peter Dittrich (Friedrich-Schiller-Universität Jena)
3. Prof. Dr. Andreas Beilhack (Universität Würzburg)

Die Disputation der Doktorarbeit erfolgte am 21.12.2016 in Jena.

Contents

Zusammenfassung

Der human-pathogene Schimmelpilz *Aspergillus fumigatus* verursacht tödliche Infektionen und Erkrankungen vorrangig bei immunsupprimierten Patienten und stellt die moderne Medizin vor zunehmende Herausforderungen. *A. fumigatus* ist ubiquitär präsent und verbreitet sich über sehr kleine Konidien durch Luftströmungen in der Athmosphäre. Mehrere Hundert bis Tausende dieser Konidien werden täglich durch jeden Menschen eingeatmet. Die geringe Größe der infektiösen Konidien erlauben es dem Pilz bis in die Alveolen der Lunge des Wirtes vorzudringen, in denen eine Primärinfektionen mit *A. fumigatus* am häufigsten stattfindet. In den Alveolen trifft der Pilz zunächst auf das angeborene Immunsystem in Form von alveolaren Epithelzellen, dem Komplementsystem, Alveolarmakrophagen und Neutrophilen, die aus dem Blutkreislauf rekrutiert werden. Gesunde Wirte können die eingeatmeten Konidien meist problemlos beseitigen, jedoch kann sich *A. fumigatus* bei beeinträchtigter Funktion des Immunsystems behaupten, invasiv werden und innerhalb von Wochen zum Tod des Patienten führen.

In dieser Arbeit wird die Interaktion zwischen *A. fumigatus* und dem angeborenen Immunsystem in der menschlichen Lunge mit Hilfe von mathematischen Modellen und Computersimulationen nachgestellt. Als Grundlage für dieses Vorhaben wurde ein modulares Software-Paket entwickelt, welches agentenbasierte Modellierung und entsprechende Simulationen in Raum und Zeit ermöglicht. Hierbei wurden einzelne biologische Zellen als virtuelle Objekte im Computer repräsentiert und deren innewohnende Eigenschaften, wie ihre Migration, Morphologie, Interaktionen mit anderen Zellen und ihre sensorische Fähigkeit, das sie umgebende Medium wahrzunehmen und darauf zu reagieren, explizit integriert. Da derartig detaillierte Darstellungen enorme Computerressourcen erfordern können, wurden in dieser Arbeit Datenstrukturen und Algorithmen entwickelt und angewendet, die in vertretbarer Rechenzeit Simulationsergebnisse generieren. Insbesondere wurde eine Methode zur Interaktionserkennung zwischen virtuellen Zellobjekten implementiert, die lokale Nachbarschaftsbeziehungen zwischen Zellen durchgehend überwacht und es damit ermöglicht in effizienter Weise alle Interaktionen zwischen Agenten aufzulösen. Des weiteren wurde der Programmcode parallelisiert und auf Mehrprozessorsystemen ausgeführt, so dass einzelne Simulationen auf mehreren Kernen parallel Ergebnisse liefern und somit in kürzerer Zeit statistische Auswertungen generiert werden konnten.

Im Labor kann eine *A. fumigatus* Infektion *in vivo* unter physiologischen Bedingungen nur sehr schwer nachgestellt werden, da die geringe Anzahl infektiöser Konidien, die täglich eingeatmet werden, keine signifikanten inflammatorischen Signale hervorrufen und eine Detektion mit heutigen Verfahren noch außer Reichweite erscheint. Aus diesem Grund wurde ein maßstabsgetreues mathematisches Infektionsmodell in einer typischen menschlichen Alveole entwickelt, mit dem es möglich ist auch die physiologische Situation, inklusive Atmung, in Computersimulationen nachzustellen. Alveolarmakrophagen sind die im Lungengewebe ansässigen Phagozyten, die als erste mit dem human-pathogenen Pilz *A. fumigatus* in Kontakt kommen. Diese Arbeit liefert statistische Belege als Antwort auf die Frage wie dieser erste Kontakt mit dem Pilz nach seinem

Eintritt in die Lunge hergestellt wird. Hierfür wurde der Auffindungsprozeß auf der Oberfläche der Alveole mit verschiedenen Migrationsmustern von Alveolarmakrophagen wiederholt und mit unterschiedlichen Parameterkonfigurationen durchsimuliert. Es zeigte sich, dass Chemotaxis, d.h. eine Bewegungstendenz, in die Richtung der Konidie notwendig ist, um die Konidie rechtzeitig vor deren Auskeimen finden zu können. Da das Chemokin, welches verantwortlich für die Chemotaxis von Alveolarmakrophagen ist, bisher noch nicht identifiziert werden konnte, wurde darauf aufbauend ein erweitertes und verfeinertes Modell entwickelt, welches das chemotaktische Signal durch diffundierende Chemokine, die mit den Oberflächenrezeptoren von Alveolarmakrophagen reagieren konnten, explizit darstellt. Um die Konzentration des Chemokins auf der Alveolenoberfläche zu beliebigen Zeitpunkten auflösen zu können, wurde die Alveolenoberfläche mit einer Delaunaytriangulation diskretisiert und darauf die Diffusionsgleichung numerisch in Zeit und Raum gelöst. Aus den Simulationen mit variierten Parameterwerten für das Chemokin konnten experimentell relevante Bereiche von Parametern ermittelt werden, welche der Identifikation des konkreten Chemokins dienlich sein können. Das virtuelle *A. fumigatus* Infektionsmodell in einer dreidimensionalen alveolaren Struktur stellt die erste Implementierung auf Zell- und Molekularebene mit Alveolarepithelium, Kohnschen Poren, beweglichen Alveolarmakrophagen, *A. fumigatus* Konidien und der Diffusion und Reaktion von Chemokinen dar.

Da sich eine Nachahmung der gesamten angeborenen Immunantwort auf eine *A. fumigatus* Infektion unter Benutzung des maßstabsgetreuen Alveolenmodells als zu anspruchsvoll für eine agentenbasierte Computersimulation erwies, wurde hierfür auf das Modellierungskonzept der evolutionären Spieltheorie auf Graphen zurückgegriffen. Hierbei wurde der Infektionsverlauf als aufeinanderfolgende Serie evolutionärer Spiele mit dem Komplementsystem, Alveolarmakrophagen und Neutrophilen nachgestellt. Auch hier wurden einzelne virtuelle *A. fumigatus* Pilzzellen und individuelle Immunzellen als virtuelle Akteure mit vordefinierten Fähigkeiten repräsentiert. *A. fumigatus* war dabei in der Lage jeweils einen seiner morphologischen Phänotypen – ruhend, aufschwellend oder auskeimend – einzunehmen, um möglichst vorteilhaft dem angeborenen Immunsystem entgegenzutreten. Die Simulationen erlaubten Fallunterscheidungen zwischen gesunden und beeinträchtigten Wirten vorzunehmen, sowie hohe und niedrige Infektionsdosen zu untersuchen. Aus den Ergebnissen konnte eine zentrale immunregulatorische Rolle von Alveolarmakrophagen entnommen werden, da diese einerseits selbst die Beseitigung des Pathogens durch Phagozytose voranbringen können, andererseits aber auch zusätzlich durch inflammatorische Signale die Rekrutierung von Neutrophilen aus dem Blutkreislauf initiieren können. Insbesondere die Säuberung von hohen Infektionsdosen erforderte, dass dem Wirt voll funktionsfähige Phagozyten, aber insbesondere Neutrophhile zur Verfügung standen.

In dieser Arbeit wurden mehrere individualbasierte Techniken angewandt und entsprechende mathematische Modelle entwickelt, um die Interaktion zwischen dem angeborenen Immunsystem und *A. fumigatus* in Raum und Zeit stochastisch zu simulieren. Aus den Simulationsergebnissen konnten mehrere Vorhersagen gewonnen werden, deren Verifikation in biologischen Experimenten noch aussteht. Die entstandenen Modelle können als Basis für Weiterentwicklungen dienen, um sowohl neue Erkenntnisse einfließen zu lassen, als auch experimentell ermittelte Parameter zu fixieren und somit Verfeinerungen vornehmen zu können. Ein weiteres Vorgehen wird stark vom systembiologischen Austausch zwischen Experimentatoren und Theoretikern profitieren, und hat das Potential Synergien zwischen Experiment und Theorie freizusetzen.

Summary

The human-pathogenic fungus *Aspergillus fumigatus* causes life-threatening infections in immunocompromised patients and poses increasing challenges for the modern medicine. *A. fumigatus* is ubiquitously present and disseminates via small conidia over the air of the athmosphere. Each human inhales several hundreds to thousands of conidia every day. The small size of conidia allows them to pass into the alveoli of the lung, where primary infections with *A. fumigatus* are typically observed. In alveoli, the fungus encounters the innate immune system of the host comprising alveolar epithelial cells, the complement system, alveolar macrophages and recruited polymorphonuclear neutrophilic granulocytes from the bloodstream. While healthy hosts master the challenge of conidial elimination on a daily basis, in immunocompromised hosts *A. fumigatus* may become persistent, invasive and may ultimately lead to death within weeks.

This thesis covers mathematical modeling and computer simulation of the interaction between *A. fumigatus* and the innate immune response in the human lung. For this purpose a modular software framework was developed and implemented, which allows for spatio-temporal agent-based modeling and simulation. Here, individual biological cells are represented as individual virtual actors in the computer and their intrinsic properties as migration, morphology, interactions with other cells as well as their sensoric ability to detect environmental signals are explicitly integrated. Since a high level of model detail may lead to the requirement of enormous computational resources, efficient algorithms and smart data structures were applied and developed to make simulation results obtainable in reasonable computation time. In particular a method for interaction detection was engineered, which continuously monitors the local neighborhood of each agent and efficiently resolves all interactions between the agents. Moreover, parallelization and execution of the program code on multi-core machines allowed for distributed processing of simulations and generated results at increased rates.

An *in vivo* laboratory study of an *A. fumigatus* infection under physiological conditions is hard to realize due to the low amount of inhaled conidia, which in turn induce too low levels of inflammatory signals. To overcome this limitation, a to-scale *A. fumigatus* infection model in a typical human alveolus was developed in order to simulate and analyze the infection scenario under physiological conditions including breathing. Alveolar macrophages are resident in alveoli and constitute the first professional phagocytes that get into contact with inhaled conidia of *A. fumigatus*. This work provides statistical evidence on how this first contact after conidial entry into alveoli is established. For this purpose the process of conidial discovery by alveolar macrophages was modeled and simulated with different migration modes and different parameter configurations. It could be shown that chemotactic migration with bias in the direction of the conidium was required to find the pathogen before the onset of its germination. Since the chemokine responsible for guiding alveolar macrophages to conidia has not been identified yet, an extended model including an explicit representation of the chemoattractant was developed. Here, a reaction-diffusion equation was numerically solved on a discretized Delaunay-triangulated

alveolar surface. From simulations with varied chemokine parameter configurations, experimentally relevant parameter regimes, subserving eventual chemokine identification, were extracted. The three-dimensional virtual *A. fumigatus* infection model constitutes the first implementation on cellular and molecular scale including alveolar epithelium, pores of Kohn, mobile alveolar macrophages, *A. fumigatus* conidia and a diffusing and reacting chemokine.

Since a three-dimensional to-scale model of the whole innate immune response against *A. fumigatus* proved to be computationally too demanding, for this purpose the modeling approach of evolutionary game theory on graphs was applied. Here, the course of infection was modeled as a consecutive sequence of evolutionary games related to the complement system, alveolar macrophages and polymorphonuclear neutrophilic granulocytes. Similarly to the agent-based approach, individual fungal cells and immune cells were represented as individual virtual actors with pre-defined properties. *A. fumigatus* was in the position to adopt one of its morphological phenotypes – resting, swollen or hyphal – to beneficially interact with the immune respone. Computational simulations allowed to delineate between healthy and immunocompromomised hosts as well as to distinguish between high- and low-dose infection scenarios. The results revealed a central immunoregulatory role of alveolar macrophages due to their ability to contribute to infection clearance via phagocytosis and to initiate the recruitment of additional phagocytes from the bloodstream. In the case of high infectious doses it was found that the host required fully active phagocytes, but in particular a qualitative response of quantitatively sufficient polymorphonuclear neutrophilic granulocytes.

In this work a number of individual-based techniques were applied and mathematical models developed in order to simulate the innate immune response against *A. fumigatus* in the human lung. From computer simulations, a number of predictions were generated, which have to be verified experimentally. The individual-based models paved the way for future investigations and may serve as a foundation on which additional findings and experimentally identified parameter values are capable of being integrated. Model extensions will strongly benefit from the exchange between theoreticians and experimentalists, which ultimately could release synergies in a Systems Biology fashion.

Abbreviations

ABM	Agent-based modeling
AM	Alveolar macrophage
AEC	Alveolar epithelial cell
CGT	Classical game theory
DNA	Deoxyribonucleic acid
EGT	Evolutionary game theory
e.g.	*exempli gratia* (for example)
et al.	*et alii* (and others)
HIV	human immunodeficiency virus
IA	Invasive aspergillosis
IDE	Integrated development environment
IL	Interleukin
i.e.	*id est* (that is)
MAC	Membrane attack complex
MIP-1	Macrophage inflammatory protein-1
NADPH	Nicotinamide adenine dinucleotide phosphate
NETs	Neutrophilic extracellular traps
PAMP	Pathogen-associated molecular pattern
PMN	Polymorphonuclear neutrophilic granulocyte
PRR	Pattern recognition receptor
SBML	Systems biology markup language
ROI	Reactive oxygen intermediate
ROS	Reactive oxygen species
TNF-α	Tumor necrosis factor α
UML	Unified modeling language
XML	Extensible markup language

Chapter 1

Introduction

Fungi are able to colonize a vast amount of different habitats like soil, water, plants and higher organisms. They constitute a major eukaryotic lineage and are termed molds, yeasts, mushrooms, smuts and polypores among others, which reflects the diversity of the fungal kingdom. Today about 10^5 fungal species are known, but current estimates expect the existence of about five million different fungal species world-wide [1]. Fungi comply essential symbiotic functions for many organisms with which they form associations, but some species pose harmful threats to particular organisms. Some species of the genus *Aspergillus* behave pathogenic against humans and have the potential to quickly invade into immunocompromised individuals and account for infections associated with high mortality rates [2]. Among the 260–837 known *Aspergillus* species, *Aspergillus fumigatus* is the infectious agent with the highest potential to harm humans [2, 3]. Over the second half of the 20th century a steady increase of fatal infections caused by *A. fumigatus* was observed, which is widely attributed to rising frequencies of those medical therapies that accompany with a downregulation of the immune system [4]. A core topic of this thesis deals with the investigation of *A. fumigatus* infection dynamics *in silico* in order to unravel and predict key mechanisms and attributes of both, the fungus and the immune system of the host.

Each scientific question raised to a biological system demands for appropriate approaches and methods to tackle the tasks leading to eventual identification of the unknowns. In many cases, experimental laboratory work in the "wet-lab" sets a solid foundation to extract the relevant entities, their relationships, important processes and their properties in the system. Mathematical models have the power to enrich the wet-lab results by incorporation of prior knowledge as well as qualitative or quantitative data into simulations in which scenarios of the biological system are probed in order to predict its potential behavior. To play the counterpart of wet-lab approaches is one opportunity for theoreticians, but an initiation of studies using computational approaches is conceivable as well. Advantages of the "dry-lab" over the wet-lab lie in the disposal of ethical concerns related to animal experiments, an enormous reduction of associated costs in terms of the materials required for the investigation and an execution of computational experiments in which everything is absolutely controllable.

There exist different types of models and related simulation tools to study dynamical biological systems. Due to the stochastic nature, the diverse and individual behavior of living organisms, like single cells, individual-based approaches are favorable to study these systems. Here, single biologically relevant entities, like cells, can be represented in a one-to-one representation *in silico*. The virtual individuals are in the position to act autonomously and according

to pre-defined features that were implemented. Computational challenges of these approaches arise due to the level of detail in which the biological system is represented. Thus, efficient algorithms and smart data structures have to be used, developed and implemented for successful application of individual-based computational methods. Computational modeling of fungal infection dynamics on the scale of cells using individual-based approaches received only limited attention in the past. This thesis aims at the application of these models in three-dimensional spatial environments related to the major sites of *A. fumigatus* infection. Their full potential is exploited by studying processes, functions and cell behavior for which space and time-resolution are inevitably required like migration, cell-cell interactions or time-limited exploration of an environment. Next to the explanation and recreation of known data *in silico*, the primary goal of performing simulations is the generation of reasonable predictions, which can be verified in future experimental research [5].

This chapter is organized as follows: First, the biological background is introduced and the topic of the thesis motivated. Here, an overview about the fungal species under consideration, *A. fumigatus*, is given in section 1.1. Furthermore, in section 1.2 its interaction with the immune system of mammalian hosts is explained. The last section of the introduction (section 1.3) considers the individual-based modeling approaches and techniques that have been carried out in this thesis.

1.1 The human-pathogenic fungus *Aspergillus fumigatus*

Aspergillus fumigatus is the most important airborne human-pathogenic fungus leading to severe infections, which are associated with high mortality rates [2]. This fungus belongs to the filamentous ascomycetes and is ubiquitously present in the nature [6]. Its natural habitat is the soil as well as decaying organic material [7, 8]. Due to its thermotolerance *A. fumigatus* is a predominant organism of the high-temperature phase of the compost-cycle. The main function of this fungus is the degradation and recycling of nitrogen and carbon sources [8].

1.1.1 Morphology and lifecycle

A. fumigatus exhibits several morphotypes related to the specific stages in its lifecycle. The grayish-green spherical asexual spores of *A. fumigatus* are called conidia, have a size of about 2–3 μm in diameter and they distribute primarily through the air of the athmosphere [7, 9, 10]. Furthermore, dissemination relies on environmental disturbances as well as strong air currents [7]. Typical spore-densities range up to 660 conidia per m^3 air, where specific values depend mainly on environmental conditions like temperature, humidity and proximity to conidial reproduction sites [11–13]. Resting *A. fumigatus* conidia are shielded by a relatively thick rodlet layer, which allows for masking itself and to reduce predation in hostile environments [14]. Conidia begin to swell depending on the availability of water, nutrients and specific temperature ranges [15–17]. The process of swelling comes along with a remodeling of the outer shield inducing the break of the rodlet layer [17]. After a phase of isotropic growth swollen conidia start to germinate and initiate polar growth, which accompanies with the creation of small filaments [8]. These elongated structures are compositions of cylindrical elements and are called hyphae, which further can branch into several directions and allow for enhanced acquisition of nutrients, spatial expansion and environmental exploration. A number of fungi in the state of filamentous growth are able to generate a mycelial network, which allows for asexual reproduction. At the boundary surface between mycelial structures and air, the mycelium forms so-called conidiophores, which produce large numbers of asexual spores that may be released into the athmosphere for dissemination [7,9].

1.1.2 Route of infection and associated diseases

Every day humans inhale several hundreds to thousands of conidia. As illustrated in Fig. 1.1, these fungal spores are small enough to evade the filter activity of the human lung and pass into the lower respiratory tract [7,18]. Normally, immunocompetent individuals manage fungal clearance without complications on a daily basis [19]. Exceptions are patients with asthma and those with cystic fibrosis. A fraction of them eventually could suffer from allergic bronchopulmonary aspergillosis [16,20,21]. In addition to that pre-existing structural lung diseases like emphysema or previous cavitary tuberculosis may lead to chronic forms of pulmonary aspergillosis, e.g. chronic necrotizing pulmonary aspergillosis or fibrocavitary aspergillosis [7,20,22]. The aforementioned diseases progress over months and years, require prolonged antifungal therapy, but are not lethal in contrast to invasive aspergillosis (IA), which is the most severe disease linked to *A. fumigatus* with mortality rates ranging from 30-90% [2,20,22]. IA is attributed to patients with impaired or altered immune status and the lung is the primary site of infection [4]. High risk of infection can be attributed to individuals with immune deficiencies like chronic granulomatous disease, hematological malignancies and patients that received a corticotherapy, cytotoxic chemotherapy, and organ- or stem-cell transplantation accompanied by immunosuppressive therapy [16,23]. For all these risk factors, an impaired function of phagocytic cells, like neutrophils and macrophages, is at least one common feature, and the crucial role of these cells in the fight against fungal infections is widely recognized [24].

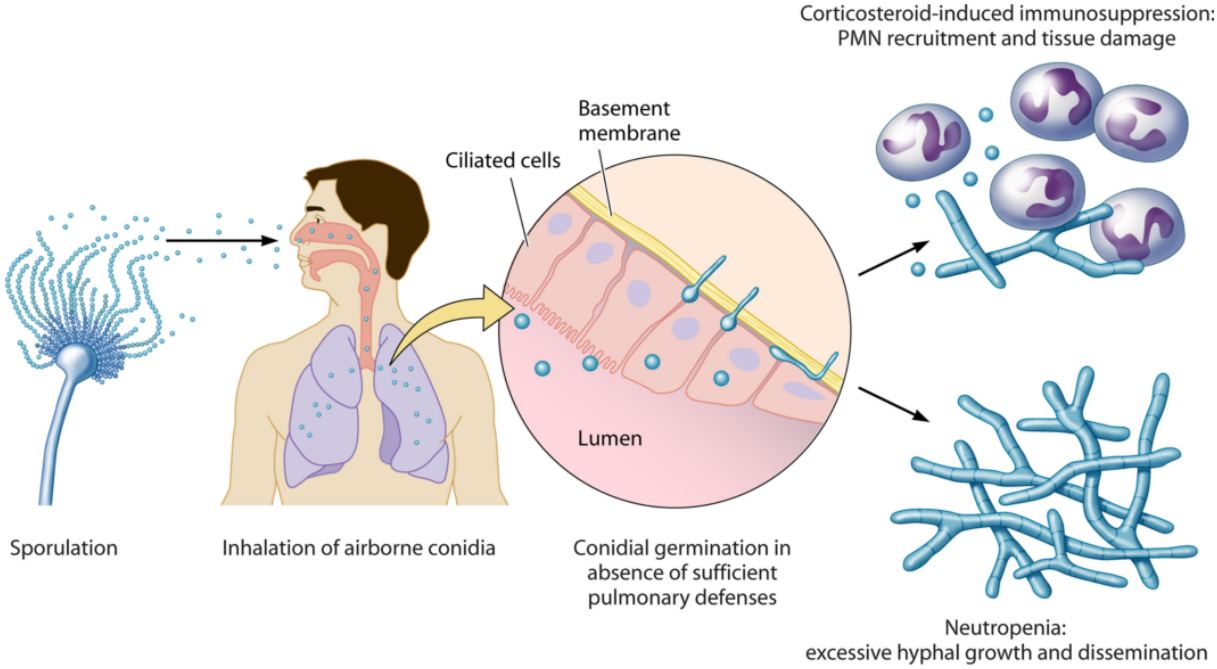

Figure 1.1: Route of *A. fumigatus* infection and typical manifestations in different patient groups (adapted from [16]). Asexual conidia distribute over the air of the athmosphere and are inhaled by individuals. Insufficient immune responses in immunocompromised patients lead to fungal germination and tissue invasion. Neutropenic hosts suffer from rapid fungal dissemination and extensive tissue damage by mycelial growth. Unbalanced immune responses can cause severe self-damage as a consequence of massive PMN recruitment.

1.2 Interaction of the host with *Aspergillus fumigatus*

1.2.1 Virulence attributes of *A. fumigatus*

A. fumigatus evolved a number of mechanisms to evade, to suppress and to counteract the immune system of mammalian hosts. Most likely several virulence attributes of this fungus evolved from interactions with other microorganisms that posed selective pressure and supported virulence long before the development of innate immune systems [24].

In the resting state, conidia are shielded by two physical barriers. A hydrophobic rodlet protein layer covers pathogen associated molecular patterns (PAMPs) rendering conidia immunologically inert [14, 24]. Furthermore, the fungus has a rough melanin layer responsible for the gray-green color. Conidia with an intact melanin layer show increased virulence over conidia with a smooth surface and disrupted melanin layer [25]. In addition to that, conidia evade the immune response by active binding of host complement regulators like factor H and plasminogen [15]. Next to properties of the conidial cell wall, *A. fumigatus* shows quick adaptation and a relatively fast reproduction in humid and nutrient rich milieus [26]. Resting conidia adapt to altered environmental conditions and initiate growth within three hours after exposure to beneficial surroundings [27]. The time period from growth initiation, *i.e.* swelling to germination and hyphal extension under optimal growth conditions takes another three hours [27, 28]. If not removed within this tight time window invasive hyphal growth may cause physical damage and allow the fungus to further spread through the organism. Resting conidia show a remarkable thermotalerance and are viable up to 70°C, whereas hyphae tolerate up to 55°C [29]. In hyphal state *A. fumigatus* has an arsenal of weapons to counteract the hosts immune response. After phagocytosis of conidia by macrophages swelling and subsequentent germination of *A. fumigatus* can kill macrophages by disruption of their cell wall due to filamentous extension [30]. Furthermore, application of physical stress on epithelial barriers by the same mechanism damages or destroys them and opens paths for enhanced nutrient acquisition [9, 31]. The secretion of proteases enables the fungus to actively downregulate the immune response by degradation of important regulatory proteins [32]. Production and secretion of gliotoxin over the course of infection reduces the phagocytic activity, cytokine secretion and the production of reactive oxygen intermediates (ROI) of macrophages and neutrophils [33]. Furthermore, the fungus is in the position to grow under hypoxic conditions as well as in iron- and zinc-limiting environments as is present in the lung [16].

1.2.2 Innate immune responses to *A. fumigatus* in lung alveoli

As soon as conidia of *A. fumigatus* get into physical contact with the bodies of mammalian organisms they are confronted with host-specific immune responses [7, 17, 26]. The innate immune system constitutes the first line of defence for microbes and foreign particles. It acts fast, unspecific and is composed of anatomical barriers like epithelial cells, circulating cells like polymorphonuclear neutrophilic granulocytes (PMN) and the complement system, which consists of several proteins that have roles in immune regulation and inflammation [34]. Due to the fast growth and reproduction of *A. fumigatus*, innate immunity is the key to eliminate this fungus on a daily basis as well as in infection scenarios.

The lung accounts for 70% of all invasive aspergillosis cases due to permanent inhalation of the ubiquitously present conidia of *A. fumigatus* [4]. The respiratory tract of humans has coarse filters starting from the nose that consists of hairs and mucus to filter and eventually get rid of inhaled foreign particles exceeding a certain size [26]. The size of resting *A. fumigatus* spores is well below the threshold and a fraction of the inhaled conidia is flowed and diffused into alveoli of the lung [7]. Alveoli are the elementary units of the lung primarily responsible for the exchange of oxygen and carbondioxide. Since gas-exchange involves diffusion of oxygen

into the blood and carbondioxide into the expiratory volume, the alveolus is composed of a thin epithelial layer separating the bloodstream and the alveolar volume [35]. Thus, the penetration and invasion of this delicate structure by pathogens would quickly result in their direct access to the bloodstream. In addition to alveolar epithelial type I cells that are dedicated to gas-exchange and make up 95% of the surface area, alveoli also include alveolar epithelial type II cells and interalveolar pores, so-called pores of Kohn [26, 35]. Type II cells permanently produce, secrete and recycle the alveolar lining layer named surfactant [36]. This is an on average 200 nm thin and viscous fluid coating the inner surface of alveoli, which reduces surface tension, thus avoiding the collapse of alveoli, and enables the diffusion of immunoregulatory proteins [37, 38]. Alveolar macrophages (AM) denote the tissue-specialized phagocytes that are resident in alveoli. The primary function of AM is the maintenance of a pathogen-free alveolar surface and to minimize the amount of foreign substances in order to allow for optimal gas-exchange [39,40]. Furthermore, AM patrol on the inner surface of alveoli shielded by the surfactant from direct contact to the alveolar volume. From here they initiate and regulate immune responses [41]. Pores of Kohn are tunnel-like connections between neighbouring alveoli filled with surfactant and permit the direct transit of immune cells [42]. They allow for direct molecular signaling between alveoli and shorten the travel-distances of immune cells compared to the route over the alveolar entrance ring.

Epithelial cells are the first host cells that get into contact with the fungus. Next to their function as a physical barrier they feature the ability of pathogen sensing and immune-cell recruitment to the site of infection by secretion of chemoattractants [34]. Whenever a conidium is inhaled, it may get trapped within the ciliated epithelium of the airways, which subsequently would transport it to the throat by rhythmical cilial movement [7]. During this process conidia of *A. fumigatus* may secrete the cytotoxic mycotoxin gliotoxin, which was shown to reduce the frequency of the cilial movement and to damage the sorrounding epithelium [43]. The other fraction of inhaled conidia will enter alveoli and get into contact with the surfactant and cells of the alveolar epithelium. Type II cells were shown to internalize conidia and to degrade them in their phagosomes [44]. Upon physical contact with live conidia and mycelial fragments type II cells released the cytokines IL-6, IL-8 and TNF-α to generate an inflammatory milieu and to attract immune cells [31]. Despite making up 95% of the alveolar surface and a high probability of physical contact to invading conidia, type I cells are poorly studied in wet-lab and their response to *A. fumigatus* remains speculative [35]. Due to their peculiar morphology type I cells are hard to cultivate and difficult to isolate [35].

The proteins of the complement system reside in the surfactant and start to opsonize the conidia, followed by the release of the proinflammatory and chemoattracting ligands C3a and the anaphylatoxin C5a into the surrounding environment [45, 46]. Furthermore, opsonization of the fungal surface leads to increased phagocytosis-, killing- and ROI production by macrophages, monocytes and neutrophils on direct physical contact [47]. Swollen conidia as well as hyphae activate the complement system via the alternative and classical pathway [46]. Resting conidia show reduced opsonization compared to swollen conidia and hyphae due to active binding of the hosts immune regulators factor-H and plasminogen [15,46]. Hyphae are in the position to produce and secrete proteases, which degrade complement proteins in order to reduce their effects [32]. Furthermore, *A. fumigatus* resists lysis by the formation of the terminal complement complex, *i.e.* the membrane attack complex (MAC), as a matter of its thick cell wall [48]. In summary, the complement system contributes mainly in opsonization, which facilitates detection and enhances recruitment of phagocytes, but the complement system is not reported to kill the fungus [49].

AM are thought to be the first professional phagocytes that get into contact with the fungus, but were shown to be not very motile *in vitro* [26]. They phagocytose resting and swollen conidia upon physical contact, but for killing the swollen morphotype is a prerequisite [50]. For the process of internal killing ROI are indispensable [51]. The exact mechanisms that lead to the successful discovery of the pathogen by AM are yet to be identified experimentally. The

mode of AM migration, a potential chemokine that might be involved in this process and its molecular properties are major subjects of this thesis. Upon physical contact with AM, conidia are detected primarily by the pattern recognition receptor (PRR) dectin-1 binding to β-glucans on the fungal surface [52]. Since β-glucans get exposed in higher amounts with the begin of swelling, the swollen morphotype is taken up more rapidly than conidia in the resting state [52]. Furthermore, the availability of fungal β-glucans to AM determines the production and secretion of the inflammatory cytokines and chemokines TNF-α and macrophage inflammatory protein-1 (MIP-1), respectively [52]. If the capacity-limits of AM to clear the lungs from the fungus are reached, like on administration of high amounts of infectious agents, further recruitment of immune cells is required. The recruitment of PMN from the bloodstream is an important feature of AM as they can not eliminate hyphae of *A. fumigatus* [50]. In the case of high doses of administered conidia, macrophages seem to be dispensable for the outcome of the infection [53]. PMN and their recruitment are essential for pathogen clearance [53]. Once recruited, neutrophilic granulocytes are able to eliminate the fungus by internalization and subsequent lysis [50]. If the fungus is too large for phagocytosis neutrophils may kill it externally by degranulation [47]. This process involves the secretion of ROI into the extracellular space, which is harmful for the pathogen but also for the tissue of the host [28]. *A. fumigatus* hyphae counteract the production of ROI via secretion of gliotoxin, which inhibits assembling of the NADPH oxidase complex responsible for ROI production [54]. In later stages of the infection, neutrophils may also commit an altruistic suicide accompanied with the formation of neutrophilic extracellular traps (NETs) [54]. Here, single neutrophils die relatively fast und release their DNA in the extracellular space. In contrast to apoptosis, which is the typical cell death, the NETs produced in the NETosis event were shown to feature fungistatic but not fungicidal properties against *A. fumigatus* [54]. Taken together, neutrophils show double-edged sword properties in host-pathogen interaction, implying the requirement of continuous regulatory control, but they play an essential and vital role in the clearance of *A. fumigatus* associated infections.

1.3 Individual-based modeling and simulation

Over the past three decades computers have made remarkable advances. In this period of time, the computational power of computers increased exponentially and allowed for more and more complex computer simulations with increased levels of detail [55]. To increase readability of this section some basic terms are defined in advance:

system: A system is a set of entities that act and interact in order to fulfill one or more specific functions and objectives. Systems have characteristic attributes [56]:

- Systems are not separable in the sense that the removal of entities and relations would make the fulfillment of inherent functions and objectives impossible.
- Systems are composed of entities and their interrelationships, which define their functions.
- Systems have boundaries and may be located in an environment. The separation between the system and the environment depends on the definition of boundaries. The system may interact with another system of the environment or may be a part of a bigger system. Interfaces of systems with their related environments allow for their observation and control.

model: A model is a system that aims to map another system. The objective of the model is the acquisition of information about the mapped system [57].

(computational) simulation: A computer simulation is a tool to experimentally investigate

a mathematically described model. Simulations may allow for the explanation of system behavior and the interrelationships between the entities [58].

The processes of mathematical modeling and computational simulation are strongly intertwined as modeling approaches typically demand for appropriate simulation tools. Thus, modeling and simulation of a system are termed computational approaches in what follows. There are a number of computational approaches each having its own advantage and disadvantage over others. An appropriate choice depends on a number of factors, listed below:

model scale: The scale of the model relates to the entities under consideration. Entities in focus of the model might be biological cells, proteins, atoms, cars, humans, animals amongst others. *E.g.* on the scale of biological cells the length scale of micrometers and the time scale of minutes to days would be considered, whereas for the scale of molecules or proteins one would consider the nanometer length scale and a time scale from milliseconds to minutes.

degree of entity individuality: Each individual of a group may act according to specific individual rules or it may act in the same manner as its group members.

deterministic or stochastic: Rules of the actors and rules for interactions and processes may be strict with well-defined conditions for their execution (deterministic case) or their execution may depend on pre-defined probabilities (stochastic case) [59].

model detail/granularity: The level of detail comprises the amount of variables, states, processes and/or rules to describe the real system [60]. The degree of granularity is restricted by the availability of data, but on the other hand it is also concievable to purposely reduce model detail in order to focus on central aspects of a system and to reduce complexity [61].

computational costs: Computational simulations cause computational costs in terms of memory and computation time. Computation time should stay within the realms of possibility and memory should not exceed the limits of the respective machine on which the simulation is going to be executed.

These factors are not completely independent of each other. Typically, simulations causing higher computational costs relate to models with higher levels of detail and vice versa. Stochastic models increase computational costs compared to deterministic approaches due to additional computations of random numbers [59]. Higher computational costs are also attributed to higher degrees of individuality.

A distinction is drawn between population-based approaches and individual-based approaches. In population-based approaches entities are grouped and each group is condensed in one variable denoting the average number or the average (local) concentration of the entity. Here, each group of entities is treated as a whole, which induces that solely results for groups or subpopulations may be obtained and analyzed. Interactions between these groups are defined as processes averaged over all individuals that belong to the groups involved in the interaction. Thus, population-based approaches are suited for low degrees of individuality and induce a relatively low computational cost. In contrast to that, individual-based approaches represent each single entity as a virtual object each having a number of attributes as well as rules to act and rules to interact with other entities of the system under consideration. The individual behavior of many so-called agents can then be used to analyze the behavior of a group or a population on the system level. Single entities may be tracked and their dynamics in relation to the whole population may get dissected. Individual-based methods are also termed agent-based approaches and may simulate the dynamics of processes in space and/or time. Since they represent a system in a higher resolution than their population-based counterparts results of agent-based approaches tend to be closer to the related real-world processes, but these results come at the price of higher computational

costs in terms of computation time and memory [6]. An appealing feature of individual-based approaches is their higher degree of comprehensibility over equation-based approaches like differential equations that are typically used to model population-based systems, which can enhance the exchange between theoreticians and experimentalists [62]. Population-based and individual-based approaches are capable of deterministic and stochastic simulations at different degrees of model granularity, but population-based approaches are restricted to stochastic effects and the implementation of increased complexity on the population level rather than on the level of single entities [63].

In this thesis, particular efforts are made to construct and to simulate biological systems in an individual-based fashion. Here, simulation of fungal infection dynamics follows primarily this paradigm of computational modeling on the scale of cells, but advantage is also taken of population-based approaches to model subcellular processes like the diffusion of cytokines and their binding dynamics with surface receptors. For this aim individual-based models were constructed on the one hand to simulate the spatio-temporal infection dynamics and on the other hand to determine the evolutionary dominant morphotypes of *A. fumigatus* at distinct stages in the infection process.

1.3.1 Spatio-temporal agent-based modeling on the scale of cells

In this subsection, attention is drawn to agent-based models of dynamic biological systems with spatial resolution on the scale of cells. In this thesis, stochastic agent-based models are considered and applied due to the stochastic and individual nature of biological cells [59].

In cell-scale agent-based models the representation of single biological cells follows an explicit one to one mapping as virtual objects. For implementation purposes, object-oriented programming languages are highly favorable due to their natural entity-based organization structure in classes and related modern tools for software development like the unified modeling language (UML). Here, cell attributes can easily be organized in structured objects and variables. Spatial position or individual lifetime can be considered as simple attributes, whereas the morphology, the mode of migration or the interaction pattern of the corresponding cellular agent easily become complex attributes. Object-oriented analysis and -design provide tools to determine an appropriate structure of the object-oriented program. This aids the developers in setting foci and also to sustain a flexible and extensible implementation.

The agents interact with each other in a spatial environment that is either modeled by grid points or by continuous length variables [62]. Cell-cell interactions require a pre-defined condition before the rules according to the cell-specific interaction definition are applied. Since interactions between cells are based on the binding of surface receptors to ligands of the cell wall of the interaction partner direct physical contact has to be established first. The determination of all pairs of interaction partners in an off-lattice spatial environment requires particular attention as checks of all possible combinations would lead to a quadratic scaling for the time complexity in the number of agents. A method to reduce the time complexity to linear scaling based on the concept of a grid-based monitoring of cell positions is presented in this thesis as well (see subsection 4.6.1).

The implementation of agent-based models requires enormous efforts in verification and validation as such models become very quickly very complex. To ease the process of model development frameworks have been made available for everyone, whereas each of these frameworks has a specific focus on a particular scale of interest and comes along with a more or less protracted period of vocational adjustment. IMMSIM, SIMMUNE, SIS are true immunesystem platforms, which allow users to set rules of interactions to define immune reactions [64]. Next to these ones, further implementations exist, which are comprehensively reviewed in [65, 66]. Each of these tools has a more or less restricted flexibility in terms of the opportunity to extend a

given model, which means that the user can operate with the features that were implemented but not beyond. A more flexible approach is featured by the agent-based open source development tool NetLogo [66]. Here, own code can be included to extend the model with desired features. Restrictions of this tools are the basic algorithms and definitions behind the program that can only be exchanged with unpleasant workarounds. To these basics belong, *e.g.*, the traversal of agents, the range of the possible morphologies and boundary conditions of the spatial environment, the allowed spatial positions of agents and the degree of freedom in handling agent-interactions. The highest flexibility in model design is achieved by own implementations using object-oriented programming languages like `C++` or `Java`. But this flexibility comes at the price of a time-intensive implementation phase. However, modern integrated development environments (IDE) help to conceptualize, object-oriented design principles increase the extensibility and readability of the code and software development tools like UML aid in the transfer of software design between different developers. Still agent-based modeling approaches lack in a generalized description framework to ease exchange between scientist, to *e.g.* easily reproduce model results. For models based on genomics-, transcriptomics- and proteomics-data the systems biology markup language (SBML) was developed, which is widely accepted, intensively used and continuously extended nowadays [67]. Agent-based modeling frameworks tend to use their own defined formats to configure and parametrize the simulation. Efforts to generalize description formats like the attempt of the framework FLAME are yet to be accepted by the scientific community [68].

Spatio-temporal agent-based models were applied in biological areas like tissue engineering, tumor growth and wound healing [69–71]. Over the last two decades the number of agent-based approaches to model and simulate immunological processes has steadily increased [62]. Here, functions of the adaptive immune system have received particular attention. The migration and development of B-cells in germinal centers were investigated in a systems biology approach with iterative cycles of exchange between theoreticians and experimentalists [72–74]. Dunbar and Bogle developed a model for the activation and proliferation of T-cells in lymph nodes in order to study the migration and population dynamics of T-cells during an inflammatory response [75–77]. Figge and Meyer-Hermann reproduced the experimentally observed pattern of the immunological synapse during the activation of T-cells using an agent-based model on the scale of molecules [78, 79]. Other models focus on responses of the immune system to diseases like HIV, malaria or cancer, reviewed in [62] and [64]. Individual-based methods to model innate immune processes in host-fungal interaction received only marginal attention but a few models focussing on specific aspects were published over the recent years. The hunt strategies of PMN to efficiently phagocytose and kill conidia of *A. fumigatus* in an infection scenario were studied by Tokarski *et al.* [80]. Lehnert and Timme *et al.* successfully transformed a time-resolved state-based model to a spatio-temporal agent-based model in order to unravel the migration parameter regimes of monocytes and PMN in response to *Candida albicans* in human blood [81]. This thesis aims at closing knowledge gaps in the early infection stages with *A. fumigatus* and contributes particular insight into the spatio-temporal dynamics of the innate immune system with fungal conidia in a realistic three-dimensional representation of lung alveoli.

1.3.2 Multi-scale hybrid agent-based modeling in biology

Multi-scale models are able to handle at least two different scales of interest. The challenge of these approaches is in managing computational costs that easily may rise as a matter of strong differences in time and length scales over several orders of magnitude. In biological systems time and length scales range from 10^{-2} s and 10^{-6} m during gene transcription at the molecular scale to 10^{6} s and several meters at the scale of the whole organism [64, 82]. The language of cell-to-cell communication are molecular substances. Cells can send messages by the production and secretion of signaling molecules and they are able to receive messages of other

cells nearby via binding their signaling molecules with surface receptors. Thus, from a cell-scale agent-based modeling perspective it is most worthwhile to also include the scale of molecules in order to attain the opportunity to map molecular processes and their interrelations with the cell-scale. However, there exist considerable differences between cells and molecules, which favor distinct modeling strategies [83]. Since the number of molecules relative to the number of cells per unit volume differs in 10^6 to 10^9, to model molecules in an individual-based fashion would render the multi-scale system computationally intractable [6]. Furthermore, molecules act relatively simple compared to cells as molecular interactions can be described collectively by chemical reactions and their movement is captured by Fick's law of diffusion at the population level [83]. The aforementioned arguments favor a population-based approach on the molecular scale for the purpose of multi-scale modeling with cells and molecules. The hybrid agent-based modeling approach transfers this concept with a spatio-temporal agent-based model on the cell-scale and a system of partial differential equations for modeling the dynamics of molecules and their interactions. Hence it balances a reasonable amount of computational costs against a considerable level of detail and unifies the advantages of both, individual- and population-based methods, in one approach.

Multi-scale approaches as introduced above have been applied multiple times to different topics in cell biology. Schaller *et al.* developed a hybrid agent-based model in continuous space including cell-cell forces to study the homeostatic behavior of the epidermis under perturbations [84]. For this aim they solve the equations of motion on the scale of cells numerically and the reaction-diffusion equation on the scale of molecules by a finite difference approach. A framework allowing for computationally efficient hybrid agent-based modeling was proposed by Guo *et al.* [83]. In order to trade off between computational costs and model granularity they presented a multi-timescale event-scheduler as well as validation procedures to verify different levels of model detail [60, 85]. On the scale of cells the migration is executed using timestep-based displacement vectors, which are the result of superpositions of random, chemotactic and fluidic flow vectors. The spatio-temporal dynamics of molecules are treated by reaction-diffusion equations [83]. Kempf *et al.* implemented and validated a multi-scale model of tumor spheroid growth and the response of the model to different irradiation therapies as well as to hypoxia [70, 86]. Similar to Schaller *et al.* [84] they solve the equations of motion on the scale of cells, whereas on the scale of molecules a homeostatic steady state equilibrium of a reaction-diffusion equation is considered.

1.3.3 Evolutionary game theory on graphs

Game theory is a mathematical framework of abstract models and methods to analyze and recast problems of *e.g.* biological, social or economic situations and contexts [87]. The metaphor of a game facilitates our understanding of complex phenomena despite the severity of the conflict between the players, which are typically animals, companies or nations [88]. The main founders, John von Neumann and Oskar Morgenstern, originally developed game theory to ease decisions in economic contexts [89]. A game in the context of game theory is an interactive decision situation in which the aims, preferences and goals of individual players are potentially in conflict with each other [87]. The players of the game are allowed to choose from a fixed number of strategies. Each player's strategy is associated with an utility, also termed payoff, which also depends on the strategy choices of the other players [88]. Nowadays, the concepts and methods related to the early years of game theory are termed classical game theory (CGT) to delimit their features from newer approaches. In classical game theory a number of severe assumptions are made to represent each player as an economic agents, termed *homo oeconomicus* defining a maximizer of the expected benefit. Consequently, this player acts perfectly rational, has the complete information about all possible strategy options of all other players and features the ability to deduce the best strategy [87]. Classical game theory was successfully applied in

sociology, psychology, politics and military strategies due to reasonable abstractions of particular real world situations [87]. Since living organisms like cells or animals do not consciously optimize over strategic alternatives the concept of classical game theory turned out to be too restrictive for biological applications [90].

The need for a paradigm shift softened the limiting assumptions made to the players in a new concept termed evolutionary game theory (EGT) in which strategies are rather genetically coded than choices resulting from cognitive efforts [90]. EGT received fundamental contributions from John Maynard Smith in the early 1970s, who studied animal behavior in contesting scenarios [91, 92]. Since the utility of an animal strategy cannot be easily determined directly by a quantitative payoff like money in economic contexts, it is linked to reproductive fitness in EGT. This quantitative measure describes the success of a living organism in terms of reproduction, survival and death (sorted by descending success). Furthermore, in EGT optimization is not a result of deductive reasoning, the improvement of a player stems from an iterative process of trial-and-error in the respective biological context [87]. Inspired by evolution theory improvement is a consequence of successive adaptation-, recombination- and mutation events in EGT.

The temporal dynamics in EGT arise from iteratively executed evolutionary steps, which do not reflect the short term evolution of a system, but the long term behavior across generations of a particular organism. Depending on the amount of individuals participating in the game and their interactions among each other, the organism itself can be resolved in a population-based or in an individual-based fashion [87]. For large and well-mixed populations population-based approaches may be applied. A popular approach is given by the replicator equation in which the per capita growth rate of individuals playing strategy s ($\partial\rho_s/\partial t$) is proportional to the difference in fitness of strategy s (f_s) over the average fitness of all strategies ($\bar{f}$) currently played [93]:

$$\frac{\partial \rho_s}{\partial t} = (f_s - \bar{f})\rho_s \quad . \tag{1.1}$$

If a limited number of individuals is present or a confined number of interactions between individuals have to be considered, then individual-based approaches would be in favor. The network of interactions between individuals can be organized as a graph on which the evolutionary game is carried out. Interactions in evolutionary games on graphs may originate from spatial proximity, social connections or genetic relationships introducing another level of detail to the model [94]. Hence, an own field studying the relation between graph properties and evolutionary dynamics emerged [95].

There exist several studies that apply EGT to unravel the pathogenic, parasitic, competitive and symbiotic behavior of cells, which are comprehensively reviewed in [88]. For the application of game theory on the scale of molecules see Bohl *et al.* [96]. Game theory was also applied in the field of fungal infections. Hummert *et al.* studied the behavior of the human-pathogen *Candida albicans* after being phagocytosed by macrophages [97]. If encountering at least two *C. albicans* cells in an macrophage the possible behavioral phenotypes were either to remain as yeast cell or to switch to the hyphal state to pierce the macrophage from inside and kill it. They found that depending on the cost for piercing all fungal cells will play the piercing strategy (low cost for piercing) or only a fraction of them pierces the macrophage from inside (high cost for piercing) [97]. In another study, the yeast-to-hyphal switch of *C. albicans* was investigated under different nutrient conditions and for different immune responses by the host [98]. Tyc *et al.* showed that the host requires a differentiated response to *C. albicans* to keep the fungal cells in the least pathogenic state. A literature search revealed that no EGT model of *A. fumigatus* infection exists today. We here develop a model comprising the most relevant stages of host-pathogen interaction with this particular fungus.

1.3.4 Nested cycles of model development and model probing *in silico*

Computational model development involves a number of steps that are iteratively and in part repeatedly applied in order to capture the essential and desired features of a system. The process of modeling is strongly data-driven. The quality and the amount of the data determines how realistic the model will behave and also which questions the model may answer by performing computational simulations. Essential steps in the development process are presented in what follows und are illistrated in Fig. 1.2.

1. *model creation:* First of all the problem has to be defined and the biological scale of interest needs to be determined. Model construction requires an intensive mining of literature to allow for adequate mapping of constituents with their interrelations and functions of the system under consideration [62]. Much of the art of modeling consists in the identification of the appropriate level of detail [61, 99]. Ockham's razor gives an important advice to meet this important requirement: The model should contain as much detail as necessary, but on the other hand as less as possible [99]. What is necessary is determined primarily by the question to be answered by the model. To get insight into the behavior of the model in a last step meaningful readouts of the model are defined.

2. *parametrisation:* Parameters serve as input for the simulation procedure. A distinction is made between fixed and variable parameters [62]. Typically, fixed parameters are known and are extracted from published or experimental data or can be deduced from these sources. If a parameter is varied in a reasonable and relevant regime, the model behavior can be analyzed under changed conditions and the influence of the respective parameter can be determined. Parameters are systematically varied in the process of calibration in order to meet particular simulation outcomes.

3. *simulation:* Simulations probe the model behavior *in silico* [99]. Stochastic simulations implement randomized processes implying that two simulations with equivalent parametrisation may lead to different results, whereas in deterministic simulations an equivalent parametrisation will lead to equivalent results. Thus, several repetitions of stochastic simulations are required to obtain statistically robust results of one parametrisation. Computer simulations convert the mathematically described model into an executable code. Since computers have only a limited amount of storage continuous fields can not be represented continuously in space with an infinite number of positions. Here, discretisations in reasonable resolutions have to be constructed in order to meet a justifiable trade-off between computational costs and accuracy [99]. In general, stable and efficient simulations require robust implementations and an adequate choice of numerical algorithms, respectively.

4. *calibration:* If the results of the simulation should fulfill one or more criteria, conditions or data, the simulation is repeatedly executed with varying parametrisation. Calibration is the systematic variation of unknown/variable parameters to minimize an objective function, that typically describes the dissimilarity between the simulation and the desired result [61]. The objective function aggregates and weighs all criteria, conditions and data that should be met in one function. There exist vast numbers of approaches to vary parameters in order to quickly arrive at the minimum, which are categorized into global and local optimization methods. For a comprehensive overview of the different approaches, their cases of application as well as their particular strengths and weaknesses see [100]. As a side effect of fitting the simulation to the desired result unknown parameters can be identified. Often, multiple parametrisations minimize the objective function equally well, which then need to be checked for rubustness via sensitivity analysis [99].

5. *model validation/refinement:* A model is considered to be valid if it correctly reproduces test- or training data. Typically, several control experiments are used to check for validity.

The validation becomes stronger the more of these test data can be successfully reproduced [99]. If the model can not stick to one ore more data of the training set the reason for the insufficient behavior has to be identified with the immediate consequence to refine the model. This may mean that extensions to the model have to be made, particular functions need to be exchanged or the resolutions of discretisations are required to be increased [62]. An iterative cycle of model refinement is applied to finally arrive at a satisfactory model fulfilling the criteria of validity [60, 62].

6. *model predictions:* After the previous steps and cycles of development, calibration and successive refinement, ideally, the model is able to capture the processes that are known to date of the system under consideration. Using pre-defined scenarios computer simulations are now in the position to predict their outcomes. These predictions may unravel as yet unknown features of constituents, may shed light into the most important interactions, processes or functions within the system or may give insight into the prospective system behavior over time from a given initial state. Furthermore, predictions can motivate future experimental research or offer new explanations for existing data [101].

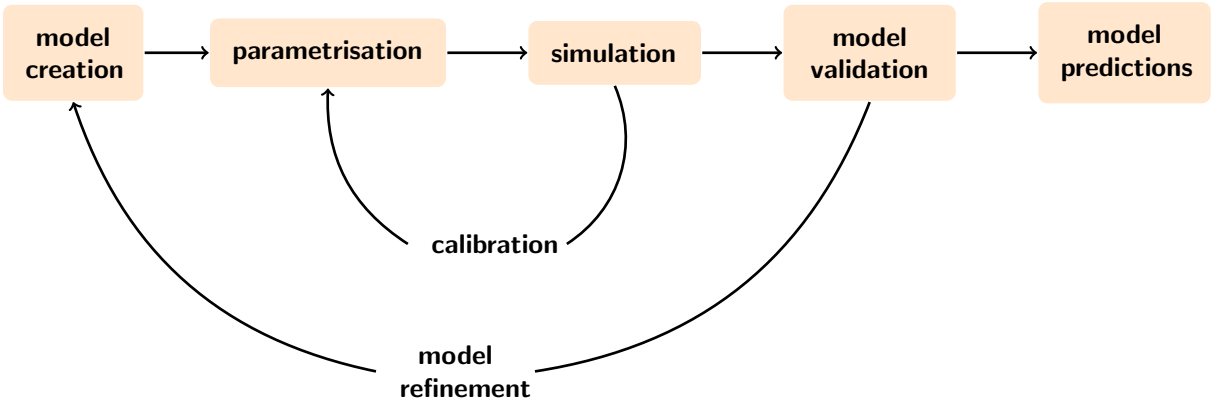

Figure 1.2: Illustration of the cyclic phases in model engineering.

The development of computational models may be embedded in a higher hierarchical process or in a wider scientific context. In the context of systems biology iterative cycles of exchange between wet- and dry-lab serve as a platform to investigate a specific biological system. Here, the main contribution of computational modeling and simulation is to generate and provide reasonable predictions and new hypotheses that can be verified in experimental laboratories [102]. Since computational models require less time and cost than laboratory experiments they allow for extensive measurements of system features that are not capable of being tracked *in vitro* or *in vivo* [62]. Systems biology has originally evolved from high-throughput omics-based approaches that allowed for the construction of gene-regulatory networks on the scale of molecules. In order to unravel the spatio-temporal dynamics of multi-cell systems the framework of image-based systems biology emerged. Within that context the construction of spatio-temporal models with high granularity gets highly conceivable. This can be attributed due to an increase of automated methods to analyze and extract information from high-resolution images and videos in a high-throughput fashion over the recent years [61].

Chapter 2

Aims and objectives of this work

The innate immune response is considered to be the key component to counteract fungal infections [50]. Responses following conidial inhalatation are concerted primarily by proteins of the complement system, by alveolar epithelial cells, alveolar macrophages and polymorphonuclear neutrophilic granulocytes [26, 47, 103]. This work focusses on the innate immune response to the human-pathogenic fungus *A. fumigatus* in the lung of the host.

Since individual-based approaches are highly valuable tools to recreate, simulate and predict infection dynamics in spatio-temporal models, this thesis takes advantage of such methods. To achieve flexibility and to guarantee the opportunity of model extension also for works and projects beyond this thesis, an agent-based framework satisfying modern software architecture was developed (see Section 4.6.2). This methodological tool originated to meet the specific requirements for the interaction between the immune system of the host and different fungal species. Furthermore, to maintain computational tractability advantage of efficient algorithms was taken and smart data structures have been developed and applied. In particular a reusable and fast method to identify interaction partners for agents that are able to occupy arbitrary positions in continuous space was engineered (see Section 4.6.1).

Methods in experimental laboratories typically require a detectable and significant inflammatory response upon host-pathogen encounter to draw reasonable conclusions. Thus, studying the interaction between the innate immune system and *A. fumigatus* is restricted to higher doses of fungal cells than those doses inhaled on a daily basis. Computational approach as the one applied in this thesis have the potential to overcome wet-lab limitations as such. Hence, a three-dimensional virtual infection scenario was simulated to unravel obscured details of the host-pathogen interaction in lung alveoli. This work aims for answers of the following questions:

1. How much time does it take alveolar macrophages to successfully find conidia of the human pathogen *A. fumigatus* after its entry into lung alveoli?
2. In which way and at which speed should macrophages migrate in order to be able to remove the fungus before the onset of germination and invasive growth?
3. Which are the relevant parameter regimes of an alveolar macrophage chemoattractant to successfully enable alveolar macrophages in finding conidia of *A. fumigatus* in time.

In addition to that the different requirements to the components of innate immunity for low and high dose administration of conidia were to be investigated. Here, the following questions were raised:

1. Which morphological states of *A. fumigatus* are the most likely ones at distinct stages in the infection process?

2. To which degree are alveolar macrophages in the position to cope with *A. fumigatus*?

3. Are there differences in the response characteristics between low and high dose conidial infections and if so: what are these differences about?

4. Which features of innate immunity are essential to clear infections induced by *A. fumigatus*?

Chapter 3

Overview of manuscripts

frontiers in MICROBIOLOGY

REVIEW ARTICLE
published: 02 April 2012
doi: 10.3389/fmicb.2012.00108

Systems biology of fungal infection

Fabian Horn[1], Thorsten Heinekamp[2], Olaf Kniemeyer[2], Johannes Pollmächer[3], Vito Valiante[2] and Axel A. Brakhage[2,4]*

[1] *Systems Biology/Bioinformatics, Leibniz Institute for Natural Product Research and Infection Biology – Hans Knöll Institute, Jena, Germany*
[2] *Molecular and Applied Microbiology, Leibniz Institute for Natural Product Research and Infection Biology – Hans Knöll Institute, Jena, Germany*
[3] *Applied Systems Biology, Leibniz Institute for Natural Product Research and Infection Biology – Hans Knöll Institute, Jena, Germany*
[4] *Department of Microbiology and Molecular Biology, Institute of Microbiology, Friedrich Schiller University, Jena, Germany*

Status

Published in Frontiers in Microbiology; 2012; 3:108.

Summary

In this review, we present current applications and trends in the utilization of systems biology to fungal infections focusing on the two pathogens *Aspergillus fumigatus* and *Candida albicans*. We discuss the impact of different studies using high-throughput data in the field of genomics, transcriptomics, and proteomics. Current approaches in computational modeling are classified into network models and spatio-temporal models, where for each class current achievements are presented and an outlook for the application of systems biology to infection biology is given. (This manuscript covers all stages of the data- and knowledge-driven analysis, but focuses on the stage of computational modeling.)

Authors' contributions

FH and AAB coordinated the review. All authors wrote parts of the manuscript and revised it critically.

OPEN ACCESS Freely available online

PLOS | ONE

Agent-Based Model of Human Alveoli Predicts Chemotactic Signaling by Epithelial Cells during Early *Aspergillus fumigatus* Infection

Johannes Pollmächer[1,2], Marc Thilo Figge[1,2]*

1 Applied Systems Biology, Leibniz-Institute for Natural Product Research and Infection Biology, Hans Knöll Institute, Jena, Germany, **2** Friedrich Schiller University, Jena, Germany

Status

Published in PLOS ONE; 2014; 9(10): e111630.

Summary

This study addresses the early immune response to *A. fumigatus* infection by alveolar macrophages in lung alveoli. We engineered a realistic agent-based model of a typical human alveolus on which computer simulations were performed. The simulations predicted that randomly migrating alveolar macrophages will not find a conidium before germination. The results provided strong evidence that alveolar macrophages require chemotactic cues to comply with their widely accepted role in the detection and recognition of conidia during the early immune response.

Authors' contributions

JP and MTF conceived and designed the experiments. JP performed the experiments. JP and MTF analyzed the data. MTF contributed reagents, materials and analysis tools. JP and MTF wrote the paper.

frontiers in Microbiology

ORIGINAL RESEARCH
published: 28 May 2015
doi: 10.3389/fmicb.2015.00503

Deciphering chemokine properties by a hybrid agent-based model of *Aspergillus fumigatus* infection in human alveoli

Johannes Pollmächer[1,2] *and Marc Thilo Figge*[1,2]*

[1] *Applied Systems Biology, Leibniz-Institute for Natural Product Research and Infection Biology – Hans Knöll Institute, Jena, Germany,* [2] *Faculty of Biology and Pharmacy, Friedrich Schiller University Jena, Jena, Germany*

Status

Published in Frontiers in Microbiology; 2015; 6:503.

Summary

In this study, the agent-based model from the PLOS ONE publication [104] was extended and refined to explicitly account for the as yet unidentified alveolar macrophage chemoattractant. The model comprises numerically solving a reaction-diffusion equation on the alveolar surface. A novel chemotaxis model was developed, which accounted for the processes of receptor-ligand binding, receptor internalization and receptor re-expression of alveolar macrophages. Computational simulations allowed for the extraction of experimentally relevant parameter regimes of the molecular diffusion coefficient as well as of the secretion and degradation rate of the chemoattractant.

Authors' contributions

JP and MTF conceived and designed the investigation and work. MTF contributed materials and computational resources. JP processed the data, implemented and applied the computational algorithm. JP and MTF evaluatuated and analyzed the results. JP and MTF drafted the manuscript and revised it critically for important intellectual content and approved the final version to be published. JP and MTF agree to be accountable for all aspects of the work in ensuring that questions related to the accuracy or integrity of any part of the work are appropriately investigated and resolved.

frontiers in Microbiology

ORIGINAL RESEARCH
published: 19 June 2015
doi: 10.3389/fmicb.2015.00608

Bottom-up modeling approach for the quantitative estimation of parameters in pathogen-host interactions

Teresa Lehnert[1,2†], Sandra Timme[1,2†], Johannes Pollmächer[1,2], Kerstin Hünniger[3], Oliver Kurzai[2,3] and Marc Thilo Figge[1,2]*

[1] Applied Systems Biology, Leibniz Institute for Natural Product Research and Infection Biology - Hans-Knöll-Institute, Jena, Germany, [2] Faculty of Biology and Pharmacy, Friedrich Schiller University Jena, Jena, Germany, [3] Fungal Septomics, Septomics Research Center, Friedrich Schiller University and Leibniz Institute for Natural Product Research and Infection Biology Hans-Knöll-Institute, Jena, Germany

OPEN ACCESS

Status

Published in Frontiers in Microbiology; 2015; 6:608.

Summary

In this study, different modeling techniques for dynamical host-pathogen interaction with increasing complexity are built on one another to finally arrive at a more and more realistic representation of an experimental infection assay for *Candida albicans* in human blood. A non-spatial state-based model of a previous study [105] is extended to account for the responses of both, the pathogen and the host's immune system. To also include spatial localisation of cells a spatio-temporal agent-based model is constructed. In both models the results of stochastic computer simulations are compared with experimental data to estimate unknown parameter values. Parameter values for state-transitions as estimated by the state-based model are used in the agent-based simulations to reduce the parameter space and to estimate migration parameters like the diffusion coefficient of monocytes and neutrophils. Furthermore, the state-based model is used to predict the system behaviour under neutropenic and monocytopenic conditions, whereas the agent-based model demonstrates the impact of hyper- and hypoinflammation in immune dysregulation.

Authors' contributions

TL, ST and MTF conceived and designed the investigation and work. MTF contributed materials and computational resources. TL, ST, JP and MTF processed the data, implementated and applied the computational algorithm. TL, ST, JP, KH, OK and MTF evaluated and analyzed the results. TL, ST, JP, KH, OK and MTF drafted the manuscript and revised it critically for important intellectual content and approved the final version to be published. TL, ST, JP, KH, OK and MTF agree to be accountable for all aspects of the work in ensuring that questions related to the accuracy or integrity of any part of the work are appropriately investigated and resolved.

SCIENTIFIC REPORTS

OPEN

Received: 16 March 2016
Accepted: 20 May 2016
Published: 13 June 2016

Deciphering the Counterplay of *Aspergillus fumigatus* Infection and Host Inflammation by Evolutionary Games on Graphs

Johannes Pollmächer[1,2], Sandra Timme[1,2], Stefan Schuster[3], Axel A. Brakhage[2,4], Peter F. Zipfel[2,5] & Marc Thilo Figge[1,2]

Status

Published in Scientific Reports; 2016; 6:27807.

Summary

Here, we engineered a sequence of evolutionary games to model immune responses by the complement system, alveolar macrophages and polymorphonuclear neutrophilic granulocytes against the human-pathogenic fungus *Aspergillus fumigatus* in alveolar sacs. Combination of the games with inflammatory signals revealed the relative importance and the respective contributions of different immune effectors and functions in the fight against the pathogen. We found that the main role of alveolar macrophages consists in their regulatory capabilities, whereas neutrophils are the key to eliminate *A. fumigatus* due to their superiority in quantity and ability to counteract the pathogen.

Authors' contributions

JP, PFZ and MTF conceived and designed the study. MTF contributed materials and computational resources. JP processed the data, implemented and applied the computational algorithm. All authors evaluated and analyzed the results. All authors wrote the manuscript and revised it critically.

Title	Status	Journal	Authors	Contribution
Manuscript 1	published	Frontiers in Microbiology	Horn F	25 %
		2012, 3:108	Heinekamp T	15 %
			Pollmächer J	15 %
			Kniemeyer O	15 %
			Valiante V	15 %
			Brakhage AA	15 %
Manuscript 2	published	PLOS ONE	**Pollmächer J**	90 %
		2014, 9(10): e111630	Figge MT	10 %
Manuscript 3	published	Frontiers in Microbiology	**Pollmächer J**	90 %
		2015, 6:503	Figge MT	10 %
Manuscript 4	published	Frontiers in Microbiology	Lehnert T	35 %
		2015, 6:608	Timme S	35 %
			Pollmächer J	15 %
			Hünniger K	5 %
			Kurzai O	5 %
			Figge MT	5 %
Manuscript 5	published	Scientific Reports	**Pollmächer J**	45 %
		2016, 6:27807	Timme S	35 %
			Schuster S	5 %
			Brakhage AA	5 %
			Zipfel PF	5 %
			Figge MT	5 %

Table 3.1: Overview of manuscripts

Chapter 4

Manuscripts and unpublished material

4.1 Systems biology of fungal infections

frontiers in MICROBIOLOGY

REVIEW ARTICLE
published: 02 April 2012
doi: 10.3389/fmicb.2012.00108

Systems biology of fungal infection

Fabian Horn[1], Thorsten Heinekamp[2], Olaf Kniemeyer[2], Johannes Pollmächer[3], Vito Valiante[2] and Axel A. Brakhage[2,4]*

[1] *Systems Biology/Bioinformatics, Leibniz Institute for Natural Product Research and Infection Biology – Hans Knöll Institute, Jena, Germany*
[2] *Molecular and Applied Microbiology, Leibniz Institute for Natural Product Research and Infection Biology – Hans Knöll Institute, Jena, Germany*
[3] *Applied Systems Biology, Leibniz Institute for Natural Product Research and Infection Biology – Hans Knöll Institute, Jena, Germany*
[4] *Department of Microbiology and Molecular Biology, Institute of Microbiology, Friedrich Schiller University, Jena, Germany*

frontiers in MICROBIOLOGY

REVIEW ARTICLE
published: 02 April 2012
doi: 10.3389/fmicb.2012.00108

Systems biology of fungal infection

Fabian Horn[1], Thorsten Heinekamp[2], Olaf Kniemeyer[2], Johannes Pollmächer[3], Vito Valiante[2] and Axel A. Brakhage[2,4]*

[1] Systems Biology/Bioinformatics, Leibniz Institute for Natural Product Research and Infection Biology – Hans Knöll Institute, Jena, Germany
[2] Molecular and Applied Microbiology, Leibniz Institute for Natural Product Research and Infection Biology – Hans Knöll Institute, Jena, Germany
[3] Applied Systems Biology, Leibniz Institute for Natural Product Research and Infection Biology – Hans Knöll Institute, Jena, Germany
[4] Department of Microbiology and Molecular Biology, Institute of Microbiology, Friedrich Schiller University, Jena, Germany

Edited by:
Jörg Linde, Leibniz Institute for Natural Product Research and Infection Biology – Hans Knöll Institute, Germany

Reviewed by:
Rene Alvarez, Naval Medical Research Unit-San Antonio, USA
Guoku Hu, Creighton University, USA
Scott G. Filler, Los Angeles Biomedical Research Institute, USA

***Correspondence:**
Axel A. Brakhage, Molecular and Applied Microbiology, Leibniz Institute for Natural Product Research and Infection Biology – Hans Knöll Institute, Beutenbergstrasse 11a, 07745 Jena, Germany.
e-mail: axel.brakhage@hki-jena.de

Elucidation of pathogenicity mechanisms of the most important human-pathogenic fungi, *Aspergillus fumigatus* and *Candida albicans*, has gained great interest in the light of the steadily increasing number of cases of invasive fungal infections. A key feature of these infections is the interaction of the different fungal morphotypes with epithelial and immune effector cells in the human host. Because of the high level of complexity, it is necessary to describe and understand invasive fungal infection by taking a systems biological approach, i.e., by a comprehensive quantitative analysis of the non-linear and selective interactions of a large number of functionally diverse, and frequently multifunctional, sets of elements, e.g., genes, proteins, metabolites, which produce coherent and emergent behaviors in time and space. The recent advances in systems biology will now make it possible to uncover the structure and dynamics of molecular and cellular cause-effect relationships within these pathogenic interactions. We review current efforts to integrate omics and image-based data of host-pathogen interactions into network and spatio-temporal models. The modeling will help to elucidate pathogenicity mechanisms and to identify diagnostic biomarkers and potential drug targets for therapy and could thus pave the way for novel intervention strategies based on novel antifungal drugs and cell therapy.

Keywords: *Aspergillus fumigatus, Candida albicans*, gene-regulatory network, network modeling, pathogenicity, pathogen-host interaction, spatio-temporal modeling, systems biology

1. BACKGROUND

1.1. HUMAN-PATHOGENIC FUNGI

It is estimated that the total number of fungal species exceeds 1.5 million (Hawksworth, 2001). However, only a small minority of approximately 100 species of fungi are associated with human diseases. Nevertheless, infections caused by fungal pathogens lead to a wide range of diseases including allergies, superficial infections, and invasive mycoses. The outcome of an infection with a human-pathogenic fungus often depends on the immune status of the host organism. Patients suffering from a weakened immune system are at high risk of developing a serious fungal infection. Continuous progress in medicine, e.g., in chemotherapy and organ or bone marrow transplantation, has led to an increasing number of patients with impaired immune status. In recent decades, the frequency of invasive fungal infections has increased steadily, resulting in considerable morbidity and mortality. In the USA, the incidence of sepsis caused by fungi has increased by more than 200% since 1991, whereas cases of bacterial sepsis have only increased moderate (Martin et al., 2003). Invasive mycoses are characterized by a high mortality rate. The increasing number of fungal infections has significantly contributed to health-related costs (Pfaller and Diekema, 2007).

The yeast *Candida albicans* and the filamentous fungus *Aspergillus fumigatus* are by far the most important causes of life-threatening invasive mycoses. Apart from *A. fumigatus*, around 10% of the more than 200 species of the genus *Aspergillus* are regarded as human pathogens or as having other adverse effects, e.g., *A. terreus*, *A. flavus*, and *A. niger* (Brakhage, 2005). The prevalence of *C. albicans* in clinical *Candida* samples is 50–70%, followed by infections with *Candida glabrata*, which is found in 20–25% of clinical *Candida* samples. Other pathogenic *Candida* species include *C. tropicalis*, *C. dubliniensis*, *C. krusei*, and *C. parapsilosis* (overview in Pfaller and Diekema, 2007). Another important human-pathogenic fungus of clinical relevance is the fungus *Cryptococcus neoformans*. The most common fungal infection among AIDS patients, cryptococcal meningitis, is caused by this basidiomycete. Furthermore, other fungal species, such as *Pneumocystis jiroveci*, *Zygomycetes*, *Fusarium* species, and *Scedosporium* species, have emerged as causal agents of invasive mycoses (Pfaller and Diekema, 2007).

Despite the different pathogenesis of infections caused by *C. albicans* and *A. fumigatus*, there are several common traits, particularly when the host response is considered: (i) the pathogens must be able to overcome epithelial barriers, (ii) innate immunity represents the major defense system, (iii) pathogenic fungi possess physiological characteristics, virulence determinants, and capabilities for immune evasion that make them aggressive pathogens, and (iv) invasive candidiasis and invasive aspergillosis are mainly found in patients with a weakened immune system either due to reduced activity of immune effector cells or defects in epithelial barriers.

Consequently, the aims of research on human-pathogenic fungi are (i) to unravel the pathogenic determinants specific to each

fungus, (ii) to investigate the distinct roles of epithelial barriers, the mechanisms of the innate immunity, and potential contributions of the adaptive immune system to the pathogenesis of fungal infections, and (iii) to elucidate the complex mechanisms of fungal infections and identify common principles of fungal pathogenesis.

1.2. PATHOBIOLOGY OF *ASPERGILLUS FUMIGATUS*: FROM ENVIRONMENTAL MICROORGANISM TO PATHOGEN

Within the last two decades, the filamentous fungus *A. fumigatus* has become one of the most important fungal pathogens. Conidia of this saprophytic fungus can be found almost everywhere, from the winds of the Sahara to the snow of the Antarctic. The most severe disease caused by *A. fumigatus* is invasive aspergillosis (IA), which occurs almost exclusively in immunocompromised patients (Brakhage, 2005). There is currently a lack of reliable diagnostic tools and effective treatment options for this condition, resulting in a high mortality rate despite therapy. Remarkably, *A. fumigatus* causes 90% of all systemic *Aspergillus* infections. This indicates that *A. fumigatus* possesses certain virulence determinants that favor this species becoming an opportunistic human pathogen. Because of their ubiquitous presence in the air, each person inhales several hundred *A. fumigatus* conidia daily. In immunosuppressed patients, the lung is the primary site of infection. In immunocompetent individuals, mucociliary clearance and phagocytic cells normally prevent the disease (Brakhage et al., 2010). However, there is a correlation between the degree of immunosuppression and the risk of contracting IA. Consequently, important risk factors include neutropenia, T cell depletion, CD34-selected stem cell products, corticosteroid therapy, and cytomegalovirus infections (Marr et al., 2002).

Since 2005, considerable progress has been made in the analysis of *A. fumigatus*. The genome sequence of *A. fumigatus* is available, and the transformation efficiency of the fungus was drastically increased by generation of *ku70* and *ku80* mutants of *A. fumigatus* (Nierman et al., 2005; da Silva Ferreira et al., 2006; Krappmann et al., 2006) making the generation of mutants by targeted gene deletion much easier. As a result of this improvement, the number of deletion mutants has increased from a handful, in the year 2000, to more than 400, today.

However, only a few virulence determinants of *A. fumigatus* have been characterized to date. These determinants include the siderophore-mediated iron uptake system (Schrettl et al., 2004) or the *pksP* gene, which is involved in the biosynthesis of the gray-green spore pigment (Langfelder et al., 1998; Thywißen et al., 2011; Volling et al., 2011). How these virulence determinants influence the infection is currently under investigation. DHN melanin was shown to inhibit both apoptosis and the acidification of conidia-containing phagolysosomes of macrophages (Thywißen et al., 2011; Volling et al., 2011). Because virulence is a multifactorial process, it can safely be expected that many more virulence-associated traits will be discovered, e.g., *A. fumigatus* is able to grow under hypoxic conditions. This ability is essential for pathogenicity (Willger et al., 2008). *A. fumigatus* also possesses immune-evasion mechanisms which reduce recognition, both by immune effector cells and the complement system (Behnsen et al., 2008, 2010; Aimanianda et al., 2009).

Innate immunity is of great importance in defense against *A. fumigatus*. Alveolar macrophages are the major resident cells of the lung alveoli and they phagocytose conidia. However, conidia have the ability to interfere with functions of the macrophages such as the maturation of phagolysosomes (Jahn et al., 2002; Ibrahim-Granet et al., 2003; Thywißen et al., 2011). Unphagocytosed conidia and outgrowing hyphae are killed by neutrophilic granulocytes, whose activity is essential for preventing IA (Feldmesser, 2006).

Also, the complement system appears to contribute to the defense mechanism (Moalli et al., 2010). Human pattern recognition receptors sensing fungal cell wall components include TLRs (Toll-like receptors), Galactin 3, DC-Sign (C-type lectin receptors), dendritic cell-specific intracellular adhesion molecule 3 (ICAM-3)-grabbing non-integrin, Dectin-1, SCARF1, and CD36. In line with the importance of these receptors for fungal recognition, a growing number of defined single nucleotide polymorphisms in the respective genes that appear to determine host susceptibility to *A. fumigatus* were identified (overview in Romani, 2011).

Furthermore, neutrophils possess recently discovered extracellular killing mechanisms: they degranulate, release DNA, and form neutrophil extracellular traps (NETs) both *in vitro* and *in vivo* against *A. fumigatus* (Bruns et al., 2010; McCormick et al., 2010). However, whether NET formation is detrimental for *A. fumigatus* overall is currently under investigation, and it remains unclear how neutrophils ultimately kill *A. fumigatus*. Reactive oxygen intermediates (ROI) most probably do not play a role as primary killing agents, but are required as signaling molecules (Lessing et al., 2007). Incubation of dendritic cells (DCs) with *A. fumigatus in vitro* resulted in the release of chemokine CXCL8, which attracts neutrophils (Gafa et al., 2007). Secretion of additional factors increased surface expression of CD11b and CD18 on neutrophils. Dectin-1, which is an important receptor on macrophages and neutrophils, is also expressed on the surface of immature DCs and is involved in the induction of a proinflammatory cytokine response (Mezger et al., 2008). DCs thus play an important role in defense against *A. fumigatus*. The pathogen recognition receptor Dectin-1 acts upstream of the Syk tyrosine kinase in response to an infection with *A. fumigatus*. Signaling via the Syk tyrosine kinase was recently found to be essential for the activation of NLRP3 inflammasome, another component of the innate immune system (Saïd-Sadier et al., 2010). Despite these findings, we are still in the early stages of understanding their role in organizing the immune defense mechanism.

Epithelial and endothelial cells in the lung can internalize conidia. It cannot, therefore, be excluded that these cells form sites of persistence and foci of infection (Latgé, 1999). The role of T cells has not yet been clarified. It appears most likely that they initiate the adaptive immune responses to *Aspergillus* species and directly influence the outcome of an infection (Dagenais and Keller, 2009). Phagocytosis of conidia by DCs leads to a protective Th1 response, whereas hyphal phagocytosis results in non-favorable Th2 responses and the generation of IL-10-producing CD4 cells (Romani, 2011).

1.3. PATHOBIOLOGY OF *CANDIDA ALBICANS*: FROM COMMENSAL TO PATHOGEN

Candida albicans normally exists as harmless commensal yeast on mucosal surfaces of the majority of the human population. Only under certain circumstances (imbalance of the normal microbial flora, immunosuppression, damage of tissue barriers), can *C. albicans* cause superficial (oral thrush in 90% of all untreated HIV patients, vaginal thrush in 75% of all women once in their lifetime) or life-threatening systemic infections (nosocomial candidiasis, candidemia; reviewed in Pfaller and Diekema, 2007; Martin et al., 2011). *C. albicans* is currently identified as the fourth most common blood isolate in US hospitals, accounting for around 10% of hospital-acquired bloodstream infections (Wisplinghoff et al., 2004). Cases of sepsis caused by this fungus lead to mortality rates of about 40% and are thus higher than observed for any bacterial sepsis (Gudlaugsson et al., 2003; Wisplinghoff et al., 2004; Picazo et al., 2008). Although *C. albicans* is an opportunistic pathogen, only a minority of cases (20%) of disseminated candidiasis occurs in patients with severe immunosuppression such as individuals with neutropenia, corticosteroid therapy, or HIV infection. Patients with severe illnesses who have prolonged periods of hospitalizations, a central venous catheter, gastrointestinal/cardiac surgery, or burns are at especially high risk of developing an invasive *Candida* infection (reviewed in Perlroth et al., 2007).

Almost all *C. albicans* infections are endogenous infections, caused by commensal strains of patients' own microflora. Despite numerous studies, it remains unclear how the transition from a harmless commensal to an aggressive pathogen is triggered. It seems certain that it is not only modifications of the microbial flora and host factors, but also specific attributes of the fungus that play an important role in this transition.

The ability to switch from yeast to pseudohyphal or hyphal growth is an important virulence trait for *C. albicans*. Several environmental conditions such as temperatures above 37°C, pH values of 7.0 or higher, high exogenous CO_2 concentrations of more than 5%, or the presence of serum (Liu, 2002) trigger this transition. Numerous genes are involved in the regulation of the morphological switch, but molecular details are still poorly understood. The transcription factor Efg1p plays a central role in the control of morphogenesis (Stoldt et al., 1997; Doedt et al., 2004) and the loss of the *EFG1* gene led to mutants which were locked in the yeast form and showed reduced virulence in a murine model of candidiasis (Lo et al., 1997; Stoldt et al., 1997). In the regulation of the Efg1p pathway, cAMP-mediated signal transduction plays an essential role and mutants lacking the adenylyl cyclase Cdc35p do not form hyphae. As well as Efg1p, a large number of other transcription factors have also been reported to inhibit or trigger the yeast to hyphal transition, e.g., Efh1p, Mcm1p, Cph2p, and Tec1p (reviewed in Whiteway and Bachewich, 2007).

Besides the morphological plasticity, the ability of *C. albicans* to adhere to host cells and tissue and form biofilms is another important virulence factor. Amongst others, the ALS (agglutinin-like sequence) proteins are a well-studied group of proteins that form a family of peptide-binding proteins and which mediate adhesion (Salgado et al., 2011). They bind to extracellular matrix proteins, such as collagen, fibronectin and laminin (Als1p, Als3p, Als5p, Als6p, Als9p), endothelial and epithelial cells (Als1p, Als3p, Als5p), and also mediate cell-to-cell aggregation (Als5p) and iron acquisition (Als3p; Filler, 2006; Almeida et al., 2009). Hwp1p is another important adhesin, expressed only on hyphae, which binds tightly to oral epithelial cells and that is involved in biofilm formation (Nobile et al., 2006).

Secreted enzymes with proteolytic or lipolytic activity represent another group of proteins which contributes significantly to *C. albicans*' pathogenicity. A large proportion of the proteolytic activity is attributed to a multigene family of secreted aspartic proteinases (SAPs). Ten different SAPs have been described in *C. albicans*, eight of which are secreted extracellularly and two of which are anchored to the membrane via GPI linkage. Their contribution to the pathogenesis of *C. albicans* infections has been extensively investigated. *SAP1–SAP3* genes were considered to play a role in localized *C. albicans* infections and complement evasion, whereas *SAP4–SAP6* were postulated to play an important role in the pathogenesis of invasive candidiasis (Schaller et al., 2005; Gropp et al., 2009). However, in a recent study by Correia et al. (2010) the importance of *SAP1* to *SAP6* for virulence was reassessed in a murine model of candidemia. In contrast to previous findings, *SAP1* to *SAP6* were found to play no significant role in disseminated *C. albicans* infections. In addition to the virulence determinants described above, physiological fitness, in other words, high stress tolerance and metabolic flexibility, is another important factor that contributes to the pathogenicity of *C. albicans* (Brown et al., 2007; Fleck et al., 2011).

The fact that *C. albicans* is a diploid fungus and was long thought to be an obligate asexual organism (Alby et al., 2009), has long hindered the production of genetically defined mutants. In contrast to the well-studied yeast *Saccharomyces cerevisiae*, *C. albicans* does not have any natural DNA plasmids that could be used for transformation. In addition to this, *C. albicans* shows a non-standard codon usage and translates the CUG codon as serine instead of leucine (Lloyd and Sharp, 1992). Only after establishing protocols for targeted gene disruptions of both alleles, creating conditional null mutants based on tetracycline-regulatable systems, sequencing of the entire genome, establishment of a genome database, production of genome-wide microarrays, and production of reporter strains and other molecular tools as well as infection models, has *C. albicans* reached the status of a model organism for yeast infections (Theiss et al., 2002; Fradin et al., 2003; Jones et al., 2004; Braun et al., 2005; Samaranayake and Hanes, 2011; Szabo and MacCallum, 2011).

Due to this technical progress, interactions of *C. albicans* with host cells and the immune system have been the focus of many studies in recent years. Fungal recognition is the first step in the antifungal immune response and is mediated by pattern recognition receptors (PRR). The mannan cell wall component is recognized by the mannose receptor, the C-type lectin-like receptor Dectin-2, and the TLR4. Furthermore, TLR2 triggers an immune response by binding to phospholipomannans, as the Dectin-1 receptor does by binding to β-glucan (Netea et al., 2008). TLR2 and Dectin-1 regulate also the gene transcription of proinflammatory cytokines such as the pro-IL-1β. This interleukin is further processed into its active mature form via the NLRP3 inflammasome, a multiprotein complex. It has recently been shown that it is crucial for antifungal host defense (Gross et al., 2009; Hise

et al., 2009). After recognition, phagocytes, like macrophages or neutrophilic granulocytes, kill *C. albicans* cells by phagocytosis or secretion of antimicrobials. One mechanism discovered recently is the formation of neutrophil extracellular traps as mentioned above in the section on *A. fumigatus* (Urban et al., 2006). To link these interactions to the highly complex setting of clinical infections, complex *in vitro*, *ex vivo*, and *in vivo* infection models have been established and genome-wide transcriptional profiles, including direct *C. albicans* transcriptomes from patient samples, have been produced (Wilson et al., 2009; Cairns et al., 2010).

1.4. SYSTEMS BIOLOGY OF INFECTION

Due to their high complexity, it is conceivable that invasive infections caused by human-pathogenic fungi can be described and understood in a comprehensive manner by taking a systems biological approach. There are two complementary strategies in systems biology: (i) Starting from smaller, even minimal models capturing the essential and abstract interactions in the system under study and (ii) using experimental measurements such as large omics datasets in combination with large-scale models. Hybrid approaches, which integrate these top-down and bottom-up perspectives, contribute to our understanding of the multiple interdependencies of different hierarchical levels in biological systems (Forst, 2006). The global dynamics of a system can only be understood and quantified if the functionality of modular subsystems is elucidated, while considering the most important interactions on different levels in the biological system. With the aim of revealing molecular and cellular cause-effect relationships within the host-pathogen interaction in a non-ambiguous and efficient way, the setup of experiments and the design of experimental series can be optimized on the basis of established mathematical and computational models. Data exchange proceeds in an iterative cycle between model and experiment, with a constant refinement and validation of the models and the model-based planning of experiments (Ideker et al., 2001).

Current experimental and modeling techniques focus on specific perspectives at different scales. At present, experimental data from high-throughput experiments are increasingly and routinely used as the basis for mathematical modeling. This wealth of information has become available recently. Nevertheless, the history of the mathematical modeling of infectious diseases can be traced back to the eighteenth century, when today's basic concepts of evolution, genetics, and molecular biology were still unknown. Back in 1760, Daniel Bernoulli predicted the life expectancy of a population which has been immunized with cowpox (Bernoulli, 1760). In the early twentieth century, mathematical models were developed that mainly focused on the spread of diseases such as measles and malaria (Ross, 1911; Bailey, 1975). Most models would be related to today's research field of *population biology*, meaning that they dealt with fluctuations in population size under different modes of disease transmission. Since the second half of the twentieth century, these models have become more sophisticated. Amongst other concepts, they incorporated new aspects (e.g., population variables, May and Anderson, 1979; transmission rates, Real and Biek, 2007; pathogen life cycles, and host specificities, Woolhouse et al., 2001; Barrett et al., 2008) and extended the model to allow multi-level modeling (Roux and Aiello, 2005) or concepts of evolution (reviewed in Tong and Ng, 2011).

Naturally, each infection process is unique. Nevertheless, the modeling makes it possible to reveal fundamental similarities and differences in the underlying processes. The influence of single model parameters and their interdependency can thus be deduced. These parameters are also assessed if they serve as effective control options for the implementation of governmental public health risk management programs (Tong and Ng, 2011).

With the progress in molecular biology, infection biology, and biotechnology, it is now possible to study species-specific host-pathogen interactions at the molecular level in order to search directly for biomarkers with diagnostic potential and drug targets for novel therapeutic treatment strategies. The focus of research has diversified, resulting in specialized databases and research groups. Only early steps toward the computational systems biology of *A. fumigatus* and *C. albicans* have been made, including genome-scale data mining and mathematical modeling of infection processes by these fungi (reviewed for human-pathogenic fungi in Albrecht et al., 2008, 2011 and Rizzetto and Cavalieri, 2011).

2. DATA BASIS AND DATA ANALYSIS

The aim of understanding the complexity of host-pathogen interactions can be achieved by exploiting the increasing amount of experimental data, including high-throughput data and information available from public repositories as well as from biomolecular databases (see **Table 1**). Typically, experimental series comprise knock-down experiments along with global and specific screening using knockout mutants of pathogenic fungi. Procedures can be designed to analyze the complex structured data obtained

Table 1 | Bioinformatic resources of special interest for fungal systems biology.

Resource	Website	Description
AsperCyc	www.aspercyc.org	*Aspergillus* metabolic pathways
Aspergillus genome DB	www.aspgd.org	*Aspergillus* genomics
BROAD	www.broadinstitute.org	Genomics
Candida genome DB	www.candidagenome.org	*Candida* genomics
CFGB	http://cfgp.riceblast.snu.ac.kr	Comparative genomics platform
Ensembl	http://fungi.ensembl.org	Genomics
FunCatDB	www.helmholtz-muenchen.de/en/mips/projects/funcat	Gene-annotations
FungiDB	www.fungidb.org	Genomics
FungiFun	https://sbi.hki-jena.de/FungiFun/	Gene set enrichment analysis
JGI	www.jgi.doe.gov	Genomics
Omnifung	www.omnifung.hki-jena.de	Data warehouse for omics data
PhiBase	www.phibase.org	Database of virulence genes
SysMo-DB	www.sysmo-db.org	Collaborative platform

from these experimental series. Standardized pre-processing of the raw data and integrative analyses allow the identification of key regulators involved in pathogenicity. The management and integrative analysis of experimental data is challenging and constitutes a research field itself within bioinformatics (Albrecht et al., 2008). It was presented exemplary for genome, transcriptome, and proteome analysis of the heat shock response of *A. fumigatus* (Albrecht et al., 2010). Each technique applied generates different types of data, which have been acquired at the various levels of information. For each level, all of the available data types and their accompanying computational methods are usually referred to as "*omics.*" New technologies, such as high-throughput sequencing, impose new challenges on efficient data storage, data retrieval, and statistical analysis. In order to handle the tremendous amount of data required for systems biology, the heterologous data has to be linked between existing databases. Automatic computer access has to be provided, and different user perspectives have to be taken into account. The standardization of biological terms (GO, FunCat, SBO, Ruepp et al., 2004; Arnaud et al., 2009; Courtot et al., 2011), data formats (SBML, Hucka et al., 2003), experimental metadata (MIBBI, Taylor et al., 2008), and operating procedures (Taverna, Hull et al., 2006) contribute to this objective.

Despite the wealth of information gained from analyzing high-throughput data, research into biological systems is mostly focused on a single data level. To overcome these limitations, data warehousing approaches (Omnifung, IntegromeDB, Albrecht et al., 2007; Kozhenkov et al., 2011) aim to integrate the different data layers. At the same time, most integration tools offer different visualization techniques as an additional key method for querying and understanding large datasets (Köhler et al., 2006; Smoot et al., 2011). Even though efforts have been made in this respect, an integrated view of different omics data levels is still a major challenge. Regulatory processes, different time scales, and non-linear processes in the biological system as well as technical limitations of omics technologies hamper the detection of causality or even correlation between different data layers (Albrecht et al., 2011).

2.1. "OMICS" BASED DATA

2.1.1. Genome

The importance of fungal-derived infections is reflected impressively by the number of fungal genomes that have been sequenced in recent years. The genome of the diploid *C. albicans* was published in 2004 (Jones et al., 2004; Braun et al., 2005), followed by the *C. neoformans* genome (Loftus et al., 2005) and by the *A. fumigatus* genome (Nierman et al., 2005). Since then, other *Candida* and *Aspergilli* genomes have been sequenced (Arnaud et al., 2007; Fedorova et al., 2008). Also, the first genomes of dermatophytes have recently been published (Burmester et al., 2011). **Table 2** lists all human-pathogenic fungi for which the full genome sequence is available. This list does not include genome projects currently in progress such as the sequencing of several *C. albicans* strains to evaluate *Candida* genome plasticity. New sequencing technologies now allow even greater numbers of genomes and transcriptomes to be deciphered, which will contribute to a better understanding of fungal pathogenesis. This information has been collected and released in suitable and easy to use web tools (see **Table 1**). For *Candida* sp., the main websites used are the CandidaDB (d'Enfert et al., 2005) and the *Candida* Genome Database (CGD; Arnaud et al., 2007). For *A. fumigatus*, the community normally refers to the Central *Aspergillus* Data REpository (CADRE, Gilsenan et al., 2012) and the new *Aspergillus* Genome Database (AspGD, Arnaud et al., 2012).

The information available in the different genome databases allowed us to apply studies of comparative genomics to human-pathogenic fungi focusing on evolutionary aspects of virulence genes. Studies of different *Candida* sp. highlighted that cell

Table 2 | List of human-pathogenic fungi of which the genomes have been sequenced.

Scientific classification	Species
ASCOMYCOTA	
Ascomycetes	*Ajellomyces dermatitidis, Aspergillus clavatus, Aspergillus fischeri, Aspergillus flavus, Aspergillus fumigatus, Aspergillus terreus, Blastomyces dermatitidis, Exophiala dermatitidis, Histoplasma capsulatum*
Euascomycetes	*Coccidioides immitis, Coccidioides posadasii, Penicillium marneffei*
Eurotiomycetes	*Arthroderma benhamiae, Arthroderma canis, Arthroderma gypseum, Arthroderma otae, Lacazia loboi, Paracoccidioides brasiliensis, Penicillium chrysogenum, Trichophyton equinum, Trichophyton rubrum, Trichophyton tonsurans, Trichophyton verrucosum*
Saccharomycetes	*Candida albicans, Candida dubliniensis, Candida glabrata, Candida guilliermondii, Candida lusitaniae, Candida parapsilosis, Candida tropicalis*
Sordariomycetes	*Chaetomium globosum, Fusarium oxysporum, Fusarium verticilloides, Nectria haematococca*
Pneumocystidomycetes	*Pneumocystis jirovecii*
BASIDIOMYCOTA	
Agaricomycetes	*Cryptococcus gattii, Cryptococcus neoformans*
Ustilaginomycetes	*Malassezia globosa, Malassezia restricta*
ZYGOMYCOTA	
Mucorales	*Rhizopus oryzae*
MICROSPORIDIA	
	Encephalitozoon cuniculi, Encephalitozoon intestinalis

wall-associated genes, important for host recognition and virulence of *Candida* sp., have been subject to gene duplications (Butler et al., 2009). Furthermore, the high number of lipases or GPI anchored proteins (normally clustered) is important for the virulence of *C. albicans* and *C. glabrata* (van het Hoog et al., 2007; Dujon, 2010). This phenomenon is known as gene family expansion and results in an increase of enzymatic power during infection processes or, where possible, easier rearrangement of the genome. In both cases, there is an increase in the competitiveness of the pathogens during infection processes (Moran et al., 2011).

Many clustered genes present in *Aspergillus* sp. encode proteins for secondary metabolite production, such as mycotoxins and antibiotics, and do not normally represent repetition of genes with similar enzymatic activity. A higher degree of genome rearrangement was observed in telomeric regions, where many of these clusters are located. The origins of these gene clusters have always been associated with the possibility of vertical gene transfer from other microbes. However, extensive comparative studies on *Aspergilli* genomes suggest that the presence of paralogs in the different species could be ascribed to gene duplication within the genus and subsequent translocation to telomere-proximal locations (Fedorova et al., 2008).

In addition to the importance for taxonomic studies, comparative genomics also highlighted peculiarities and similarities between different fungal species. One example was given by comparing signaling pathways in different pathogenic fungi. The mitogen activated protein kinase (MAPK) signaling pathways and the calcineurin pathway have been extensively studied in pathogenic fungi because of their involvement in pathogenesis. Global sequence similarity analysis indicated that, on the one hand, core structures involved in signaling are highly conserved while, on the other hand, upstream (e.g., receptors) and downstream factors (e.g., transcription factors) are far more species-specific (Rispail et al., 2009). Knowledge obtained in these studies can be used to identify suitable intraspecific or interspecific targets for therapeutic intervention.

2.1.2. Transcriptome

A genome, apart from its arrangement and complexity, can always be regarded as a static feature. In contrast to this, transcriptome analysis provides information about the dynamics of a genome's expression. Due to the availability of fungal genome data, it is now possible to design microarrays for genome-wide expression analysis.

For more than 10 years, scientists have had access to various *C. albicans* transcriptome studies. Many experiments have focused on studying gene expression in response to antifungal agents (e.g., azole derivatives, amphotericin B, echinocandins; Backer et al., 2001; Barker et al., 2004; Liu et al., 2005) but also at different stages of development and during biofilm formation (Doedt et al., 2004; Murillo et al., 2005). For *C. albicans*, already in 2005 a comparative gene expression analysis was published (Ihmels et al., 2005).

Aspergillus fumigatus' transcriptome history is comparatively recent. The first entire global transcriptome analysis was published together with the release of the first genome sequence (Nierman et al., 2005). After that, scientists had access to various transcriptome studies of developmental stages, during iron starvation, of biofilm formation, and response to antifungals (e.g., da Silva Ferreira et al., 2006; Schrettl et al., 2008; Bruns et al., 2010; Cagas et al., 2011; Jain et al., 2011). Fewer transcriptome studies have been carried out for *A. fumigatus* than for *C. albicans*. Furthermore, the comparability of transcriptome data is low. One reason for this is the development of different microarray platforms that made it harder to compare different gene expression data. In addition to this, the experimental design of transcriptome studies has been quite heterogenous with respect to media, strains, and general growth conditions. At present, we can only reliably compare different transcriptome data on the basis of genes that have high fold-changes in expression levels.

The main challenge in infection biology is to understand gene responses during infection. Such studies have been performed in several ways (co-culture of fungi and immune cells or direct tissue infection). The main problem remains the enrichment of the RNA from the pathogen prior to the hybridization step in order to avoid a decrease in data quality caused by cross-hybridization. This step is normally performed by separation of the different RNA species that can eventually be amplified to increase the nucleic acid quantity (Nygaard and Hovig, 2006). Previous studies identified genes involved in nutrient acquisition, oxidative stress response, and metal homeostasis, which are differentially regulated in *C. albicans* when co-cultured with macrophages and neutrophils (Lorenz and Fink, 2001; Lorenz et al., 2004; Wilson et al., 2009). Similar results have also been found in *A. fumigatus* when co-cultured with neutrophils and dendritic cells (Lessing et al., 2007; Sugui et al., 2008; Morton et al., 2011). A recent review described a comparison of transcriptome data obtained from pathogenic fungi during organ or tissue infections (Cairns et al., 2010). Many genes involved in primary metabolism appeared to be differentially expressed during infection in both human and plant pathogens. This data suggested that physiological reprogramming during infection remains relatively well conserved among various pathogens. On the other hand, these types of studies highlighted the limitations of hybridization-based techniques such as microarrays.

Recently, new techniques based on deep RNA sequencing have been introduced, i.e., the RNA-seq technique to analyze transcriptomes (Wang et al., 2009). Recent work on *C. albicans* and *A. fumigatus* indicated that with this technology it is possible to identify misannotated genes and differences in the level of low expressed genes which, for example, is relevant for many secondary metabolite gene clusters (Bruno et al., 2010; Gibbons et al., 2012). Furthermore, in infection biology it is important to study the gene expression profiles during infection, not only from the pathogen side, but also from the host side. To date, microarray analysis was limited in this respect, because separation of organism-specific RNA prior the hybridization is hard to achieve. Theoretically, RNA-seq analysis is capable of handling this problem. Technically, RNA from different species can be pooled, and then the data obtained can be separated during the analysis by aligning raw sequence data to different genomes. This approach seems possible because the sequences not matching a genome are normally discarded. The RNA-seq technique could potentially give us a way of monitoring gene expression profiles from the pathogen and the host simultaneously.

2.1.3. Proteome

To gain global insights into the biology of fungal pathogens and their interactions, genome-wide studies should focus not only on the transcript level, but also on the protein level. Proteins are the molecules that are catalytically active, build up the cellular structure, and mediate signal transduction and gene regulation. The release of the genome sequences of *C. albicans* and *A. fumigatus* paved the way for studies on the fungal proteome, i.e., the entire set of proteins which is synthesized and modified at a given time under defined conditions. Two dimensional-gel electrophoresis, a method invented in the mid-1970s, was the first technique used to study the presence of proteins on a global scale (O'Farrell, 1975; Klose and Kobalz, 1995). Meanwhile, mass spectrometry (MS)-based methods have become more and more popular. Here, the separation of tryptically digested peptides by liquid chromatography is coupled to mass spectrometry (reviewed in Aebersold and Mann, 2003). Despite the significant technical progress made in recent years in the field of MS-based proteomics, no technique currently available allows us to entirely profile the highly dynamic range and complexity of the protein set of a eukaryotic organism. However, a lot of knowledge about the proteome of *C. albicans* and *A. fumigatus* has already been obtained, which is summarized in several recent reviews (Rupp, 2004; Thomas et al., 2006; Kim et al., 2008; Kniemeyer and Brakhage, 2008; Andersen and Nielsen, 2009; Kniemeyer, 2011; Kniemeyer et al., 2011). Here, a brief overview will be given and current trends will be highlighted.

For *C. albicans*, the first studies on the extent of changes in cytoplasmic proteins during yeast-mycelial transition were conducted in the early 1980s, 25 years before the start of the post-genomic era in the field of fungal pathogenicity (Manning and Mitchell, 1980). More 2D-PAGE studies followed (Niimi et al., 1996), and differences in protein expression between the two morphotypes were also analyzed using MS-based techniques (Melanson et al., 2006). Several proteins that also play a role in the virulence of *C. albicans* were found to have increased expression levels in hyphal cells (reviewed in Kniemeyer and Brakhage, 2008). Recently, a study by Monteoliva et al. (2011) indicated that the primary metabolism undergoes a reorganization during morphotype-switching. Also, the composition of the *C. albicans* cell surface proteome undergoes changes during the yeast-mycelial transition. Several extraction techniques have been established in recent years to study this phenomenon (Pitarch et al., 2002; de Groot et al., 2004; Castillo et al., 2008; Hernáez et al., 2010). Heilmann et al. (2011) gave a first quantitative proteomic snapshot of the changes occurring in the cell wall proteome of *C. albicans* during the transition from yeast to hyphal cells. Several proteins were identified as indicators of hyphal growth, including the adhesin Als3p.

Due to the fact that *C. albicans* faces a multitude of diverse stresses, e.g., oxidative stress, higher temperatures, hypoxia, and low pH during infection, the proteomic response to these and other adverse conditions have been investigated by many groups. Kusch et al. (2007) and Yin et al. (2009) showed that the levels of many proteins with antioxidative functions were significantly increased during the oxidative stress response. Sosinska et al. (2008) and Sosinska et al. (2011) investigated the variability of the cell wall proteome during iron depletion, hypoxia, and at different pH values (pH 4 and 7).

Proteomics is also a suitable approach for gaining a deeper insight into the response of *C. albicans* toward antifungal compounds. Bruneau et al. (2003) characterized the proteome changes in *C. albicans* induced by triazoles (fluconazole and itraconazole) and an echinocandin-like lipopeptide (mulundocandin). The different modes of action of triazoles and echinocandins, two different classes of antifungal agents, were also reflected at the protein level. Similar results were obtained by Hoehamer et al. (2010), who additionally included the polyene amphotericin B in their study. Results of a recent study using a liquid chromatography–mass spectrometry (LC-MS) based approach suggested a cell wall destabilizing effect of the triazole fluconazole (Sorgo et al., 2011). Other studies addressed the mechanism of drug resistance by comparing the proteome of a drug-resistant mutant strain with a drug-susceptible wild-type strain (Hooshdaran et al., 2004; Yan et al., 2007).

A lot of progress has also been made in the field of *A. fumigatus* proteomics. In contrast to *C. albicans*, this pathogenic mold shows not only a mycelial growth form, but also produces spores for dispersal. Proteome maps of both morphotypes and the composition of the secretome have been established (Vödisch et al., 2009; Teutschbein et al., 2010; Cagas et al., 2011; Wartenberg et al., 2011). Also, the stress response to oxidative and heat stress was characterized (Lessing et al., 2007; Albrecht et al., 2010). Chaperones and antioxidative enzymes were produced under both conditions. Additionally, the results showed that the thioredoxin system seems to play an important role in maintaining the cellular redox balance for *A. fumigatus*. Recent findings revealed that *A. fumigatus* is exposed to oxygen-depleted microenvironments during infection (Grahl et al., 2011). The response to hypoxia was also studied at the protein level using an oxygen-controlled chemostat (Vödisch et al., 2011). Under hypoxic conditions, *A. fumigatus* cells developed a higher respiratory capacity, induced the synthesis of enzymes of the nitrosative stress response, and activated a secondary metabolite gene cluster (pseurotin A). Also, other growth conditions triggered the production of secondary metabolites with biological activity. When *A. fumigatus* attaches to surfaces, it can grow into a biofilm-like structure including the formation of an extracellular matrix. Under these conditions, higher levels of the immunosuppressive secondary metabolite gliotoxin were produced (Bruns et al., 2010).

Several groups profiled the *A. fumigatus* proteome in response to the antifungal compounds caspofungin (Cagas et al., 2011) and amphotericin B (Gautam et al., 2008). Amphotericin B influenced various metabolic processes including the ergosterol pathway, whereas caspofungin induced a strong increase in levels of ribosomal proteins.

The study of the interplay between fungal pathogens and human cells at the level of the proteome remains a challenging task due to the complexity and the limited number of methods available for the separation of fungal cells from the human effector cells. Several studies characterized the proteome of murine macrophages, which had been exposed to living or heat-inactivated *C. albicans* yeast cells (Shin et al., 2005; Martínez-Solano et al., 2006, 2009). To complement these studies, proteomic changes of *C. albicans* yeast cells due to macrophage confrontation were investigated and revealed an increase of the level of chaperones and

other stress-related proteins. No proteomic data is available on the interaction with other cells of the immune system or on the interaction of *A. fumigatus* with cells of the immune system. Nevertheless, proteomic technologies, such as targeted MS methods with high-performance instruments, have the potential to determine the mode of interaction between pathogenic fungi and their host. Targeted proteomic approaches are based on the selection of specific peptides of a protein for mass analysis. This process is termed *multiple reaction monitoring* (MRM). It allows the identification of very low-abundance proteins (Domon and Aebersold, 2010). However, this technique is still limited to the analysis of several hundred proteins in a single LC-MS/MS run, but technical progress in this field can be expected and may help to make a leap forward to the systematic investigation of host-pathogen interplay.

2.2. IMAGE-BASED DATA

Investigation and elucidation of the pathobiology of fungal infections strictly requires analysis of the interaction of the pathogen with the host immune effector cells (Brakhage et al., 2010). Image analysis is an indispensable tool for doing this. In combination with advances in computer performance and computing resources, the use of several imaging technologies led to the generation of large amounts of data (Behnsen et al., 2007; Hickey and Read, 2009; Brock, 2012) awaiting integration via a systems biological approach for analysis and interpretation. In general, image data can be obtained by different experimental approaches, e.g., microscopy, positron emission tomography (PET)/computer tomography (CT), or bioluminescence imaging. Due to the fact that the latter two techniques for monitoring fungal infections in living hosts are still in the early stages of development (Avet et al., 2009; Ibrahim-Granet et al., 2010), we focus here on recent studies using microscopy-generated image data. A good example of such data is represented by monitoring the interaction of labeled fungal cells, i.e., conidia, germlings, or hyphae, with immune effector cells using microscopy, especially fluorescence microscopy or confocal laser scanning microscopy (CLSM). Interaction of *A. fumigatus* and phagocytes based on fluorescence microscopy and manual image analysis was described, for example, by Ibrahim-Granet et al. (2003) and Jahn et al. (2002). In theses studies, interaction of *A. fumigatus* with phagocytes was monitored in detail, which revealed that *A. fumigatus* is able to inhibit acidification of phagolysosomes. More recently, Thywißen et al. (2011) were able to assign this ability to the presence of an active PksP, the polyketide synthase involved in dihydroxynaphthalene melanin biosynthesis. All of these studies were based on differentially labeled conidia, germlings, phagocytes, and their structures and compartments. It is even possible to monitor different pH values within distinct compartments of the phagocytes, allowing us to monitor phagocytosis rates in general and the fate of conidia after confrontation with immune cells in detail (Thywißen et al., 2011). In the future, a large number of mutants can be screened using this assay to identify further pathogen-derived components interfering with phagocytosis. Although phagocytosis of *A. fumigatus* by different phagocytes from both human and mouse has been analyzed in detail in several studies (Jahn et al., 2002; Ibrahim-Granet et al., 2003), only a limited amount of data is available with regard to direct observation of the phagocytosis process itself by live cell imaging. This applies to live cell imaging of phagocytosis of *Candida* species. Cell motility, however, is an essential requirement for the function of phagocytes. A detailed spatio-temporal analysis of the dynamics of the interaction of phagocytes with *A. fumigatus* and *C. albicans* using time-lapse microscopy and single-cell tracking was performed by Behnsen et al. (2007). In this study, the natural environments of different phagocytes were simulated by 2D liquid cultures and by generation of a 3D collagen environment. Live imaging showed that the interaction of phagocytes with *A. fumigatus* conidia or *C. albicans* cells in both 2D and 3D environments is a highly dynamic process that includes touching, dragging, and phagocytosis of fungal structures. Interestingly, the different immune cells, i.e., neutrophils, macrophages, and dendritic cells, exhibited different behavior with regard to the dependence on environmental dimensionality and as well as to the processing of *A. fumigatus* and *C. albicans*. Whereas neutrophils and alveolar macrophages efficiently phagocytosed or dragged *A. fumigatus* conidia in a 2D environment, their function was severely impaired in a 3D matrix. The opposite was found for processing of *C. albicans* cells. Phagocytosis was reduced in 2D environments, while in 3D environments most neutrophils internalized multiple yeast cells. These differences were also found in competitive assays, when both *C. albicans* and *A. fumigatus* were confronted with immune cells in the respective environment. Despite frequent touching of the other pathogen, neutrophils primarily incorporated *A. fumigatus* conidia in 2D and *C. albicans* yeast cells in a 3D environment. It is therefore conceivable that the activity and efficacy of the different phagocytes is best in the environment where a pathogen is naturally encountered.

Analysis of image data with regard to host-pathogen interaction was performed almost exclusively manually, with all of the inherent drawbacks and disadvantages. Manual data analysis is very time-consuming, error-prone, and last but not least, dependent on subjective criteria of the person performing the analysis. A first approach to automatize image analysis was performed by Mech et al. (2011). As a proof of principle, the interaction of *A. fumigatus* conidia with macrophages was monitored (see **Figure 1**). Data was collected by CLSM using cells labeled with different fluorescent dyes. The ruleset developed for processing microscopic raw data allows fully automated and context-based analysis of image data. By applying this method, discrimination between different cell types, i.e., phagocytes and conidia, was facilitated. Furthermore, cell counting based on discrimination between phagocytosed, adherent and non-adherent exterior conidia was performed. This is of particular importance since the different steps in conidia-macrophage interaction, i.e., recognition, adherence, ingestion, and intracellular processing of inhaled spores, define important pathogenesis-related processes. A prerequisite for automated image analysis, e.g., to determine phagocytosis rates, is the digitization of images. However, due to the fact that phagocytosis of *A. fumigatus* conidia by macrophages is a complex process, current image analysis tools that require precisely defined and homogeneous objects (overview in Shamir et al., 2010; Sysko and Davis, 2010) cannot be applied here. During co-incubation, conidia and macrophages tend to attach and form clusters. In addition to this, the relevant structures vary in their intensities as a result of different labeling efficacies and, last but not least,

the background differs considerably. These parameters were taken into consideration by the ruleset developed by Mech et al. (2011) and thereby allowed fully automated and context-based analysis of spatially resolved biological data, i.e., phagocytosis rates of *A. fumigatus* conidia. As this ruleset can be easily transferred to high-throughput microscopy measurements of other pathogens, e.g., *Candida* sp. or *Cryptococcus neoformans*, it will contribute to the further elucidation of host-pathogen interactions.

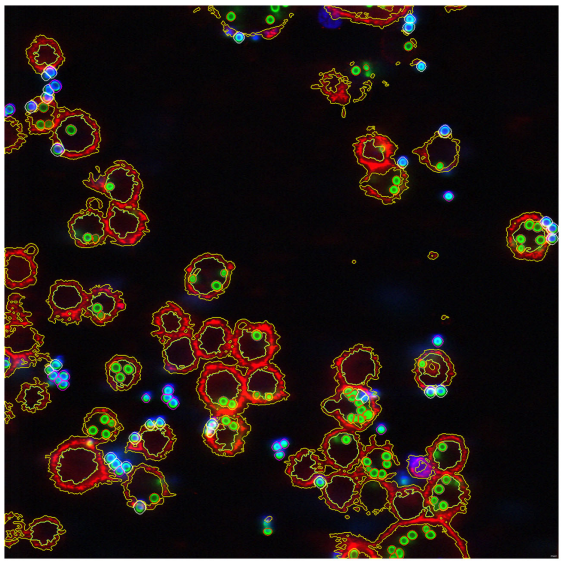

FIGURE 1 | Image of the phagocytosis assay showing all conidia and macrophages after segmentation and classification. Exterior non-adherent conidia outlined in magenta, adherent conidia outlined in white, interior conidia outlined in orange, and macrophages outlined in yellow. (Taken from Mech et al., 2011.)

3. MODELING

The identification of pathogenic traits will increasingly be supported by mathematical and computational modeling and by the integration of experimental data and prior knowledge into complex models that describe the underlying virulence mechanisms. The generation of models and their subsequent application aim to support the optimal and standardized design of experiments and to generate and validate hypotheses. This allows that new knowledge is gained and predictions for novel strategies for diagnostics (biomarker design) and therapy (drug discovery, drug administration, therapy decision support) are made.

Systems biology of fungal infections describes and analyses various aspects of the confrontation of the host and its pathogen under defined conditions. The interactions and co-evolution of host and pathogen can be described with the help of evolutionary models (May and Anderson, 1979). Currently, molecular modeling of the host-pathogen interaction generally takes a reductionistic approach.

In general, models either describe a biological perspective on a single scale, or they span several different orders of magnitude (see **Figure 2**). Molecular mechanisms of host-pathogen interaction were identified with the help of statistical and integrated analysis of experimental data (see section 2). Single interactions represent only a reduced level of complexity, and a combination of several different mechanisms is capable of reflecting the global behavior at a cellular level. Such multi-systems interactions will become more complex when several species are considered. More recent approaches incorporate different biological levels to

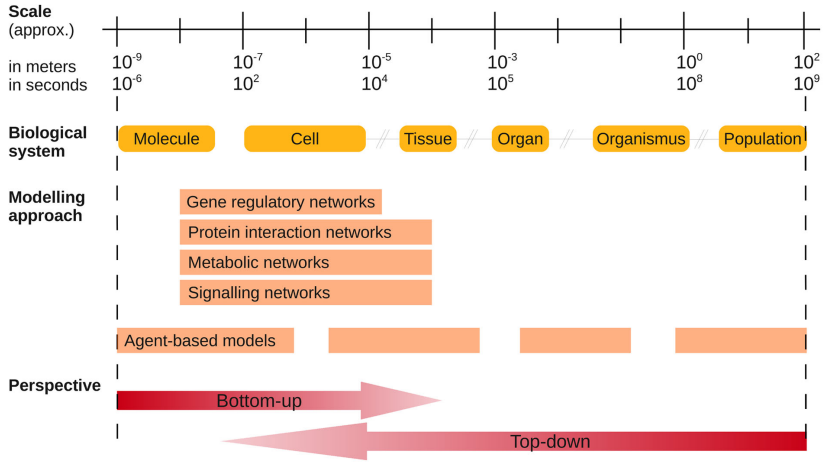

FIGURE 2 | Schematic diagram of different biological and modeling levels of systems biology of infectious diseases. Biological systems span several orders of magnitude. Mathematical methods, which are presented in this paper, focus on different biological levels of a fungal or similar infection. Modeling approaches can be applied to host and pathogen systems and their interplay. The flexibility and adaptability of agent-based modeling allows analysis at multiple levels without any restrictions with respect to the biological system. In order to generate new hypotheses, the advantages of bottom-up and top-down models are usually incorporated into the analysis. (Figure adapted from Forst, 2006.)

get an interrelated view of fungal infections. These multi-scale approaches need to integrate data from experiments on two or more scales (Walker and Southgate, 2009). The greatest challenge arises from the fact that an effective computational framework has to deal with the complexity of different length and time scales spanning several orders of magnitude. This leads to quantifiable differences of crucial constituents (e.g., one cell and its sizeable number of molecules) and to newly considered events (e.g., movement of the cell and the corresponding events at the molecular scale).

To date, only a few models of fungal infections of humans have been studied, which is mainly due to the complex modeling challenges and the previous lack of measurements of model parameters. In perspective, the host-pathogen interaction should be described by a combination of spatio-temporal models with interacting molecular network models.

3.1. NETWORK MODELING

Nodes in networks stand for interacting molecular entities (e.g., genes, proteins, metabolites) whose concentration or activity can be quantified by discrete or continuous variables. Edges, which stand for the relationships between the nodes, can be modeled in different ways, e.g., by directed or undirected edges and labeled by linear or non-linear functionality (Hecker et al., 2009). The cellular behavior of a system is usually represented by gene-regulatory networks, signaling networks, protein-protein interaction networks (PPI), and metabolic networks (see **Figure 3**). In addition to this, a confrontation between pathogen and host can be viewed as two interacting molecular networks, for example one within the host epithelial or immune cells and the other in the colonizing, persisting, or invading pathogens. Network models are capable of reflecting the non-linear dynamic behavior of the systems. Despite the fact that network visualization and handling is not scalable, its representation is intuitive and, as an example, there are ongoing projects which aim to standardize the graphical representation (BioPax, PSI-MI, SBGN, Hermjakob et al., 2004; Strömbäck and Lambrix, 2005; Le Novère et al., 2009). Basic networks only model the coordinated behavior of biological entities, and experimental data can be mapped to the network in order to confirm and annotate experimental results. The integration of general and specific knowledge transforms those "influence networks" into "mechanistic networks" of higher quality (Hecker et al., 2009; Santamaría et al., 2011) which themselves already represent a molecular interaction model that can be tested with the help of perturbation experiments. The dynamic nature of a system is partly reflected in the network topology. The investigation of the interactivity, the distribution and regulation of hubs, network motifs, and cross-talk of functional modules and reaction sets (e.g., coupled reaction sets and elementary flux patterns in metabolic networks) contribute to our understanding of the robustness and flexibility of a system (Barabási and Oltvai, 2004).

The major challenge of a systems biology-based approach to understanding the host-pathogen interaction arises from the robustness of the pathogenic system. The robustness originates from the network structure of the biological system that makes it unlikely that it will be possible to develop a single biomarker or drug against fungal infection. In the interests of clinical success, a system-oriented drug design with multiple antifungal strategies needs to affect sufficient points in the infection process (Kitano, 2007).

3.1.1. *Gene-regulatory networks*

Gene expression is mainly regulated by transcription factors and co-factors and additionally by post-transcriptional modification as well as mRNA and protein degradation. The reverse engineering of genome-wide interdependencies between these molecular entities relies on comprehensive datasets. Since there are only a few datasets on infectious processes available, one of the major tasks is to collect and process data and prior knowledge required for the development of novel parsimonious network models, describing essential fungus-host interactions. The inference process is mathematically challenging because the search space (number of possible gene regulations) increases exponentially with the number of nodes (genes). The modeling, on the other hand, relies on a small amount of data, which is usually obtained from microarray time series experiments. The experimental design is a trade-off that minimizes the cost and effort of the experiment, while ensuring that the data reliably reflects the underlying processes of the perturbation experiment. Many different network model architectures and inference methods have been proposed (reviewed in Hecker et al., 2009; Marbach et al., 2010). As part of the DREAM5-initiative[1] (Dialog for Reverse Engineering Assessments and Methods), gene expression data of the bacterial pathogen *Staphylococcus aureus* was presented to infer large-scale gene-regulatory networks. The inferred networks have been used to create a predictive community network of 1054 genes and 1688 edges, which need to be validated experimentally (Stolovitzky,

[1] http://wiki.c2b2.columbia.edu/dream/

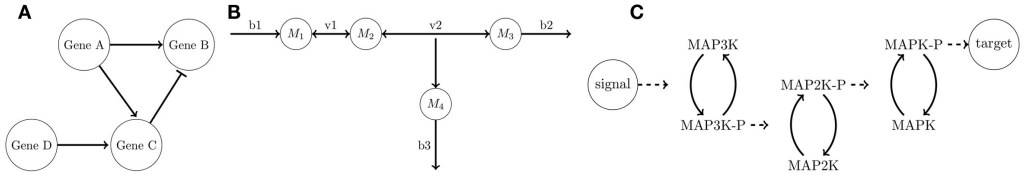

FIGURE 3 | Graphical representation of (A) gene-regulatory network, (B) metabolic network, and (C) signaling network. (A) The activation of genes is shown by arrows whereas repression is marked by bars. **(B)** Metabolites (M_i) are connected with internal (v_i) or external (b_i) metabolic fluxes. **(C)** A signal can lead to a phosphorylation ("-P") cascade of MAP kinases, and eventually the target is activated or repressed.

2011). The infection process of the fungi *C. albicans* and *A. fumigatus* were modeled using tools such as NetGenerator (Guthke et al., 2005; Toepfer et al., 2007), which are based on ordinary differential equation systems and linear regression methods that are capable of describing the dynamic behavior of systems, even on a global scale (Altwasser et al., 2012). The high dimensionality of the mathematical problem can be reduced at several stages in the network reconstruction process (Hecker et al., 2009). For example, Guthke et al. (2007) reconstructed the underlying gene-regulatory events when *A. fumigatus* was exposed to a temperature shift. In order to select features for the network modeling, expression profiles with similar significantly regulated time courses were clustered to functional entities. Cluster representatives, indicating main biological functions, were assigned to these entities using gene annotation (Priebe et al., 2011).

The dimensionality of the problem can be further reduced when known global characteristics of a gene-regulatory network are taken into account. The observed high modularity, hierarchical structure, and over-representation of network motifs can guide the optimization of the structure of the model. A widely used criterion is the network sparseness, meaning that each gene is regulated only by a small number of regulatory genes. This feature of gene networks was incorporated in studies by Linde et al. (2010, 2012), who analyzed transcriptomic data focused on the iron homeostasis of *C. albicans* during infection and of *A. fumigatus* after a change in available iron concentration. The authors also used prior knowledge in order to reduce the search space. Interactions between genes and transcription factors found in literature were used to build a network template, and this prior knowledge was integrated into the network reconstruction procedures with the help of a weighting function. Currently, prior knowledge about fungi is scarcely available in databases and needs to be extracted from literature or genome sequences, e.g., by predicting transcription factor binding sites (Fazius et al., 2011). The prior knowledge also forms the basis for the analysis of the validity of the inferred network and the performance of the applied reconstruction method.

Recently, the inference of gene-regulatory network was applied to predict host-pathogen interactions (Tierney et al., 2012). RNA-seq data from a *C. albicans* infection of *Mus musculus* were used to predict subnetworks which were subsequently combined into an interspecies network. This model contained predicted regulations between the two species during the infection process. The results were supported by experimental findings which, overall, demonstrated that network inference can be used to support the deciphering of complex infectious processes.

3.1.2. Protein-protein interaction network

The biological function of genes originates from encoded proteins which form molecular structures, catalyze metabolic reactions, and are involved in signaling and regulation. With the help of technologies such as yeast two-hybrid or tandem affinity purification combined with mass spectrometry, it is possible to identify interacting protein partners which form an "interactome" network. The interactome shifts the focus from the detection of single protein interactions to the decoding of the global organization of proteomes (Barabási and Oltvai, 2004). Protein networks are increasingly used to identify host immune molecules and pathogenic effector proteins associated with host infection and drug targets (reviewed in Ideker and Sharan, 2008). For fungal infections, the main challenge is the lack of experimental protein interaction data, which is required to (semi)automatically construct such a network. The bioinformatic approaches either rely on text-mining (Zhou and He, 2008; Rao et al., 2010), or the interaction is predicted on the basis of sequence analyses (Dyer et al., 2007; Skrabanek et al., 2008). For the modeling of infectious diseases, Dyer et al. (2008) mapped all available host-pathogen protein interactions to a single protein network. Many pathogens were found to target the same process and therefore supported the hypothesis that topological properties of the protein-protein interaction network can be used to identify pathogenetic traits (Mukhtar et al., 2011) and drug targets (Hase et al., 2009; Zhu et al., 2009). In addition to this, the functional annotation of single gene products is supported by the interaction context of proteins within the global protein-protein interaction network (Xu and Li, 2006; Sharan et al., 2007).

3.1.3. Signaling Networks

The cell's response to an internal and external stimulus is triggered by a signaling network whose regulation is the key control for cellular behavior. The understanding and modeling of this network holds great promise for the development of new therapeutic strategies and, consequently, many different modeling techniques have been developed (reviewed in Aldridge et al., 2006). The elements of the signal transduction networks help to identify the effect of positive or negative feedback loops (Blüthgen et al., 2009) and also shed light on the cross-talk between different signaling pathways (Borisov et al., 2009).

Successful application of signaling models depends on careful validation of the underlying data, especially since molecular signals are hard to measure experimentally. This is one reason why many applications in this research area concentrate on the perspective of the human host where, for example, the JAK/Stat pathway (Vera et al., 2011) and macrophage activation (Raza et al., 2008) have been modeled. Currently, the yeast *Saccharomyces cerevisiae* is a model organism for the analysis of fungal signaling networks (Waltermann and Klipp, 2010). The modeling of fungal pathogen signaling is still in its early stages. Efforts are being made to reconstruct the underlying signaling network, e.g., for *C. albicans*, with the help of sequence analysis and molecular biological experiments (Rispail et al., 2009). Additionally, the effects of host-pathogen interaction on the signaling pathways of the host are the subject of several studies (reviewed in Brodsky and Medzhitov, 2009; Hajishengallis and Lambris, 2011). For example, Franke et al. (2008) modeled the c-Met signaling network of hepatocytes after infection with the pathogenic bacterium *Helicobacter pylori* and predicted the effects of gene knock-outs, which were subsequently confirmed experimentally.

3.1.4. Metabolic networks

Supported by the increasing number of sequenced fungal genomes, the modeling of host-pathogen interactions with the help of genome-scale metabolic networks is feasible. The functionality of thousands of genes can be associated with a set of metabolic

reactions, because they either encode enzymes or they regulate related reactions (Cavalieri and Filippo, 2005). The steady state of metabolic fluxes through a metabolic network structure can be understood as a phenotypic state of an organism. For example, the metabolic capacity of the pathogen needs to be able to produce a variety of secretory metabolites and proteins which correspond to the pathogenic traits of the species and which are interesting drug targets (Fang et al., 2009). On the other hand, fungi also rely on the uptake of essential minerals which are bound to storage proteins in the host, e.g., iron bound to hemoglobin or ferritin during *C. albicans* infection (Almeida et al., 2009). The intertwined nature of the host-pathogen interaction can thus be modeled by two interacting metabolic networks (Raghunathan et al., 2009).

Despite the increasing number of sequencing projects for pathogenic fungi (see **Table 2**), the number of reconstructed networks is limited to species which are in the focus of metabolic engineering. To the best of our knowledge, only two large-scale, manually curated metabolic network reconstructions of fungal pathogens exist, namely for *A. fumigatus* (Tuckwell et al., 2011) and *C. albicans*[2]. Despite the recent efforts made at automation, a high quality network reconstruction process needs manual curation, a step which acts as the bottleneck in this modeling technique (Pitkänen et al., 2010). During the curation of specific metabolic pathways, genes that encode missing enzymes are annotated with the help of bioinformatic tools or experimental validation (Pitkänen et al., 2010). The reconstruction process itself thus already contributes to the elucidation of the underlying molecular processes.

The mathematical modeling and simulation of metabolic networks allow us to address questions such as (i) the influence of single enzymes (and corresponding genes) within the network, (ii) the search for invariant steady states, (iii) the prediction of elementary flux modes, and even (iv) the consideration of different optimization strategies for the organism (Ruppin et al., 2010). With these objectives in mind, specific methods and concepts of metabolic modeling, which do not rely on mostly unknown specific kinetic parameters, can be applied to fungi.

Nevertheless, it is promising to compare metabolic networks of closely related pathogenic and non-pathogenic species in order to understand the physical features of pathogenicity (Lee et al., 2009). Recently, Oberhardt et al. (2011) examined differences and similarities between a pathogenic and non-pathogenic *Pseudomonas* species. Prior to analysis, the authors reconciled both metabolic networks in order to minimize the influence of different reconstruction approaches on the results. The subsequent analysis confirmed the multifactorial aspect of pathogenicity, but differences in the flexibility of sulfur related pathways were also found.

3.2. SPATIO-TEMPORAL MODELING

In contrast to the network models discussed in section 3.1, which are based on "omics"-data that does not contain any spatial information, spatio-temporal models are developed to include this type of information. For example, modeling the affinity maturation of antibodies in germinal centers in response to the recognition of antigens has been successfully performed in recent years in joint experimental and theoretical studies (Figge, 2005; Figge et al., 2008; Garin et al., 2010). Similarly, this modeling approach can be applied to the field of fungal infections to model the innate immune response (see **Figure 4**). With the application of special imaging techniques to generate spatially and spatio-temporally resolved data and their automated analysis (see section 2.2), the way has been paved to model, simulate, and study interactions between the host and pathogenic fungi from this point of view.

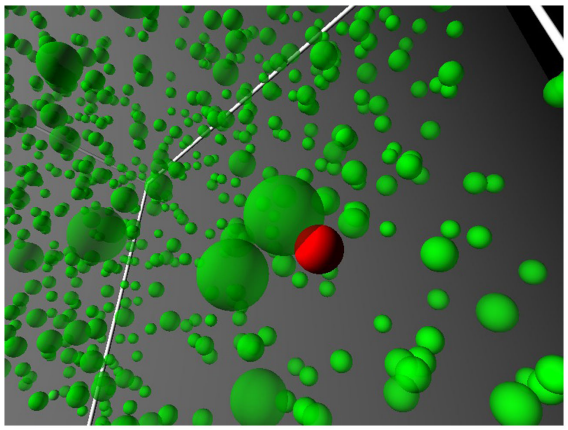

FIGURE 4 | Schematic illustration of a continuous 3D spatial environment *in silico* within an agent-based model. Spherical objects represent cells, the different colors depict different cell types.

Two common approaches to model spatio-temporally resolved systems are *partial differential equations* (PDEs) and *agent-based models* (ABMs). The former treats systemic constituents (e.g., molecules or cells) as concentrations (or populations), whereas the latter deals with them as discrete objects. When it comes to the number of constituents and their quantities, scalability is one of the computational strengths of PDEs. Apart from this advantage, crucial limitations such as the identification of single objects, their specific local interactions and their particular internal states exist (Van Dyke Parunak et al., 1998). ABMs can cope with all of the constraints mentioned above, but come at the price of more expensive computer resources in terms of computer memory and computing time (Chavali et al., 2008).

Each modeling approach has its own right to exist. ABM systems proved to have the necessary properties when higher levels of granularity for single constituents are considered. PDEs are adequate when the general behavior, such as Brownian motion, for a whole population of constituents is considered (Guo and Tay, 2005). Another criterion for making the right choice is the amount of data and knowledge available for the scale under consideration. Cells can be differentiated in various states. They may either move in a straight line or show random migration behavior and interact individually, depending on the interaction partners involved. These characteristics favor the choice of an ABM. However, modeling molecules at the level of individual molecules also has several advantages. Nevertheless, describing innate immune responses against fungal infections at all levels within ABMs renders the

[2]http://www.candidagenome.org and commercially available at Insilico Biotechnology AG and ERGO

multi-scale system intractable because of the overwhelmingly large number of cells and molecules. A promising approach toward modeling multi-scale systems was proposed by Guo et al. (2008), where, within a hybrid model, cells are described in continuous space as individual agents by an ABM approach, while molecular interaction is described by PDEs via reaction-diffusion equations for molecular populations. Such a hybrid multi-scale approach has the potential to model fungal infections since it is adaptable and extensible, thus providing the required flexibility.

At the beginning of the modeling process of this multi-scale system, one major issue is the definition of the necessary features of cells at the cellular scale. Examples of macroscopic characteristics are the cellular migration type as well as their morphology and interaction with other cells. A major source of these essential parameters are images and time-lapse videos, which are recorded during microscopy experiments. With the analysis of single frames, cellular sizes, morphological properties, and population quantities can be computationally extracted in an automated fashion (see **Figure 1**). An automated analysis of the interaction between macrophages and *A. fumigatus* was recently presented by Mech et al. (2011). Furthermore, the analysis of cell tracks extracted from videos plays an important role in the calculation of characteristic properties of the cellular movement such as speed, motility coefficient, and diffusion constant. The intercellular interactions can be defined at both the cellular and molecular scale. The initial setup of the interaction model can be arranged by implementing simple interaction rules of cellular behavior based on phenomenological knowledge. An extension toward a complex rule-system is also conceivable as well as the implementation of specific strategic behavior of the pathogenic fungi, as recently unraveled by Hummert et al. (2010), by applying methods of game theory. It would also be conceivable to include cell-cell interactions by considering interacting molecules at the cellular surface and their subsequent impact on internal and external signaling. These processes, taking place at the molecular level, require the data basis that underlies the network models (see section 3.1) and can be integrated together with the microscopy data basis into one and the same multi-scale model.

In addition to the integration of data, there are also other challenging tasks, such as the estimation of unknown parameters and the establishment of efficient algorithms and adequate data structures, in order to make simulations computational feasible. The former issue is strongly related to the generation of hypotheses. The efficiency of the applied algorithms needs to be verified experimentally in further studies. We are still at the beginning of the systems biology cycle regarding the spatio-temporal modeling of fungal infections, but the first promising steps have successfully been made.

4. OUTLOOK

Although great advances have been made in the understanding of molecular and cellular mechanisms of fungal infections, they do not currently provide a genome-wide view on the pathogenic processes of both fungal pathogens and hosts. New technologies such as RNA-seq, single-cell measurements, and PET/CT imaging open up new opportunities to unravel molecular and cellular mechanisms in greater detail and complexity. However, integrative analysis of high-throughput and spatio-temporal data on several molecular and cellular levels is increasingly becoming the limiting step when identifying molecular key regulators and mechanisms involved in fungal pathogenicity. Efforts to standardize data management and annotation promise advances for computational approaches to the mathematical modeling of host-pathogen interactions. Bioinformatic tools also need to be further adapted to the specific biological context of fungi. The current focus of systems biology is on the application of network and agent-based modeling techniques to genome-wide and spatio-temporally resolved dynamic systems thus exploiting the full range of high-throughput and image data available. In order to fully facilitate existing computational methods, it is necessary to deepen our understanding of molecular mechanisms thus improving gene annotation and establishing wider knowledge bases.

Genomic knowledge, coupled with high-throughput gene knock-out methodologies, are already advancing. The availability of mutant strains has grown rapidly over the last 10 years (McCluskey et al., 2010). We now have the possibility to screen more than 3,000 *C. albicans* single deletion mutants, but we still lack complete *A. fumigatus* or *C. albicans* knock-out libraries. At present, many high-throughput investigations are performed using complete gene knock-out libraries from *S. cerevisiae* or *Neurospora crassa*. This approach can be exploited to discover wide spectra of antimycotic drugs, but is not helpful for virulence studies. However, complete sets of viable genome-wide mutants for many pathogenic fungi are expected to become available in the next few years. In parallel, many efforts are being made to create high-throughput screening infection model systems. Recently, alternative systems using insects, nematodes, or embryonated eggs have been used (Ferrandon et al., 2007; Mylonakis, 2008; Moy et al., 2009; Jacobsen et al., 2010).

In the meantime, the scientific community continues to investigate the role of innate immunity during fungal infections. It has yet to be explored how neutrophil granulocytes actually kill outgrowing hyphae of *A. fumigatus*. The cellular mechanisms can be explored with the help of images which are a promising data source for driving the systems biology cycle. *Image-based Systems Biology* focuses on spatial properties such as cellular morphology or the mechanical features of interactions, and allows further insights which contribute to a better understanding of biological systems.

In clinical practice, differential diagnosis of infectious diseases and sepsis is based primarily on clinical criteria. These criteria lack the required sensitivity and specificity (Alberti et al., 2003) making the identification of novel biomarkers essential to identify the pathogen causing the infection on time. In clinical decision-making, fast and reliable diagnosis of specific pathogens is required. Theranostics (Chen, 2011) is a novel concept of combining novel platforms and technologies in clinical diagnostics and therapy such as image-guided therapy by, e.g., PET (Walther et al., 2011) or Raman spectroscopy (Neugebauer et al., 2006). There is currently a great deal of effort being made to push commercialization and collaboration strategies to establish the so-called companion diagnostics (CDx) marketplace. So-called *Translational Systems Biology* describes the clinical application of mathematical or computational models by enhancing the understanding of the complex dynamics of biomedical processes in an integrative, genome-wide way (Vodovotz et al., 2008). It integrates the scientific background of these trends and is based on current

experimental findings. Apart from integrating different "omics" data levels, models should not exclusively focus on the host's and the pathogen's aspects of the infection process, but also on the interaction between both biological systems. This interconnected perspective supports the elucidation of mechanisms underlying the complex process of fungal pathogenicity. Translational Systems Biology is primarily directed at drug target identification and validation as well as rational drug design, supported by analysis of the inferred molecular network models (Klipp et al., 2010). Furthermore, Translational Systems Biology of infection aims (i) to recognize pathogens by their molecular signatures, (ii) to make the outcome and responsiveness of therapeutic interventions more predictable, and (iii) to identify more effective therapies using mathematical and computational models. The first steps in Translational Systems Biology were taken in the area of sepsis control (Vodovotz et al., 2008) and tuberculosis research (Day et al., 2010). Translational Systems Biology of fungal infections with applications in personalized medicine (Willard and Ginsburg, 2009) can be expected to be developed in the near future.

ACKNOWLEDGMENTS

Part of this work was supported by the excellence graduate school Jena School for Microbial Communication (JSMC), funded by the Deutsche Forschungsgemeinschaft, as part o fit, by the International Leibniz Research School for Microbial and Biomolecular Interactions (ILRS Jena) and by a grant from the Federal Ministry of Education and Research (BMBF) in the frame of ERA-NetPathoGenoMics.

REFERENCES

Aebersold, R., and Mann, M. (2003). Mass spectrometry-based proteomics. *Nature* 422, 198–207.

Aimanianda, V., Bayry, J., Bozza, S., Kniemeyer, O., Perruccio, K., Elluru, S. R., Clavaud, C., Paris, S., Brakhage, A. A., Kaveri, S. V., Romani, L., and Latgé, J.-P. (2009). Surface hydrophobin prevents immune recognition of airborne fungal spores. *Nature* 460, 1117–1121.

Alberti, C., Brun-Buisson, C., Goodman, S. V., Guidici, D., Granton, J., Moreno, R., Smithies, M., Thomas, O., Artigas, A., Gall, J. R. L., and Group, E. S. (2003). Influence of systemic inflammatory response syndrome and sepsis on outcome of critically ill infected patients. *Am. J. Respir. Crit. Care Med.* 168, 77–84.

Albrecht, D., Guthke, R., Brakhage, A. A., and Kniemeyer, O. (2010). Integrative analysis of the heat shock response in *Aspergillus fumigatus*. *BMC Genomics* 11, 32. doi:10.1186/1471-2164-11-32

Albrecht, D., Guthke, R., Kniemeyer, O., and Brakhage, A. A. (2008). "Systems biology of human-pathogenic fungi," in *Handbook of Research on Systems Biology Applications in Medicine*, Vol. 1, ed. A. Daskalaki (Hershey: IGI Global), 400–418.

Albrecht, D., Kniemeyer, O., Brakhage, A. A., Berth, M., and Guthke, R. (2007). Integration of transcriptome and proteome data from human-pathogenic fungi by using a data warehouse. *J. Integr. Bioinform.* 4, 52.

Albrecht, D., Kniemeyer, O., Mech, F., Gunzer, M., Brakhage, A. A., and Guthke, R. (2011). On the way toward systems biology of *Aspergillus fumigatus* infection. *Int. J. Med. Microbiol.* 301, 453–459.

Alby, K., Schaefer, D., and Bennett, R. J. (2009). Homothallic and heterothallic mating in the opportunistic pathogen *Candida albicans*. *Nature* 460, 890–893.

Aldridge, B. B., Burke, J. M., Lauffenburger, D. A., and Sorger, P. K. (2006). Physicochemical modelling of cell signalling pathways. *Nat. Cell Biol.* 8, 1195–1203.

Almeida, R. S., Wilson, D., and Hube, B. (2009). *Candida albicans* iron acquisition within the host. *FEMS Yeast Res.* 9, 1000–1012.

Altwasser, R., Linde, J., Buyko, E., Hahn, U., and Guthke, R. (2012). Genome-wide scale-free network inference for *Candida albicans*. *Front. Microbiol.* 3:51. doi:10.3389/fmicb.2012.00051

Andersen, M. R., and Nielsen, J. (2009). Current status of systems biology in aspergilli. *Fungal Genet. Biol.* 46(Suppl. 1), S180–S190.

Arnaud, M. B., Cerqueira, G. C., Inglis, D. O., Skrzypek, M. S., Binkley, J., Chibucos, M. C., Crabtree, J., Howarth, C., Orvis, J., Shah, P., Wymore, F., Binkley, G., Miyasato, S. R., Simison, M., Sherlock, G., and Wortman, J. R. (2012). The Aspergillus Genome Database (AspGD): recent developments in comprehensive multispecies curation, comparative genomics and community resources. *Nucleic Acids Res.* 40, D653–D659.

Arnaud, M. B., Costanzo, M. C., Shah, P., Skrzypek, M. S., and Sherlock, G. (2009). Gene ontology and the annotation of pathogen genomes: the case of *Candida albicans*. *Trends Microbiol.* 17, 295–303.

Arnaud, M. B., Costanzo, M. C., Skrzypek, M. S., Shah, P., Binkley, G., Lane, C., Miyasato, S. R., and Sherlock, G. (2007). Sequence resources at the Candida Genome Database. *Nucleic Acids Res.* 35, D452–D456. [Database issue].

Avet, J., Granjon, D., Prevot-Bitot, N., Isnardi, V., Berger, C., Stephan, J. L., and Dubois, F. (2009). Monitoring of systemic candidiasis by 18F-FDG PET/CT. *Eur. J. Nucl. Med. Mol. Imaging* 36, 1900.

Backer, M. D. D., Ilyina, T., Ma, X. J., Vandoninck, S., Luyten, W. H., and Bossche, H. V. (2001). Genomic profiling of the response of *Candida albicans* to itraconazole treatment using a DNA microarray. *Antimicrob. Agents Chemother.* 45, 1660–1670.

Bailey, N. J. T. (1975). *The Mathematical Theory of Infectious Diseases and its Application*. London: Griffin.

Barabási, A.-L., and Oltvai, Z. N. (2004). Network biology: understanding the cell's functional organization. *Nat. Rev. Genet.* 5, 101–113.

Barker, K. S., Crisp, S., Wiederhold, N., Lewis, R. E., Bareither, B., Eckstein, J., Barbuch, R., Bard, M., and Rogers, P. D. (2004). Genome-wide expression profiling reveals genes associated with amphotericin B and fluconazole resistance in experimentally induced antifungal resistant isolates of *Candida albicans*. *J. Antimicrob. Chemother.* 54, 376–385.

Barrett, L. G., Thrall, P. H., Burdon, J. J., and Linde, C. C. (2008). Life history determines genetic structure and evolutionary potential of host-parasite interactions. *Trends Ecol. Evol. (Amst.)* 23, 678–685.

Behnsen, J., Hartmann, A., Schmaler, J., Gehrke, A., Brakhage, A. A., and Zipfel, P. F. (2008). The opportunistic human pathogenic fungus *Aspergillus fumigatus* evades the host complement system. *Infect. Immun.* 76, 820–827.

Behnsen, J., Lessing, F., Schindler, S., Wartenberg, D., Jacobsen, I. D., Thoen, M., Zipfel, P. F., and Brakhage, A. A. (2010). Secreted *Aspergillus fumigatus* protease Alp1 degrades human complement proteins C3, C4, and C5. *Infect. Immun.* 78, 3585–3594.

Behnsen, J., Narang, P., Hasenberg, M., Gunzer, F., Bilitewski, U., Klippel, N., Rohde, M., Brock, M., Brakhage, A. A., and Gunzer, M. (2007). Environmental dimensionality controls the interaction of phagocytes with the pathogenic fungi *Aspergillus fumigatus* and *Candida albicans*. *PLoS Pathog.* 3, e13. doi:10.1371/journal.ppat.0030013

Bernoulli, D. (1760). Essai d'une nouvelle analyse de la mortalité causée par la petite vérole et des avantages de l'inoculation pour la prévenir. *Mémoires de Mathématiques et de Physique Paris Académie Royale des Sciences* 1, 1–45.

Blüthgen, N., Legewie, S., Kielbasa, S. M., Schramme, A., Tchernitsa, O., Keil, J., Solf, A., Vingron, M., Schäfer, R., Herzel, H., and Sers, C. (2009). A systems biological approach suggests that transcriptional feedback regulation by dual-specificity phosphatase 6 shapes extracellular signal-related kinase activity in RAS-transformed fibroblasts. *FEBS J.* 276, 1024–1035.

Borisov, N., Aksamitiene, E., Kiyatkin, A., Legewie, S., Berkhout, J., Maiwald, T., Kaimachnikov, N. P., Timmer, J., Hoek, J. B., and Kholodenko, B. N. (2009). Systems-level interactions between insulin-EGF networks amplify mitogenic signaling. *Mol. Syst. Biol.* 5, 256.

Brakhage, A. A. (2005). Systemic fungal infections caused by *Aspergillus* species: epidemiology, infection process and virulence determinants. *Curr. Drug Targets* 6, 875–886.

Brakhage, A. A., Bruns, S., Thywissen, A., Zipfel, P. F., and Behnsen, J. (2010). Interaction of phagocytes with filamentous fungi. *Curr. Opin. Microbiol.* 13, 409–415.

Braun, B. R., van Het Hoog, M., d'Enfert, C., Martchenko, M., Dungan, J., Kuo, A., Inglis, D. O., Uhl, M. A., Hogues, H., Berriman, M., Lorenz, M., Levitin, A., Oberholzer, U., Bachewich, C., Harcus, D., Marcil, A., Dignard, D., Iouk, T., Zito, R., Frangeul, L., Tekaia, F., Rutherford, K., Wang, E., Munro, C. A., Bates, S., Gow, N. A., Hoyer, L. L., Köhler, G., Morschhäuser, J., Newport, G., Znaidi, S., Raymond, M., Turcotte, B., Sherlock, G., Costanzo, M., Ihmels, J., Berman, J., Sanglard, D., Agabian, N., Mitchell, A. P., Johnson, A. D., Whiteway, M., and Nantel, A. (2005). A human-curated annotation of the *Candida albicans* genome. *PLoS Genet.* 1, 36–57.

Brock, M. (2012). Application of bioluminescence imaging for in vivo monitoring of fungal infections. *Int. J. Microbiol.* 2012, 956794.

Brodsky, I. E., and Medzhitov, R. (2009). Targeting of immune signalling networks by bacterial pathogens. *Nat. Cell Biol.* 11, 521–526.

Brown, A. J. P., Odds, F. C., and Gow, N. A. R. (2007). Infection-related gene expression in *Candida albicans*. *Curr. Opin. Microbiol.* 10, 307–313.

Bruneau, J. -M., Maillet, I., Tagat, E., Legrand, R., Supatto, F., Fudali, C., Caer, J.-P. L., Labas, V., Lecaque, D., and Hodgson, J. (2003). Drug induced proteome changes in *Candida albicans*: comparison of the effect of beta(1,3) glucan synthase inhibitors and two triazoles, fluconazole and itraconazole. *Proteomics* 3, 325–336.

Bruno, V. M., Wang, Z., Marjani, S. L., Euskirchen, G. M., Martin, J., Sherlock, G., and Snyder, M. (2010). Comprehensive annotation of the transcriptome of the human fungal pathogen *Candida albicans* using RNA-seq. *Genome Res.* 20, 1451–1458.

Bruns, S., Seidler, M., Albrecht, D., Salvenmoser, S., Remme, N., Hertweck, C., Brakhage, A. A., Kniemeyer, O., and Müller, F.-M. C. (2010). Functional genomic profiling of *Aspergillus fumigatus* biofilm reveals enhanced production of the mycotoxin gliotoxin. *Proteomics* 10, 3097–3107.

Burmester, A., Shelest, E., Glöckner, G., Heddergott, C., Schindler, S., Staib, P., Heidel, A., Felder, M., Petzold, A., Szafranski, K., Feuermann, M., Pedruzzi, I., Priebe, S., Groth, M., Winkler, R., Li, W., Kniemeyer, O., Schroeckh, V., Hertweck, C., Hube, B., White, T. C., Platzer, M., Guthke, R., Heitman, J., Wöstemeyer, J., Zipfel, P. F., Monod, M., and Brakhage, A. A. (2011). Comparative and functional genomics provide insights into the pathogenicity of dermatophytic fungi. *Genome Biol.* 12, R7.

Butler, G., Rasmussen, M. D., Lin, M. F., Santos, M. A. S., Sakthikumar, S., Munro, C. A., Rheinbay, E., Grabherr, M., Forche, A., Reedy, J. L., Agrafioti, I., Arnaud, M. B., Bates, S., Brown, A. J. P., Brunke, S., Costanzo, M. C., Fitzpatrick, D. A., de Groot, P. W. J., Harris, D., Hoyer, L. L., Hube, B., Klis, F. M., Kodira, C., Lennard, N., Logue, M. E., Martin, R., Neiman, A. M., Nikolaou, E., Quail, M. A., Quinn, J., Santos, M. C., Schmitzberger, F. F., Sherlock, G., Shah, P., Silverstein, K. A. T., Skrzypek, M. S., Soll, D., Staggs, R., Stansfield, I., Stumpf, M. P. H., Sudbery, P. E., Srikantha, T., Zeng, Q., Berman, J., Berriman, M., Heitman, J., Gow, N. A. R., Lorenz, M. C., Birren, B. W., Kellis, M., and Cuomo, C. A. (2009). Evolution of pathogenicity and sexual reproduction in eight *Candida* genomes. *Nature* 459, 657–662.

Cagas, S. E., Jain, M. R., Li, H., and Perlin, D. S. (2011). Profiling the *Aspergillus fumigatus* proteome in response to caspofungin. *Antimicrob. Agents Chemother.* 55, 146–154.

Cairns, T., Minuzzi, F., and Bignell, E. (2010). The host-infecting fungal transcriptome. *FEMS Microbiol. Lett.* 307, 1–11.

Castillo, L., Calvo, E., Martínez, A. I., Ruiz-Herrera, J., Valentín, E., Lopez, J. A., and Sentandreu, R. (2008). A study of the *Candida albicans* cell wall proteome. *Proteomics* 8, 3871–3881.

Cavalieri, D., and Filippo, C. D. (2005). Bioinformatic methods for integrating whole-genome expression results into cellular networks. *Drug Discov. Today* 10, 727–734.

Chavali, A. K., Gianchandani, E. P., Tung, K. S., Lawrence, M. B., Peirce, S. M., and Papin, J. A. (2008). Characterizing emergent properties of immunological systems with multi-cellular rule-based computational modeling. *Trends Immunol.* 29, 589–599.

Chen, X. S. (2011). Introducing Theranostics journal – from the editor-in-chief. *Theranostics* 1, 1–2.

Correia, A., Lermann, U., Teixeira, L., Cerca, F., Botelho, S., da Costa, R. M. G., Sampaio, P., Gärtner, F., Morschhäuser, J., Vilanova, M., and Pais, C. (2010). Limited role of secreted aspartyl proteinases Sap1 to Sap6 in *Candida albicans* virulence and host immune response in murine hematogenously disseminated candidiasis. *Infect. Immun.* 78, 4839–4849.

Courtot, M., Juty, N., Knüpfer, C., Waltemath, D., Zhukova, A., Dräger, A., Dumontier, M., Finney, A., Golebiewski, M., Hastings, J., Hoops, S., Keating, S., Kell, D. B., Kerrien, S., Lawson, J., Lister, A., Lu, J., Machne, R., Mendes, P., Pocock, M., Rodriguez, N., Villeger, A., Wilkinson, D. J., Wimalaratne, S., Laibe, C., Hucka, M., and Novère, N. L. (2011). Controlled vocabularies and semantics in systems biology. *Mol. Syst. Biol.* 7, 543.

da Silva Ferreira, M. E., Malavazi, I., Savoldi, M., Brakhage, A. A., Goldman, M. H. S., Kim, H. S., Nierman, W. C., and Goldman, G. H. (2006). Transcriptome analysis of *Aspergillus fumigatus* exposed to voriconazole. *Curr. Genet.* 50, 32–44.

Dagenais, T. R. T., and Keller, N. P. (2009). Pathogenesis of *Aspergillus fumigatus* in invasive aspergillosis. *Clin. Microbiol. Rev.* 22, 447–465.

Day, J., Schlesinger, L. S., and Friedman, A. (2010). Tuberculosis research: going forward with a powerful "translational systems biology" approach. *Tuberculosis (Edinb.)* 90, 7–8.

de Groot, P. W. J., de Boer, A. D., Cunningham, J., Dekker, H. L., de Jong, L., Hellingwerf, K. J., de Koster, C., and Klis, F. M. (2004). Proteomic analysis of *Candida albicans* cell walls reveals covalently bound carbohydrate-active enzymes and adhesins. *Eukaryotic Cell* 3, 955–965.

d'Enfert, C., Goyard, S., Rodriguez-Arnaveilhe, S., Frangeul, L., Jones, L., Tekaia, F., Bader, O., Albrecht, A., Castillo, L., Dominguez, A., Ernst, J. F., Fradin, C., Gaillardin, C., Garcia-Sanchez, S., de Groot, P., Hube, B., Klis, F. M., Krishnamurthy, S., Kunze, D., Lopez, M.-C., Mavor, A., Martin, N., Moszer, I., Onésime, D., Martin, J. P., Sentandreu, R., Valentin, E., and Brown, A. J. P. (2005). CandidaDB: a genome database for *Candida albicans* pathogenomics. *Nucleic Acids Res.* 33, D353–D357. [Database issue].

Doedt, T., Krishnamurthy, S., Bockmühl, D. P., Tebarth, B., Stempel, C., Russell, C. L., Brown, A. J. P., and Ernst, J. F. (2004). APSES proteins regulate morphogenesis and metabolism in *Candida albicans*. *Mol. Biol. Cell* 15, 3167–3180.

Domon, B., and Aebersold, R. (2010). Options and considerations when selecting a quantitative proteomics strategy. *Nat. Biotechnol.* 28, 710–721.

Dujon, B. (2010). Yeast evolutionary genomics. *Nat. Rev. Genet.* 11, 512–524.

Dyer, M. D., Murali, T. M., and Sobral, B. W. (2007). Computational prediction of host-pathogen protein-protein interactions. *Bioinformatics* 23, i159–i166.

Dyer, M. D., Murali, T. M., and Sobral, B. W. (2008). The landscape of human proteins interacting with viruses and other pathogens. *PLoS Pathog.* 4, e32. doi:10.1371/journal.ppat.0040032

Fang, X., Wallqvist, A., and Reifman, J. (2009). A systems biology framework for modeling metabolic enzyme inhibition of *Mycobacterium tuberculosis*. *BMC Syst. Biol.* 3, 92.

Fazius, E., Shelest, V., and Shelest, E. (2011). SiTaR: a novel tool for transcription factor binding site prediction. *Bioinformatics* 27, 2806–2811.

Fedorova, N. D., Khaldi, N., Joardar, V. S., Maiti, R., Amedeo, P., Anderson, M. J., Crabtree, J., Silva, J. C., Badger, J. H., Albarraq, A., Angiuoli, S., Bussey, H., Bowyer, P., Cotty, P. J., Dyer, P. S., Egan, A., Galens, K., Fraser-Liggett, C. M., Haas, B. J., Inman, J. M., Kent, R., Lemieux, S., Malavazi, I., Orvis, J., Roemer, T., Ronning, C. M., Sundaram, J. P., Sutton, G., Turner, G., Venter, J. C., White, O. R., Whitty, B. R., Youngman, P., Wolfe, K. H., Goldman, G. H., Wortman, J. R., Jiang, B., Denning, D. W., and Nierman, W. C. (2008). Genomic islands in the pathogenic filamentous fungus *Aspergillus fumigatus*. *PLoS Genet.* 4, e1000046. doi:10.1371/journal.pgen.1000046

Feldmesser, M. (2006). Role of neutrophils in invasive aspergillosis. *Infect. Immun.* 74, 6514–6516.

Ferrandon, D., Imler, J.-L., Hetru, C., and Hoffmann, J. A. (2007). The *Drosophila* systemic immune response: sensing and signalling during bacterial and fungal infections. *Nat. Rev. Immunol.* 7, 862–874.

Figge, M. T. (2005). Stochastic discrete event simulation of germinal center reactions. *Phys. Rev. E Stat. Nonlin. Soft Matter Phys.* 71, 051907.

Figge, M. T., Garin, A., Gunzer, M., Kosco-Vilbois, M., Toellner, K.-M., and Meyer-Hermann, M. (2008). Deriving a germinal center lymphocyte migration model from two-photon data. *J. Exp. Med.* 205, 3019–3029.

Filler, S. G. (2006). *Candida*-host cell receptor-ligand interactions. *Curr. Opin. Microbiol.* 9, 333–339.

Fleck, C. B., Schöbel, F., and Brock, M. (2011). Nutrient acquisition by pathogenic fungi: nutrient availability, pathway regulation, and differences in substrate utilization. *Int. J. Med. Microbiol.* 301, 400–407.

Forst, C. V. (2006). Host-pathogen systems biology. *Drug Discov. Today* 11, 220–227.

Fradin, C., Kretschmar, M., Nichterlein, T., Gaillardin, C., d'Enfert, C., and Hube, B. (2003). Stage-specific gene expression of *Candida albicans* in human blood. *Mol. Microbiol.* 47, 1523–1543.

Franke, R., Müller, M., Wundrack, N., Gilles, E.-D., Klamt, S., Kähne, T., and Naumann, M. (2008). Host-pathogen systems biology: logical modelling of hepatocyte growth factor and *Helicobacter pylori* induced c-Met signal transduction. *BMC Syst. Biol.* 2, 4. doi:10.1186/1752-0509-2-4

Gafa, V., Remoli, M. E., Giacomini, E., Gagliardi, M. C., Lande, R., Severa, M., Grillot, R., and Coccia, E. M. (2007). In vitro infection of human dendritic cells by *Aspergillus fumigatus* conidia triggers the secretion of chemokines for neutrophil and Th1 lymphocyte recruitment. *Microbes Infect.* 9, 971–980.

Garin, A., Meyer-Hermann, M., Contie, M., Figge, M. T., Buatois, V., Gunzer, M., Toellner, K. -M., Elson, G., and Kosco-Vilbois, M. H. (2010). Toll-like receptor 4 signaling by follicular dendritic cells is pivotal for germinal center onset and affinity maturation. *Immunity* 33, 84–95.

Gautam, P., Shankar, J., Madan, T., Sirdeshmukh, R., Sundaram, C. S., Gade, W. N., Basir, S. F., and Sarma, P. U. (2008). Proteomic and transcriptomic analysis of *Aspergillus fumigatus* on exposure to amphotericin B. *Antimicrob. Agents Chemother.* 52, 4220–4227.

Gibbons, J. G., Beauvais, A., Beau, R., McGary, K. L., Latge, J.-P., and Rokas, A. (2012). Global transcriptome changes underlying colony growth in the opportunistic human pathogen *Aspergillus fumigatus*. *Eukaryotic Cell.* 11, 68–78.

Gilsenan, J. M., Cooley, J., and Bowyer, P. (2012). CADRE: The Central Aspergillus Data Repository 2012. *Nucleic Acids Res.* 40, D660–D666.

Grahl, N., Puttikamonkul, S., MacDonald, J. M., Gamcsik, M. P., Ngo, L. Y., Hohl, T. M., and Cramer, R. A. (2011). In vivo hypoxia and a fungal alcohol dehydrogenase influence the pathogenesis of invasive pulmonary aspergillosis. *PLoS Pathog.* 7, e1002145. doi:10.1371/journal.ppat.1002145

Gropp, K., Schild, L., Schindler, S., Hube, B., Zipfel, P. F., and Skerka, C. (2009). The yeast *Candida albicans* evades human complement attack by secretion of aspartic proteases. *Mol. Immunol.* 47, 465–475.

Gross, O., Poeck, H., Bscheider, M., Dostert, C., Hannesschläger, N., Endres, S., Hartmann, G., Tardivel, A., Schweighoffer, E., Tybulewicz, V., Mocsai, A., Tschopp, J., and Ruland, J. (2009). Syk kinase signalling couples to the Nlrp3 inflammasome for anti-fungal host defence. *Nature* 459, 433–436.

Gudlaugsson, O., Gillespie, S., Lee, K., Berg, J. V., Hu, J., Messer, S., Herwaldt, L., Pfaller, M., and Diekema, D. (2003). Attributable mortality of nosocomial candidemia, revisited. *Clin. Infect. Dis.* 37, 1172–1177.

Guo, Z., Sloot, P. M., and Tay, J. C. (2008). A hybrid agent-based approach for modeling microbiological systems. *J. Theor. Biol.* 255, 163–175.

Guo, Z., and Tay, J. (2005). A comparative study on modeling strategies for immune system dynamics under HIV-1 infection. *Artif. Immune Syst.* 3627, 220–233.

Guthke, R., Kniemeyer, O., Albrecht, D., Brakhage, A. A., and Möller, U. (2007). Discovery of gene regulatory networks in *Aspergillus fumigatus*. *Lect. Notes Bioinform.* 4366, 22–41.

Guthke, R., Möller, U., Hoffmann, M., Thies, F., and Töpfer, S. (2005). Dynamic network reconstruction from gene expression data applied to immune response during bacterial infection. *Bioinformatics* 21, 1626–1634.

Hajishengallis, G., and Lambris, J. D. (2011). Microbial manipulation of receptor crosstalk in innate immunity. *Nat. Rev. Immunol.* 11, 187–200.

Hase, T., Tanaka, H., Suzuki, Y., Nakagawa, S., and Kitano, H. (2009). Structure of protein interaction networks and their implications on drug design. *PLoS Comput. Biol.* 5, e1000550. doi:10.1371/journal.pcbi.1000550

Hawksworth, D. (2001). The magnitude of fungal diversity: the 1.5 million species estimate revisited. *Mycol. Res.* 105, 1422–1432.

Hecker, M., Lambeck, S., Toepfer, S., van Someren, E., and Guthke, R. (2009). Gene regulatory network inference: data integration in dynamic models – a review. *BioSystems* 96, 86–103.

Heilmann, C. J., Sorgo, A. G., Siliakus, A. R., Dekker, H. L., Brul, S., de Koster, C. G., de Koning, L. J., and Klis, F. M. (2011). Hyphal induction in the human fungal pathogen *Candida albicans* reveals a characteristic wall protein profile. *Microbiology* 157, 2297–2307.

Hermjakob, H., Montecchi-Palazzi, L., Bader, G., Wojcik, J., Salwinski, L., Ceol, A., Moore, S., Orchard, S., Sarkans, U., von Mering, C., Roechert, B., Poux, S., Jung, E., Mersch, H., Kersey, P., Lappe, M., Li, Y., Zeng, R., Rana, D., Nikolski, M., Husi, H., Brun, C., Shanker, K., Grant, S. G. N., Sander, C., Bork, P., Zhu, W., Pandey, A., Brazma, A., Jacq, B., Vidal, M., Sherman, D., Legrain, P., Cesareni, G., Xenarios, I., Eisenberg, D., Steipe, B., Hogue, C., and Apweiler, R. (2004). The HUPO PSI's molecular interaction format – a community standard for the representation of protein interaction data. *Nat. Biotechnol.* 22, 177–183.

Hernáez, M. L., Ximénez-Embún, P., Martínez-Gomariz, M., Gutiérrez-Blázquez, M. D., Nombela, C., and Gil, C. (2010). Identification of *Candida albicans* exposed surface proteins in vivo by a rapid proteomic approach. *J. Proteomics* 73, 1404–1409.

Hickey, P. C., and Read, N. D. (2009). Imaging living cells of *Aspergillus* in vitro. *Med. Mycol.* 47(Suppl. 1), S110–S119.

Hise, A. G., Tomalka, J., Ganesan, S., Patel, K., Hall, B. A., Brown, G. D., and Fitzgerald, K. A. (2009). An essential role for the NLRP3 inflammasome in host defense against the human fungal pathogen *Candida albicans*. *Cell Host Microbe* 5, 487–497.

Hoehamer, C. F., Cummings, E. D., Hilliard, G. M., and Rogers, P. D. (2010). Changes in the proteome of *Candida albicans* in response to azole, polyene, and echinocandin antifungal agents. *Antimicrob. Agents Chemother.* 54, 1655–1664.

Hooshdaran, M. Z., Barker, K. S., Hilliard, G. M., Kusch, H., Morschhäuser, J., and Rogers, P. D. (2004). Proteomic analysis of azole resistance in *Candida albicans* clinical isolates. *Antimicrob. Agents Chemother.* 48, 2733–2735.

Hucka, M., Finney, A., Sauro, H. M., Bolouri, H., Doyle, J. C., Kitano, H., Arkin, A. P., Bornstein, B. J., Bray, D., Cornish-Bowden, A., Cuellar, A. A., Dronov, S., Gilles, E. D., Ginkel, M., Gor, V., Goryanin, I. I., Hedley, W. J., Hodgman, T. C., Hofmeyr, J.-H., Hunter, P. J., Juty, N. S., Kasberger, J. L., Kremling, A., Kummer, U., Novère, N. L., Loew, L. M., Lucio, D., Mendes, P., Minch, E., Mjolsness, E. D., Nakayama, Y., Nelson, M. R., Nielsen, P. F., Sakurada, T., Schaff, J. C., Shapiro, B. E., Shimizu, T. S., Spence, H. D., Stelling, J., Takahashi, K., Tomita, M., Wagner, J., Wang, J., and Forum, S. B. M. L. (2003). The systems biology markup language (SBML): a medium for representation and exchange of biochemical network models. *Bioinformatics* 19, 524–531.

Hull, D., Wolstencroft, K., Stevens, R., Goble, C., Pocock, M. R., Li, P., and Oinn, T. (2006). Taverna: a tool for building and running workflows of services. *Nucleic Acids Res.* 34, W729–W732. [Web Server issue].

Hummert, S., Hummert, C., Schröter, A., Hube, B., and Schuster, S. (2010). Game theoretical modelling of survival strategies of *Candida albicans* inside macrophages. *J. Theor. Biol.* 264, 312–318.

Ibrahim-Granet, O., Jouvion, G., Hohl, T. M., Droin-Bergère, S., Philippart, F., Kim, O. Y., Adib-Conquy, M., Schwendener, R., Cavaillon, J.-M., and Brock, M. (2010). In vivo bioluminescence imaging and histopathopathologic analysis reveal distinct roles for resident and recruited immune effector cells in defense against invasive aspergillosis. *BMC Microbiol.* 10, 105. doi:10.1186/1471-2180-10-105

Ibrahim-Granet, O., Philippe, B., Boleti, H., Boisvieux-Ulrich, E., Grenet, D., Stern, M., and Latgé, J. P. (2003). Phagocytosis and intracellular fate of *Aspergillus fumigatus* conidia in alveolar macrophages. *Infect. Immun.* 71, 891–903.

Ideker, T., Galitski, T., and Hood, L. (2001). A new approach to decoding life: systems biology. *Annu. Rev. Genomics Hum. Genet.* 2, 343–372.

Ideker, T., and Sharan, R. (2008). Protein networks in disease. *Genome Res.* 18, 644–652.

Ihmels, J., Bergmann, S., Berman, J., and Barkai, N. (2005). Comparative gene expression analysis by differential clustering approach: application to the *Candida albicans* transcription program. *PLoS Genet.* 1, e39. doi:10.1371/journal.pgen.0010039

Jacobsen, I. D., Grosse, K., Slesiona, S., Hube, B., Berndt, A., and Brock, M. (2010). Embryonated eggs as an alternative infection model to investigate *Aspergillus fumigatus* virulence. *Infect. Immun.* 78, 2995–3006.

Jahn, B., Langfelder, K., Schneider, U., Schindel, C., and Brakhage, A. A. (2002). PKSP-dependent reduction

of phagolysosome fusion and intracellular kill of *Aspergillus fumigatus* conidia by human monocyte-derived macrophages. *Cell. Microbiol.* 4, 793–803.

Jain, R., Valiante, V., Remme, N., Docimo, T., Heinekamp, T., Hertweck, C., Gershenzon, J., Haas, H., and Brakhage, A. A. (2011). The MAP kinase MpkA controls cell wall integrity, oxidative stress response, gliotoxin production and iron adaptation in *Aspergillus fumigatus*. *Mol. Microbiol.* 82, 39–53.

Jones, T., Federspiel, N. A., Chibana, H., Dungan, J., Kalman, S., Magee, B. B., Newport, G., Thorstenson, Y. R., Agabian, N., Magee, P. T., Davis, R. W., and Scherer, S. (2004). The diploid genome sequence of *Candida albicans*. *Proc. Natl. Acad. Sci. U.S.A.* 101, 7329–7334.

Kim, Y., Nandakumar, M. P., and Marten, M. R. (2008). The state of proteome profiling in the fungal genus *Aspergillus*. *Brief. Funct. Genomic. Proteomic.* 7, 87–94.

Kitano, H. (2007). A robustness-based approach to systems-oriented drug design. *Nat. Rev. Drug Discov.* 6, 202–210.

Klipp, E., Wade, R. C., and Kummer, U. (2010). Biochemical network-based drug-target prediction. *Curr. Opin. Biotechnol.* 21, 511–516.

Klose, J., and Kobalz, U. (1995). Two-dimensional electrophoresis of proteins: an updated protocol and implications for a functional analysis of the genome. *Electrophoresis* 16, 1034–1059.

Kniemeyer, O. (2011). Proteomics of eukaryotic microorganisms: the medically and biotechnologically important fungal genus *Aspergillus*. *Proteomics* 11, 3232–3243.

Kniemeyer, O., and Brakhage, A. A. (2008). "Proteomics and its application to the human-pathogenic fungi," in *Human and Animal Relationships: The Mycota VI*, eds A. A. Brakhage and P. F. Zipfel (Berlin: Springer), 154–186.

Kniemeyer, O., Schmidt, A. D., Vödisch, M., Wartenberg, D., and Brakhage, A. A. (2011). Identification of virulence determinants of the human pathogenic fungi *Aspergillus fumigatus* and *Candida albicans* by proteomics. *Int. J. Med. Microbiol.* 301, 368–377.

Köhler, J., Baumbach, J., Taubert, J., Specht, M., Skusa, A., Rüegg, A., Rawlings, C., Verrier, P., and Philippi, S. (2006). Graph-based analysis and visualization of experimental results with ONDEX. *Bioinformatics* 22, 1383–1390.

Kozhenkov, S., Sedova, M., Dubinina, Y., Gupta, A., Ray, A., Ponomarenko, J., and Baitaluk, M. (2011). Biological networks – tools enabling the integration of multi-scale data for the host-pathogen studies. *BMC Syst. Biol.* 5, 7. doi:10.1186/1752-0509-5-7

Krappmann, S., Sasse, C., and Braus, G. H. (2006). Gene targeting in *Aspergillus fumigatus* by homologous recombination is facilitated in a nonhomologous end-joining-deficient genetic background. *Eukaryotic Cell* 5, 212–215.

Kusch, H., Engelmann, S., Albrecht, D., Morschhäuser, J., and Hecker, M. (2007). Proteomic analysis of the oxidative stress response in *Candida albicans*. *Proteomics* 7, 686–697.

Langfelder, K., Jahn, B., Gehringer, H., Schmidt, A., Wanner, G., and Brakhage, A. A. (1998). Identification of a polyketide synthase gene (pksP) of *Aspergillus fumigatus* involved in conidial pigment biosynthesis and virulence. *Med. Microbiol. Immunol.* 187, 79–89.

Latgé, J. P. (1999). *Aspergillus fumigatus* and aspergillosis. *Clin. Microbiol. Rev.* 12, 310–350.

Le Novère, N., Hucka, M., Mi, H., Moodie, S., Schreiber, F., Sorokin, A., Demir, E., Wegner, K., Aladjem, M. I., Wimalaratne, S. M., Bergman, F. T., Gauges, R., Ghazal, P., Kawaji, H., Li, L., Matsuoka, Y., Villéger, A., Boyd, S. E., Calzone, L., Courtot, M., Dogrusoz, U., Freeman, T. C., Funahashi, A., Ghosh, S., Jouraku, A., Kim, S., Kolpakov, F., Luna, A., Sahle, S., Schmidt, E., Watterson, S., Wu, G., Goryanin, I., Kell, D. B., Sander, C., Sauro, H., Snoep, J. L., Kohn, K., and Kitano, H. (2009). The systems biology graphical notation. *Nat. Biotechnol.* 27, 735–741.

Lee, D.-S., Burd, H., Liu, J., Almaas, E., Wiest, O., Barabási, A.-L., Oltvai, Z. N., and Kapatral, V. (2009). Comparative genome-scale metabolic reconstruction and flux balance analysis of multiple *Staphylococcus aureus* genomes identify novel antimicrobial drug targets. *J. Bacteriol.* 191, 4015–4024.

Lessing, F., Kniemeyer, O., Wozniok, I., Loeffler, J., Kurzai, O., Haertl, A., and Brakhage, A. A. (2007). The *Aspergillus fumigatus* transcriptional regulator AfYap1 represents the major regulator for defense against reactive oxygen intermediates but is dispensable for pathogenicity in an intranasal mouse infection model. *Eukaryotic Cell* 6, 2290–2302.

Linde, J., Hortschansky, P., Fazius, E., Brakhage, A. A., Guthke, R., and Haas, H. (2012). Regulatory interactions for iron homoeostatis in *Aspergillus fumigatus* inferred by a systems biology approach. *BMC Syst. Biol.* 6, 6. doi:10.1186/1752-0509-6-6

Linde, J., Wilson, D., Hube, B., and Guthke, R. (2010). Regulatory network modelling of iron acquisition by a fungal pathogen in contact with epithelial cells. *BMC Syst. Biol.* 4, 148. doi:10.1186/1752-0509-4-148

Liu, H. (2002). Co-regulation of pathogenesis with dimorphism and phenotypic switching in *Candida albicans*, a commensal and a pathogen. *Int. J. Med. Microbiol.* 292, 299–311.

Liu, T. T., Lee, R. E. B., Barker, K. S., Lee, R. E., Wei, L., Homayouni, R., and Rogers, P. D. (2005). Genome-wide expression profiling of the response to azole, polyene, echinocandin, and pyrimidine antifungal agents in *Candida albicans*. *Antimicrob. Agents Chemother.* 49, 2226–2236.

Lloyd, A. T., and Sharp, P. M. (1992). Evolution of codon usage patterns: the extent and nature of divergence between *Candida albicans* and *Saccharomyces cerevisiae*. *Nucleic Acids Res.* 20, 5289–5295.

Lo, H. J., Köhler, J. R., DiDomenico, B., Loebenberg, D., Cacciapuoti, A., and Fink, G. R. (1997). Nonfilamentous *C. albicans* mutants are avirulent. *Cell* 90, 939–949.

Loftus, B. J., Fung, E., Roncaglia, P., Rowley, D., Amedeo, P., Bruno, D., Vamathevan, J., Miranda, M., Anderson, I. J., Fraser, J. A., Allen, J. E., Bosdet, I. E., Brent, M. R., Chiu, R., Doering, T. L., Donlin, M. J., D'Souza, C. A., Fox, D. S., Grinberg, V., Fu, J., Fukushima, M., Haas, B. J., Huang, J. C., Janbon, G., Jones, S. J. M., Koo, H. L., Krzywinski, M. I., Kwon-Chung, J. K., Lengeler, K. B., Maiti, R., Marra, M. A., Marra, R. E., Mathewson, C. A., Mitchell, T. G., Pertea, M., Riggs, F. R., Salzberg, S. L., Schein, J. E., Shvartsbeyn, A., Shin, H., Shumway, M., Specht, C. A., Suh, B. B., Tenney, A., Utterback, T. R., Wickes, B. L., Wortman, J. R., Wye, N. H., Kronstad, J. W., Lodge, J. K., Heitman, J., Davis, R. W., Fraser, C. M., and Hyman, R. W. (2005). The genome of the basidiomycetous yeast and human pathogen *Cryptococcus neoformans*. *Science* 307, 1321–1324.

Lorenz, M. C., Bender, J. A., and Fink, G. R. (2004). Transcriptional response of *Candida albicans* upon internalization by macrophages. *Eukaryotic Cell* 3, 1076–1087.

Lorenz, M. C., and Fink, G. R. (2001). The glyoxylate cycle is required for fungal virulence. *Nature* 412, 83–86.

Manning, M., and Mitchell, T. G. (1980). Morphogenesis of *Candida albicans* and cytoplasmic proteins associated with differences in morphology, strain, or temperature. *J. Bacteriol.* 144, 258–273.

Marbach, D., Prill, R. J., Schaffter, T., Mattiussi, C., Floreano, D., and Stolovitzky, G. (2010). Revealing strengths and weaknesses of methods for gene network inference. *Proc. Natl. Acad. Sci. U.S.A.* 107, 6286–6291.

Marr, K. A., Carter, R. A., Boeckh, M., Martin, P., and Corey, L. (2002). Invasive aspergillosis in allogeneic stem cell transplant recipients: changes in epidemiology and risk factors. *Blood* 100, 4358–4366.

Martin, G. S., Mannino, D. M., Eaton, S., and Moss, M. (2003). The epidemiology of sepsis in the United States from 1979 through 2000. *N. Engl. J. Med.* 348, 1546–1554.

Martin, R., Wächtler, B., Schaller, M., Wilson, D., and Hube, B. (2011). Host-pathogen interactions and virulence-associated genes during *Candida albicans* oral infections. *Int. J. Med. Microbiol.* 301, 417–422.

Martínez-Solano, L., Nombela, C., Molero, G., and Gil, C. (2006). Differential protein expression of murine macrophages upon interaction with *Candida albicans*. *Proteomics* 6(Suppl. 1), S133–S144.

Martínez-Solano, L., Reales-Calderón, J. A., Nombela, C., Molero, G., and Gil, C. (2009). Proteomics of RAW 264.7 macrophages upon interaction with heat-inactivated *Candida albicans* cells unravel an anti-inflammatory response. *Proteomics* 9, 2995–3010.

May, R. M., and Anderson, R. M. (1979). Population biology of infectious diseases. Part II. *Nature* 280, 455–461.

McCluskey, K., Wiest, A., and Plamann, M. (2010). The Fungal Genetics Stock Center: a repository for 50 years of fungal genetics research. *J. Biosci.* 35, 119–126.

McCormick, A., Heesemann, L., Wagener, J., Marcos, V., Hartl, D., Loeffler, J., Heesemann, J., and Ebel, F. (2010). NETs formed by human neutrophils inhibit growth of the pathogenic mold *Aspergillus fumigatus*. *Microbes Infect.* 12, 928–936.

Mech, F., Thywissen, A., Guthke, R., Brakhage, A. A., and Figge, M. T. (2011). Automated image analysis

of the host-pathogen interaction between phagocytes and *Aspergillus fumigatus*. *PLoS ONE* 6, e19591. doi:10.1371/journal.pone.0019591

Melanson, J. E., Chisholm, K. A., and Pinto, D. M. (2006). Targeted comparative proteomics by liquid chromatography/matrix-assisted laser desorption/ionization triple-quadrupole mass spectrometry. *Rapid Commun. Mass Spectrom.* 20, 904–910.

Mezger, M., Kneitz, S., Wozniok, I., Kurzai, O., Einsele, H., and Loeffler, J. (2008). Proinflammatory response of immature human dendritic cells is mediated by dectin-1 after exposure to *Aspergillus fumigatus* germ tubes. *J. Infect. Dis.* 197, 924–931.

Moalli, F., Doni, A., Deban, L., Zelante, T., Zagarella, S., Bottazzi, B., Romani, L., Mantovani, A., and Garlanda, C. (2010). Role of complement and fcgamma receptors in the protective activity of the long pentraxin PTX3 against *Aspergillus fumigatus*. *Blood* 116, 5170–5180.

Monteoliva, L., Martinez-Lopez, R., Pitarch, A., Hernaez, M. L., Serna, A., Nombela, C., Albar, J. P., and Gil, C. (2011). Quantitative proteome and acidic subproteome profiling of *Candida albicans* yeast-to-hypha transition. *J. Proteome Res.* 10, 502–517.

Moran, G. P., Coleman, D. C., and Sullivan, D. J. (2011). Comparative genomics and the evolution of pathogenicity in human pathogenic fungi. *Eukaryotic Cell* 10, 34–42.

Morton, C. O., Varga, J. J., Hornbach, A., Mezger, M., Sennefelder, H., Kneitz, S., Kurzai, O., Krappmann, S., Einsele, H., Nierman, W. C., Rogers, T. R., and Loeffler, J. (2011). The temporal dynamics of differential gene expression in *Aspergillus fumigatus* interacting with human immature dendritic cells in vitro. *PLoS ONE* 6, e16016. doi:10.1371/journal.pone.0016016

Moy, T. I., Conery, A. L., Larkins-Ford, J., Wu, G., Mazitschek, R., Casadei, G., Lewis, K., Carpenter, A. E., and Ausubel, F. M. (2009). High-throughput screen for novel antimicrobials using a whole animal infection model. *ACS Chem. Biol.* 4, 527–533.

Mukhtar, M. S., Carvunis, A.-R., Dreze, M., Epple, P., Steinbrenner, J., Moore, J., Tasan, M., Galli, M., Hao, T., Nishimura, M. T., Pevzner, S. J., Donovan, S. E., Ghamsari, L., Santhanam, B., Romero, V., Poulin, M. M., Gebreab, F., Gutierrez, B. J., Tam, S., Monachello, D., Boxem, M., Harbort, C. J., McDonald, N., Gai, L., Chen, H., He, Y.,, E. U. E. C., Vandenhaute, J., Roth, F. P., Hill, D. E., Ecker, J. R., Vidal, M., Beynon, J., Braun, P., and Dangl, J. L. (2011). Independently evolved virulence effectors converge onto hubs in a plant immune system network. *Science* 333, 596–601.

Murillo, L. A., Newport, G., Lan, C.-Y., Habelitz, S., Dungan, J., and Agabian, N. M. (2005). Genome-wide transcription profiling of the early phase of biofilm formation by *Candida albicans*. *Eukaryotic Cell* 4, 1562–1573.

Mylonakis, E. (2008). *Galleria mellonella* and the study of fungal pathogenesis: making the case for another genetically tractable model host. *Mycopathologia* 165, 1–3.

Netea, M. G., Brown, G. D., Kullberg, B. J., and Gow, N. A. R. (2008). An integrated model of the recognition of *Candida albicans* by the innate immune system. *Nat. Rev. Microbiol.* 6, 67–78.

Neugebauer, U., Schmid, U., Baumann, K., Holzgrabe, U., Ziebuhr, W., Kozitskaya, S., Kiefer, W., Schmitt, M., and Popp, J. (2006). Characterization of bacterial growth and the influence of antibiotics by means of UV resonance Raman spectroscopy. *Biopolymers* 82, 306–311.

Nierman, W. C., Pain, A., Anderson, M. J., Wortman, J. R., Kim, H. S., Arroyo, J., Berriman, M., Abe, K., Archer, D. B., Bermejo, C., Bennett, J., Bowyer, P., Chen, D., Collins, M., Coulsen, R., Davies, R., Dyer, P. S., Farman, M., Fedorova, N., Fedorova, N., Feldblyum, T. V., Fischer, R., Fosker, N., Fraser, A., García, J. L., García, M. J., Goble, A., Goldman, G. H., Gomi, K., Griffith-Jones, S., Gwilliam, R., Haas, B., Haas, H., Harris, D., Horiuchi, H., Huang, J., Humphray, S., Jiménez, J., Keller, N., Khouri, H., Kitamoto, K., Kobayashi, T., Konzack, S., Kulkarni, R., Kumagai, T., Lafon, A., Lafton, A., Latgé, J.-P., Li, W., Lord, A., Lu, C., Majoros, W. H., May, G. S., Miller, B. L., Mohamoud, Y., Molina, M., Monod, M., Mouyna, I., Mulligan, S., Murphy, L., O'Neil, S., Paulsen, I., Peñalva, M. A., Pertea, M., Price, C., Pritchard, B. L., Quail, M. A., Rabbinowitsch, E., Rawlins, N., Rajandream, M.-A., Reichard, U., Renauld, H., Robson, G. D., de Córdoba, S. R., and Rodríguez-Peña, J. M., Ronning, C. M., Rutter, S., Salzberg, S. L., Sanchez, M., Sánchez-Ferrero, J. C., Saunders, D., Seeger, K., Squares, R., Squares, S., Takeuchi, M., Tekaia, F., Turner, G., de Aldana, C. R. V., Weidman, J., White, O., Woodward, J., Yu, J. H., Fraser, C., Galagan, J. E., Asai, K., Machida, M., Hall, N., Barrell, B., and Denning, D. W. (2005). Genomic sequence of the pathogenic and allergenic filamentous fungus *Aspergillus fumigatus*. *Nature* 438, 1151–1156.

Niimi, M., Shepherd, M. G., and Monk, B. C. (1996). Differential profiles of soluble proteins during the initiation of morphogenesis in *Candida albicans*. *Arch. Microbiol.* 166, 260–268.

Nobile, C. J., Nett, J. E., Andes, D. R., and Mitchell, A. P. (2006). Function of *Candida albicans* adhesin Hwp1 in biofilm formation. *Eukaryotic Cell* 5, 1604–1610.

Nygaard, V., and Hovig, E. (2006). Options available for profiling small samples: a review of sample amplification technology when combined with microarray profiling. *Nucleic Acids Res.* 34, 996–1014.

Oberhardt, M. A., Puchalka, J., Martins dos Santos, V. A. P., and Papin, J. A. (2011). Reconciliation of genome-scale metabolic reconstructions for comparative systems analysis. *PLoS Comput. Biol.* 7, e1001116. doi:10.1371/journal.pcbi.1001116

O'Farrell, P. H. (1975). High resolution two-dimensional electrophoresis of proteins. *J. Biol. Chem.* 250, 4007–4021.

Perlroth, J., Choi, B., and Spellberg, B. (2007). Nosocomial fungal infections: epidemiology, diagnosis, and treatment. *Med. Mycol.* 45, 321–346.

Pfaller, M. A., and Diekema, D. J. (2007). Epidemiology of invasive candidiasis: a persistent public health problem. *Clin. Microbiol. Rev.* 20, 133–163.

Picazo, J. J., González-Romo, F., and Candel, F. J. (2008). Candidemia in the critically ill patient. *Int. J. Antimicrob. Agents* 32(Suppl. 2), S83–S85.

Pitarch, A., Sánchez, M., Nombela, C., and Gil, C. (2002). Sequential fractionation and two-dimensional gel analysis unravels the complexity of the dimorphic fungus *Candida albicans* cell wall proteome. *Mol. Cell Proteomics* 1, 967–982.

Pitkänen, E., Rousu, J., and Ukkonen, E. (2010). Computational methods for metabolic reconstruction. *Curr. Opin. Biotechnol.* 21, 70–77.

Priebe, S., Linde, J., Albrecht, D., Guthke, R., and Brakhage, A. A. (2011). FungiFun: a web-based application for functional categorization of fungal genes and proteins. *Fungal Genet. Biol.* 48, 353–358.

Raghunathan, A., Reed, J., Shin, S., Palsson, B., and Daefler, S. (2009). Constraint-based analysis of metabolic capacity of *Salmonella typhimurium* during host-pathogen interaction. *BMC Syst. Biol.* 3, 38. doi:10.1186/1752-0509-3-38

Rao, A., Kumar, M. K., Joseph, T., and Bulusu, G. (2010). Cerebral malaria: insights from host-parasite protein-protein interactions. *Malar. J.* 9, 155.

Raza, S., Robertson, K. A., Lacaze, P. A., Page, D., Enright, A. J., Ghazal, P., and Freeman, T. C. (2008). A logic-based diagram of signalling pathways central to macrophage activation. *BMC Syst. Biol.* 2, 36. doi:10.1186/1752-0509-2-36

Real, L. A., and Biek, R. (2007). Infectious disease modeling and the dynamics of transmission. *Curr. Top. Microbiol. Immunol.* 315, 33–49.

Rispail, N., Soanes, D. M., Ant, C., Czajkowski, R., Grünler, A., Huguet, R., Perez-Nadales, E., Poli, A., Sartorel, E., Valiante, V., Yang, M., Beffa, R., Brakhage, A. A., Gow, N. A. R., Kahmann, R., Lebrun, M.-H., Lenasi, H., Perez-Martin, J., Talbot, N. J., Wendland, J., and Di Pietro, A. (2009). Comparative genomics of MAP kinase and calcium-calcineurin signalling components in plant and human pathogenic fungi. *Fungal Genet. Biol.* 46, 287–298.

Rizzetto, L., and Cavalieri, D. (2011). Friend or foe: using systems biology to elucidate interactions between fungi and their hosts. *Trends Microbiol.* 19, 509–515.

Romani, L. (2011). Immunity to fungal infections. *Nat. Rev. Immunol.* 11, 275–288.

Ross, R. (1911). *The Prevention of Malaria, with Addendum on the Theory of Happenings*. London: Murray.

Roux, A. V. D., and Aiello, A. E. (2005). Multilevel analysis of infectious diseases. *J. Infect. Dis.* 191(Suppl. 1), S25–S33.

Ruepp, A., Zollner, A., Maier, D., Albermann, K., Hani, J., Mokrejs, M., Tetko, I., Güldener, U., Mannhaupt, G., Münsterkötter, M., and Mewes, H. W. (2004). The FunCat, a functional annotation scheme for systematic classification of proteins from whole genomes. *Nucleic Acids Res.* 32, 5539–5545.

Rupp, S. (2004). Proteomics on its way to study host-pathogen interaction in *Candida albicans*. *Curr. Opin. Microbiol.* 7, 330–335.

Ruppin, E., Papin, J. A., de Figueiredo, L. F., and Schuster, S. (2010). Metabolic reconstruction, constraint-based analysis and game theory to probe genome-scale metabolic networks. *Curr. Opin. Biotechnol.* 21, 502–510.

Saïd-Sadier, N., Padilla, E., Langsley, G., and Ojcius, D. M. (2010). *Aspergillus fumigatus* stimulates the NLRP3 inflammasome through a pathway requiring ROS production and the Syk tyrosine kinase. *PLoS ONE* 5, e10008. doi:10.1371/journal.pone.0010008

Salgado, P. S., Yan, R., Taylor, J. D., Burchell, L., Jones, R., Hoyer, L. L., Matthews, S. J., Simpson, P. J., and Cota, E. (2011). Structural basis for the broad specificity to host-cell ligands by the pathogenic fungus *Candida albicans*. *Proc. Natl. Acad. Sci. U.S.A.* 108, 15775–15779.

Samaranayake, D. P., and Hanes, S. D. (2011). Milestones in *Candida albicans* gene manipulation. *Fungal Genet. Biol.* 48, 858–865.

Santamaría, R., Rizzetto, L., Bromley, M., Zelante, T., Lee, W., Cavalieri, D., Romani, L., Miller, B., Gut, I., Santos, M., Pierre, P., Bowyer, P., and Kapushesky, M. (2011). Systems biology of infectious diseases: a focus on fungal infections. *Immunobiology* 216, 1212–1227.

Schaller, M., Korting, H. C., Borelli, C., Hamm, G., and Hube, B. (2005). *Candida albicans*-secreted aspartic proteinases modify the epithelial cytokine response in an in vitro model of vaginal candidiasis. *Infect. Immun.* 73, 2758–2765.

Schrettl, M., Bignell, E., Kragl, C., Joechl, C., Rogers, T., Arst, H. N., Haynes, K., and Haas, H. (2004). Siderophore biosynthesis but not reductive iron assimilation is essential for *Aspergillus fumigatus* virulence. *J. Exp. Med.* 200, 1213–1219.

Schrettl, M., Kim, H. S., Eisendle, M., Kragl, C., Nierman, W. C., Heinekamp, T., Werner, E. R., Jacobsen, I., Illmer, P., Yi, H., Brakhage, A. A., and Haas, H. (2008). SreA-mediated iron regulation in *Aspergillus fumigatus*. *Mol. Microbiol.* 70, 27–43.

Shamir, L., Delaney, J. D., Orlov, N., Eckley, D. M., and Goldberg, I. G. (2010). Pattern recognition software and techniques for biological image analysis. *PLoS Comput. Biol.* 6, e1000974. doi:10.1371/journal.pcbi.1000974

Sharan, R., Ulitsky, I., and Shamir, R. (2007). Network-based prediction of protein function. *Mol. Syst. Biol.* 3, 88.

Shin, Y.-K., Kim, K.-Y., and Paik, Y.-K. (2005). Alterations of protein expression in macrophages in response to *Candida albicans* infection. *Mol. Cells* 20, 271–279.

Skrabanek, L., Saini, H. K., Bader, G. D., and Enright, A. J. (2008). Computational prediction of protein-protein interactions. *Mol. Biotechnol.* 38, 1–17.

Smoot, M. E., Ono, K., Ruscheinski, J., Wang, P.-L., and Ideker, T. (2011). Cytoscape 2.8: new features for data integration and network visualization. *Bioinformatics* 27, 431–432.

Sorgo, A. G., Heilmann, C. J., Dekker, H. L., Bekker, M., Brul, S., de Koster, C. G., de Koning, L. J., and Klis, F. M. (2011). Effects of fluconazole on the secretome, the wall proteome, and wall integrity of the clinical fungus *Candida albicans*. *Eukaryotic Cell* 10, 1071–1081.

Sosinska, G. J., de Groot, P. W. J., de Mattos, M. J. T., Dekker, H. L., de Koster, C. G., Hellingwerf, K. J., and Klis, F. M. (2008). Hypoxic conditions and iron restriction affect the cell-wall proteome of *Candida albicans* grown under vagina-simulative conditions. *Microbiology* 154(Pt 2), 510–520.

Sosinska, G. J., de Koning, L. J., de Groot, P. W. J., Manders, E. M. M., Dekker, H. L., Hellingwerf, K. J., de Koster, C. G., and Klis, F. M. (2011). Mass spectrometric quantification of the adaptations in the wall proteome of *Candida albicans* in response to ambient pH. *Microbiology* 157(Pt 1), 136–146.

Stoldt, V. R., Sonneborn, A., Leuker, C. E., and Ernst, J. F. (1997). Efg1p, an essential regulator of morphogenesis of the human pathogen *Candida albicans*, is a member of a conserved class of bHLH proteins regulating morphogenetic processes in fungi. *EMBO J.* 16, 1982–1991.

Stolovitzky, G. (2011). "Wisdom of crowds for gene network inference," in *12th International Conference on Systems Biology*, August 28 to September 1st, 2011, Heidelberg.

Strömbäck, L., and Lambrix, P. (2005). Representations of molecular pathways: an evaluation of SBML, PSI MI and BioPAX. *Bioinformatics* 21, 4401–4407.

Sugui, J. A., Kim, H. S., Zarember, K. A., Chang, Y. C., Gallin, J. I., Nierman, W. C., and Kwon-Chung, K. J. (2008). Genes differentially expressed in conidia and hyphae of *Aspergillus fumigatus* upon exposure to human neutrophils. *PLoS ONE* 3, e2655. doi:10.1371/journal.pone.0002655

Sysko, L. R., and Davis, M. A. (2010). From image to data using common image-processing techniques. *Curr. Protoc. Cytom.* Chapter 12, Unit 12.21.

Szabo, E. K., and MacCallum, D. M. (2011). The contribution of mouse models to our understanding of systemic candidiasis. *FEMS Microbiol. Lett.* 320, 1–8.

Taylor, C. F., Field, D., Sansone, S.-A., Aerts, J., Apweiler, R., Ashburner, M., Ball, C. A., Binz, P.-A., Bogue, M., Booth, T., Brazma, A., Brinkman, R. R., Clark, A. M., Deutsch, E. W., Fiehn, O., Fostel, J., Ghazal, P., Gibson, F., Gray, T., Grimes, G., Hancock, J. M., Hardy, N. W., Hermjakob, H., Julian, R. K., Kane, M., Kettner, C., Kinsinger, C., Kolker, E., Kuiper, M., Novère, N. L., Leebens-Mack, J., Lewis, S. E., Lord, P., Mallon, A.-M., Marthandan, N., Masuya, H., McNally, R., Mehrle, A., Morrison, N., Orchard, S., Quackenbush, J., Reecy, J. M., Robertson, D. G., Rocca-Serra, P., Rodriguez, H., Rosenfelder, H., Santoyo-Lopez, J., Scheuermann, R. H., Schober, D., Smith, B., Snape, J., Stoeckert, C. J., Tipton, K., Sterk, P., Untergasser, A., Vandesompele, J., and Wiemann, S. (2008). Promoting coherent minimum reporting guidelines for biological and biomedical investigations: the MIBBI project. *Nat. Biotechnol.* 26, 889–896.

Teutschbein, J., Albrecht, D., Pötsch, M., Guthke, R., Aimanianda, V., Clavaud, C., Latgé, J.-P., Brakhage, A. A., and Kniemeyer, O. (2010). Proteome profiling and functional classification of intracellular proteins from conidia of the human-pathogenic mold *Aspergillus fumigatus*. *J. Proteome Res.* 9, 3427–3442.

Theiss, S., Köhler, G. A., Kretschmar, M., Nichterlein, T., and Hacker, J. (2002). New molecular methods to study gene functions in *Candida* infections. *Mycoses* 45, 345–350.

Thomas, D. P., Bachmann, S. P., and Lopez-Ribot, J. L. (2006). Proteomics for the analysis of the *Candida albicans* biofilm lifestyle. *Proteomics* 6, 5795–5804.

Thywißen, A., Heinekamp, T., Dahse, H.-M., Schmaler-Ripcke, J., Nietzsche, S., Zipfel, P. F., and Brakhage, A. A. (2011). Conidial dihydroxynaphthalene melanin of the human pathogenic fungus *Aspergillus fumigatus* interferes with the host endocytosis pathway. *Front. Microbiol.* 2, 96. doi:10.3389/fmicb.2011.00096

Tierney, L., Linde, J., Müller, S., Brunke, S., Molina, J., Hube, B., Schöck, U., Guthke, R., and Kuchler, K. (2012). An interspecies regulatory network inferred from simultaneous RNA-seq of *Candida albicans* invading innate immune cells. *Front. Microbiol.* 3, 85. doi:10.3389/fmicb.2012.00085

Toepfer, S., Guthke, R., Driesch, D., Woetzel, D., and Pfaff, M. (2007). The NetGenerator algorithm: reconstruction of gene regulatory networks. *Lect. Notes Bioinform.* 4366, 119–130.

Tong, J. C., and Ng, L. F. P. (2011). Understanding infectious agents from an in silico perspective. *Drug Discov. Today* 16, 42–49.

Tuckwell, D., Denning, D. W., and Bowyer, P. (2011). A public resource for metabolic pathway mapping of *Aspergillus fumigatus* Af293. *Med. Mycol.* 49(Suppl 1), S114–S119.

Urban, C. F., Reichard, U., Brinkmann, V., and Zychlinsky, A. (2006). Neutrophil extracellular traps capture and kill *Candida albicans* yeast and hyphal forms. *Cell. Microbiol.* 8, 668–676.

Van Dyke Parunak, H., Savit, R., and Riolo, R. (1998). "Agent-based modeling vs. equation-based modeling: a case study and users' guide," in *Multi-Agent Systems and Agent-Based Simulation*, eds J. Sichman, R. Conte, and N. Gilbert, *Lecture Notes in Computer Science*, Vol. 1534 (Berlin: Springer), 277–283.

van het Hoog, M., Rast, T. J., Martchenko, M., Grindle, S., Dignard, D., Hogues, H., Cuomo, C., Berriman, M., Scherer, S., Magee, B. B., Whiteway, M., Chibana, H., Nantel, A., and Magee, P. T. (2007). Assembly of the *Candida albicans* genome into sixteen supercontigs aligned on the eight chromosomes. *Genome Biol.* 8, R52.

Vera, J., Rateitschak, K., Lange, F., Kossow, C., Wolkenhauer, O., and Jaster, R. (2011). Systems biology of JAK-STAT signalling in human malignancies. *Prog. Biophys. Mol. Biol.* 106, 426–434.

Vödisch, M., Albrecht, D., Lessing, F., Schmidt, A. D., Winkler, R., Guthke, R., Brakhage, A. A., and Kniemeyer, O. (2009). Two-dimensional proteome reference maps for the human pathogenic filamentous fungus *Aspergillus fumigatus*. *Proteomics* 9, 1407–1415.

Vödisch, M., Scherlach, K., Winkler, R., Hertweck, C., Braun, H.-P., Roth, M., Haas, H., Werner, E. R., Brakhage, A. A., and Kniemeyer, O. (2011). Analysis of the *Aspergillus fumigatus* proteome reveals metabolic changes and the activation of the pseurotin A biosynthesis gene cluster in response to hypoxia. *J. Proteome Res.* 10, 2508–2524.

Vodovotz, Y., Csete, M., Bartels, J., Chang, S., and An, G. (2008). Translational systems biology of inflammation. *PLoS Comput. Biol.*

4, e1000014. doi:10.1371/journal.pcbi.1000014

Volling, K., Thywissen, A., Brakhage, A. A., and Saluz, H. P. (2011). Phagocytosis of melanized *Aspergillus conidia* by macrophages exerts cytoprotective effects by sustained PI3K/Akt signalling. *Cell. Microbiol.* 13, 1130–1148.

Walker, D. C., and Southgate, J. (2009). The virtual cell – a candidate co-ordinator for 'middle-out' modelling of biological systems. *Brief. Bioinformatics* 10, 450–461.

Waltermann, C., and Klipp, E. (2010). Signal integration in budding yeast. *Biochem. Soc. Trans.* 38, 1257–1264.

Walther, M., Gebhardt, P., Grosse-Gehling, P., Würbach, L., Irmler, I., Preusche, S., Khalid, M., Opfermann, T., Kamradt, T., Steinbach, J., and Saluz, H.-P. (2011). Implementation of 89Zr production and in vivo imaging of B-cells in mice with 89Zr-labeled anti-B-cell antibodies by small animal PET/CT. *Appl. Radiat. Isot.* 69, 852–857.

Wang, Z., Gerstein, M., and Snyder, M. (2009). RNA-seq: a revolutionary tool for transcriptomics. *Nat. Rev. Genet.* 10, 57–63.

Wartenberg, D., Lapp, K., Jacobsen, I. D., Dahse, H.-M., Kniemeyer, O., Heinekamp, T., and Brakhage, A. A. (2011). Secretome analysis of *Aspergillus fumigatus* reveals Asp-hemolysin as a major secreted protein. *Int. J. Med. Microbiol.* 301, 602–611.

Whiteway, M., and Bachewich, C. (2007). Morphogenesis in *Candida albicans*. *Annu. Rev. Microbiol.* 61, 529–553.

Willard, H., and Ginsburg, G. (2009). *Genomic and Personalized Medicine. Number Vol. 2 in Genomic and Personalized Medicine.* Amsterdam: Academic Press.

Willger, S. D., Puttikamonkul, S., Kim, K.-H., Burritt, J. B., Grahl, N., Metzler, L. J., Barbuch, R., Bard, M., Lawrence, C. B., and Cramer, R. A. (2008). A sterol-regulatory element binding protein is required for cell polarity, hypoxia adaptation, azole drug resistance, and virulence in *Aspergillus fumigatus*. *PLoS Pathog.* 4, e1000200. doi:10.1371/journal.ppat.1000200

Wilson, D., Thewes, S., Zakikhany, K., Fradin, C., Albrecht, A., Almeida, R., Brunke, S., Grosse, K., Martin, R., Mayer, F., Leonhardt, I., Schild, L., Seider, K., Skibbe, M., Slesiona, S., Waechtler, B., Jacobsen, I., and Hube, B. (2009). Identifying infection-associated genes of *Candida albicans* in the postgenomic era. *FEMS Yeast Res.* 9, 688–700.

Wisplinghoff, H., Bischoff, T., Tallent, S. M., Seifert, H., Wenzel, R. P., and Edmond, M. B. (2004). Nosocomial bloodstream infections in US hospitals: analysis of 24,179 cases from a prospective nationwide surveillance study. *Clin. Infect. Dis.* 39, 309–317.

Woolhouse, M. E., Taylor, L. H., and Haydon, D. T. (2001). Population biology of multihost pathogens. *Science* 292, 1109–1112.

Xu, J., and Li, Y. (2006). Discovering disease-genes by topological features in human protein-protein interaction network. *Bioinformatics* 22, 2800–2805.

Yan, L., Zhang, J.-D., Cao, Y.-B., Gao, P.-H., and Jiang, Y.-Y. (2007). Proteomic analysis reveals a metabolism shift in a laboratory fluconazole-resistant *Candida albicans* strain. *J. Proteome Res.* 6, 2248–2256.

Yin, Z., Stead, D., Walker, J., Selway, L., Smith, D. A., Brown, A. J. P., and Quinn, J. (2009). A proteomic analysis of the salt, cadmium and peroxide stress responses in *Candida albicans* and the role of the Hog1 stress-activated MAPK in regulating the stress-induced proteome. *Proteomics* 9, 4686–4703.

Zhou, D., and He, Y. (2008). Extracting interactions between proteins from the literature. *J. Biomed. Inform.* 41, 393–407.

Zhu, M., Gao, L., Li, X., Liu, Z., Xu, C., Yan, Y., Walker, E., Jiang, W., Su, B., Chen, X., and Lin, H. (2009). The analysis of the drug-targets based on the topological properties in the human protein-protein interaction network. *J. Drug Target* 17, 524–532.

Conflict of Interest Statement: The authors declare that the research was conducted in the absence of any commercial or financial relationships that could be construed as a potential conflict of interest.

Received: 12 December 2011; accepted: 05 March 2012; published online: 02 April 2012.

*Citation: Horn F, Heinekamp T, Kniemeyer O, Pollmächer J, Valiante V and Brakhage AA (2012) Systems biology of fungal infection. Front. Microbio. **3**:108. doi: 10.3389/fmicb.2012.00108*

This article was submitted to Frontiers in Microbial Immunology, a specialty of Frontiers in Microbiology.

Copyright © 2012 Horn, Heinekamp, Kniemeyer, Pollmächer, Valiante and Brakhage. This is an open-access article distributed under the terms of the Creative Commons Attribution Non Commercial License, which permits non-commercial use, distribution, and reproduction in other forums, provided the original authors and source are credited.

4.2 Agent-based model of human alveoli predicts chemotactic signaling by epithelial cells during early *Aspergillus fumigatus* infection

OPEN ACCESS Freely available online

PLOS ONE

Agent-Based Model of Human Alveoli Predicts Chemotactic Signaling by Epithelial Cells during Early *Aspergillus fumigatus* Infection

Johannes Pollmächer[1,2], Marc Thilo Figge[1,2]*

1 Applied Systems Biology, Leibniz-Institute for Natural Product Research and Infection Biology, Hans Knöll Institute, Jena, Germany, **2** Friedrich Schiller University, Jena, Germany

OPEN ACCESS Freely available online

PLOS ONE

Agent-Based Model of Human Alveoli Predicts Chemotactic Signaling by Epithelial Cells during Early *Aspergillus fumigatus* Infection

Johannes Pollmächer[1,2], Marc Thilo Figge[1,2]*

1 Applied Systems Biology, Leibniz-Institute for Natural Product Research and Infection Biology, Hans Knöll Institute, Jena, Germany, **2** Friedrich Schiller University, Jena, Germany

Abstract

Aspergillus fumigatus is one of the most important human fungal pathogens, causing life-threatening diseases. Since humans inhale hundreds to thousands of fungal conidia every day, the lower respiratory tract is the primary site of infection. Current interaction networks of the innate immune response attribute fungal recognition and detection to alveolar macrophages, which are thought to be the first cells to get in contact with the fungus. At present, these networks are derived from *in vitro* or *in situ* assays, as the peculiar physiology of the human lung makes *in vivo* experiments, including imaging on the cell-level, hard to realize. We implemented a spatio-temporal agent-based model of a human alveolus in order to perform *in silico* experiments of a virtual infection scenario, for an alveolus infected with *A. fumigatus* under physiological conditions. The virtual analog captures the three-dimensional alveolar morphology consisting of the two major alveolar epithelial cell types and the pores of Kohn as well as the dynamic process of respiration. To the best of our knowledge this is the first agent-based model of a dynamic human alveolus in the presence of respiration. A key readout of our simulations is the first-passage-time of alveolar macrophages, which is the period of time that elapses until the first physical macrophage-conidium contact is established. We tested for random and chemotactic migration modes of alveolar macrophages and varied their corresponding parameter sets. The resulting first-passage-time distributions imply that randomly migrating macrophages fail to find the conidium before the start of germination, whereas guidance by chemotactic signals derived from the alveolar epithelial cell associated with the fungus enables a secure and successful discovery of the pathogen in time.

Citation: Pollmächer J, Figge MT (2014) Agent-Based Model of Human Alveoli Predicts Chemotactic Signaling by Epithelial Cells during Early *Aspergillus fumigatus* Infection. PLoS ONE 9(10): e111630. doi:10.1371/journal.pone.0111630

Editor: Joy Sturtevant, Louisiana State University, United States of America

Received June 20, 2014; **Accepted** October 2, 2014; **Published** October 31, 2014

Copyright: © 2014 Pollmächer, Figge. This is an open-access article distributed under the terms of the Creative Commons Attribution License, which permits unrestricted use, distribution, and reproduction in any medium, provided the original author and source are credited.

Data Availability: The authors confirm that all data underlying the findings are fully available without restriction. All relevant data are within the paper and its Supporting Information files.

Funding: This work was financially supported by the excellence graduate school Jena School for Microbial Communication (JSMC: https://www.jsmc.uni-jena.de/) and the CRC/TR124 FungiNet (http://www.funginet.de/), Project B4, which are both funded by the Deutsche Forschungsgemeinschaft (DFG). The funders had no role in study design, data collection and analysis, decision to publish, or preparation of the manuscript.

Competing Interests: The authors have declared that no competing interests exist.

* Email: thilo.figge@hki-jena.de

Introduction

Aspergillus fumigatus is the most frequently isolated invasive mould in clinical patients [1]. With an increasing number of severe infections over the last two decades this ubiquitous saprophytic fungus has become one of the most important fungal pathogens [2]. The fungus exhibits its pathogenic behaviour primarily in immunosuppressed individuals, leading to life-threatening diseases with invasive aspergillosis being the most lethal one [3,4]. Depending on the environmental conditions humans inhale several hundreds up to thousands of conidia of *A. fumigatus* every day [5]. Due to their small size of about 2–3 μm in diameter, a fraction of the inhaled conidia is able to evade the filter activity of the human lung and reaches the alveoli [6,7]. Here, conidia are controlled and eliminated predominantly by innate immune responses [8].

Alveolar macrophages (AM) are professional phagocytes of the innate immune system resident in alveoli, where they trigger immune-responses to a vast amount of inhaled substances and particles [9]. They are located on the surface of alveolar epithelial cells (AEC) and shielded from direct contact to the alveolar airspace by the thin surfactant film [10]. AM are able to detect and phagocytose resting and swollen conidia of *A. fumigatus*, whereas the swollen phenotype is a prerequisite for killing [8]. Typical *in vitro* assays of host-pathogen interaction use high cell densities [11,12], *i.e.* at any time phagocytes and pathogens are in close range and these unphysiological conditions render the experiments unrealistic with regard to the active search of phagocytes for pathogens. Similarly, animal models of aspergillus infection deal with the application of several millions of conidia in one shot in order to measure survival rates [12,13]. Such approaches do not reflect the actual physiological conditions under which aspergillosis develops and consequently important aspects of the host response, such as the dynamics of phagocytes searching for pathogens, are obscured. Due to the peculiar physiology of the human lung, various measures are also not directly accessible *in vivo*. For example, the migration mode and speed of AM could not be investigated today *in vivo*. *In vitro* studies of AM motility [10,11]

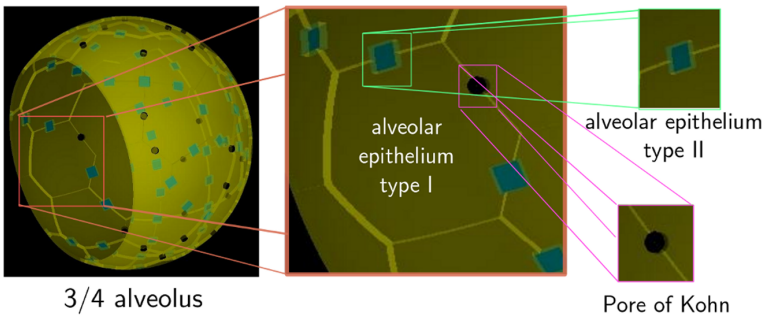

Figure 1. Three-dimensional reconstruction of the human three-quarter alveolus. Based on a literature survey (parameters are shown in Table 1) we reconstructed the spatial environment of one typical human alveolus, including the spherical shape of the system, the two major AEC types present in alveoli and the pores of Kohn as interalveolar connections (see Video S1).
doi:10.1371/journal.pone.0111630.g001

generally revealed low speeds of AM with an average value of four micrometer per minute under chemotactic conditions [14]. Nevertheless, it may well be that AM present their true migration activity only in their natural environment.

By means of agent-based modelling and computer simulation we are in the position to study the early immune response in human alveoli by establishing a virtual infection model in space and time. This is similar to the virtual infection model for *Candida albicans* in human blood that was recently established by [15] to quantify immune effector mechanisms. Two important aspects regarding the early immune response upon the encounter with *A. fumigatus* have been investigated *in silico*. One aspect of phagocyte activity is the search strategy allowing to rapidly find the pathogen and to efficiently clear the infection. This was studied before by [16] and [17] using agent-based modelling. Tokarski *et al.* compared the performance of various search strategies by measuring the amount of pathogens that were phagocytozed by a large number of phagocytes in the course of time, whereas Charnick *et al.* investigated single phagocyte-pathogen encounters for varying search strategies. Both models comprise active phagocyte migration with and without chemotactic signalling on a two-dimensional grid representing the surface of the lung, but do not account for the three-dimensional morphology and peculiar boundary conditions of alveoli.

In this study, we put special emphasis on the spatio-temporal reconstruction of the human alveolus, including the spherical morphology [18], the composition of the alveolar surface by AEC type I and type II cells [19] and the pores of Kohn, representing connections between adjacent alveoli [20]. We investigate the dynamics of the alveolus under typical respiration conditions and for potential active migration modes of AM during the early immune response. An important readout of our simulations is the *first-passage time* (FPT), *i.e.* the time required for a phagocyte to find a pathogen in this complex biological structure. It is well known that analytical solutions for the FPT probability distribution can only be obtained for relatively simple systems with low spatial dimensions, whereas for higher spatial dimensions and complex geometries only the mean value of the FPT may be analytically tractable [21]. Therefore, computer simulations are required to numerically retrieve the distribution of FPT in the agent-based model. In combination with typical times of *A. fumigatus* germination, it is possible to assess the migration behaviour of AM with regard to infection clearance. Our results clearly indicate that random migration of AM is not an adequate type of migration for searching alveoli and detecting conidia before germination starts. In order to realize this in time, chemotactic signals are required that guide AM toward positions of conidia and we propose how this prediction could be tested in experiment.

Model

A spatio-temporal agent-based model is implemented to perform *in silico* experiments on first-passage-time (FPT) measurements for *A. fumigatus* conidia being found by AM in alveoli. We take advantage of a cell-scale model, where each single cell of the system is represented by one discrete entity in the computer. In what follows, we present a detailed description of each cell-type, *i.e.* its static and dynamic attributes, as well as of the biological environment.

Setup of the alveolus

The three-dimensional spatial environment of the model represents a typical human alveolus. The morphology of alveoli is polyhedral, resulting in a large surface-to-volume ratio in comparison to a sphere [10]. Previous *in silico* models, e.g. for aerosol transport and particle deposition in the human lung [22], were successfully based on a sphere-approximation of alveoli. A geometrical structure with spherical symmetry is most convenient for computational simulation models as the surface can be mathematically represented using spherical coordinates and was also used in the present study. We consider the most frequent case in human beings, corresponding to a three-quarter spherical alveolus [18] of radius $r_{\mathrm{Alv,min}}$ in the deflated state (see Fig. 1 and Video S1). The alveolus is constructed from a full sphere with surface points $\vec{x}=(r_{\mathrm{Alv,min}},\vartheta,\varphi)$ that is reduced to a three-quarter sphere regarding the volume fraction by using a lower threshold ϑ_c of the polar angle $\vartheta_c \le \vartheta \le \pi$. The alveolar entrance ring is defined by the positions $\vec{x}_{\mathrm{entrance}}=(r_{\mathrm{Alv,min}},\vartheta_c,\varphi)$ with $\varphi\in[0,2\pi)$.

Based on a literature survey on alveolar ducts (see Table 1), we reconstruct the cell-types belonging to the alveolar epithelium and the pores of Kohn, which represent inter-alveolar connections between neighbouring alveoli (see Fig. 1). Cell-numbers are estimated from the proportions of surface coverage and their respective sizes. To realize a realistic construction of the alveolus we proceed as follows. We first place centroids of type I AEC on the surface of the three-quarter sphere in a close-to-equidistant fashion (see Text S1 further details). Next, a Voronoi tesselation based on these centroids is projected onto the spherical surface of the alveolus to obtain type I AEC on the curved geometry as

Table 1. Model parameters for entities in the human alveolus.

parameter	description	value	comments
$r_{\mathrm{Alv,min}}$	radius of one alveolus in deflated state	$116.5\,\mu$m	[22]
n_{Alv}	overall number of alveoli in adult human	4.8×10^{8}	[36]
V_{AECT1}	volume of alveolar epithelial type I cells	$2391\,\mu\mathrm{m}^3$	[37]
V_{AECT2}	volume of alveolar epithelial type II cells	$815\,\mu\mathrm{m}^3$	[37]
n_{AECT1}	number of alveolar epithelial type I per alveolus	39–45	estimation
n_{AECT2}	number of alveolar epithelial type II per alveolus	74–84	estimation
r_{PoK}	radius of one pore of Kohn	$2.99\,\mu$m	[38], estimation
n_{PoK}	number of pores of Kohn per alveolus	24	[38]

doi:10.1371/journal.pone.0111630.t001

depicted in Fig. 1. Alveolar epithelial type II cells have a cuboidal shape and are randomly placed at the edges of neighbouring type I cells. A similar random procedure is used for positioning pores of Kohn with cylindrical shape (see Fig. 1). Note that pores of Kohn as well as the alveolar entrance ring represent open boundaries of the system through which AM can enter or exit the alveolus. The distributed open boundaries of the system strongly contribute to the complexity of alveoli.

The alveolus with constant radius $r_{\mathrm{Alv,min}}$ is extended by the implementation of two respiration modes, referred to as *resting condition* and *heavy exercise*, that differ in the respiration frequencies and spherical maximum radii (see Table 2 for values). The volume change of the alveolus by inflation and deflation during each respiration cycle is assumed to occur with equal time intervals for inspiration and expiration. We incorporate the increase and the decrease of the three-quarter sphere by periodically changing its time-dependent radius $r_{\mathrm{Alv}}(t)$ according to a piecewise linear function for the gain and the loss in the alveolar volume:

$$V_{\mathrm{Alv}}(t)=V_{\min}+(V_{\max}-V_{\min})\times(1-2|(tf_{\mathrm{Alv}}-\lfloor tf_{\mathrm{Alv}}\rfloor)-0.5|). \quad (1)$$

Here, f_{Alv} denotes the respiration frequency and $V_{\min}$ and $V_{\max}$ are the volumes of the three-quarter sphere in the deflated and inflated state, respectively.

Passive movement of *A. fumigatus* conidia

We account for the passive movement of conidia that is induced by the contraction and expansion of the alveolus due to respiration. This is modeled by random walk migration with a speed that depends on the difference between the minimum radius $r_{\mathrm{Alv,min}}$ and the maximum radius $r_{\mathrm{Alv,max}}$ of the alveolus, on the frequency of respiration f_{Alv} and on the radius of the conidium $r_{\mathrm{con}}=1.25\,\mu$m:

$$v_{\mathrm{con}}=r_{\mathrm{con}}f_{\mathrm{Alv}}(r_{\mathrm{Alv,max}}/r_{\mathrm{Alv,min}}-1). \quad (2)$$

This speed value assures that - in going from the deflated to the inflated state of the alveolus - the displacement d_{con} of the conidium during one respiratory cycle does not exceed the maximum value $d_{\mathrm{con,max}}=0.5v_{\mathrm{con}}/f_{\mathrm{Alv}}$. As follows from the theorem of intersecting lines, $d_{\mathrm{con,max}}$ corresponds to the radius of the additional area that becomes available to the location of the conidium by the expansion of the alveolus.

Active migration of alveolar macrophages

AM migrate on the surface of the AEC inside the alveolus and can enter or exit it via the entrance ring or the pores of Kohn. In the agent-based model, this is realized by migration vectors that connect positions on the inner surface of the three-quarter sphere. Migration vectors represent arc-elements to meet the bound-to-surface condition and have a geodesic length of $v\Delta t$, where v is the

Table 2. Model parameters for the static case and the two breathing conditions.

		values			
			resting	heavy	
parameter	description	static	condition	exercise	unit
Δt	global timestep of the simulation	0.1	0.001	0.001	min
$r_{\mathrm{Alv,min}}$	radius of one alveolus in deflated state	116.5	116.5	116.5	μm
$r_{\mathrm{Alv,max}}$	radius of one alveolus in expanded state	116.5	125	136.5	μm
f_{Alv}	frequency of respiration	0	12	26	min^{-1}
v_{con}	turbulence speed of *A. fumigatus*	0	2.19	11.16	μm/min
n	number of simulation runs per parameter-set	10^5	10^3	10^3	

doi:10.1371/journal.pone.0111630.t002

specified speed of the AM and Δt is the timestep. A migration vector $\Delta\vec{s}$ from a given position $(x,y,z)_{\text{cart}}=(r,\vartheta,\varphi)_{\text{spher}}$ on the surface of the sphere is computed by

$$\Delta\vec{s}(\alpha,v,\Delta t)=\begin{pmatrix}\cos\varphi & -\sin\varphi & 0\\ \sin\varphi & \cos\varphi & 0\\ 0 & 0 & 1\end{pmatrix}\begin{pmatrix}\cos\vartheta & 0 & \sin\vartheta\\ 0 & 1 & 0\\ -\sin\vartheta & 0 & \cos\vartheta\end{pmatrix}\begin{pmatrix}r\sin\left(\frac{v\Delta t}{r}\right)\cos\alpha\\ r\sin\left(\frac{v\Delta t}{r}\right)\sin\alpha\\ r(\cos\left(\frac{v\Delta t}{r}\right)-1)\end{pmatrix}, \quad (3)$$

where α is the direction angle, comparable to the polar angle in a two-dimensional polar coordinate system.

We implemented two migration modes for AM: (i) persistent random walk (PRW) and (ii) biased persistent random walk (BPRW). The PRW is realized by randomly choosing a new direction α_{rand} from a uniform distribution over $[0,2\pi)$ after expiration of the persistence time t_{P}. In each timestep $\Delta\vec{s}_{\text{rand}}=\Delta\vec{s}(\alpha_{\text{rand}},v,\Delta t)$ is computed to account for the curvature of the alveolus. We implemented this migration model for constant speed v and constant persistence time t_{P}.

The BPRW assumes that the migration of AM is not purely random but is biased by additional signals. This means that the cell follows the combination of the random migration vector $\Delta\vec{s}_{\text{rand}}$ and the signal migration vector $\Delta\vec{s}_{\text{sig}}$ that will be described in the next paragraph. The relative contributions of the two vectors depend on the geodesic distance of the AM from the signal source.

Chemotactic signalling by alveolar epithelial cells

The signal that induces the BPRW is derived from the AEC being in close contact with the conidium. We assume chemokine secretion from either type I or type II AEC in order to direct AM to itself as shown in Fig. 2. The distribution of the secreted molecules follows a two-dimensional diffusion equation with constant source term. We use the steady state solution for the planar case (see Text S1), where the concentration gradient only depends on the distance d from the source and is proportional to d^{-1}. AM migrate with probability $p_{\text{sig}}(d)$ in the direction of the gradient until they reach the AEC associated with the conidum:

$$p_{\text{sig}}(d)=\begin{cases}0 & \text{for } d<r_0\\ r_0/d & \text{for } d\geq r_0\end{cases}. \quad (4)$$

Here, d is the geodesic distance from the source of the signal to the centroid of the AM and r_0 defines the radius of a circular shape with the centroid of the occupied AEC as origin. For our studies we set $r_0=30\,\mu$m and $5.27\,\mu$m, respectively, for the typical radii of AEC of type I and type II. The resulting migration vector for BPRW is computed as follows: First, we apply the relative contributions of random migration

$$\Delta\vec{s}_{\text{rand}}=\Delta\vec{s}(\alpha_{\text{rand}},(1-p_{\text{sig}}(d))v,\Delta t) \quad (5)$$

and directed migration

$$\Delta\vec{s}_{\text{sig}}=\Delta\vec{s}(\alpha_{\text{sig}},p_{\text{sig}}(d)v,\Delta t) \quad (6)$$

in random order. Since the resulting shift of their linear combination has not necessarily a geodesic length of $v\Delta t$, we scale to the geodesic length that corresponds to speed v. As in the case of PRW, the direction angles α_{rand} and α_{sig} are updated after the persistence time t_{p} has elapsed. By using the function $p_{\text{sig}}(d)$ we set a vanishing gradient on the AEC associated with the conidium, assuming a fairly homogeneous chemokine-concentration on the AEC leading to a random migration within the distance r_0. Outside this circular area of radius r_0, the strength of the gradient is used as a measure for the impact of directed migration.

Distribution of cells in the alveolus

Assuming that n_{AM} AM are distributed randomly over the n_{Alv} alveoli in the human lung, a n_{AM}-ary Bernoulli experiment with $p=1/n_{\text{Alv}}$ leads to a Binomial distribution

$$B_{\text{AM}}(n_{\text{AM}},p,k)=\binom{n_{\text{AM}}}{k}p^k(1-p)^{n_{\text{AM}}-k}, \quad (7)$$

denoting the probability of having k AM per alveolus. For the n_{con} *A. fumigatus* conidia we derive with the same approach the probability $B_{\text{con}}(n_{\text{con}},p,j)$ for j conidia per alveolus. In Table 3 we present the values for parameters used in formula 7.

Dynamics and boundary conditions

The alveolus consists of two different types of boundaries, where AM can enter and exit: the alveolar entrance ring and the pores of Kohn. We implemented absorbing boundaries with a constant input rate λ_{in} in order to reproduce the Binomial distribution of AM at any time $t\geq 0$ *in silico*. A migrating AM is removed from the virtual alveolus as soon as its centroid has crossed one of the boundary segments. For each parameter combination of AM speed and persistence time the input parameter λ_{in} is calibrated to the corresponding Binomial distribution of AM per alveolus (see Text S1). An AM enters the alveolus after the exponentially distributed waiting time

$$t_{\text{wait}}=\frac{1}{\lambda_{\text{in}}}\ln\left(\frac{1}{u}\right), \quad (8)$$

is elapsed. Here, u is a uniformly distributed variate in $(0,1]$. Note that we always draw a new waiting time after the previous waiting time is elapsed. The position of AM insertion into the system follows a uniform random distribution over the length of the line elements belonging to all boundaries. If the position at the boundary is occupied by either an AM or the conidium, we reject that position and choose a new one until a non-occupied boundary position is found.

Virtual infection scenario and first-passage-time measurements

We vary the corresponding parameter sets in typical ranges in order to analyze the resulting FPT. The Binomial distribution for the number of conidia per alveolus gives evidence for only one conidium in one alveolus as by far the most probable situation in non-empty alveoli. The alveolus is constructed by randomly placing the AEC and the pores of Kohn as explained in the paragraph *Setup of the alveolus*. We start simulating at time $t = 0$, at which the conidium has entered the alveolus. The number of initial AM is chosen according to the Binomial distribution of AM per alveolus. These AM are placed randomly over the entire surface of the three-quarter sphere. The system dynamics is

simulated over time until the first physical cell-cell contact is detected between one of the AM and the conidium of *A. fumigatus*. This is the event of first passage and the time associated with it is referred to as first-passage-time (FPT). The whole scenario is repeated n times for each parameter configuration to account for the stochasticity in the computer simulations of the agent-based model (see Table 2). From the distribution of FPT for a given parameter configuration, we calculate the mean, the standard deviation and the median. The results are compared with the typical time of six hours required for *A. fumigatus* conidia to germinate [23]. In the unlikely event that a conidium exits the alveolus due to passive movement in the presence of breathing, the simulation is discarded and a new one is initiated.

Algorithm and implementation

A general object-oriented framework for agent-based simulations is implemented in the programming language C++. We apply an asynchronous random order updating scheme to integrate the dynamics of the system over time [24]. Here, for each timestep a uniform random permutation $\sigma_{N_{\mathrm{Cell}}}$ of all cells present in the system at time t (N_{Cell}) is generated. The flowchart of the agent-based simulation framework is presented in Fig. 3.

The handling of interactions is divided into two parts: First, the currently enabled interactions have to be detected and, second, they are executed. Two dynamic cells interact if their associated spheres overlap or touch each other. Here, we implement a mechanism that avoids overlaps between the spheres of the cells by shifting the most recently moved cell back to a position where it only touches its interaction partner. The simulation ends in the case of an AM touching a conidium for the first time.

Simulations are carried out on a SUSE Linux Enterprise Server version 11 on a x86-64 architecture with 512 GB RAM and 48 AMD Opteron processors, each running on 1781 MHz. Run-time measurements are presented in Table S1. We effectively reduce the run-time over n repetitions by executing FPT simulations in parallel.

Results

Virtual infection model reveals most probable configuration

The *in silico* experiments were performed for a three-quarter spherical alveolus corresponding to the configuration with highest frequency of occurrence in humans [18]. Alveolar macrophages (AM) were positioned in the alveolus and could migrate on the inner surface and enter or exit the alveolus via the alveolar entrance ring and the pores of Kohn (see Fig. 1 and Video S1). The Binomial distribution of AM in the alveolus was obtained as the result of balancing stochastic AM exiting from the alveolus by fitting a constant input rate λ_{in} of AM entering the alveolus (Table S2). This input rate was calibrated for each set of migration parameters, *i.e.* AM speed and persistence time, but were found to be fairly independent of the applied migration mode and breathing scenario (see Figs. 4A and S1).

The resulting fits to the Binomial distribution are presented in Fig. 4A for two different sets of migration patterns. We found that each alveolus is on average occupied by 4.4 ± 2.1 AM over time. As can be seen in Fig. 4B by far the most of all alveoli do not contain a conidium, irrespective of the inhaled dose within the tested range of 10^3 to 10^6 conidia. Of all alveoli that do contain conidia, the configuration with one single conidium is by far the most probable one and it is more than three orders of magnitude less probable to find an alveolus with two or more conidia. The most probable configuration as revealed by the virtual infection model, therefore, corresponds to an alveolus with one conidium and a dynamically varying number of about two to seven AM. In other words, the relevant physiological scenario that we will focus on in the following resembles the problem of finding the needle in the haystack within a time limit that is set by the germination time of about six hours for *A. fumigatus* conidia.

Randomly migrating AM do not find fungal conidia before germination

Since it is not possible to observe AM migration *in vivo* with today's imaging techniques, nothing is known about their migration behaviour under physiological conditions. However, the virtual infection model allows investigating different hypotheses for AM migration. Here, we started with the hypothesis that AM perform a persistent random walk (PRW) and we scanned the parameter space, which is spanned by the constant speed and persistence time, within reasonable ranges of the parameter values.

A simulation was performed starting from a random initial configuration, *i.e.* the spatial arrangement of alveolar epithelial cells (AEC) forming the alveolus and of the pores of Kohn were randomly chosen within the three-quarter spherical alveolus. Furthermore, the initial condition with regard to the number and position of AM as well as the position of the conidium were also randomly set. We computed the first-passage-time (FPT), *i.e.* the minimal time it takes an arbitrary AM to find the conidium in the alveolus, and repeated this simulation for 10^5 random realizations (Video S2).

In Fig. 5, we show the result of the FPT distribution for a PRW with parameter values speed $v = 4\ \mu\mathrm{m/min}$ and persistence time $t_p = 2\ \mathrm{min}$. Of note, these distributions typically show long tails, such that despite of the peak value with a FPT well below six hours the probability to find the conidium at more than six hours post infection, $p(\mathrm{FPT} > 6\ \mathrm{h}) = 0.68$, is relatively high. In fact, the median and mean of this distribution was found to be 11.5 hours and 17.5 hours, respectively, thus, reaching inacceptable high values of the order of one day.

The results of a systematic investigation of the parameter space for the migration mode PRW are presented in Fig. 6A–C in terms of the mean, the median and the probability $p(\mathrm{FPT} > 6\ \mathrm{h})$. Here, we scanned the parameter values in the range $4\ \mu\mathrm{m/min} \le v \le 10\ \mu\mathrm{m/min}$ and $0.5\ \mathrm{min} \le t_{\mathrm{p}} \le 4\ \mathrm{min}$. It is observed that the mean FPT and the median FPT decrease with increasing speed and/or persistence time. For example, for a speed of $10\ \mu\mathrm{m/min}$ and a persistence time of $4\ \mathrm{min}$, the mean FPT reaches values below three hours. However, even for these extremely high values, the probability that the conidium is not found within six hours post infection remains at relatively high values of 15%.

In addition to studying static alveoli, we also investigated two breathing conditions – referred to as resting and heavy exercise – that differ in the breathing frequency and in the dynamic change of the alveolar volume (see Table 1 and Video S3). As explained in detail in the Model section, breathing conditions are associated with the passive random movement of the *A. fumigatus* conidium due to expansion of the inner surface of the alveolus. The results are shown in Fig. 6A–C by the dashed (resting condition) and dotted (heavy exercise) lines. It is observed that, while the overall change compared with the static alveolus is small, the induced random migration of the conidium generally has a prolonging effect on the mean and median of the FPT as well as on increasing effect on the probability $p(\mathrm{FPT} > 6\ \mathrm{h})$. This result can be explained by the fact that the surface area during each cycle of breathing is increased compared with the static case of the deflated state alveolus. Correspondingly, the observed deviations are larger

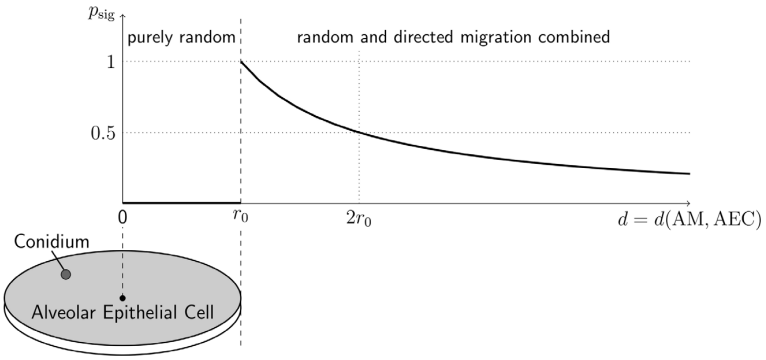

Figure 2. Chemotaxis model for signalling alveolar epithelial cells. Probability of directed migration by AM towards the AEC associated with the conidium as a function of geodesic distance *d* between the centroids of the AEC and the AM. See text for details.
doi:10.1371/journal.pone.0111630.g002

for the heavy exercise condition than for the resting condition. However, the main result of investigating breathing conditions is that their general impact on the FPT is small.

Virtual infection model predicts chemoattraction of alveolar macrophages

To accomplish the task of finding the needle in a haystack within a time limit, we investigated a second migration mode of AM assuming that they are directed towards the conidium by chemokines released from AEC. More specifically, it is assumed that the AEC associated with the conidium senses the pathogen and in response releases a chemoattractant that diffuses in the surfactant on the inner surface of the alveolus and guides AM the way to the AEC (see Fig. 2). Once a randomly migrating AM detects the chemotactic gradient, it becomes attracted to the respective AEC and arriving at this cell continues with a random search for the conidium on its surface (see Video S4). Since this migration mode is both random and transiently directed (see Eqs. 5 and 6), we refer to it as biased persistent random walk (BPRW).

In Fig. 6D–F, we present the results of FPT measurements for the BPRW. In comparison with the PRW (see Fig. 6A–C), it is observed that the mean and the median of the FPT were significantly reduced by one order of magnitude. Only in the case of very small speed values for AM, e.g. $v = 2\ \mu\text{m/min}$, we found for the probability $p(\text{FPT} > 6\ \text{h}) > 10\%$ over the whole range of tested persistence times. In general, this AM migration mode does accomplish the task of finding the conidium reasonably well, because $p(\text{FPT} > 6\ \text{h})$ remains well below 5% for all combinations of $v \geq 4\ \mu\text{m/min}$ and $t_p \geq 1\ \text{min}$. These observations remained again largely unchanged for both breathing conditions (see Fig. 6D–F), which motivated us to concentrate on the static alveolus in what follows.

As mentioned above, for this migration mode the FPT consists of two parts: First, randomly migrating AM are biased by the chemotactic signal attracting them towards the AEC associated with the conidium and the duration of time that this process takes was measured by t_{sig}. Second, the search for the conidium on the respective AEC obeys a persistent random walk and is associated with the time duration t_{rand}. We analyzed the relative contributions of these time durations for different parameter values of speed and persistence time by computing the time fraction of the purely random migration on the AEC, i.e. $\tau_{\text{rand}} = t_{\text{rand}}/(t_{\text{sig}} + t_{\text{rand}})$, and that of the chemotactic migration towards this AEC: $\tau_{\text{sig}} = t_{\text{sig}}/(t_{\text{sig}} + t_{\text{rand}})$. This computation was done in retrospect for the AM that successfully found the conidium. The results for selected speeds of 4 and $10\ \mu\text{m/min}$ and selected persistence times of 1 and $4\ \text{min}$ are presented in Fig. 7. In agreement with our earlier observations for PRW migration in the alveolus, we find that higher AM speeds and/or persistence times also reduce τ_{rand} relative to τ_{sig}, if the random search is restricted to a single AEC. Thus, low speed values and/or persistence times result in the major contribution to the FPT associated with the random search of AM on the AEC.

Next, we computed the distance corresponding to a geodesic in the spherical geometry denoting the shortest distance between the conidium and the successful AM on first occurrence in the system (see Fig. 8A and B). It is observed that for both migration modes the average geodesic distances typically level off at about $250\ \mu\text{m}$, implying that successful AM are closer to the conidium than one third of the circumference of the spherical alveolus. The magnitude of this distance is consistent with theoretical estimates for maximal communication distances between single cells by chemokines [25]. Furthermore, geodesic distances for higher persistence times or higher speeds are larger suggesting advantages

Table 3. Model parameters for human alveolar macrophages.

parameter	description	value	comments
V_{AM}	volume	$4989.9\ \mu\text{m}^3$	[39]
r_{AM}	radius	$10.6\ \mu\text{m}$	[39]
ρ_{AM}	surface density	$29.4\ \text{mm}^{-2}$	[40]
n_{AM}	overall number	2.1×10^9	[40], estimation

doi:10.1371/journal.pone.0111630.t003

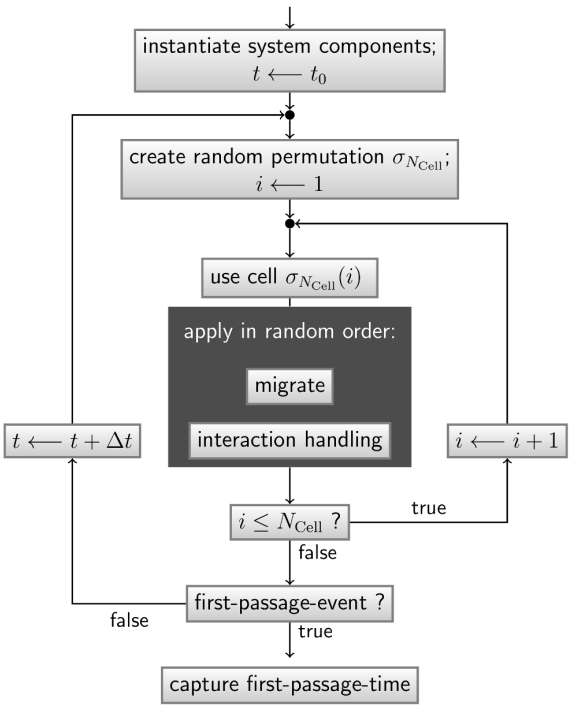

Figure 3. Flowchart of the agent-based simulation procedure for first-passage-time measurements. Integration of the system dynamics over time with timestep Δt by using an asynchronous random order updating scheme [24]. Here, the recording of one first-passage-time sample is shown. N_{Cell} is the total number of cells in the system at time t and σ_m denotes a uniform random permutation of m elements. See text for further details.
doi:10.1371/journal.pone.0111630.g003

for a fast exploration of the spatial environment, thus, having reduced FPT.

Search strategies of AM disentangled

The virtual infection model allows for the disentanglement of AM search strategies. This is achieved by comparing the two migration modes through an in-retrospect analysis of AM properties that successfully found the conidium. In other words, we investigated what was special about the AM that accomplished the task of finding the needle in a haystack most quickly. The results of this analysis are summarized in Fig. 8, where we computed the retention time distribution, *i.e.* the distribution of times that the successful AM was in the system. Interestingly, we found that this distribution is diverging at short time durations for the PRW resembling an exponential distribution. This is shown in Fig. 8C and D for two different sets of parameter values $(v; t_{\mathrm{p}}) = (4\ \mu\mathrm{m/min}; 1\ \mathrm{min})$ and $(v; t_{\mathrm{p}}) = (10\ \mu\mathrm{m/min}; 4\ \mathrm{min})$. In contrast, in the case of the BPRW this distribution showed a peak at some finite time and this peak time was lower for higher values of speed and/or persistence time. This suggests that in the case of PRW migration, successful AM were mostly those that happened to enter the alveolus at entry points close to the position of the conidium and could find them right away. Inspecting again the geodesic distances – being the shortest distance between the successful AM on first occurrence in the system and the conidium – confirms this interpretation. As can be seen in Fig. 8A and B, the distance of the successful AM that performed PRW migration is vanishing, whereas for BPRW migration this distance remains finite. The average geodesic distance of the successful AM from the conidium for $(v; t_{\mathrm{p}}) = (4\ \mu\mathrm{m/min}; 1\ \mathrm{min})$ was found to be 52.8 μm for the PRW and attained a higher value of 77.7 μm for the BPRW (see Fig. 8A). Similarly, for $(v; t_{\mathrm{p}}) = (10\ \mu\mathrm{m/min}; 4\ \mathrm{min})$ we found an average geodesic distance of 83.6 μm for the PRW and 82.0 μm for the BPRW (see Fig. 8B).

These observations were further investigated by averaging over the mean values extracted for each of the 20 parameter combinations, *i.e.* $(t_{\mathrm{p}}, v) \in \{0.5,1,2,4\}\ \mathrm{min} \times \{2,4,6,8,10\}\ \mu\mathrm{m/min}$. This revealed the geodesic distance of the successful AM from the conidium to be $d^{\mathrm{PRW}}_{\mathrm{geodesic}} = 60.3 \pm 10.2\ \mu\mathrm{m}$ for the PRW and to attain the significantly higher value of $d^{\mathrm{BPRW}}_{\mathrm{geodesic}} = 78.1 \pm 2.4\ \mu\mathrm{m}$ for the BPRW. Thus, the successful AM performing PRW start closer to the conidium than is the case for the BPRW, but this proximity can only be realized by random entries into the alveolus (via the alveolar entrance ring or the numerous pores of Kohn). Since it is statistically more likely that AM enter the system within the area defined by the larger distance, $d^{\mathrm{BPRW}}_{\mathrm{geodesic}} > d^{\mathrm{PRW}}_{\mathrm{geodesic}}$, the successful AM of the BPRW will find the conidium earlier than the successful AM of the PRW. This also explains why the FPT of AM that are migrating by a PRW is significantly longer: they do not find their target by capability but mostly by the luck of a fortunate initial condition or of entering the alveolus at an entry point being close to the conidium. In contrast, for BPRW migration the impact of luckily entering the alveolus close to the conidium is less important and AM find their target more by the capability of following the chemotactic signal.

Discussion

In this study, we investigated the early immune response to *A. fumigatus* infection involving the recognition of conidia by alveolar macrophages (AM). Computer simulations of a realistic agent-based model for the human alveolus predicted that randomly migrating AM will not find a conidium before germination. The results provided strong evidence that chemotactic signals released by the alveolar epithelial cell (AEC) associated with the conidium are required to comply with the widely accepted role of AM in the detection and recognition of conidia during the early immune response [10,26].

Due to the peculiar physiology of the human lung and the small number of conidia relative to the number of alveoli, the infection scenario is not directly observable *in vivo* under realistic conditions. Therefore, computer simulations of the agent-based model providing the distribution of first-passage-time (FPT) as simulation readout of the virtual infection scenario for varying parameters of different AM migration modes represent a most appropriate approach for this feasibility study. The human alveolus was implemented in the agent-based model as a three-quarter sphere, *i.e.* corresponding to the most common alveolar structure [18], with type I and type II AEC as well as pores of Kohn of realistic morphologies and population numbers [19]. As the number of interacting cells involved in the simulations is low, the model may appear simple on first sight; however, the complexity of the model is associated with the system's open boundaries. Since AM can only exit the alveolus by approaching the entrance ring or the randomly positioned pores of Kohn, balancing the equilibrium distribution is a critical issue in this dynamic system and was solved by the concept of waiting times for entering AM. To the best of our knowledge this is the first agent-based model of a human alveolus in the presence of respiration.

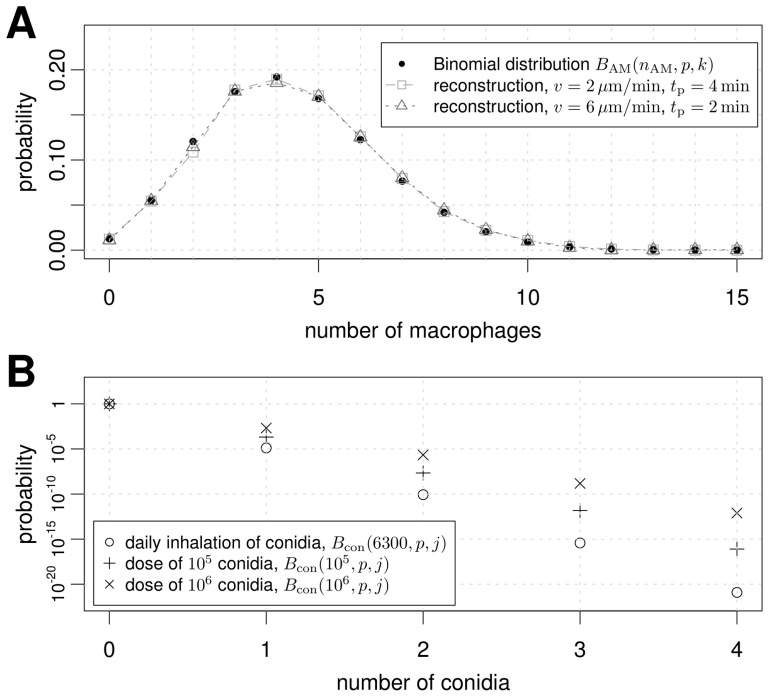

Figure 4. Number of conidia and alveolar macrophages per alveolus. A Binomial distribution is used to get insight into the number of cells per alveolus. (A) The probability distribution of AM per alveolus derived from their overall number (see Table 3) is shown in blue. The quality of the calibration can be seen by means of two example simulations of the persistent random walk migration mode with breathing being disabled. (B) Probability for the distribution of *A. fumigatus* in one alveolus is plotted on a logarithmic scale. Different typical doses as used in experiments are plotted for comparison. Daily inhalation refers to a dose of 6300 conidia, which is taken as the upper threshold of the lungs' daily exposure toward *A. fumigatus*.
doi:10.1371/journal.pone.0111630.g004

At first, we computed the FPT distribution for a persistent random walk as migration mode of AM. For reasonable AM speed values of 4 μm/min, we obtained relatively high FPT values of 10–48 hours on average for persistence times in the range of 0.5–4 minutes. This result has two possible implications: (i) the role of AM in *A. fumigatus* infection, which recently was controversially discussed [13,26], may be overestimated or (ii) the persistent random walk (PRW) hypothesis may not be valid for AM migration. Therefore, in a second step, we investigated the possibility that AM perform a biased persistent random walk, *i.e.* AM migration is not purely random but guided by chemotaxis towards the AEC that is associated with the conidium. In this case, our computer simulations revealed a significant drop in the FPT of about one order of magnitude. In particular, for reasonable AM

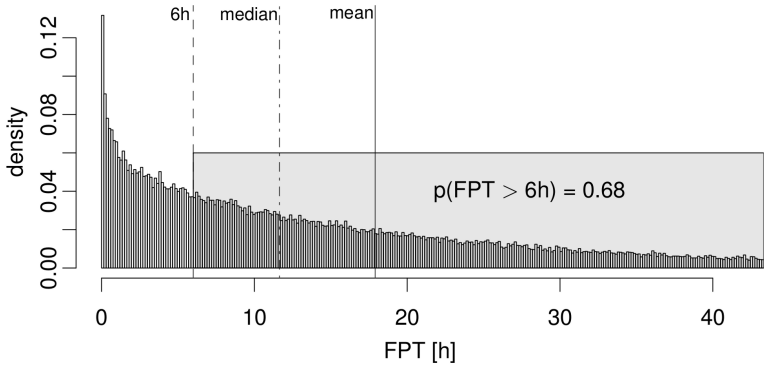

Figure 5. Typical measures of the first-passage-time density distribution used in this study. Here, we show an example-distribution for a persistent random walk scenario with the parameters $v = 4$ μm/min and $t_{\mathrm{p}} = 2$ min based on 10^5 samples (the corresponding distribution for biased persistent random walk is shown in Fig. S2). One sample of these simulations can be viewed in Video S2.
doi:10.1371/journal.pone.0111630.g005

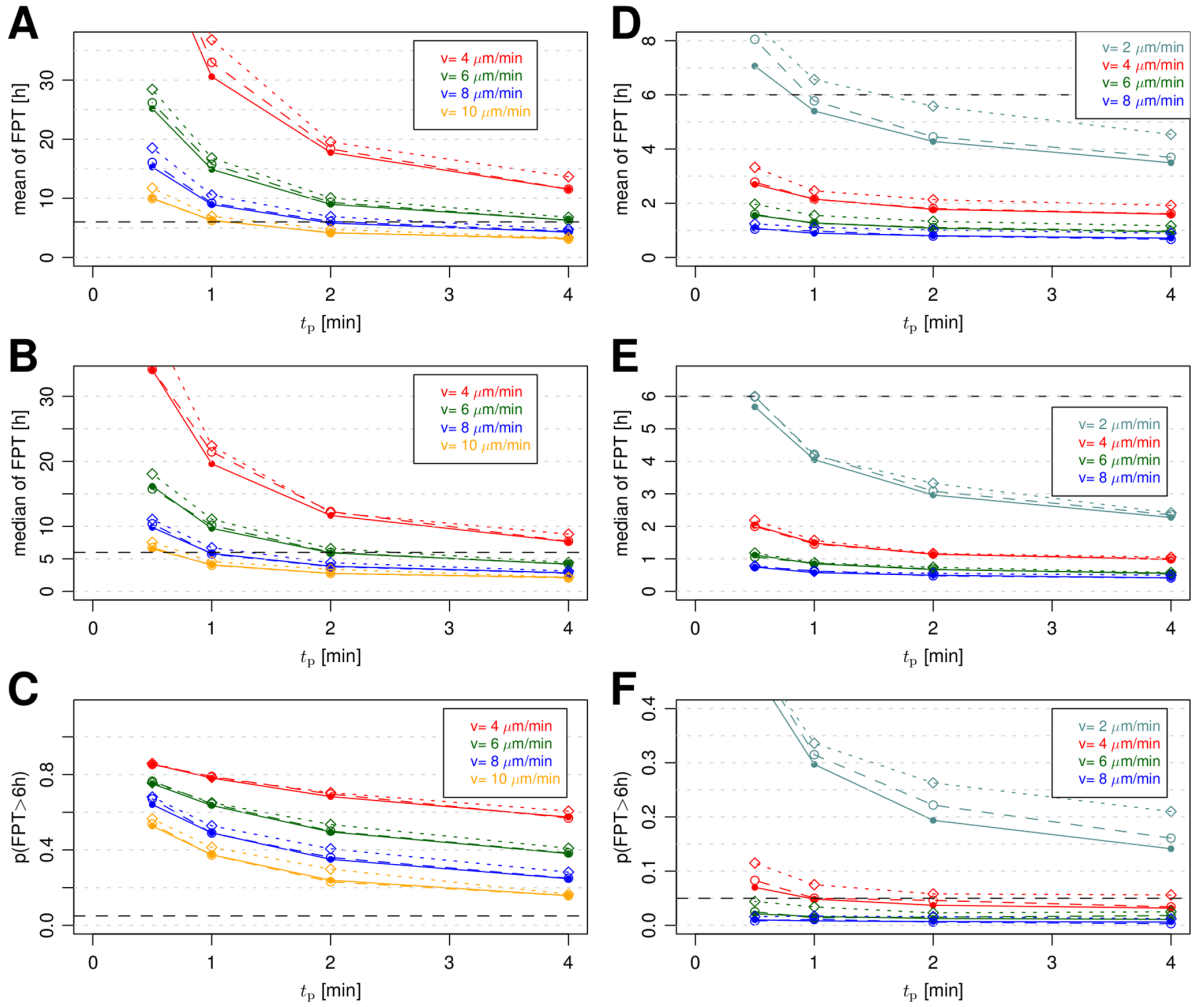

Figure 6. Comparison of first-passage-time distribution measures with and without breathing for both migration modes. Subfigures (A)–(C) show the FPT measures mean, median and probabilities of FPT above six hours for persistent random walk migration mode. Subfigures (D)–(F) show these measures for biased persistent random walk. The two breathing scenarios, resting condition (dashed lines) and heavy exercise (dotted lines) are shown together with the static case (lines) of a constant deflated alveolus. The parameters for the static case and the breathing scenarios are summarized in Table 2.
doi:10.1371/journal.pone.0111630.g006

speeds starting from 4 μm/min the conidium was detected within six hours post infection in more than 95% of all cases. It should be noted that these results were obtained for a conservative implementation of chemotaxis, where AM migration was composed of random and directed contributions to the AEC but not directly to the conidium on the AEC itself. Thus, the current implementation assumed that, once AM arrived at the AEC associated with the conidium, the conidium itself had to be searched randomly on this AEC. Furthermore, a geodesic distance analysis showed that successful AM typically catched the chemotactic signal within a geodesic distance of at most 250 μm, which is in good agreement with theoretical estimations of maximal cell-to-cell communication distances [25].

Furthermore, we considered the possibility that the onset of chemotaxis is retarded because swelling of conidia associated with the exposure of their surface molecules might be required for AEC to initiate chemokine release. If chemotactic signalling is initiated by swollen conidia only, a time lag of about three hours post infection applies [23]. Nevertheless, our simulations of the BPRW revealed that conidium detection within six hours post infection was maintained in 95% of the cases, as long as AM attained speed values of 8 μm/min or higher (see Fig. S3 in comparison with Fig. 6F).

Recently, evidence is emerging that neutrophils rather than AM may be the predominant phagocytes to detect and clear *A. fumigatus* infection [13]. In contrast to our study, millions of conidia were administered to each mouse, which is far from normal conditions for humans that inhale between four and five conidia per minute. As a consequence of providing a superdose of conidia, strong and immediate inflammation, e.g. induction of neutrophil recruitment, can be expected. In this context, the question arises how the recruitment of neutrophils is regulated by

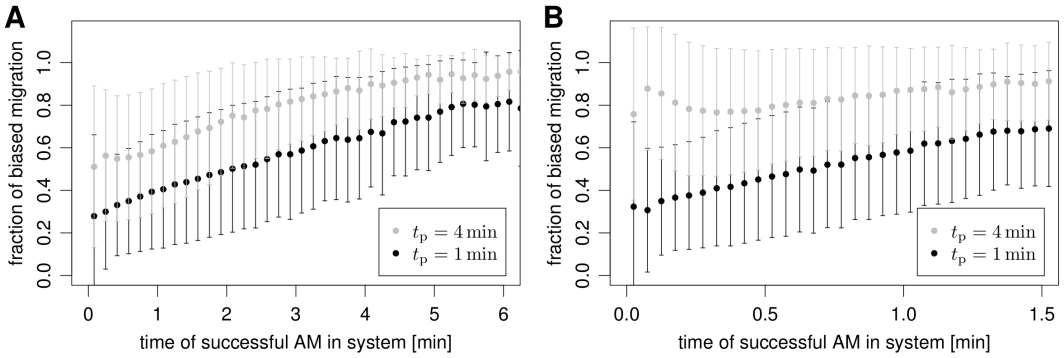

Figure 7. Time fractions for successful AM performing biased persistent random walk migration. The fraction of the biased migration part ($t_{sig}/(t_{sig}+t_{rand})$, see text for details). (A) Mean and standard deviation of the fraction of biased migration for $v=4\ \mu$m/min, (B) for $v=10\ \mu$m/min. The overall number of samples is 10^5.
doi:10.1371/journal.pone.0111630.g007

the inflammatory response. It is well-known that neutrophils can be attracted by activated AM trough the secretion of IL-8 [6]. However, while this would imply that detection of conidia by AM precedes, one could as well imagine that neutrophils are recruited by other signals, e.g. by chemokines released from AEC of type II directly [27]. In any case, our computer simulations revealed that a chemotactic signal would as well be required for neutrophils, because PRW requires speed values of phagocytes well above 10 μm/min for timely detection of the conidium to achieve a success probability of at least 95%.

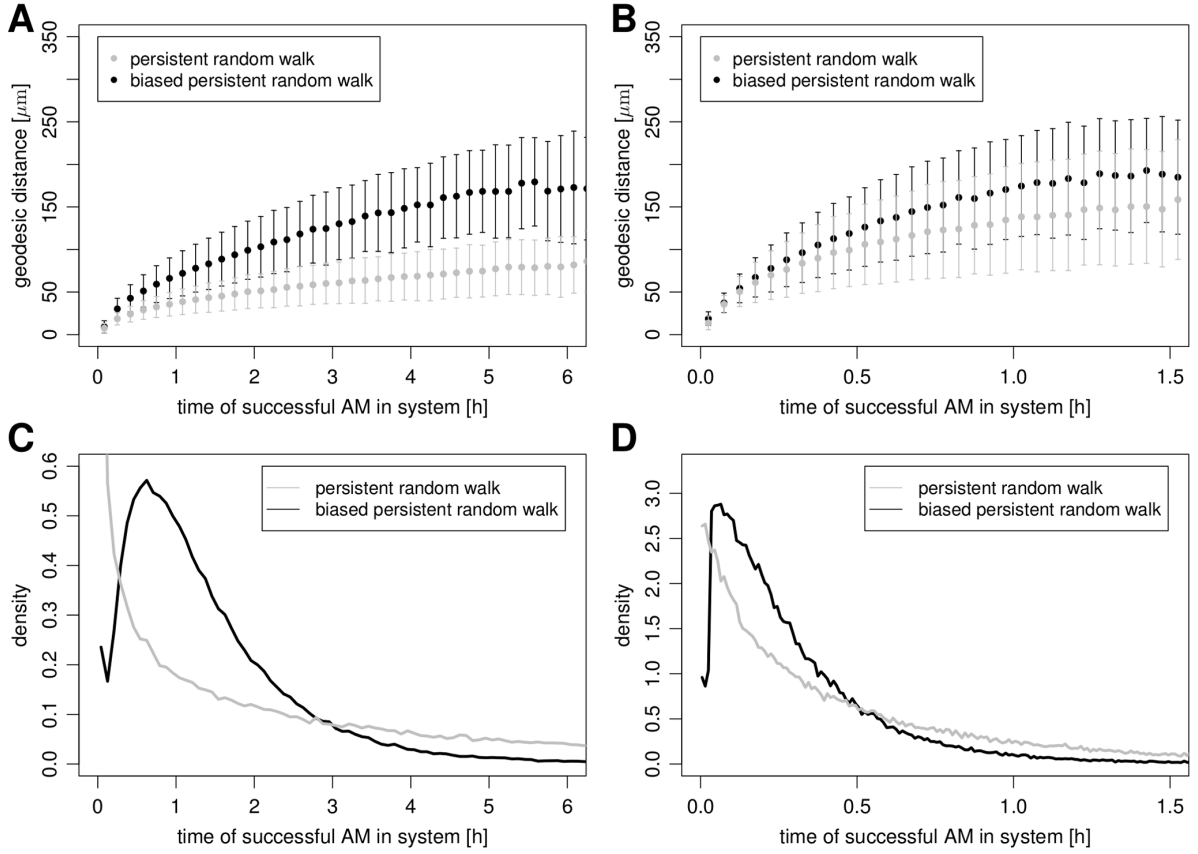

Figure 8. Geodesic distances and the retention time distribution of successful macrophages for different migration modes in the static case. (A) and (C) are based on $v=4\ \mu$m/min and $t_p=1$ min, whereas (B) and (D) are based on $v=10\ \mu$m/min and $t_p=4$ min.
doi:10.1371/journal.pone.0111630.g008

Another option for the realization of pathogen detection arises from a recent *in situ* setup, which suggests that sessile AM located at certain spots in the alveoli detect pathogens that are washed towards these phagocytes [28]. However, this process was not quantified and it remains unclear to what extent AM migration activity is directly affected in this *in situ* study. For the sake of completeness, we scanned the whole range of measured speed values for AM. Furthermore, the fluidic surfactant lining layer could also contribute to the recruitment of neutrophils to the site of infection by pro-inflammatory- and chemoattracting anaphylatoxin and C3a molecules that are cleaved from C3 molecules on the fungal surface [29,30]. However, the impact of complement molecules on the early inflammatory response against *A. fumigatus* is currently unknown [31]. Note that AEC may also play a part in this regard, since these are in direct contact with the conidia from the time of their entry. AEC of type II were shown to secrete IL-8 on contact with swollen conidia of *A. fumigatus* in a TLR-independent fashion [27] and are able to uptake condia within two hours of co-incubation *in vitro* [32]. Due to the fact that type I AEC are diffcult to isolate, immune-regulatory functions were so far exclusively investigated for AEC of type II. It should be noted that type I cells comprise 95% of the alveolar surface [19], which means that a vast majority of conidia entering the alveoli will most certainly make contact with type I AEC.

Search-strategies of AM in the human alveolus are of general interest, because apart from *A. fumigatus* several other harmful fungal spores as well as pathogenic bacteria may cause damage or lead to infectious diseases. In the present study, we focused on *A. fumigatus* because this pathogen sets a tight time scale for removal by phagocytes before germination and invasion of AEC. AM own the capability of recognition and phagocytosis of resting conidia [26], as rigorously quantified by automated image analysis [33], but to figure out the exact mechanisms that lie behind the process of seeking the fungal intruder, we suggest an experimental setup that allows distinguishing the interactions of the different AEC types with AM in the presence of various pathogens. For example, using transwell assays, the hypothesis of directed AM migration due to chemotactic signalling by AEC may be experimentally investigated [34]. Furthermore, if *in vivo* imaging of alveolar ducts could be performed under physiological conditions, typical migration modes in the presence and absence of *A. fumigatus* conidia may be revealed by automated characterization and parameter-free classification of cell tracks [35]. Based on such data, the parameters of the agent-based model could be refined and initiate the iterative cycle between experiment and theory within an image-based systems biology approach.

Supporting Information

Figure S1 *In silico* reconstruction of the Binomial distribution for AM under different breathing conditions and migration modes.
(TIF)

Figure S2 Typical first-passage-time density distribution for biased persistent random walk. Biased persistent random walk migration of alveolar macrophages with parameters $v = 4\ \mu\mathrm{m/min}$ and $t_p = 2\ \mathrm{min}$ based on 10^5 samples.
(TIF)

Figure S3 Probability of FPT being above three hours for biased persistent random walk migration. The reduction of the maximal FPT from six to three hours mimics the case where fungal swelling is required for type I AEC to release chemokines.
(TIF)

Table S1 Average run-time for one timestep $t_{\mathrm{run},\Delta t}$ of agent-based simulations for different breathing conditions and migration modes. Mean run-times and their corresponding standard deviation are averaged over 10^5 runs in the static case and averaged over 10^3 runs under resting and heavy exercise breathing conditions.
(PDF)

Table S2 Calibrated input rates λ_{in} for the different migration mode parameter configurations of AM.
(PDF)

Text S1 Construction of the alveolus and its composition, estimation of cell numbers, diffusion of chemokines and run-time profiling of the simulations.
(PDF)

Video S1 Reconstruction of the spherical three-quarter alveolus. Sizes, shapes and cell numbers are summarized in the Table 1 and in the Model section of the main article. AEC of type I (yellow), AEC of type II (blue) and the pores of Kohn (black) are visible in the morphology of the three-quarter alveolus.
(MP4)

Video S2 Virtual infection scenario with persistent random walk migration of alveolar macrophages. Alveolar macrophages (green) perform persistent random walk migration with parameters $v = 4\ \mu\mathrm{m/min}$ and $t_p = 2\ \mathrm{min}$ in order to find the conidium of *A. fumigatus* (red) in the alveolus. In a time period of $1000\ \mathrm{min}$ the alveolar macrophages did not complete the first-passage. The video is sampled at a rate of 25 frames per second and the time between two frames corresponds to $0.5\ \mathrm{min}$ real time.
(MP4)

Video S3 Alveolar macrophages in an alveolus with resting breathing condition. Inflation and deflation of the three-quarter alveolus are shown in real time. In the resting breathing condition, we apply a respiration frequency of $f_{\mathrm{Alv}} = 12\ \mathrm{min}^{-1}$. A fixed cubic bounding box around the alveolus is used as static reference.
(MP4)

Video S4 Virtual infection scenario with biased persistent random walk migration of alveolar macrophages. Alveolar macrophages (green) perform biased persistent random walk migration with parameters $v = 4\ \mu\mathrm{m/min}$ and $t_p = 2\ \mathrm{min}$ in order to find the conidium of *A. fumigatus* (red) in the alveolus. The alveolar macrophages realized the first-passage in 90 min of time. The video is sampled at a rate of 25 frames per second and the time between two frames corresponds to 0.5 min real time.
(MP4)

Author Contributions

Conceived and designed the experiments: JP MTF. Performed the experiments: JP. Analyzed the data: JP MTF. Contributed reagents/materials/analysis tools: MTF. Wrote the paper: JP MTF.

References

1. Enoch DA, Ludlam HA, Brown NM (2006) Invasive fungal infections: a review of epidemiology and management options. Journal of Medical Microbiology 55: 809–818.
2. Horn F, Heinekamp T, Kniemeyer O, Pollmächer J, Valiante V, et al. (2012) Systems biology of fungal infection. Frontiers in Microbiology 3: 108.
3. Walsh TJ, Groll AH (1999) Emerging fungal pathogens: evolving challenges to immunocompromised patients for the twenty-first century. Transplant Infectious Disease: an Official Journal of the Transplantation Society 1: 247–61.
4. Brakhage AA (2005) Systemic fungal infections caused by Aspergillus species: epidemiology, infection process and virulence determinants. Current Drug Targets 6: 875–886.
5. Codina R, Fox R, Lockey R (2008) Typical levels of airborne fungal spores in houses without obvious moisture problems during a rainy season in Florida, USA. Journal of Investigational Allergology & Clinical Immunology 18: 156–162.
6. McCormick A, Loeffler J, Ebel F (2010) Aspergillus fumigatus: contours of an opportunistic human pathogen. Cellular Microbiology 12: 1535–43.
7. Sibille Y, Reynolds HY (1990) Macrophages and polymorphonuclear neutrophils in lung defense and injury. The American Review of Respiratory Disease 141: 471–501.
8. Balloy V, Chignard M (2009) The innate immune response to Aspergillus fumigatus. Microbes and Infection/Institut Pasteur 11: 919–27.
9. Lambrecht BN (2006) Alveolar macrophage in the driver's seat. Immunity 24: 366–368.
10. Hasenberg M, Stegemann-Koniszewski S, Gunzer M (2013) Cellular immune reactions in the lung. Immunological Reviews 251: 189–214.
11. Behnsen J, Narang P, Hasenberg M, Gunzer F, Bilitewski U, et al. (2007) Environmental dimensionality controls the interaction of phagocytes with the pathogenic fungi Aspergillus fumigatus and Candida albicans. PLOS Pathogens 3: e13.
12. Philippe B, Ibrahim-Granet O, Prévost MC, Gougerot-Pocidalo MA, Sanchez Perez M, et al. (2003) Killing of Aspergillus fumigatus by alveolar macrophages is mediated by reactive oxidant intermediates. Infection and Immunity 71: 3034–3042.
13. Mircescu MM, Lipuma L, van Rooijen N, Pamer EG, Hohl TM (2009) Essential role for neutrophils but not alveolar macrophages at early time points following Aspergillus fumigatus infection. The Journal of Infectious Diseases 200: 647–56.
14. Glasgow JE, Farrell BE, Fisher ES, Lauffenburger DA, Daniele RP (1989) The motile response of alveolar macrophages. An experimental study using single-cell and cell population approaches. The American Review of Respiratory Disease 139: 320–329.
15. Hünniger K, Lehnert T, Bieber K, Martin R, Figge MT, et al. (2014) A Virtual Infection Model Quantifies Innate Effector Mechanisms and Candida albicans Immune Escape in Human Blood. PLOS Computational Biology 10: e1003479.
16. Charnick SB, Fisher ES, Lauffenburger DA (1991) Computer simulations of cell-target encounter including biased cell motion toward targets: single and multiple cell-target simulations in two dimensions. Bulletin of Mathematical Biology 53: 591–621.
17. Tokarski C, Hummert S, Mech F, Figge MT, Germerodt S, et al. (2012) Agent-based modeling approach of immune defense against spores of opportunistic human pathogenic fungi. Frontiers in Microbiology 3: 129.
18. Hansen JE, Ampaya EP (1975) Human air space shapes, sizes, areas, and volumes. Journal of Applied Physiology 38: 990–5.
19. Herzog EL, Brody AR, Colby TV, Mason R, Williams MC (2008) Knowns and unknowns of the alveolus. Proceedings of the American Thoracic Society 5: 778–82.
20. Bastacky J, Goerke J (1992) Pores of Kohn are filled in normal lungs: low-temperature scanning electron microscopy. Journal of Applied Physiology (Bethesda, Md: 1985) 73: 88–95.
21. Condamin S, Bénichou O, Tejedor V, Voituriez R, Klafter J (2007) First-passage times in complex scale-invariant media. Nature 450: 77–80.
22. Balásházy I, Hofmann W, Farkas A, Madas BG (2008) Three-dimensional model for aerosol transport and deposition in expanding and contracting alveoli. Inhalation Toxicology 20: 611–21.
23. Latgé JP, Steinbach W (2009) Aspergillus fumigatus and aspergillosis. ASM Press.
24. Harvey I, Bossomaier T (1997) Time out of joint: Attractors in asynchronous random boolean networks. In: Proceedings of the Fourth European Conference on Artificial Life. Cambridge: MIT Press, pp. 67–75.
25. Francis K, Palsson BO (1997) Effective intercellular communication distances are determined by the relative time constants for cyto/chemokine secretion and diffusion. Proceedings of the National Academy of Sciences of the United States of America 94: 12258–62.
26. Brakhage AA, Bruns S, Thywissen A, Zipfel PF, Behnsen J (2010) Interaction of phagocytes with filamentous fungi. Current Opinion in Microbiology 13: 409–15.
27. Balloy V, Sallenave JM, Wu Y, Touqui L, Latgé JP, et al. (2008) Aspergillus fumigatus-induced interleukin-8 synthesis by respiratory epithelial cells is controlled by the phosphatidylinositol 3-kinase, p38 MAPK, and ERK1/2 pathways and not by the toll-like receptor-MyD88 pathway. The Journal of Biological Chemistry 283: 30513–21.
28. Westphalen K, Gusarova G (2014) Sessile alveolar macrophages communicate with alveolar epithelium to modulate immunity. Nature 506: 503–506.
29. Kozel TR, Wilson MA, Farrell TP, Levitz SM (1989) Activation of C3 and binding to Aspergillus fumigatus conidia and hyphae. Infection and Immunity 57: 3412–7.
30. Zipfel PF, Skerka C (2009) Complement regulators and inhibitory proteins. Nature Reviews Immunology 9: 729–40.
31. Faro-Trindade I, Willment JA, Kerrigan AM, Redelinghuys P, Hadebe S, et al. (2012) Characterisation of innate fungal recognition in the lung. PLOS ONE 7: e35675.
32. Paris S, Boisvieux-Ulrich E, Crestani B, Houcine O, Taramelli D, et al. (1997) Internalization of Aspergillus fumigatus conidia by epithelial and endothelial cells. Infection and Immunity 65: 1510–4.
33. Mech F, Thywissen A, Guthke R, Brakhage AA, Figge MT (2011) Automated image analysis of the host-pathogen interaction between phagocytes and Aspergillus fumigatus. PLOS ONE 6: e19591.
34. Entschladen F, Drell TL, Lang K, Masur K, Palm D, et al. (2005) Analysis methods of human cell migration. Experimental Cell Research 307: 418–26.
35. Mokhtari Z, Mech F, Zitzmann C, Hasenberg M, Gunzer M, et al. (2013) Automated characterization and parameter-free classification of cell tracks based on local migration behavior. PLOS ONE 8: e80808.
36. Ochs M, Nyengaard JR, Jung A, Knudsen L, Voigt M, et al. (2004) The number of alveoli in the human lung. American Journal of Respiratory and Critical Care Medicine 169: 120–4.
37. Stone KC, Mercer RR, Gehr P, Stockstill B, Crapo JD (1992) Allometric relationships of cell numbers and size in the mammalian lung. American Journal of Respiratory Cell and Molecular Biology 6: 235–243.
38. Kawakami M, Takizawa T (1987) Distribution of pores within alveoli in the human lung. Journal of Applied Physiology (Bethesda, Md: 1985) 63: 1866–70.
39. Krombach F, Münzing S (1997) Cell size of alveolar macrophages: an interspecies comparison. Environmental Health Perspectives 105: 1261–1263.
40. Wallace W, Gillooly M, Lamb D (1992) Intra-alveolar macrophage numbers in current smokers and non-smokers: a morphometric study of tissue sections. Thorax 47: 437–440.

Supporting Information S1: Construction of the alveolus and its composition, estimation of cell numbers, diffusion of chemokines and run-time profiling of the simulations.

Construction of the Alveolus and its Composition

The most frequent shape of alveoli in humans was found to be the three-quarter alveolus [1]. In order to construct the spherical shape according to the volume fraction, we use a lower threshold for ϑ_c of the polar angle $\vartheta_c \leq \vartheta \leq \pi$. ϑ_c is computed with the help of the following equation:

$$\pi r^3 = \int \mathrm{dV} = \int_0^{2\pi} \int_{\vartheta_c}^{\pi} \int_0^{\mathrm{r}} \mathrm{r}'^2 \sin\vartheta \mathrm{dr}' \mathrm{d}\vartheta \mathrm{d}\varphi \quad , \tag{1}$$

which leads to $\vartheta_c = \pi/3$. It follows that the epithilial surface of the three-quarter alveolus equals $A_{\mathrm{Alv}} = 3\pi r^2$.

The total number of alveoli in the human lung was estimated in Ochs *et al.* [2]. Here, a stereological analysis was performed to estimate the overall number of alveoli in the lung of adult humans. This yielded the average number of 4.8×10^8, with all measurements being in the range $[2.74, 7.9] \times 10^8$ alveoli.

The spatial arrangement and dynamics of single alveoli are governed by the influx of air and the respiration frequency. The International Commission on Radiological Protection (ICRP) designed a standard model of the human lung and also displayed standard values for the respiration of human beings at different ages and different states of effort [3]. Breathing frequencies and tidal volumes are the important parameters in this respect. Balashazy *et al.* calculated based on the tidal volume of $V_{\mathrm{T}} = 750\,\mathrm{ml}$ per breath and from an average alveolar radius of $r_{\mathrm{Alv,max}} = 125\,\mu\mathrm{m}$ in the resting state, the average minimum alveolar radius $r_{\mathrm{Alv,min}} = 116.5\,\mu\mathrm{m}$ under the assumption that alveoli resize in the same way during one breathing cycle [4]. Under this assumption and for a tidal volume of $V_{\mathrm{T}} = 1923\,\mathrm{ml}$ per breath during heavy exercise, the maximum alveolar radius reaches $136.5\,\mu\mathrm{m}$.

For the construction of the epithelium it is necessary to know the numbers and sizes of the alveolar epithelial cells (AEC), which consist predominantly of type I and type II AEC. In Herzog *et al.*, it is described that type I cells cover 95% of the surface area in alveoli and the remaining 5% are covered by type II cells [5]. Type I cells have a flat morphology and are huge in comparison to type II cells, which have a cuboidal shape. The proportions of the number of cells differ strongly from the surface coverage relation between type I and type II cells as a matter of the size-differences of the cells. Herzog

et al. reported that type I cells make up 8% of all cells in the adult human lung, whereas type II cells amount to 15%. Stone *et al.* measured the mean cell-volume of AEC type II of human lungs, which was $V_{\mathrm{AECT2,avg}} = 815\,\mu\mathrm{m}^3$ on average [6]. With this value we are able to estimate the number of cells in one alveolus. The length of one AEC type II edge assuming cubic symmetry is given by

$$a_{\mathrm{AECT2}} = V_{\mathrm{AECT2,avg}}^{1/3} \approx 9.3\,\mu m \tag{2}$$

This leads to a surface coverage of the alveolus (assuming a three-quarter sphere) of $A_{\mathrm{AECT2}} = a_{\mathrm{AECT2}}^2$ per type II cell. Knowing that type II cells cover 5% of the alveolar surface, we are able to determine the number of cells in inflated and deflated alveolar state by

$$n_{\mathrm{AECT2,max}} = \frac{0.05 \times 3\pi r_{\mathrm{Alv,max}}^2}{A_{\mathrm{AECT2}}} \approx 84\,, \tag{3}$$

$$n_{\mathrm{AECT2,min}} = \frac{0.05 \times 3\pi r_{\mathrm{Alv,min}}^2}{A_{\mathrm{AECT2}}} \approx 74\,. \tag{4}$$

This leads to the number of type I cells by the relation of the fraction of both cell types:

$$n_{\mathrm{AECT1,max}} = \frac{8\%}{15\%} n_{\mathrm{AECT2,max}} \approx 45\,, \tag{5}$$

$$n_{\mathrm{AECT1,min}} = \frac{8\%}{15\%} n_{\mathrm{AECT2,min}} \approx 39\,. \tag{6}$$

In the model, the AEC of type I are placed first. To reach the amount of cells calculated for a three-quarter sphere it is necessary to introduce the parameter $n_{\mathrm{AECT1,pgc}}$, which is a natural number that defines how many cells occur along a great circles of the sphere. The centroids of the type I cells are placed equidistantly by geodesic length $(2\pi r_{\mathrm{Alv,max}})/n_{\mathrm{AECT1,pgc}}$ over parallels of the sphere, whereas the parallels themselves are equidistantly distributed over the whole sphere by the same geodesic length in the interval $\vartheta \in [\vartheta_c, \pi]$ starting from $\vartheta_c = \pi/3$. The amount of centroids of AEC of type I varies per parallel depending on the fraction of its length to the length of a great circle. The amount of cells per parallel equals $n_{\mathrm{AECT1,pgc}} \sin\vartheta$, where ϑ is the polar angle of the parallel under consideration. Note that parameter $n_{\mathrm{AECT1,pgc}}$ determines the total number of type I AEC n_{AECT1} per three-quarter alveolus. We varied $n_{\mathrm{AECT1,pgc}}$ in order to get a total type I cell number with $n_{\mathrm{AECT1,min}} \leq n_{\mathrm{AECT1}} \leq n_{\mathrm{AECT1,max}}$. We determined a value of $n_{\mathrm{AECT1,pgc}} = 13$ leading to $n_{\mathrm{AECT1}} = 39$ and $n_{\mathrm{AECT2}} = 74$ for the alveolus

model and the simulations. From the centroids of the AEC of type I the three-dimensional Voronoi tesselation is calculated and mapped onto the surface of the sphere. Each Voronoi cell represents the spatial dimensions of one AEC of type I. The pores of Kohn and the AEC of type II are subsequently placed randomly over distinct edges of neighbouring type I cells.

Regarding the pores of Kohn, Kawakami *et al.* performed a study comparing different measures like number per alveolus and axial length of a pore in humans [7]. From an average surface of $11.1 \times 10^3\,\mu\mathrm{m}^2$ for the bottom part of the alveolus and an average of 8.9 pores per bottom part, we are able to estimate the average surface density of the pores of Kohn to be $802\,\mathrm{mm}^{-2}$. From the average fraction of the covered area by pores of Kohn of the bottom part being 0.0225, we obtain a coverage surface of $28.1\,\mu\mathrm{m}^2$ per pore which leads to an average radius of $2.99\,\mu\mathrm{m}$ for a pore assuming circular symmetry of its cross section.

Estimation of Cell Numbers

The density of alveolar macrophages ρ_{AM} is taken from the study of Wallace *et al.*, where smokers and non-smokers were compared [8]. For non-smokers the surface density is $\rho_{\mathrm{AM}} = 29.4\,\mathrm{mm}^{-2}$ on average. Note that the alveoli were in expanded state when they sampled the macrophages in order to compute the density. From the surface density ρ_{AM}, the area covered by one lung alveolus A_{Alv} and the overall number of lung alveoli $n_{\mathrm{Alv}} = 4.8 \times 10^8$, we are able to estimate the total number of alveolar macrophages on average in the following way:

$$\begin{aligned} n_{\mathrm{AM}} &= \rho_{\mathrm{AM}} A_{\mathrm{Alv}} n_{\mathrm{Alv}} = \rho_{\mathrm{AM}} \times 3\pi r_{\mathrm{Alv,max}}^2 n_{\mathrm{Alv}} \\ &\approx 2.1 \times 10^9 \,. \end{aligned} \tag{7}$$

Here, we assume that each alveolus has the surface area of a three-quarter sphere in expanded state under resting breathing conditions, which relates to an alveolus radius of $r_{\mathrm{Alv,max}} = 125\,\mu\mathrm{m}$.

From the density of conidia $\rho_{\mathrm{con}} = 194\,\mathrm{m}^{-3}$ [9], we derive the frequencey of spore-inhalation f_{inh} as follows:

$$f_{\mathrm{inh}} = \rho_{\mathrm{con}} V_{\mathrm{T}} f_{\mathrm{Alv}} \quad , \tag{8}$$

where V_{T} is the tidal volume per breath and f_{Alv} the frequency of respiration. Considering resting

breathing conditions, we find $f_{\mathrm{inh}} \approx 6300\,\mathrm{d}^{-1}$. Note that this number relates to the amount of spores that pass into the thorax, but it remains unknown what fraction conidia are able to evade the filter activity of the lung and reach the alveolar ducts.

Diffusion of Chemokines

We apply the two-dimensional planar diffusion equation with a source term:

$$\frac{\partial}{\partial t}c(\vec{d},t) = D\nabla^2 c(\vec{d},t) + S(\vec{d},t) \quad , \tag{9}$$

where $c(\vec{d},t)$ is the molecule concentration at position $\vec{d} = (x,y)^{\mathrm{T}}$ and time t, ∇ is the Nabla operator and D the diffusion constant. We start from the initial condition $c(\vec{d},0) = 0$ and set a constant source term $S(\vec{d},t) = S_0\delta(\vec{d_S})$, where $\vec{d_S}$ is the location of the point source and $\delta(\cdot)$ is the Dirac delta distribution.

The analytical solution of equation 9 with $\vec{d}_{\mathrm{S}} = (0,0)^{\mathrm{T}}$ is given by:

$$c(d,t) = \frac{S_0}{4\pi D} \times \gamma\left(0, \frac{d^2}{4Dt}\right) \quad , \tag{10}$$

where $d = \sqrt{x^2+y^2}$ and $\gamma(\cdot,\cdot)$ is the lower incomplete Gamma-function. The gradient of the chemokine distribution is then given by

$$\frac{\partial}{\partial d}c(d,t) = \frac{S_0}{2\pi D}\frac{1}{d} \times \gamma\left(1, \frac{d^2}{4Dt}\right) \quad . \tag{11}$$

Note that $\gamma(1, \frac{d^2}{4Dt}) \to 1$ for $t \gg d^2/(4D)$, leading to a $1/d$ proportionality of the concentration gradient in the steady state. The $1/d$ relation enters the expression for the probability $p_{\mathrm{sig}}(d)$ of alveolar macrophages to perform directed migration towards the AEC associated with the fungus. The maximum intensity of the signal is set at the edge of the AEC with $r_0 = 30\,\mu$m for type I and $r_0 = 5.27\,\mu$m for type II from its centroid. This yields the distance-dependent probability $p_{\mathrm{sig}}(d) = r_0/d$ for $d \geq r_0$ that is used in this study.

We assume that mapping the two-dimensional planar solution of the diffusion equation to the two-dimensional spherical inner surface of the alveolus is a reasonable assumption in the limit of $r_0/(\pi r_{\mathrm{Alv,max}}) \approx 0.076 \ll 1$.

Run-time Profiling of the Simulations

The execution time of the simulation program depends linearly on the timesteps required for the first passage of one of the alveolar macrophages. The average run-time, $t_{\mathrm{run},\Delta\mathrm{t}}$, for one timestep is independent of the spread of the first-passage-time distribution and of the scenarios (static case $\Delta t = 0.1\,\mathrm{min}$, breathing cases $\Delta t = 0.001\,\mathrm{min}$). However, this measure depends on the dynamically changing number of agents to be simulated in the timestep under consideration.

In Table S1 we show the average run-time per timestep for the different scenarios tested in this study. We see slight differences among persistent random walk and biased persistent random walk, since directions of migration have to be computed additionally in the simulations where chemotaxis is involved. Despite having spatial rescaling of all agents in the breathing scenarios in order to meet the bound-to-surface condition, run-time does not increase in comparison to the static case. The small timestep reduces the average load, since interaction events or the exit and input of AM from or into the system become rare cases. Note, however, that the overall runtime of the breathing scenarios is indeed much higher than for the static case by about two orders of magnitude, as the timesteps Δt differ by two orders of magnitude.

References Supporting Information

1. Hansen JE, Ampaya EP (1975) Human air space shapes, sizes, areas, and volumes. Journal of Applied Physiology 38: 990–5.

2. Ochs M, Nyengaard JR, Jung A, Knudsen L, Voigt M, et al. (2004) The number of alveoli in the human lung. American Journal of Respiratory and Critical Care Medicine 169: 120–4.

3. ICRP (1994) Deposition model. Annals of the ICRP 24: 36–54.

4. Balásházy I, Hofmann W, Farkas A, Madas BG (2008) Three-dimensional model for aerosol transport and deposition in expanding and contracting alveoli. Inhalation Toxicology 20: 611–21.

5. Herzog EL, Brody AR, Colby TV, Mason R, Williams MC (2008) Knowns and unknowns of the alveolus. Proceedings of the American Thoracic Society 5: 778–82.

6. Stone KC, Mercer RR, Gehr P, Stockstill B, Crapo JD (1992) Allometric relationships of cell numbers and size in the mammalian lung. American Journal of Respiratory Cell and Molecular Biology 6: 235–243.

7. Kawakami M, Takizawa T (1987) Distribution of pores within alveoli in the human lung. Journal of Applied Physiology (Bethesda, Md : 1985) 63: 1866–70.

8. Wallace W, Gillooly M, Lamb D (1992) Intra-alveolar macrophage numbers in current smokers and non-smokers: a morphometric study of tissue sections. Thorax 47: 437–440.

9. Codina R, Fox R, Lockey R (2008) Typical levels of airborne fungal spores in houses without obvious moisture problems during a rainy season in Florida, USA. Journal of Investigational Allergology & Clinical Immunology 18: 156–162.

4.3 Deciphering chemokine properties by a hybrid agent-based model of *Aspergillus fumigatus* infection in human alveoli

frontiers in Microbiology

ORIGINAL RESEARCH
published: 28 May 2015
doi: 10.3389/fmicb.2015.00503

Deciphering chemokine properties by a hybrid agent-based model of *Aspergillus fumigatus* infection in human alveoli

Johannes Pollmächer[1,2] *and Marc Thilo Figge*[1,2]*

[1] *Applied Systems Biology, Leibniz-Institute for Natural Product Research and Infection Biology – Hans Knöll Institute, Jena, Germany,* [2] *Faculty of Biology and Pharmacy, Friedrich Schiller University Jena, Jena, Germany*

frontiers in Microbiology

ORIGINAL RESEARCH
published: 28 May 2015
doi: 10.3389/fmicb.2015.00503

Deciphering chemokine properties by a hybrid agent-based model of *Aspergillus fumigatus* infection in human alveoli

Johannes Pollmächer[1,2] *and Marc Thilo Figge*[1,2]*

[1] Applied Systems Biology, Leibniz-Institute for Natural Product Research and Infection Biology – Hans Knöll Institute, Jena, Germany, [2] Faculty of Biology and Pharmacy, Friedrich Schiller University Jena, Jena, Germany

The ubiquitous airborne fungal pathogen *Aspergillus fumigatus* is inhaled by humans every day. In the lung, it is able to quickly adapt to the humid environment and, if not removed within a time frame of 4–8 h, the pathogen may cause damage by germination and invasive growth. Applying a to-scale agent-based model of human alveoli to simulate early *A. fumigatus* infection under physiological conditions, we recently demonstrated that alveolar macrophages require chemotactic cues to accomplish the task of pathogen detection within the aforementioned time frame. The objective of this study is to specify our general prediction on the as yet unidentified chemokine by a quantitative analysis of its expected properties, such as the diffusion coefficient and the rates of secretion and degradation. To this end, the rule-based implementation of chemokine diffusion in the initial agent-based model is revised by numerically solving the spatio-temporal reaction-diffusion equation in the complex structure of the alveolus. In this hybrid agent-based model, alveolar macrophages are represented as migrating agents that are coupled to the interactive layer of diffusing molecule concentrations by the kinetics of chemokine receptor binding, internalization and re-expression. Performing simulations for more than a million virtual infection scenarios, we find that the ratio of secretion rate to the diffusion coefficient is the main indicator for the success of pathogen detection. Moreover, a subdivision of the parameter space into regimes of successful and unsuccessful parameter combination by this ratio is specific for values of the migration speed and the directional persistence time of alveolar macrophages, but depends only weakly on chemokine degradation rates.

Keywords: *Aspergillus fumigatus*, fungal infection, agent-based modeling, reaction-diffusion equation, chemotaxis, human alveolus, alveolar macrophage, alveolar epithelial cell

OPEN ACCESS

Edited by:
Tunahan Cakir,
Gebze Technical University, Turkey

Reviewed by:
Joachim Selbig,
University of Potsdam, Germany
Mark Read,
The University of Sydney, Australia

***Correspondence:**
Marc Thilo Figge,
Applied Systems Biology,
Leibniz-Institute for Natural Product Research and Infection Biology – Hans Knöll Institute, Adolf-Reichwein-Str. 23, Jena 07749, Germany
thilo.figge@hki-jena.de

Specialty section:
This article was submitted to Infectious Diseases, a section of the journal Frontiers in Microbiology

Received: *19 February 2015*
Accepted: *06 May 2015*
Published: *28 May 2015*

Citation:
Pollmächer J and Figge MT (2015) Deciphering chemokine properties by a hybrid agent-based model of Aspergillus fumigatus infection in human alveoli. Front. Microbiol. 6:503. doi: 10.3389/fmicb.2015.00503

1. Introduction

Aspergillus fumigatus is the most dangerous airborne fungal pathogen in humans leading to high mortality rates (Heinekamp et al., 2014). Immunocompetent individuals are able to prevail over inhaled conidia of the fungus in an everyday challenge. In contrast, patients with an altered immune system, e.g., as a consequence of organ transplantation or an underlying disease like HIV, are at high risk to die from invasive aspergillosis (Horn et al., 2012), where the lung is the site of infection

in 70 % of the cases (Lin et al., 2001). *A. fumigatus* is able to adapt within hours to the humid and nutrient rich milieu of the lung (Hohl, 2008; Hasenberg et al., 2011), by this setting a tight time scale for phagocytes to find, detect and remove the pathogenic fungus before the onset of germination and hyphal invasion of alveolar epithelium.

Alveolar macrophages (AM) reside on the inner surface of lung alveoli and are the first professional motile phagocytes that get in contact with inhaled conidia of *A. fumigatus* (Hasenberg et al., 2013). AM are capable of clearing the lower respiratory tract from all kinds of inhaled particles and microbes in order to maintain a pathogen-free alveolar surface and to ensure optimal exchange of oxygen and carbon-dioxide (Fels and Cohn, 1986). The migration of AM takes place within the alveolar lining layer, which is a viscous fluid—referred to as surfactant—that coats the alveolar surface with an average thickness of about 200 nm (Bastacky and Lee, 1995). Apart from the stabilizing effect of the surfactant avoiding alveolus collapse, it also provides the environment for diffusive transport of molecules, such as lipids and immunoregulatory proteins SP-A and SP-D, that are continuously produced, secreted and recycled by alveolar epithelial cells (AEC) (Herzog et al., 2008).

For over one decade computational approaches have proven to successfully complement wet-lab studies in the frame of systems biology (Kitano, 2002; Horn et al., 2012). Computer modeling and simulation are nowadays important tools to verify hypotheses in advance of cost- and time intensive experimental investigations to narrow down the range of possible wet-lab experiments to the most promising ones. Furthermore, predictions may be derived from virtual models, which subsequently can be tested in experiment. The present study aims at predicting AM chemokine properties from an existing agent-based virtual infection model of human alveoli under physiological conditions (Pollmächer and Figge, 2014). Due to the peculiar physiology of the human lung, investigations *in vivo*, including live-cell imaging, are hard to realize. Thus, quantitative measures like AM motility, chemokine secretion rates of AEC or the diffusion coefficient of molecules within the surfactant are not directly accessible. AEC type II cell lines have been studied intensively in the past, but as they do account for only five percent of the alveolar surface, experimental investigations of type I AEC would be highly appreciated. However, isolation and cultivation of type I AEC with current methods are demanding tasks due to their thin and delicate morphology. The present computational modeling approach enables us studying *A. fumigatus* infection in alveoli for varying parameter sets of AM motility and of chemokine properties in order to reveal the relative importance of each of the parameters and their potential regimes in healthy individuals.

Recently, we established an agent-based model (ABM) of *A. fumigatus* infection in the human alveolus to study the early immune response under physiological conditions (Pollmächer and Figge, 2014). In this three-dimensional to-scale model, we represented the human alveolus by a three-quarter spherical structure consisting of type I and type II AEC as well as pores of Kohn. Our computations of the first-passage-time, i.e., the time it takes until the conidium is detected by an AM for the first time, clearly showed that pathogen detection by AM resembles the problem of finding the needle in the haystack within a time limit that is set by the germination time for *A. fumigatus* conidia of about 6 h. Statistical analyses based on hundreds of thousands of computer simulations revealed that for AM to successfully accomplish finding the conidium within 6 h time, chemotactic cues are required that guide AM to the AEC associated with a conidium. Chemotaxis was implemented in the ABM based on a probabilistic rule, i.e., AM were directed toward the AEC associated with the fungus with a probability that was defined by the distance-dependent strength of the chemokine gradient (Pollmächer and Figge, 2014). The gradient of the chemokine concentration in the alveolus was approximated by the analytical steady state solution of the two-dimensional diffusion equation for a point source on a planar surface. We demonstrated that this level of detail was sufficient to arrive at the conclusion that chemotactic cues are required for directing AM migration in the alveolus to the site of the pathogen. However, the specific chemokine remains as of yet unknown, including its characteristic parameters such as the secretion rate, diffusion coefficient and rate of degradation. In order to arrive at quantitative predictions of characteristic parameters that may narrow down the regime of candidate chemokines, the ABM has to be revised to describe the spatio-temporal dynamics of chemokine diffusion in the alveolus and the receptor binding on AM at a higher level of detail.

Mathematical models of chemotaxis typically set focus on one of the three key aspects that are associated with the directed migration of cells: gradient-sensing, polarization and motility. While integrative models combining all three aspects are still rare today (Iglesias and Devreotes, 2008), a chemotaxis model including the processes of gradient-sensing and motility was developed by Guo and Tay (2008). In this approach, a hybrid ABM (hABM) was used to simulate the migration behavior of leucocytes and to compare with experimental results of under-agarose assays. A hABM is a multi-scale model where cells are represented as migrating and interacting agents that are coupled to the interactive layer of diffusing molecule concentrations by the kinetics of chemokine receptor binding, internalization and re-expression (see **Figure 1**). From a technical point of view, this requires the implementation of a solver for the spatio-temporal reaction-diffusion equation of molecule concentrations in the complex alveolar structure with spherical symmetry and peculiar boundary conditions as imposed by the pores of Kohn and the alveolar entrance ring. This is achieved by generating a Delaunay triangulation of the alveolar surface for close-to-equidistant surface points. The geometric quantities of the corresponding Voronoi tesselation, i.e., the dual graph of the Delaunay triangulation, can then be used to solve the reaction-diffusion equation by a finite difference method on unstructured grids (Sukumar, 2003). We perform a numerical study of the steady state behavior of molecules for typical values of the diffusion coefficient, chemokine secretion rate and the rate of molecular degradation. Furthermore, performing statistical analyses of first-passage-time distributions we narrow down the regime of characteristic parameters required for the time-limited detection of *A. fumigatus* conidia by AM.

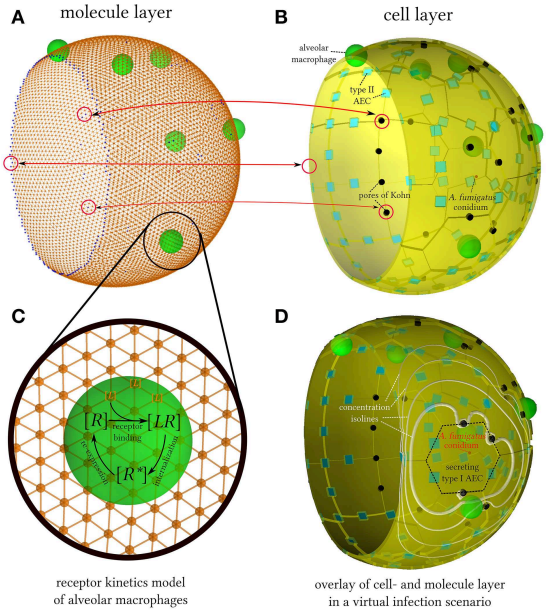

FIGURE 1 | Schematic overview and structural relations between different components of the hybrid agent-based model. (A) Close-to-equidistant discretization of the three-quarter alveolus with 10,000 grid points. Grid points with label alveolar surface point (*orange spheres*) are connected with their neighboring grid points (*orange lines*) and those with label boundary point (*blue spheres*) correspond to either pores of Kohn or the alveolar entrance ring. **(B)** To-scale reconstruction of the human three-quarter alveolus from Pollmächer and Figge (2014) including alveolar epithelial cells (AEC) of type I (*yellow*) and type II (*blue*) as well as the pores of Kohn (*black*). **(C)** Receptor kinetics model that drives the chemotaxis of alveolar macrophages (AM). Free chemokine receptors [*R*] bind to chemokine ligands [*L*] located at grid points associated with the AM. Bound receptors [*LR*] are processed into internalized receptors [*R**] and are re-expressed subsequently. **(D)** Snapshot of a virtual infection scenario where AM (*green*) aim to find a conidium of *A. fumigatus* (*red*). The information contained in the molecule layer is integrated using chemokine concentration isolines (*white*), which are plotted proportional to their respective values with different sizes.

2. Materials and Methods

2.1. Hybrid Agent-Based Model

In this study, we revised our agent-based model (ABM) of the human alveolus to explicitly account for the dynamics of molecular diffusion and reactions with cells, which were previously modeled in a simple rule-based fashion using a steady-state approximation (Pollmächer and Figge, 2014). We refer to the revised model as hybrid agent-based model (hABM), because single cells are represented as individual agents that migrate and interact in continuous space, whereas chemokine concentrations are represented as spatio-temporal distributions on a discrete grid. In this multi-scale approach, interactions between cellular agents and the layer of diffusing molecular concentrations are realized via modeling the kinetics of chemokine receptor binding, internalization and re-expression on alveolar macrophages (AM) as shown in **Figure 1**. The present agent-based simulation algorithm has linear time complexity in the number of agents and in the number of timesteps. Thus, treating single molecules as single virtual agents would render the simulations computationally intractable. Scalability in terms of constituent quantities is one of the strengths of partial differential equations (Horn et al., 2012) as the time complexity of our numerical method is linear in the number of grid points, molecule species and timesteps. In summary, treating cells at the microscopic level of discrete agents and molecules at the macroscopic level of continuous distributions ensures keeping the balance between computational tractability and detailed modeling across interwoven time- and length-scales (Guo et al., 2008). The source code of the hABM is available from the authors upon request.

2.2. Numerical Solution of the Reaction-Diffusion Equation in the Alveolus

2.2.1. Reaction-diffusion equation

The spatio-temporal distribution of chemokines on the inner surface of the alveolus is described by the following reaction-diffusion equation:

$$\frac{\partial c(\vec{r},t)}{\partial t} = D\Delta c(\vec{r},t) - \lambda\, c(\vec{r},t) + S(\vec{r},t) - Q(\vec{r},t). \qquad (1)$$

Here $c(\vec{r},t)$ denotes the molecular concentration of chemokines at position $\vec{r}$ and time t and Δ is the Laplace operator. The chemokine's isotropic diffusion coefficient is given by D and its degradation rate is given by λ. The spatio-temporal source of molecular concentration is represented by the term $S(\vec{r},t)$ associated with chemokine producing alveolar epithelial cells (AEC) of type I and type II. The term $Q(\vec{r},t)$ represents the uptake of chemokines by AM and is explained in detail below. Numerical integration of the reaction-diffusion Equation (1) within the surfactant on the inner alveolar surface requires a discretization of the thin fluidic lining layer by a grid with close-to-equidistant grid points.

2.2.2. Discretization of the Surfactant

Generating a grid with an arbitrary number of close-to-equidistant grid points on the surface of a spherical geometry is related to the Thomson problem (Thomson, 1904). This problem was raised more than a century ago in the context of finding the minimal electrostatic potential energy configuration for n equally charged particles that repel each other by Coulomb forces on the surface of a unit sphere. An equidistant distribution of points is beneficial for the numerical solution of the reaction-diffusion equation with regard to computing time and numerical stability. We take advantage of a crowd-based numerical approximation platform that determines the global minima using a variety of different optimization algorithms (MacWilliam and Cecka, 2013). Next, in order to obtain the neighborhood relationship between the grid points, we use the close-to regular distribution of points as inputs and compute the convex hull, where each of its edges corresponds to a pair of neighboring grid points. Note that the triangulation of discrete points on a sphere surface using the convex hull is equivalent to the Delaunay triangulation of these points in three dimensions (Brown, 1979). Finally, the dual

graph of the Delaunay triangulation, i.e., the Voronoi tesselation (De Berg et al., 2008), was computed in order to obtain the surface-area associated with each grid point, i.e., the area of the corresponding Voronoi cell. As will be shown below, this measure together with the length of the Voronoi edge between neighboring Voronoi cells are required for solving the reaction-diffusion Equation (1) numerically.

It should be noted that, since the human alveolus does not correspond to a full sphere, not each grid point belongs to the alveolar surface. In fact, each point of the grid can be labeled as one of the three categories: (i) alveolar surface point, (ii) boundary point, (iii) outside point. A point is considered to be an alveolar surface point if it is part of the alveolar three-quarter sphere and does not cover a pore of Kohn. All other points are outside points, except for boundary points which have at least one neighboring point being an alveolar surface point (see Supplementary Figure S1A and Video S1). We use absorbing boundary conditions in each simulation scenario, i.e., the concentration at each boundary point is kept fixed at zero for all times. The representation of the surfactant with an average thickness of only 200 nm (Bastacky and Lee, 1995) is based on 10^4 close-to-equidistant grid points of the spherical surface at an average distance of $4.45 \pm 0.16\,\mu$m (see Video S1). This allows resolving AEC of type I and type II that are, respectively, 60 μm and 9.3 μm in diameter, as well as the pores of Kohn that are 6 μm in diameter as estimated from literature data in Pollmächer and Figge (2014).

2.2.3. Numerical integration of the reaction-diffusion equation

The reaction-diffusion Equation (1) is numerically integrated in time using a finite difference method for unstructured grids as described by Sukumar (2003). Here, Voronoi cells are the placeholders of the chemokine concentrations, where each Voronoi cell may contain several molecular species. The kth Voronoi cell is associated with grid point $\vec{r}_k$ of the Delaunay triangulation and has area A_k and a finite set of neighbors $\mathcal{N}(k)$. The relation with neighboring Voronoi cells $\ell \in \mathcal{N}(k)$ is defined by the length of the Voronoi edge $h_{k\ell}$ and the Euclidean distance between the two Voronoi cells $d_{k\ell}$, as depicted in Supplementary Figure S1B. The numerical integration is then performed in a straightforward fashion over each Voronoi cell k that is associated with a grid point of the category alveolar surface point:

$$\tilde{c}(\vec{r}_k, t+\Delta t) = \tilde{c}(\vec{r}_k, t) + \Delta t\Big(\sum_{\ell \in \mathcal{N}(k)} D \frac{h_{k\ell}}{d_{k\ell} A_k} \big[\tilde{c}(\vec{r}_\ell, t) - \tilde{c}(\vec{r}_k, t)\big] - \lambda\, \tilde{c}(\vec{r}_k, t) + S(\vec{r}_k, t) - Q(\vec{r}_k, t)\Big)\,. \quad (2)$$

Here and in what follows the discretized concentration values are indicated by the symbol $\tilde{c}$. In our model, both AEC of type I and type II may secrete chemokines, which is appropriately captured by a non-vanishing source term $S(\vec{r}_k, t)$ at all grid points of the AEC associated with the conidium.

2.2.4. Validation of the numerical solution

In order to validate the implementation of the close-to-equidistant grid for the spherical system and the algorithm for the numerical solution of the reaction-diffusion Equation (1), we performed simulations of scenarios for which the analytical solutions are known. These scenarios were based on the analytical solution of the isotropic diffusion equation in terms of spherical harmonics (Sbalzarini et al., 2006). For a sphere with radius r and molecular diffusion coefficient D on its surface an analytical solution of the reaction-diffusion Equation (1) for vanishing molecule degradation and absent source- and reaction-term is given by

$$c(\vec{r} = (r, \vartheta, \varphi), t) = \sqrt{\frac{3}{4\pi}} \cos(\vartheta) \exp\left(-\frac{2D}{r^2} t\right). \quad (3)$$

Here, surface positions $\vec{r}$ are represented using spherical coordinates with polar angle ϑ and azimuthal angle φ. Simulations were started from the initial condition $c(\vec{r}, t=0) = \sqrt{3/(4\pi)}\cos(\vartheta)$. The accuracy of the numerical solution was evaluated by comparing with the analytical solution on the spherical surface using biquadratic interpolation at 2×10^4 pre-defined close-to-equidistant points.

2.3. Chemotaxis Model of Alveolar Macrophages

The previously established agent-based model of the human alveolus (Pollmächer and Figge, 2014) is extended by modeling the interactions between molecule concentrations and chemokine receptors of AM, including the internalization of bound receptors and their subsequent re-expression on the AM surface. This enables AM to sense chemokine gradients that ultimately drive the migratory response of the phagocytes. Here, we essentially follow the receptor kinetics model as previously presented in Guo and Tay (2008) and Guo et al. (2008), apart from modifications required in the present context of modeling the dynamics of infection in the curved environment of a human three-quarter alveolus.

Since the average distance between neighboring grid points is four to five times smaller than the AM diameter of $r_{\mathrm{AM}} = 10.6\ \mu m$ (Krombach and Münzing, 1997), each AM is an agent associated with on average 20 grid points on the interactive molecule layer. In the reaction-diffusion Equation (1), the interaction between chemokines and AM receptors is represented by the term

$$Q(\vec{r}, t) = \sum_{m \in \mathcal{M}(t)} Q_m(\vec{r}, t)\,, \quad (4)$$

where $\mathcal{M}(t)$ is the set of AM present in the alveolus at time t. $Q_m(\vec{r}, t)$ denotes the reaction term of the mth AM with the chemokines in the surfactant, which is defined at each grid point q as follows:

$$Q_m(\vec{r}_q, t) = \begin{cases} \frac{k_b}{A_{\mathrm{AM}}}\, \tilde{c}(\vec{r}_q, t)\, [R]_m(t) & , \text{if } q \in \mathrm{cov}_m(t) \\ 0 & \text{otherwise,} \end{cases} \quad (5)$$

where $\mathrm{cov}_m(t)$ represents the set of covered grid points by the mth AM (see Supplementary Figure S2), $[R]_m(t)$ is the current

number of free receptors on the AM and k_b is the binding rate between AM receptors and the chemotactic cytokines in the surfactant. The interaction surface for the reaction between the receptors of the AM cell wall and the chemokines in the surfactant is denoted by $A_{\mathrm{AM}} = \pi r_{\mathrm{AM}}^2$. Beside the number of free receptors, each AM m is an agent keeping track of its current number of bound ($[LR]_m$) and internalized receptors ($[R^*]_m$). The kinetics of ligand-binding, receptor internalization and re-expression is described by a system of ordinary differential equations:

$$\frac{\mathrm{d}[R]_m(t)}{\mathrm{d}t} = k_r\,[R^*]_m(t) - A_{\mathrm{AM}} \sum_q Q_m(\vec{r}_q, t)\ , \quad (6)$$

$$\frac{\mathrm{d}[RL]_m(t)}{\mathrm{d}t} = A_{\mathrm{AM}} \sum_q Q_m(\vec{r}_q, t) - k_i\,[LR]_m(t)\ , \quad (7)$$

$$\frac{\mathrm{d}[R^*]_m(t)}{\mathrm{d}t} = k_i\,[LR]_m(t) - k_r\,[R^*]_m(t)\ . \quad (8)$$

Here, k_i is the internalization rate of bound receptors and k_r is the recycling rate associated with the re-expression of internalized receptors. All model parameters together with their experimentally relevant regimes of values are listed in **Table 1**. The parameters related to the receptor-kinetics model of AM, k_b, k_i and k_r, are fixed to the geometric means of their corresponding experimental range.

In our model, the kinetics of bound receptor differences along the current chemokine gradient is coupled to the directional persistence time of migrating AM (Farrell et al., 1990). Thus, as shown in Supplementary Figure S2, we consider that the mth AM weights the direction of the average chemokine concentration gradient $\vec{g}_m(t)$ in each timestep by the difference in newly bound receptors at the front and rear of the cell along the gradient.

The difference in the chemokine concentration across the interaction surface of the mth AM between its front and rear, $\Delta c_{m,\mathrm{diff}}$, is computed using the distance between the respective barycenters of the front und rear of this AM and its corresponding concentration gradient:

$$\Delta c_{m,\mathrm{diff}}(t) = \frac{8\,r_{\mathrm{AM}}}{3\pi} ||\vec{g}_m(t)||\ , \quad (9)$$

where the chemokine concentration gradient $\vec{g}_m(t)$ over the mth AM is obtained from averaging over the local gradients of all grid points covered by the mth AM ($\mathrm{cov}_m(t)$). Then, the difference in newly bound receptors between the front and rear of the AM along the current gradient per timestep Δt is

$$\Delta[LR]_{m,\mathrm{diff}}(t) = k_b\,\Delta c_{m,\mathrm{diff}}(t)\,\frac{[R]_m(t)}{2}\,\Delta t\ . \quad (10)$$

The most favorable direction of migrating AM is determined by computing the sum of weighted gradients over one period of directional persistence:

$$\vec{g}_{m,\mathrm{cum}}(t^*_{\mathrm{begin}}, t^*_{\mathrm{end}}) = \sum_{t=t^*_{\mathrm{begin}}}^{t^*_{\mathrm{end}}} \Delta[LR]_{m,\mathrm{diff}}(t)\,\frac{\vec{g}_m(t)}{||\vec{g}_m(t)||}\ , \quad (11)$$

where t^*_{begin} and t^*_{end} denote the start and the end time for the period of directional persistence.

Finally, after each period of directional persistence, the respective AM migrates in the direction of the weighted cumulative gradient $\vec{g}_{m,\mathrm{cum}}(t^*_{\mathrm{begin}}, t^*_{\mathrm{end}})$ with probability

$$p_{\mathrm{directed}} = \min(||\vec{g}_{m,\mathrm{cum}}(t^*_{\mathrm{begin}}, t^*_{\mathrm{end}})||\sigma_{\mathrm{AM}}\ ,\ 1)\ . \quad (12)$$

This probability is proportional to the bound receptor differences along the cumulative gradient (Devreotes and Zigmond, 1988) and the constant of proportionality is the AM sensitivity σ_{AM} that was determined by Tranquillo et al. (1988) (see **Table 1**).

2.4. System Setup for Simulation Studies

2.4.1. Steady state analysis

Initially, all grid points were set to zero molecular concentration and one permanently and homogenously secreting AEC of type I at the bottom of an otherwise empty three-quarter alveolus was placed. Keeping track of the time-dependent relative concentration change,

$$\Delta\tilde{c}_{\mathrm{rel}}(\vec{r}_k, t) \equiv \frac{\tilde{c}(\vec{r}_k, t+\Delta t) - \tilde{c}(\vec{r}_k, t)}{\tilde{c}(\vec{r}_k, t)}\ , \quad (13)$$

at grid points k, the steady state of the molecular distribution was considered to be reached when the maximum value of $\Delta\tilde{c}_{\mathrm{rel}}$ over all grid points fell below a threshold value of one permille. Measurements were repeated 50 times per parameter configuration and the results were averaged, keeping the number of randomly positioned pores of Kohn in the alveolus constant.

TABLE 1 | Parameters used for the chemotaxis model of alveolar macrophages.

Symbol	Description	Unit	Value	Experimental range	References
D	Chemokine diffusion coefficient (in water)	$\mu\mathrm{m}^2 \times \mathrm{min}^{-1}$	Varied	$6 \times 10^2 - 3.5 \times 10^4$	Francis and Palsson (1997); Randolph et al. (2005)
s_{AEC}	Chemokine secretion rate of AEC	min^{-1}	Varied	Unknown	
λ	Chemokine degradation rate	min^{-1}	Varied	$3 \times 10^{-3} - 4.2 \times 10^{-2}$	Beyer and Meyer-Hermann (2008)
k_b	Ligand-receptor binding rate	$\mu\mathrm{m}^2 \times \mathrm{min}^{-1}$	1×10^{-2}	$7 \times 10^{-4} - 0.3$	Sklar (1984); Pelletier (2000); Guo et al. (2008)
k_i	Receptor internalisation rate	min^{-1}	7×10^{-2}	$3 \times 10^{-3} - 1.8$	Beyer and Meyer-Hermann (2008); Guo et al. (2008)
k_r	Receptor recycling rate	min^{-1}	5×10^{-2}	$6 \times 10^{-3} - 0.5$	Beyer and Meyer-Hermann (2008); Guo et al. (2008)
R_0	Initial number of chemokine receptors		5×10^4	$2 \times 10^4 - 2 \times 10^5$	Beyer and Meyer-Hermann (2008); Guo et al. (2008)
σ_{AM}	Sensitivity to bound-receptor differences		1.2×10^{-3}	1.2×10^{-3}	Devreotes and Zigmond (1988); Farrell et al. (1990)

2.4.2. Virtual infection scenario

For studying *A. fumigatus* infection in a three-quarter alveolus with constant radius, the virtual infection scenario from Pollmächer and Figge (2014) was followed. At $t = 0$ a binomially distributed number of AM and the conidium were placed randomly over the surface of the three-quarter alveolus and all grid points were set to zero molecular concentration. AM migrated according to a biased persistent random walk with constant speed v and constant directional persistence time t_p and were able to leave or enter the alveolus at either a pore of Kohn or the alveolar entrance ring. The position of the conidium was fixed over the whole simulation and migration of AM followed the chemotaxis model that was here previously introduced. In each virtual infection scenario the AEC of type I or II that was associated with the randomly positioned conidium released the chemoattractant permanently and homogenously with a constant secretion rate s_{AEC}. The simulation ended at the first physical contact between an arbitrary AM and the conidium. The diffusion coefficient D of the chemokine was varied over a wide range in order to account for the viscosity of the surfactant that is expected to be higher than that of water and to which experimental ranges are typically referring. In **Table 1**, the parameter regimes of the chemotaxis model are summarized and the values that were varied in the simulations are indicated.

2.4.3. Virtual infection scenario including gradient-based recruitment of alveolar macrophages

In Pollmächer and Figge (2014), AM insertion into the three-quarter alveolus followed a uniform distribution over the length of the boundary line elements. Numerical values of chemokine concentrations allow for recruitment of AM from neighboring alveoli based on the strength of the gradient. Realization of gradient-based recruitment was implemented in the following way. First, on AM entrance into the alveolus the maximum gradient was computed, $\max\{||\vec{g}_b(t)||\}$, over the finite set of edges of the triangulated grid that cross the boundary. The pairs of vertices corresponding to these edges each held one vertex labeled as boundary point and the other one labeled as alveolar surface point. Secondly, a uniformly distributed random boundary point $\vec{r}_{b,random}$ was drawn from all possible boundary points and the corresponding probability of AM insertion was calculated as follows:

$$p_{in}(\vec{r}_{b,random}, t) = \frac{||\vec{g}(\vec{r}_{b,random}, t)||}{\max\{||\vec{g}_b(t)||\}} . \quad (14)$$

This probability was used for stochastic AM insertion at position $\vec{r}_{b,random}$ and was realized by a Monte Carlo acceptance-rejection method to sample the gradient-based probability distribution of AM insertion over the boundary points. On rejection of a boundary point a new one was drawn with probability $p_{in}(\vec{r}_{b,random}, t)$ followed by another Monte Carlo decision until a boundary point was accepted. As before, first-passage-time simulations were performed over 10^3 repetitions for each parameter configuration.

3. Results

3.1. Hybrid Agent-Based Model Reproduces Analytical Solutions

We evaluated and validated the numerical solution of our PDE solver by comparison with an analytical solution over the surface of a full sphere (see Section 2.2.4 for details). The mean of the absolute and relative errors per timestep were computed for both varying timesteps and varying numbers of grid points in order to demonstrate the accuracy of the numerical method (see **Figure 2**). The method shows first-order accuracy in the timestep as the absolute and relative mean errors per timestep scale quadratically. Furthermore, it is observed that numerical instability occurs for too large values of Δt, as is expected for an explicit forward-Euler approach. To guarantee

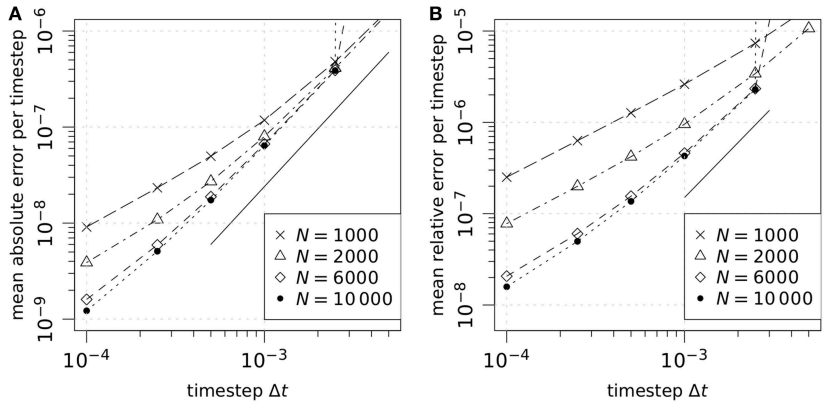

FIGURE 2 | Numerical error analysis of the PDE solver for Equation (2) on the spherical surface with $\lambda = 0$, $S(\vec{r}_k, t) = 0$, and $Q(\vec{r}_k, t) = 0$ at each grid point k. Simulations were carried out in an alveolus with a radius $r = 116.5\,\mu$m from time $t = 0$ min to a final time $t = 1$ min with an isotropic diffusion coefficient of $D = 2000\,\mu m^2$/min. The mean absolute error **(A)** and mean relative error **(B)** per timestep of our PDE solver for different numbers of grid points N and timesteps Δt are compared to the theoretically expected quadratic scaling (*solid line*).

numerical stability in our simulations, we determined the limits of numerical stability for different diffusion coefficients D over the set of grid points $\mathcal{G}$ using the condition

$$\Delta t \leq \min_{k \in \mathcal{G}} \left[\left(D \sum_{l \in \mathcal{N}(k)} \frac{h_{kl}}{d_{kl} A_k} \right)^{-1} \right] \tag{15}$$

and adjusted the global simulation timestep Δt one order of magnitude lower than the respective limits.

3.2. Steady State of Alveolar Chemokine Distribution Reached within Hours

We performed a numerical study to characterize the steady state of the alveolar chemokine distribution in terms of the concentration profile and the time required to reach the steady state (see Video S2 for the transition from the onset of AEC secretion into steady state). Simulations were carried out using one permanently and homogenously secreting AEC of type I in the bottom of an empty alveolus (see Section 2.4.1 for details) In **Figure 3**, we summarize the results of the steady state analysis for varied diffusion coefficients, degradation rates and secretion rates of the chemokine. Interestingly, we found that the time required to reach the steady state depends on the values for the diffusion coefficient D and the degradation rate λ but not on the amount of chemokine secretion s_{AEC} per time (**Figure 3A**). In the absence of degradation, the time required to reach the steady state ranges from 4 min for a diffusion coefficient of $D = 6000\,\mu\mathrm{m}^2/\mathrm{min}$ to 8.5 h for a diffusion coefficient of $D = 20\,\mu\mathrm{m}^2/\mathrm{min}$. In the presence of degradation, the times required to reach the steady

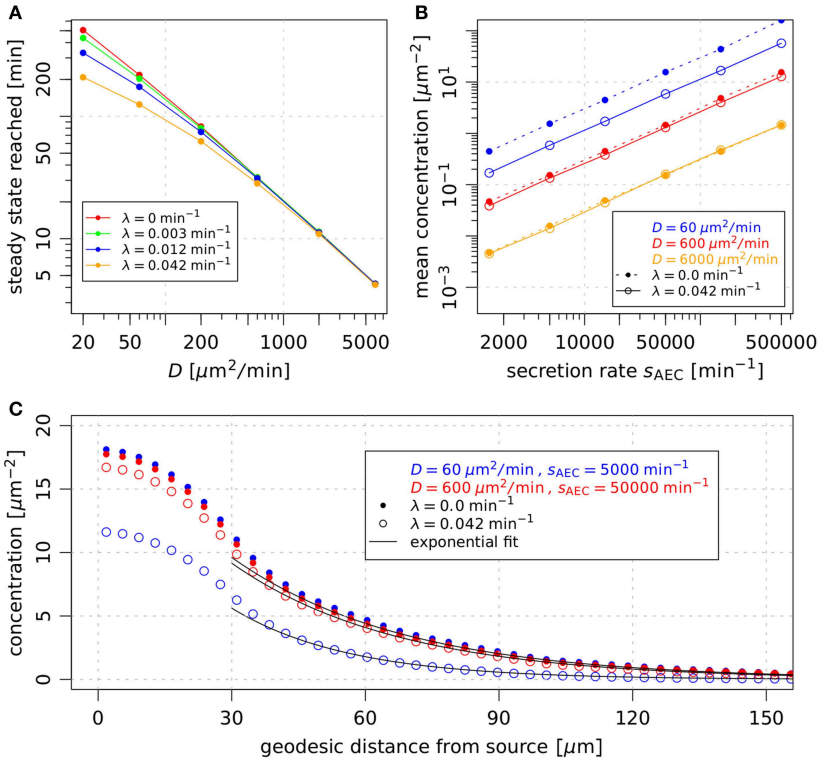

FIGURE 3 | Steady state analysis of the concentration profile in the alveolus for varied diffusion coefficients *D*, secretion rates s_{AEC} and degradation rate λ. One permanently and homogenously secreting source with radius $r_{\mathrm{AEC}} = 30\,\mu$m was placed in the bottom of the three-quarter alveolus and tthe relative concentration changes $\Delta\tilde{c}_{\mathrm{rel}}$ (see Equation 13) were tracked over time at each grid point k. The steady state of the molecular distribution was considered to be reached when the maximum value of $\Delta\tilde{c}_{\mathrm{rel}}$ over all grid points fell below a threshold value of 0.001. **(A)** Comparison of the mean values of the time when steady state was reached for different degradation rates and diffusion coefficients averaging over the secretion rates $\{1.5 \times 10^3, 5 \times 10^3, 1.5 \times 10^4, 5 \times 10^4, 1.5 \times 10^5, 5 \times 10^5\}\,\mathrm{min}^{-1}$. Each mean value has a relative standard deviation less than five percent. **(B)** Average concentration over all grid points labeled as alveolar surface point at steady state. **(C)** Concentration profile at steady state as a function of the geodesic distance from the center of the source. In each simulation concentration values were averaged over points of the three-quarter sphere with equivalent geodesic distance from the center of the source. Here biquadratic interpolation was used to obtain the concentration value at arbitrary points on the alveolar surface. Afterwards the means over simulation runs with identical parameter configuration were computed. We applied exponential fits to each concentration profile using least squares to optimize the parameters a and b in the function $c(x) = a\exp(bx)$ over concentration values at geodesic distances above the AEC radius $r_{\mathrm{AEC}} = 30\,\mu$m.

state were systematically decreasing with increasing degradation rates in a diffusion-dependent fashion (**Figure 3A**).

In **Figure 3B** it can be seen that the parameter variation lead to average concentration values that span a range of five orders of magnitude from $10^{-2}\,\mu\text{m}^{-2}$ to $10^{2}\,\mu\text{m}^{-2}$. The mean concentration was observed to increase linearly with increasing secretion rate s_{AEC}. We found that different parameter combinations showed similar mean concentration values and almost identical concentration profiles over the geodesic distance from the secreting AEC (see **Figure 3C**). Irrespective of the secretion rate, diffusion coefficient and degradation rate the profile of concentration over the surface of the alveolus showed an exponential distance-dependence from the secreting AEC for geodesic distances larger than the radius of the secreting AEC.

We generally observed that the impact of chemokine degradation on the time to reach the steady state and on the amount and profile of the chemokine concentration is largest for small diffusion coefficients (see **Figures 3A–C**). This is a direct consequence of reduced molecule motion, because on average molecules remain in the alveolus for a longer time period before leaving through a pore of Kohn or through the alveolar entrance ring. In particular, the time required to reach the steady state, the average chemokine concentration as well as the level of the concentration profile were lowered for elevated degradation rates. These effects were depending on the diffusion coefficient: While for diffusion coefficents $D \geq 2000\,\mu\text{m}^2/\text{min}$ all three observables were reduced by less than 5% relative to the case with absent degradation, for $D \leq 60\,\mu\text{m}^2/\text{min}$ this reduction was observed to increase up to 85%. For example, in the extreme case of the small diffusion coefficient $D = 20\,\mu\text{m}^2/\text{min}$ and at a secretion rate of 1.5×10^4 molecules per minute, the average concentration ranges between 2.3 and 14.7 molecules per μm^2 and the time required to reach the steady state varied in a degradation-dependent fashion between 3.5 and 8.5 h.

3.3. Virtual Infection Model Reveals Relevant Parameter Regimes

We performed computer simulations on the early immune response against *A. fumigatus* infection mediated by chemokines that are released from the AEC associated with the conidium. In contrast to our previous study, where chemotaxis was modeled in a simplified fashion by a probabilistic rule (Pollmächer and Figge, 2014), we here implemented a numerical solver for the reaction-diffusion equation extending over the inner surface of the alveolus. Thus, in the present implementation AM performed a biased persistent random walk and the directional bias was derived from local sensing of the current chemokine gradient by AM. The relative impact of directional over random migration was inferred from the difference in newly bound AM receptors along the gradient. Computer simulations with the refined AM chemotaxis model, which is described in the Section 2 and depicted in Supplementary Figure S2, enabled us to narrow down the regime of relevant parameters in terms of the diffusion coefficient, the degradation rate and the secretion rate of the postulated chemokine.

3.3.1. First-passage-times are mainly determined by diffusion coefficients and secretion rates

We measured first-passage-times in the alveolus, i.e., the time of first contact between AM and the conidium (see Video S3), in order to determine the requirements on the chemokine properties for a successful discovery of the fungal pathogen before the onset of germination (see Section 2.4.2 for details). First-passage-times were computed for 864 different parameter combinations (see Supplementary data in Supplementary Material) and for each combination 10^3 simulations of the *A. fumigatus* infection scenario were performed to obtain statistically firm results. From the distributions of first-passage-times, we computed the fraction of first-passage-times above 6 h, $p(\text{FPT} > 6\,\text{h})$, where 6 h were chosen based on the typical time period required for *A. fumigatus* germination. The results are presented in **Figure 4** and demonstrate, in agreement with our previous study (Pollmächer and Figge, 2014), that AM with migration speed $v = 2\,\mu\text{m/min}$ exceeded the first-passage-time of 6 h in more than 5 % of the simulations for all parameter combinations (see short-dashed lines in **Figures 4A,D,G**). A comparison of **Figures 4A,D** shows that an increase in the persistence time from $t_{\text{p}} = 1\,\text{min}$ to $t_{\text{p}} = 2\,\text{min}$ was always associated with a decrease of $p(\text{FPT} > 6\,\text{h})$. Next, we found that taking molecular degradation into account did not have a strong impact on $p(\text{FPT} > 6\,\text{h})$, as can be observed by comparing **Figures 4D,G** for $t_{\text{p}} = 2\,\text{min}$. These observations remain qualitatively the same for higher migration speeds of AM, see **Figures 4B,E,H** for $v = 4\,\mu\text{m/min}$ and **Figures 4C,F,I** for $v = 6\,\mu\text{m/min}$. However, higher migration speeds of AM do have a quantitative impact on $p(\text{FPT} > 6\,\text{h})$.

The dashed-dotted and long-dashed lines in **Figure 4** indicate the values of $p(\text{FPT} > 6\,\text{h})$ for AM performing, respectively, a persistent random walk and a biased persistent random walk, as previously simulated in Pollmächer and Figge (2014). The persistent random walk of AM always marks an upper limit for $p(\text{FPT} > 6\,\text{h})$, i.e., first-passage-times are on average always decreased in the presence of chemotaxis, as could be expected for a low concentration of chemokines in the alveolus. On the other hand, compared to the biased persistent random walk model the performance of the chemotaxis model could yield lower values for $p(\text{FPT} > 6\,\text{h})$, depending on the combination of parameters. In particular, we found that this is the case for combinations of a relatively high secretion rate and a relatively low diffusion constant. Note that the probabilistic rule for biased persistent random walk as previously simulated in Pollmächer and Figge (2014) was coupled to the direction of the shortest path from the AM to the AEC associated with the conidium. Occasionally, AM could leave the alveolus through a pore of Kohn if one of them was along the respective path of migration. In the present approach the frequency of this event was reduced, due to preferred AM migration in the direction of the chemokine gradient, which generally pointed away from pores of Kohn (see Videos S2 and S3). In summary, the diffusion coefficient and the secretion rate were again found to be the most important parameters, whereas the value of the degradation rate had only minor impact on $p(\text{FPT} > 6\,\text{h})$ (see **Figures 4G–I**).

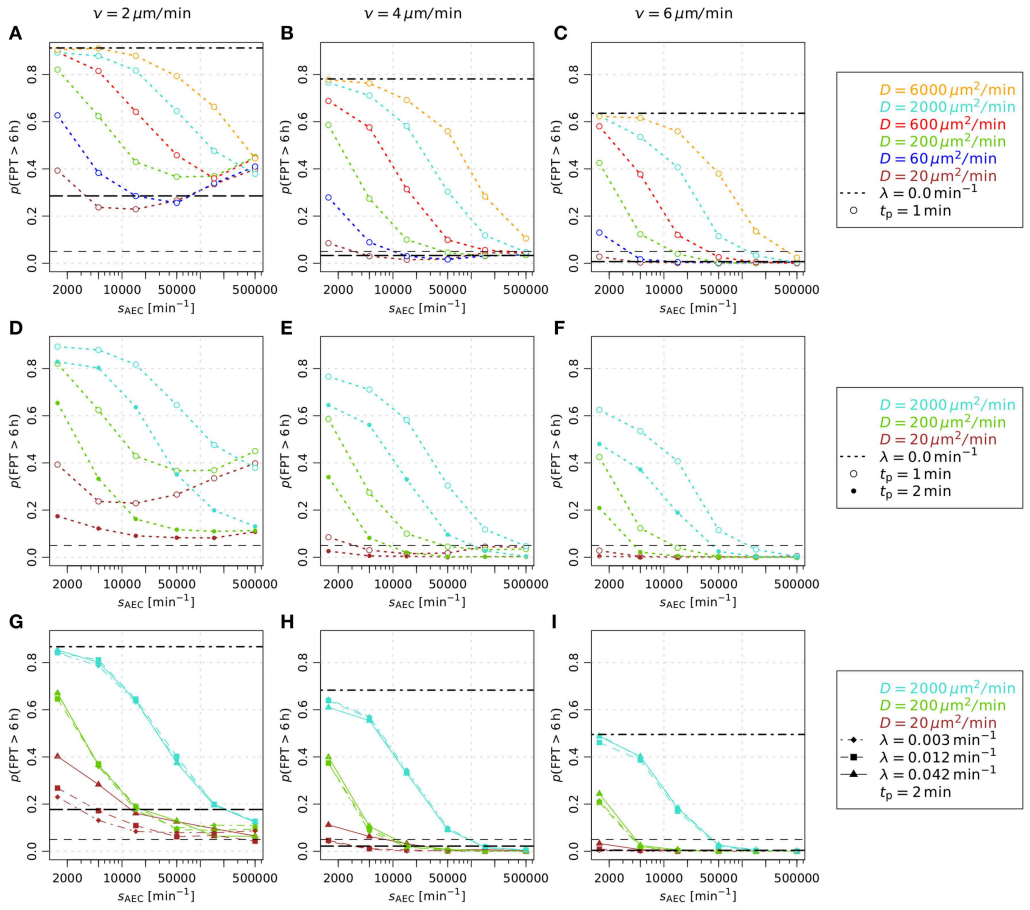

FIGURE 4 | Analysis of first-passage-time distributions varying the macrophage related parameters migration speed and persistence time and varying the chemokine related parameters diffusion coefficient, secretion rate and degradation rate. In each subfigure **(A–I)** the fraction of first-passage-times above 6 h, $p(\text{FPT} > 6\,\text{h})$, is plotted against the secretion rate of the AEC associated with the fungal conidi. The calculation of this fraction is based on the first-passage-time distribution which was derived performing 1000 first-passage-time simulations per parameter configuration. The results of the present study are compared to the biased persistent random walk (*long-dashed black line*) and the persistent random walk (*dashed-dotted black line*) by Pollmächer and Figge (2014). The *short-dashed black line* denotes the threshold $p(\text{FPT} > 6\,\text{h}) = 0.05$. In **(A–C)** the focus is on the variation of diffusion coefficients, **(D–F)** show the results for different persistence times t_p and **(G–I)** demonstrate the influence of the degradation rate λ.

Interestingly, we observed a minimum of $p(\text{FPT} > 6\,\text{h})$ as a function of the secretion rate for various diffusion coefficients in the case of AM migration speed $v = 2\,\mu\text{m/min}$ and persistence time $t_p = 1\,\text{min}$ (see **Figure 4A**). This system behavior reflects the fact that an optimal concentration of chemokines exists for an efficient guidance of AM. The value of the optimal concentration is determined by the interplay of several factors, e.g., the secretion rate, diffusion coefficient and degradation rate of the chemokine as well as the number of AM receptors and their dynamics of binding, internalization and re-expression. For example, a too high chemokine concentration is associated with a low number of unbound AM receptors limiting the adaptation of AM migration along the chemokine gradient. We further analyzed this situation by computing the probability of directed AM migration for different secretion rates and for AM migration speeds $v = 2\,\mu\text{m/min}$ and $v = 4\,\mu\text{m/min}$. The resulting probability distributions are shown in **Figure 5** as a function of the geodesic distance of AM from the AEC associated with the conidium. We found that optimal values of $p(\text{FPT} > 6\,\text{h})$ in **Figure 4A** correspond to probability distributions with a narrow and peaked maximum (see red curves in **Figure 5**). For a constant diffusion coefficient, lower secretion rates were associated with less prominent maxima in the probability distribution (see blue curves in **Figure 5**), which in turn increased $p(\text{FPT} > 6\,\text{h})$. On the other hand, higher secretion rates were associated with extended and flat maxima at relatively large geodesic distances

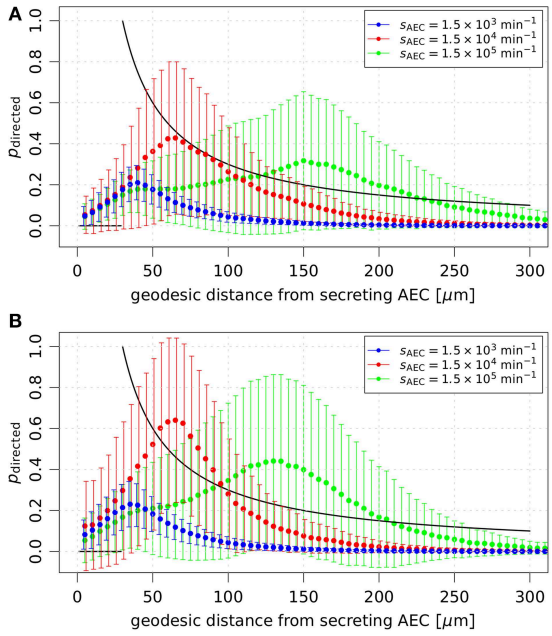

FIGURE 5 | Probabilities of directed AM migration over the geodesic distance from the AEC associated with the conidium. The mean and standard deviation of the probability $p_{directed}$ are shown in the absence of chemokine degradation for the diffusion coefficient $D = 60\,\mu m^2$/min with AM directional persistence time $t_p = 1$ min. In **(A)** AM migrate with speed $v = 2\,\mu$m/min and in **(B)** with speed $v = 4\,\mu$m/min. Averages and standard deviations were determined using the probabilities of directed AM migration that were drawn over the whole simulation time in all simulation runs. The present results are compared to the probabilistic rule for directed migration (*solid black line*) used in Pollmächer and Figge (2014).

from the boundary of the secreting AEC (see green curves in **Figure 5**). It should be noted that the profiles of the determined probability distributions are the results of various factors, such as the chemokine concentration and the receptor dynamics of AM. For example, in the case of high secretion rates, many AM receptors were already bound to the chemokine at early time points due to its relatively high concentration in the alveolus. As a result, AM were guided to the AEC associated with the conidium relatively early in time. However, the relatively high concentration of chemokines also had the adverse effect that the number of free AM receptors was decreased at distances close to the secreting AEC. Consequently, fewer events of receptor-ligand binding lead to relatively low probabilities for directed AM migration and ultimately increased $p(\text{FPT} > 6\,\text{h})$.

An overview of the relevant combinations of model parameters for successful detection of the *A. fumigatus* conidium by AM is given in **Figure 6** for AM migration speed $v = 4\,\mu$m/min (A) and $v = 6\,\mu$m/min (B). As in Pollmächer and Figge (2014), we considered a parameter combination to be successful, if the value of $p(\text{FPT} > 6\,\text{h})$ was below five percent. Interestingly, the ratio between the secretion rate and the diffusion coefficient, s_{AEC}/D, was found to subdivide the parameter space into regimes of successful and unsuccessful parameter combinations. For $v = 4\,\mu$m/min and $t_p = 1$ min, successful detection occurred for $s_{AEC}/D \geq 250\,\mu m^{-2}$ (see **Figure 6A**). Moreover, with increasing directional persistence time and/or migration speed of AM this threshold was found to be systematically reduced. While the combinations $(v, t_p) = (4\,\mu\text{m/min}, 2\,\text{min})$ and $(v, t_p) = (6\,\mu\text{m/min}, 1\,\text{min})$ both shared the condition $s_{AEC}/D \geq 75\,\mu m^{-2}$, for $(v, t_p) = (6\,\mu\text{m/min}, 2\,\text{min})$ this threshold s_{AEC}/D was lowered to the value $25\,\mu m^{-2}$. To summarize, we found that the successful detection of the conidium by AM required the ratio between the secretion rate and the diffusion coefficient to be above a specific threshold, whereas the degradation rate had only minor impact on the first-passage-time (see **Figures 4**, **6**).

3.3.2. Gradient-based recruitment of AM increases relevant parameter regimes

Next, we studied a modification of AM insertion into the system at the boundaries, i.e., the alveolar entrance ring and the pores of Kohn. Previously, AM entered the three-quarter alveolus following a uniform random distribution over the length of the line elements belonging to all boundaries (Pollmächer and Figge, 2014). In the modified setup, we accounted for the time-evolution of the chemokine gradients at the boundaries by specifying probabilities for AM insertion according to the respective gradient strengths. In other words, AM insertion is more likely at boundaries with higher chemokine gradients (see Section 2.4.3 for details).

In **Figures 6C–E** it can be seen that gradient-based recruitment of AM generally increased the regime of parameter combinations for successful detection. At AM speeds of $4\,\mu$m/min and $6\,\mu$m/min the ratio of secretion rate to diffusion coefficient was systematically reduced (see **Figures 6D,E**). In contrast to the case where AM insertion was not gradient-based, in the present case a successful detection was also achieved at the migration speed of $2\,\mu$m/min for specific parameter combinations (see **Figure 6C**). Interestingly, for the AM parameters $(v, t_p) = (2\,\mu\text{m/min}, 1\,\text{min})$ the subdivision of the parameter space into regimes of successful and unsuccessful parameter combinations was not only determined by the ratio s_{AEC}/D. We checked that $p(\text{FPT} > 6\,\text{h})$ has a dependence on the secretion rate similar to the simulations in the absence of gradient-based AM insertion (see **Figure 4A**). However, in the present case the minimum of $p(\text{FPT} > 6\,\text{h})$ reached values below the five percent threshold for a limited range of the secretion rates that gave rise to the triangular region (see **Figure 6C**, blue area). The virtual infection model with gradient-based recruitment underlines the importance of chemokine-induced AM insertion points relative to the conidium position, as the results display a beneficial effect for the immune response of the host.

4. Discussion

In this study, we implemented a hybrid agent-based model (hABM) for *A. fumigatus* infection in human alveoli under physiological conditions to decipher the properties of a chemoattractant responsible for guiding alveolar macrophages

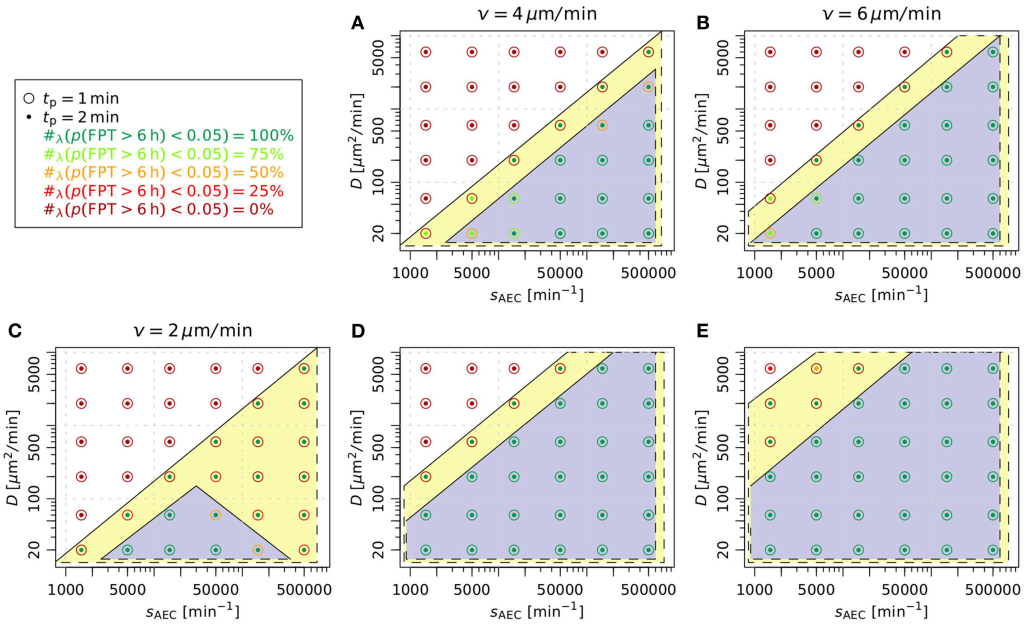

FIGURE 6 | Evaluation of parameters related to the AM chemoattractant based on the fraction of first-passage-times above 6 h. (A,B) summarize the results from **Figure 4**, where AM insertion followed a uniform random distribution over the length of the boundaries of the three-quarter alveolus. The case $v = 2\,\mu$m/min was left out as all parameter combinations lead to $p(\text{FPT} > 6\,\text{h}) \geq 0.05$. In **(C–E)** AM were inserted into the alveolus following a gradient-based probability distribution over the line elements belonging to the boundaries. The highlighted areas denote the regimes of parameters leading to timely detection of the conidium for the directional persistence times $t_p = 1$ min (*blue area*) and $t_p = 2$ min (*yellow area*) of AM under different migration speeds v. The variable $\#_\lambda(p(\text{FPT} > 6\,\text{h}) < 0.05)$ denotes the fraction of simulated degradation rates that lead to $p(\text{FPT} > 6\,\text{h}) < 0.05$ for a specific combination of parameters D and s_{AEC}.

(AM). The multi-scale simulations account for the dynamics at the cellular and molecular level, as well as the kinetics of binding, internalization and re-expression of chemokine receptors on AM. To scan the parameter space for combinations of parameters that ensure the timely detection of a conidium in the alveolus, we performed more than a million simulations of virtual infection scenarios in the experimentally relevant regimes. We were able to show that successful detection of the pathogen by AM is governed by the choice of five experimentally undetermined parameters: migration speed v and directional persistence time t_p of AM as well as the secretion rate s_{AEC}, diffusion coefficient D and the degradation rate λ of the chemokine.

Simulations of the chemokine dynamics on the inner surface of the alveolus with its peculiar boundary conditions were performed using an efficient and accurate finite difference method on Voronoi cells (Sukumar, 2003) to solve the reaction-diffusion equation on an unstructured triangular Delaunay grid with close-to-equidistant grid points. We first studied the chemokine profile in steady state under varying conditions in an empty three-quarter spherical alveolus. Our results show that, depending on the diffusion coefficient of the chemokine, the time until a steady state is reached can vary from several minutes for $D \geq 2000\ \mu\text{m}^2/\text{min}$ to several hours for $D \leq 60\ \mu\text{m}^2/\text{min}$. This revealed that our previous study, where the chemokine dynamics was simplified by a probabilistic rule, is limited to infection scenarios in the limit of high diffusion coefficients (Pollmächer and Figge, 2014). In contrast, using the present approach we are in the position to study *A. fumigatus* infection from the onset of chemokine secretion by alveolar epithelial cells (AEC) induced by the conidium and extending over the time period of establishing a concentration profile until the conidium is successfully found by one of the AM.

Since it was shown that AM require chemotactic cues in order to timely detect the conidium before the start of germination (Pollmächer and Figge, 2014), we here developed the hABM to account for the spatio-temporal concentration of chemokines in the alveolus. We implemented the receptor-kinetics chemotaxis model of Guo et al. (2008) for AM migration on a grid with high spatial resolution to capture the spherical alveolar surface with the pores of Kohn. The chemotaxis model accounts for the binding of G protein-coupled receptors on the surface of AM to the AEC-derived chemoattracting ligands in the alveolar lining layer (surfactant). In general, eukaryotic cells are able to sense spatial differences in receptor occupation along the chemokine gradient by their relatively large size of at least $10\,\mu m$ (van Haastert and Postma, 2007). In order to sense shallow gradients in the chemokine concentration of 1–5 %, chemotactic cells are in addition able to sense temporal differences in receptor occupation, which increases the signal-to-noise ratio and implies higher probabilities of polarization

directed along the gradient (van Haastert and Postma, 2007). We extended the chemotaxis model of Guo et al. (2008) by implementing AM sensing of the cumulated number of newly bound receptors over directional persistence times. This approach advances our previously applied phenomenological chemotaxis model, which was based on a constant function for the distance-dependent gradient strength (Pollmächer and Figge, 2014). In the present study, AM were enabled to sense dynamically changing local chemokine gradient strengths, which implicitly contained morphological information, e.g., concentration gradients pointing away from boundary elements. Simulations of the virtual infection scenario indicated that the present AM chemotaxis model unifies the random migration and chemotactic migration modes of our previous study in one model. In particular, we showed that persistent random walk was resembled for relatively low chemokine concentrations in the alveolus.

The computation of the first-passage-time, i.e., the duration until the conidium is detected by an AM for the first time, revealed the relative importance of the parameters associated with the chemokine distribution: the diffusion coefficient and the rate of chemokine secretion by the AEC associated with the conidium turned out to have a major impact, whereas chemokine degradation played a minor role. In particular, we found that the AEC secretion rate and the diffusion coefficient had counteractive effects regarding the average concentration of chemokines in the surfactant, i.e., decreasing the secretion rate lowered the average concentration whereas decreasing the diffusion coefficient increased it. Chemokines are diffusing in the alveolar lining layer (surfactant), which shields AM from the alveolar airspace, reduces surface tension and provides immunoregulatory proteins (Herzog et al., 2008; Hasenberg et al., 2013). In comparison with chemokine diffusion in water, the relatively high viscosity of the surfactant (Alonso et al., 2005) has the crucial effect to reduce the diffusivity of chemokines and by that to lower the AEC secretion rate required for the timely detection of the pathogen. We found the ratio of the AEC secretion rate to the diffusion coefficient, s_{AEC}/D, to be the main indicator for the outcome of the infection scenario. For specific values of the AM migration speed and directional persistence time, this ratio subdivided the parameter space into regimes of successful and unsuccessful parameter combinations, whereas this separation was only weakly depending on relevant degradation rates. The degradation rate showed to have some impact in virtual infection scenarios with relatively low diffusion coefficients, which was also the case in the simulations associated with the steady state analysis. Thus, decisive reduction of the chemokine amount available to AM due to molecular degradation is only of importance for a highly viscous surfactant. The specific morphology of human alveoli plays an important role in this regard as chemokine reduction was also a consequence of chemokine absorption at the pores of Kohn and the alveolar entrance ring. A relative dominance of chemokine decrease due to alveolar boundaries was determined for relatively high diffusion coefficients, whereas relatively low diffusion coefficients were accompanied with relatively high chemokine degradation. This was attributed to reduced molecule motion for reduced diffusion coefficients, thus, on average molecules remained in the alveolus for a longer time period before leaving through the alveolar boundaries. As observed in our previous study (Pollmächer and Figge, 2014), AM required a minimal migration speed of at least $4\,\mu$m/min to discover the fungal conidium before the onset of germination. However, as shown in the present study, assuming a recruitment of AM from neighboring alveoli that was based on the local chemokine gradient, an average speed of $2\,\mu$m/min was as well successful for a specific subset of parameter combinations. This finding is particularly interesting, because the actual AM migration speed in the alveolus is not known today, but is typically expected to be low (Hasenberg et al., 2013). Generally, our results show that the communication between different types of host immune cells and their reaction to threatening invaders needs to be finely tuned in order to mount and orchestrate a fast and adequate response.

The specific chemokine and AM receptor that are involved in the directed migration are not known today. It is well-known that AM express, for example, the chemokine receptor CXCR2 (Miller et al., 2003) that binds to the cytokine IL-8. Moreover, the presence of complement proteins in the surfactant yields the cleavage product C5a, and this anaphylatoxin is a potential candidate for which AM chemoattraction was observed (Farrell et al., 1990; Zipfel and Skerka, 2009). Resting conidia of *A. fumigatus* activate the complement system entirely by the alternative pathway (Kozel et al., 1989). Upon activation, C3 is cleaved into C3b and C3a, with C3b opsonizing the fungal surface and increasing uptake rates by macrophages (van Lookeren Campagne et al., 2007). Furthermore, C3b induces cleavage of C5 which leads to the production of the prominent proinflammatory and chemoattracting cytokine C5a (Brakhage et al., 2010). However, it is also known that resting *A. fumigatus* conidia reduce the impact of the complement cascade by binding complement regulatory proteins—such as factor H, FHL-1, CFHR-1, C4BP and plasminogon—and by that reducing the deposition of C3b molecules on their surface (Behnsen and Hartmann, 2008). These data suggest that single conidia do both trigger and counteract the complement cascade, such that the mediated stimulus of chemoattraction and inflammation is relatively weak and spatially confined. Nevertheless, it is conceivable that these signals can be detected by the AEC associated with the conidium and that this cell responds with the secretion of the chemokines for AM recruitment. Supporting evidence for this hypothesis is provided by a study of rat AEC of type II: binding of C5a to these cells lead to increased expression of the C5a receptor on the AEC surface and to the production of macrophage inflammatory protein-2 as well as neutrophil-chemoattractant-1 (Riedemann et al., 2002).

Our computational approach to investigate *A. fumigatus* infection complements wet lab experiments. *In vivo* measurements suffer from the circumstance that they can only be carried out with high doses of conidia that do not reflect the physiological condition of daily inhalation rates of a few thousand conidia (O'Gorman and Fuller, 2008; Pollmächer and Figge, 2014). The agent-based modeling approach allows studying the early immune response, i.e., we modeled a setting with those immune cells that are resident in alveoli and

performed virtual infection simulations to low numbers of conidia in a physiologically reasonable host-setting. Simulations enabled narrowing down the experimentally relevant regime of parameters to a subset of potential parameter combinations for healthy individuals. These predictions may initiate further wet lab investigations that should focus on quantitative aspects of the early immune response, e.g., the relative contributions of the complement system and the alveolar epithelial cells to the daily challenge with *A. fumigatus* or the identification of the specific chemokine for AM and the rate at which it is secreted by AEC. Furthermore, if possible by sophisticated imaging techniques in the future, it will be highly interesting to determine values of AM migration speed and migration mode in their natural environment to clarify their general role in the immune response, e.g., as compared to neutrophil migration in the alveolus (Mircescu et al., 2009).

In the context of studying fungal infections, image-based systems biology is able to serve as a well-founded framework with iterative cycles of exchange between experiment and theory and involves imaging, quantitative characterization and modeling of infection processes (Medyukhina et al., 2015). Methods for image-analysis of fungal-host interactions (Mech et al., 2011; Kraibooj et al., 2014; Brandes et al., 2015) and parameter-free classification of cell-tracks (Mokhtari et al., 2013) have been developed over the recent years and have paved the way for the quantification and extraction of the information contained in image- and video data. Furthermore, different individual-based modeling approaches were successfully carried out in combination with automated image-analysis to test hypotheses and to draw predictions that might be tested in future experimental research (Tokarski et al., 2012; Mech et al., 2013; Hünniger et al., 2014). Experimental studies including live-cell imaging in alveolar ducts would give the opportunity to refine, to review and to extend the present virtual infection model.

Author Contributions

Conception and design of the investigation and work: JP, MTF. Contribution of materials and computational resources: MTF. Data processing, implementation and application of the computational algorithm: JP. Evaluation and analysis of the results: JP, MTF. Drafting the manuscript and revising it critically for important intellectual content and final approval of the version to be published: JP, MTF. Agreement to be accountable for all aspects of the work in ensuring that questions related to the accuracy or integrity of any part of the work are appropriately investigated and resolved: JP, MTF.

Acknowledgments

This work was financially supported by the excellence graduate school Jena School for Microbial Communication (JSMC) and the CRC/TR124 FungiNet, Project B4, that are both funded by the Deutsche Forschungsgemeinschaft (DFG).

Supplementary Material

The Supplementary Material for this article can be found online at: http://journal.frontiersin.org/article/10.3389/fmicb.2015.00503/abstract

References

Alonso, C., Waring, A., and Zasadzinski, J. A. (2005). Keeping lung surfactant where it belongs: protein regulation of two-dimensional viscosity. *Biophys. J.* 89, 266–273. doi: 10.1529/biophysj.104.052092

Bastacky, J., and Lee, C. (1995). Alveolar lining layer is thin and continuous: low-temperature scanning electron microscopy of rat lung. *J. Appl. Physiol.* 79, 1615–1628.

Behnsen, J., and Hartmann, A. (2008). The opportunistic human pathogenic fungus *Aspergillus fumigatus* evades the host complement system. *Infect. Immun.* 76, 820–827. doi: 10.1128/IAI.01037-07

Beyer, T., and Meyer-Hermann, M. (2008). Cell transmembrane receptors determine tissue pattern stability. *Phys. Rev. Lett.* 101:148102. doi: 10.1103/PhysRevLett.101.148102

Brakhage, A. A., Bruns, S., Thywissen, A., Zipfel, P. F., and Behnsen, J. (2010). Interaction of phagocytes with filamentous fungi. *Curr. Opin. Microbiol.* 13, 409–415. doi: 10.1016/j.mib.2010.04.009

Brandes, S., Mokhtari, Z., Essig, F., Hünniger, K., Kurzai, O., and Figge, M. T. (2015). Automated segmentation and tracking of non-rigid objects in time-lapse microscopy videos of polymorphonuclear neutrophils. *Med. Image Anal.* 20, 34–51. doi: 10.1016/j.media.2014.10.002

Brown, K. (1979). Voronoi diagrams from convex hulls. *Inf. Process. Lett.* 9:1979. doi: 10.1016/0020-0190(79)90074-7

De Berg, M., Cheong, O., Van Kreveld, M., and Overmars, M. (2008). *Computational Geometry: Algorithms and Applications*, Vol. 17. (Berlin; Heidelberg: Springer-Verlag).

Devreotes, P. N., and Zigmond, S. H. (1988). Chemotaxis in eukaryotic cells: a focus on leukocytes and Dictyostelium. *Annu. Rev. Cell Biol.* 4, 649–686. doi: 10.1146/annurev.cb.04.110188.003245

Farrell, B. E., Daniele, R. P., and Lauffenburger, D. A. (1990). Quantitative relationships between single-cell and cell-population model parameters for chemosensory migration responses of alveolar macrophages to C5a. *Cell Motil. Cytoskeleton* 16, 279–293. doi: 10.1002/cm.970160407

Fels, A., and Cohn, Z. (1986). The alveolar macrophage. *J. Appl. Physiol.* 60, 353–369.

Francis, K., and Palsson, B. O. (1997). Effective intercellular communication distances are determined by the relative time constants for cyto/chemokine secretion and diffusion. *Proc. Natl. Acad. Sci. U.S.A.* 94, 12258–12262. doi: 10.1073/pnas.94.23.12258

Guo, Z., Sloot, P. M. A., and Tay, J. C. (2008). A hybrid agent-based approach for modeling microbiological systems. *J. Theor. Biol.* 255, 163–175. doi: 10.1016/j.jtbi.2008.08.008

Guo, Z., and Tay, J. (2008). "Granularity and the validation of agent-based models," in *Proceedings of the 2008 Spring Simulation Multiconference* (San Diego, CA), 153–161.

Hasenberg, M., Behnsen, J., Krappmann, S., Brakhage, A., and Gunzer, M. (2011). Phagocyte responses towards *Aspergillus fumigatus*. *Int. J. Med. Microbiol.* 301, 436–444. doi: 10.1016/j.ijmm.2011.04.012

Hasenberg, M., Stegemann-Koniszewski, S., and Gunzer, M. (2013). Cellular immune reactions in the lung. *Immunol. Rev.* 251, 189–214. doi: 10.1111/imr.12020

Heinekamp, T., Schmidt, H., Lapp, K., Pähtz, V., Shopova, I., Köster-Eiserfunke, N., et al. (2014). Interference of *Aspergillus fumigatus* with the immune

response. *Semin. Immunopathol.* 37, 141–152. doi: 10.1007/s00281-014-0465-1

Herzog, E. L., Brody, A. R., Colby, T. V., Mason, R., and Williams, M. C. (2008). Knowns and unknowns of the alveolus. *Proc. Am. Thoracic Soc.* 5, 778–782. doi: 10.1513/pats.200803-028HR

Hohl, T. M. (2008). Stage-specific innate immune recognition of *Aspergillus fumigatus* and modulation by echinocandin drugs. *Med. Mycol.* 47(Suppl. I), 1–7. doi: 10.1080/13693780802078131

Horn, F., Heinekamp, T., Kniemeyer, O., Pollmächer, J., Valiante, V., and Brakhage, A. A. (2012). Systems biology of fungal infection. *Front. Microbiol.* 3:108. doi: 10.3389/fmicb.2012.00108

Hünniger, K., Lehnert, T., Bieber, K., Martin, R., Figge, M. T., and Kurzai, O. (2014). A virtual infection model quantifies innate effector mechanisms and candida albicans immune escape in human blood. *PLOS Comput. Biol.* 10:e1003479. doi: 10.1371/journal.pcbi.1003479

Iglesias, P. A., and Devreotes, P. N. (2008). Navigating through models of chemotaxis. *Curr. Opin. Cell Biol.* 20, 35–40. doi: 10.1016/j.ceb.2007.11.011

Kitano, H. (2002). Systems biology: a brief overview. *Science* 295, 1662–1664. doi: 10.1126/science.1069492

Kozel, T. R., Wilson, M. A., Farrell, T. P., and Levitz, S. M. (1989). Activation of C3 and binding to *Aspergillus fumigatus* conidia and hyphae. *Infect. Immun.* 57, 3412–3417.

Kraibooj, K., Park, H.-R., Dahse, H.-M., Skerka, C., Voigt, K., and Figge, M. T. (2014). Virulent strain of Lichtheimia corymbifera shows increased phagocytosis by macrophages as revealed by automated microscopy image analysis. *Mycoses* 57, 56–66. doi: 10.1111/myc.12237

Krombach, F., and Münzing, S. (1997). Cell size of alveolar macrophages: an interspecies comparison. *Environ. Health Perspect.* 105, 1261–1263. doi: 10.1289/ehp.97105s51261

Lin, S., Schranz, J., and Teutsch, S. (2001). Aspergillosis case-fatality rate: systematic review of the literature. *Clin. Infect. Dis.* 32, 358–366. doi: 10.1086/318483

MacWilliam, T., and Cecka, C. (2013). "CrowdCL: web-based volunteer computing with WebCL," in *2013 IEEE High Performance Extreme Computing Conference (HPEC)* (Waltham, MA), 1–6.

Mech, F., Thywissen, A., Guthke, R., Brakhage, A. A., and Figge, M. T. (2011). Automated image analysis of the host-pathogen interaction between phagocytes and *Aspergillus fumigatus*. *PLoS ONE* 6:e19591. doi: 10.1371/journal.pone.0019591

Mech, F., Wilson, D., Lehnert, T., Hube, B., and Thilo Figge, M. (2013). Epithelial invasion outcompetes hypha development during Candida albicans infection as revealed by an image-based systems biology approach. *Cytometry A.* 85, 126–139. doi: 10.1002/cyto.a.22418

Medyukhina, A., Timme, S., Mokhtari, Z., and Figge, M. T. (2015). Image-based systems biology of infection. *Cytometry A.* doi: 10.1002/cyto.a.22638. [Epub ahead of print].

Miller, A. L., Strieter, R. M., Gruber, A. D., Ho, S. B., and Lukacs, N. W. (2003). CXCR2 regulates respiratory syncytial virus-induced airway hyperreactivity and mucus overproduction. *J. Immunol.* 170, 3348–3356. doi: 10.4049/jimmunol.170.6.3348

Mircescu, M. M., Lipuma, L., van Rooijen, N., Pamer, E. G., and Hohl, T. M. (2009). Essential role for neutrophils but not alveolar macrophages at early time points following *Aspergillus fumigatus* infection. *J. Infect. Dis.* 200, 647–656. doi: 10.1086/600380

Mokhtari, Z., Mech, F., Zitzmann, C., Hasenberg, M., Gunzer, M., and Figge, M. T. (2013). Automated characterization and parameter-free classification of cell tracks based on local migration behavior. *PLoS ONE* 8:e80808. doi: 10.1371/journal.pone.0080808

O'Gorman, C. M., and Fuller, H. T. (2008). Prevalence of culturable airborne spores of selected allergenic and pathogenic fungi in outdoor air. *Atmos. Environ.* 42, 4355–4368. doi: 10.1016/j.atmosenv.2008.01.009

Pelletier, A. (2000). Presentation of chemokine SDF-1α by fibronectin mediates directed migration of T cells. *Blood* 96, 2682–2690.

Pollmächer, J., and Figge, M. T. (2014). Agent-based model of human alveoli predicts chemotactic signaling by epithelial cells during early *Aspergillus fumigatus* infection. *PLoS ONE* 9:e111630. doi: 10.1371/journal.pone.0111630

Randolph, G. J., Angeli, V., and Swartz, M. A. (2005). Dendritic-cell trafficking to lymph nodes through lymphatic vessels. *Nat. Rev. Immunol.* 5, 617–628. doi: 10.1038/nri1670

Riedemann, N. C., Guo, R.-F., Sarma, V. J., Laudes, I. J., Huber-Lang, M., Warner, R. L., et al. (2002). Expression and function of the C5a receptor in rat alveolar epithelial cells. *J. Immunol.* 168, 1919–1925. doi: 10.4049/jimmunol.168.4.1919

Sbalzarini, I. F., Hayer, A., Helenius, A., and Koumoutsakos, P. (2006). Simulations of (an)isotropic diffusion on curved biological surfaces. *Biophys. J.* 90, 878–885. doi: 10.1529/biophysj.105.073809

Sklar, L. A. (1984). The dynamics of ligand-receptor interactions. *J. Biol. Chem.* 259, 5661–5669.

Sukumar, N. (2003). Voronoi cell finite difference method for the diffusion operator on arbitrary unstructured grids. *Int. J. Numer. Methods Eng.* 57, 1–34. doi: 10.1002/nme.664

Thomson, J. (1904). XXIV. On the structure of the atom: an investigation of the stability and periods of oscillation of a number of corpuscles arranged at equal intervals around the circumference of a circle; with application of the results to the theory of atomic structure. *Philos. Mag. Ser.* 7, 237–265. doi: 10.1080/14786440409463107

Tokarski, C., Hummert, S., Mech, F., Figge, M. T., Germerodt, S., Schroeter, A., et al. (2012). Agent-based modeling approach of immune defense against spores of opportunistic human pathogenic fungi. *Front. Microbiol.* 3:129. doi: 10.3389/fmicb.2012.00129

Tranquillo, R., Fisher, E., Farrell, B., and Lauffenburger, D. (1988). A stochastic model for chemosensory cell movement: application to neutrophil and macrophage persistence and orientation. *Math. Biosci.* 90, 287–303. doi: 10.1016/0025-5564(88)90071-5

van Haastert, P. J. M., and Postma, M. (2007). Biased random walk by stochastic fluctuations of chemoattractant-receptor interactions at the lower limit of detection. *Biophys. J.* 93, 1787–1796. doi: 10.1529/biophysj.107.104356

van Lookeren Campagne, M., Wiesmann, C., and Brown, E. J. (2007). Macrophage complement receptors and pathogen clearance. *Cell. Microbiol.* 9, 2095–2102. doi: 10.1111/j.1462-5822.2007.00981.x

Zipfel, P. F., and Skerka, C. (2009). Complement regulators and inhibitory proteins. *Nat. Rev. Immunol.* 9, 729–740. doi: 10.1038/nri2620

Conflict of Interest Statement: The authors declare that the research was conducted in the absence of any commercial or financial relationships that could be construed as a potential conflict of interest.

Copyright © 2015 Pollmächer and Figge. This is an open-access article distributed under the terms of the Creative Commons Attribution License (CC BY). The use, distribution or reproduction in other forums is permitted, provided the original author(s) or licensor are credited and that the original publication in this journal is cited, in accordance with accepted academic practice. No use, distribution or reproduction is permitted which does not comply with these terms.

Frontiers

Supplementary Material
19 May 2015

Supplementary Material: Deciphering chemokine properties by a hybrid agent-based model of *Aspergillus fumigatus* infection in human alveoli

Johannes Pollmächer [1,2] **and Marc Thilo Figge** [1,2,*]

[1] *Applied Systems Biology, Leibniz-Institute for Natural Product Research and Infection Biology – Hans Knöll Institute, Jena, Germany*
[2] *Friedrich Schiller University Jena, Jena, Germany*

Correspondence*:
Marc Thilo Figge
Applied Systems Biology, Leibniz-Institute for Natural Product Research and Infection Biology – Hans Knöll Institute, Adolf-Reichwein-Str. 23, Jena , 07749, Germay, thilo.figge@hki-jena.de

Computational Systems Biology of Pathogen-Host Interactions

1 SUPPLEMENTARY DATA

1.1 SIMULATED PARAMETER COMBINATIONS

Simulations of the virtual *A. fumigatus* infection scenario were carried out using 864 different parameter combinations of the chemokine diffusion coefficient D, the chemokine secretion rate s_{AEC}, the degradation rate λ, the AM migration speed v and the AM directional persistence time t_{p}. We performed simulations with 10^3 repetitions for each parameter configuration

$$(D, s_{\mathrm{AEC}}, \lambda, v, t_{\mathrm{p}}) \quad \in \quad \mathcal{D} \times \mathcal{S}_{\mathrm{AEC}} \times \Lambda \times \mathcal{V} \times \mathcal{T}_{\mathrm{p}} \quad ,$$

with the following sets of parameters for the distinct system variables:

$$\begin{aligned} \mathcal{D} &= \{20, 60, 200, 600, 2000, 6000\}\,\mu\mathrm{m}^2/\mathrm{min} \quad , \\ \mathcal{S}_{\mathrm{AEC}} &= \{1\,500, 5\,000, 1.5\times10^4, 5\times10^4, 1.5\times10^5, 5\times10^5\}\,\mathrm{min}^{-1} \quad , \\ \Lambda &= \{0, 0.003, 0.012, 0.042\}\,\mathrm{min}^{-1} \quad , \\ \mathcal{T}_p &= \{1, 2\}\,\mathrm{min} \quad , \\ \mathcal{V} &= \{2, 4, 6\}\,\mu\mathrm{m}/\mathrm{min} \quad . \end{aligned}$$

Parameters related to the chemokine were scanned logarithmically and AM migration parameters were scanned linearly in their respective experimental ranges.

2 SUPPLEMENTARY TABLES AND FIGURES

Figure S1. Macro- and microscopic view on the surface discretization of the three-quarter alveolus. **(A)** A grid with 5000 Voronoi cells, where grid points of category *boundary* and *outside* are left blank. **(B)** Neighbourhood-relationship between the grid points of the triangulated lattice with Voronoi cells providing the measures that are required to numerically solve the PDE.

Figure S2. Chemotaxis model of the mth alveolar macrophage (AM) in the computer simulations. AM (*light green*) are initialized with a population of R_0 free chemokine receptors at $t = 0$ or on boundary insertion into the alveolus during simulation time. Free receptors of each AM bind with the chemokine ligands at grid points covered by the corresponding shape in order to sense the chemokine gradient in the surfactant. Over the time segment of each directional persistence time AM register the accumulation of receptor-ligand bindings which is then used to determine the local AM gradient. Finally, the probability to migrate in the direction of the local gradient is proportional to the difference in bound receptors between the front and the rear of the cell. Thus, the velocity of AM not necessarily point in the direction of the chemokine gradient, but displays a bias depending on the strength of the gradient. See Materials and Methods section of the main document for further details.

3 SUPPLEMENTARY VIDEOS

Video S1. Dynamic overlay of the three-quarter alveolus simulation environment and the Delaunay triangulation of the alveolar surface using $10\,000$ grid points.

Video S2. Time evolution of chemokine distribution in a human three-quarter alveolus in the absence of alveolar macrophages. The alveolar epithelial cell (*yellow*) associated with the conidium of *A. fumigatus* (*red*) secretes chemokines at a rate of $1.5 \times 10^4\,\mathrm{min}^{-1}$, which diffuses with $D = 200\,\mu\mathrm{m}^2/\mathrm{min}$ and $\lambda = 0\,\mathrm{min}^{-1}$. Isolines (*white*) of the concentration values $\{2, 1, 0.5, 0.25\}\,\mu\mathrm{m}^{-2}$ are plotted proportional to their respective values with different sizes. The video is sampled at a rate of 12 frames per second and the time between two frames corresponds to 0.5 minutes real time.

Video S3. Virtual infection scenario of *A. fumigatus* (*red*) in a human three-quarter alveolus. Alveolar macrophages (*green*) migrate with speed $v = 4\,\mu\mathrm{m}/\mathrm{min}$ and with directional persistence time $t_\mathrm{p} = 2\,\mathrm{min}$. The alveolar epithelial cell (*yellow*) associated with the conidium of *A. fumigatus* (*red*) secretes chemokines at a rate of $1.5 \times 10^4\,\mathrm{min}^{-1}$, which diffuses with $D = 200\,\mu\mathrm{m}^2/\mathrm{min}$ in the absence of degradation. Isolines (*white*) of the concentrations $\{2, 1, 0.5, 0.25\}\,\mu\mathrm{m}^{-2}$ are plotted proportional to their respective values with different sizes. The video is sampled at a rate of 12 frames per second and the time between two frames corresponds to 0.5 minutes real time.

4.4 Bottom-up modeling approach for the quantitative estimation of parameters in pathogen-host interactions

frontiers in Microbiology

ORIGINAL RESEARCH
published: 19 June 2015
doi: 10.3389/fmicb.2015.00608

Bottom-up modeling approach for the quantitative estimation of parameters in pathogen-host interactions

Teresa Lehnert[1,2†], *Sandra Timme*[1,2†], *Johannes Pollmächer*[1,2], *Kerstin Hünniger*[3], *Oliver Kurzai*[2,3] *and Marc Thilo Figge*[1,2*]

[1] *Applied Systems Biology, Leibniz Institute for Natural Product Research and Infection Biology - Hans-Knöll-Institute, Jena, Germany,* [2] *Faculty of Biology and Pharmacy, Friedrich Schiller University Jena, Jena, Germany,* [3] *Fungal Septomics, Septomics Research Center, Friedrich Schiller University and Leibniz Institute for Natural Product Research and Infection Biology Hans-Knöll-Institute, Jena, Germany*

OPEN ACCESS

frontiers in Microbiology

ORIGINAL RESEARCH
published: 19 June 2015
doi: 10.3389/fmicb.2015.00608

Bottom-up modeling approach for the quantitative estimation of parameters in pathogen-host interactions

Teresa Lehnert[1,2†], *Sandra Timme*[1,2†], *Johannes Pollmächer*[1,2], *Kerstin Hünniger*[3], *Oliver Kurzai*[2,3] *and Marc Thilo Figge*[1,2*]

[1] Applied Systems Biology, Leibniz Institute for Natural Product Research and Infection Biology - Hans-Knöll-Institute, Jena, Germany, [2] Faculty of Biology and Pharmacy, Friedrich Schiller University Jena, Jena, Germany, [3] Fungal Septomics, Septomics Research Center, Friedrich Schiller University and Leibniz Institute for Natural Product Research and Infection Biology Hans-Knöll-Institute, Jena, Germany

OPEN ACCESS

Edited by:
Saliha Durmus, Gebze Technical University, Turkey

Reviewed by:
Reiko Tanaka, Imperial College London, UK
Muhammed Erkan Karabekmez, Bogazici University, Turkey

***Correspondence:**
Marc Thilo Figge, Applied Systems Biology, Leibniz Institute for Natural Product Research and Infection Biology - Hans Knöll Institute, Adolf-Reichwein-Straße 23, Beutenberg Str 11a, 07745 Jena Germany
thilo.figge@hki-jena.de

[†] *These authors have contributed equally to this work.*

Specialty section:
This article was submitted to Infectious Diseases, a section of the journal Frontiers in Microbiology

Received: *15 April 2015*
Accepted: *02 June 2015*
Published: *19 June 2015*

Citation:
Lehnert T, Timme S, Pollmächer J, Hünniger K, Kurzai O and Figge MT (2015) Bottom-up modeling approach for the quantitative estimation of parameters in pathogen-host interactions. Front. Microbiol. 6:608. doi: 10.3389/fmicb.2015.00608

Opportunistic fungal pathogens can cause bloodstream infection and severe sepsis upon entering the blood stream of the host. The early immune response in human blood comprises the elimination of pathogens by antimicrobial peptides and innate immune cells, such as neutrophils or monocytes. Mathematical modeling is a predictive method to examine these complex processes and to quantify the dynamics of pathogen-host interactions. Since model parameters are often not directly accessible from experiment, their estimation is required by calibrating model predictions with experimental data. Depending on the complexity of the mathematical model, parameter estimation can be associated with excessively high computational costs in terms of run time and memory. We apply a strategy for reliable parameter estimation where different modeling approaches with increasing complexity are used that build on one another. This bottom-up modeling approach is applied to an experimental human whole-blood infection assay for *Candida albicans*. Aiming for the quantification of the relative impact of different routes of the immune response against this human-pathogenic fungus, we start from a non-spatial state-based model (SBM), because this level of model complexity allows estimating *a priori* unknown transition rates between various system states by the global optimization method *simulated annealing*. Building on the non-spatial SBM, an agent-based model (ABM) is implemented that incorporates the migration of interacting cells in three-dimensional space. The ABM takes advantage of estimated parameters from the non-spatial SBM, leading to a decreased dimensionality of the parameter space. This space can be scanned using a local optimization approach, i.e., *least-squares error estimation* based on an *adaptive regular grid search*, to predict cell migration parameters that are not accessible in experiment. In the future, spatio-temporal simulations of whole-blood samples may enable timely stratification of sepsis patients by distinguishing hyper-inflammatory from paralytic phases in immune dysregulation.

Keywords: state-based model, agent-based model, pathogen-host interaction, parameter estimation, whole-blood infection assay, *Candida albicans*

1. Introduction

The human fungal pathogen *Candida albicans* is part of the normal microbial flora in more than half of the global population. In immunocompromised patients it can become invasive and may enter the blood stream via medical devices, e.g., catheters, or translocation in the gut and can cause severe systemic infections. The immune response against *C. albicans* in human blood comprises the interplay of various complex biological processes involving different immune mechanisms (Duggan et al., 2015b). Most importantly, the whole-blood infection assay allows multiple immune effector mechanisms to occur at the same time and thus modulate the overall outcome (Luo et al., 2013; Cunha et al., 2014; Hünniger et al., 2015). Applying a systems biology approach, we quantified individual processes and in this way revealed the main route of the immune response against *C. albicans* in human blood (Hünniger et al., 2014). This was achieved by an iterative systems biology cycle involving experiment, mathematical modeling, hypothesis generation and further experimental investigation.

The choice of an appropriate mathematical modeling approach strongly depends on the questions to be answered and the hypothesis, as well as the characteristics of the underlying experimental data with regard to temporal and spatial information. A wide range of modeling approaches exists that differ by their computational complexity and can be classified depending on the degree of spatial representation as well as the internal degrees of freedom attributed to the model entities. The computationally cheapest modeling approach for dynamic systems is represented by ordinary differential equations (ODE), where biological entities are assumed to be present in high numbers and spatial information is not required such that they can be collectively represented by a homogeneously distributed concentration variable. State-based models (SBM) resolve the biological entities as individuals that occupy states and are able to perform transitions between states representing dynamic processes. In contrast to ODE, this approach allows modeling discrete events for any entity number in a biological system. However, SBM are in turn limited in that they do not represent spatial aspects. Individual-based models (IBM) such as cellular automata (CA) and agent-based models (ABM) do simulate discrete entities in space and time (Medyukhina et al., 2015). In a CA simulation, these entities can undergo state changes associated with their internal degrees of freedom as well as positional changes on a pre-defined spatial grid of computational cells (Von Neumann, 1951; Bittig and Uhrmacher, 2010). The discrete number of individual entities as well as the spatial representation of the environment result in increasing computational costs in terms of run-time and memory. Even more computationally expensive but biologically more realistic simulations can be performed by the ABM approach. Here, biological objects are represented as individual entities, so-called agents, that are able to move in space and can act as well as interact with other agents according to individual properties. Examples of ABM for the pathogen-host interaction between the human-pathogenic fungus *Aspergillus fumigatus* and phagocytes were presented by Tokarski et al. (2012) and Pollmächer and Figge (2014). In particular, the ABM developed by Pollmächer and Figge (2014) simulates the detection of *A. fumigatus* conidia by macrophages in a to-scale representation of human alveoli and predicts the requirement of a chemotactic signal guiding the phagocytes to the spatial positions of conidia.

In general, parameters of bio-mathematical models characterize the components by their morphology and their dynamic behavior. For example, cells may be defined by parameters for size and shape as well as by parameters for interactions in the spatial environment that are associated with the typical frequency of interaction processes. Model parameters associated with dynamical, functional and morphological aspects of biological processes may be extracted from microscopic images by applying an image-based systems biology approach (Horn et al., 2012; Mech et al., 2014; Medyukhina et al., 2015). However, in many cases microscopy experiments cannot be performed for technical reasons, as is also the case for whole-blood infection assays where the majority of cells are erythrocytes blocking the view on leukocytes, let alone fungal pathogens that are present in even lower numbers. In situations like these, numerical estimation of *a priori* unknown parameter values by comparison with experimental time-series data becomes a highly relevant issue. Parameter estimation algorithms are applied to find the optimal match between the experimental data and simulated model data. These optimization algorithms can be characterized by their search technique within the parameter space, i.e., as global or local approaches, and their mathematical procedures, i.e., as stochastic or deterministic approaches (Moles et al., 2003; Ashyraliyev et al., 2009). Local optimization techniques search for better parameter values within a locally restricted parameter space, where the direct search method and gradient based methods are widely used (Ashyraliyev et al., 2009). They show fast convergence to the optimal parameter values, but since local optimization algorithms will get stuck in a nearby local optimum, an educated guess of the initial parameter values is absolutely required. In contrast, global optimization strategies search a wide range of the parameter space with possibly various local optima and the subclass of deterministic optimization strategies can find the global optimum with pre-defined accuracy (Ashyraliyev et al., 2009). High-dimensional parameter spaces may be searched by stochastic optimization algorithms that make use of probabilistic elements to avoid getting trapped in local optima in order to find the global optimum. Common stochastic search algorithms of this type are Metropolis Monte Carlo (MMC) (Metropolis et al., 1953), adaptive random search and evolutionary computation techniques such as differential evolution (DE) (Storn and Price, 1997). Additionally, heuristics can be applied in support of a fast convergence rate of global or local optimization strategies, e.g., simulated annealing (SA) (Kirkpatrick et al., 1983; Gonzalez et al., 2007), great deluge (Dueck, 1993), or performing multiple searches from random start parameters. The selection of the most suitable optimization algorithm depends on specific model properties, such as the dimension of the parameter space and the computational costs for the model simulations that have to be repeatedly performed. For computationally cheap ODE models, the computationally expensive stochastic global optimization algorithms may be used,

such as DE applied by Hernandez-Vargas et al. (2014) and SA based on MMC applied by Hünniger et al. (2014) and Mech et al. (2014).

The non-spatial virtual infection model of the immune response against *C. albicans* in human blood was formulated as a SBM and its parameters were fitted to the experimentally determined time-evolution of concentrations for *C. albicans* cells that are alive or killed and that can either reside in extracellular space or inside immune cells of different types, i.e., monocytes or granulocytes (polymorphonuclear neutrophils, PMN) (Hünniger et al., 2014). Furthermore, we observed a cell population of *C. albicans* that remained alive or killed in extracellular space, i.e., these fungal cells are resistant against phagocytosis and/or killing. The different *C. albicans* cell populations were assigned states and individual cells could perform transitions between states, such as phagocytosis by immune cells, subsequent intracellular killing, extracellular killing by antimicrobial peptides or acquiring resistance against phagocytosis and/or killing. Resistant *C. albicans* cells are a population of cells that were found to be protected against phagocytosis and/or killing and that remained in the extracellular space of the whole-blood infection assay (Hünniger et al., 2014). Since the model is restricted to the dynamics of states occupied by pathogenic cells we refer to the model by Hünniger et al. (2014) as P-SBM. In the present study, motivated by newly measured experimental data regarding the immune cell number of monocytes and PMN in the whole-blood assays, we take the next step and modify the P-SBM to drop its implicit assumption that the number of immune cells for samples from different individuals would be the same. Since in the modified SBM states are assigned to the pathogenic cells as well as to the two types of immune cells, which have been found to actively participate in *C. albicans* elimination, we will refer to this model as PI-SBM. Taking individual immune cells explicitly into account obviously makes the simulations of the whole-blood infection assay more realistic, albeit at the expense of higher computational costs for global parameter optimization that will be performed using SA based on the MMC scheme as was the case for the P-SBM.

A timely stratification of sepsis patients in different phases of immune dysregulation requires spatio-temporal simulations of whole-blood samples. To achieve this goal, an ABM of the whole-blood infection assay was established that builds on the PI-SBM and incorporates spatial properties of the blood sample in a three-dimensional continuous representation. In particular, in the ABM *C. albicans* cells as well as monocytes and PMN are agents that can migrate in the environment and interact with each other. Apart from the model parameters associated with the migration of cells, the ABM was based on the transition rates of the PI-SBM after appropriate conversion. This procedure strongly reduces the number of *a priori* unknown parameters of agents to the subset of migration parameters. The latter can be estimated using the computationally cheap grid search algorithm and enables the prediction of the migration behavior for the different immune cell types that are otherwise not directly accessible in experiment. The interrelations between the different modeling approaches are schematically shown in **Figure 1** demonstrating that results are re-used across different modeling approaches to simultaneously facilitate an increase in model complexity and a decrease in computational expense for parameter estimation. Our step-wise computational biology approach avoids typical limitations of realistic models by focusing parameter estimation on those parameters that arise at the next level of model complexity.

2. Materials and Methods

2.1. Non-spatial State-based Model

The initial version of the non-spatial SBM describes the dynamics of state transitions for the human-pathogenic fungus *C. albicans* in whole-blood samples of healthy donors (Hünniger et al., 2014). In agreement with experimental data, the time-evolution of different *C. albicans* cells that are alive or killed and in extracellular space or phagocytosed by either monocytes or PMN can be simulated in this way. Since this SBM assumes the number of immune cells to be constant across blood samples of different donors and does only simulate the dynamics of the pathogenic (P) cells, it is hereafter referred to as P-SBM. However, it is known that the number of immune cells may strongly vary across human individuals and in particular for patients. Therefore, we increase the model complexity by advancing the P-SBM to a model that does explicitly account for the number of immune cells being present in a hemogram. Data including immune cell counts can easily be obtained both in an experimental as well as in a clinical setting. This model is hereafter referred to as PI-SBM to indicate that state transitions are computed for pathogenic (P) as well as immune (I) cells.

For comparison between the model predictions and the experimentally determined kinetics in the whole-blood infection assay, we introduce specific combinations of states, referred to as *combined units*, that are measurable and useable for the parameter estimation. These comprise all extracellular *C. albicans* cells C_E,

$$C_E \equiv C_{AE} + C_{KE} + C_{AR} + C_{KR}\,, \tag{1}$$

that are either alive (C_{AE}) or killed (C_{KE}) cells in extracellular space as well as cells resistant against killing and/or phagocytosis that are either alive (C_{AR}) or killed (C_{KR}). Next, the combined units C_M and C_G refer to *C. albicans* cells that are phagocytosed, respectively, by monocytes

$$C_M \equiv \sum_{i\geq 0}\sum_{j\geq 0} M_{i,j}\,(i+j)\,, \tag{2}$$

or by granulocytes

$$C_G \equiv \sum_{i\geq 0}\sum_{j\geq 0} G_{i,j}\,(i+j)\,. \tag{3}$$

Here, $M_{i,j}$ and $G_{i,j}$ refer to the number of monocytes and granulocytes (PMN), respectively, with i alive and j killed phagocytosed *C. albicans* cells. We limit the maximal number of *C. albicans* cells that can be phagocytosed by an immune

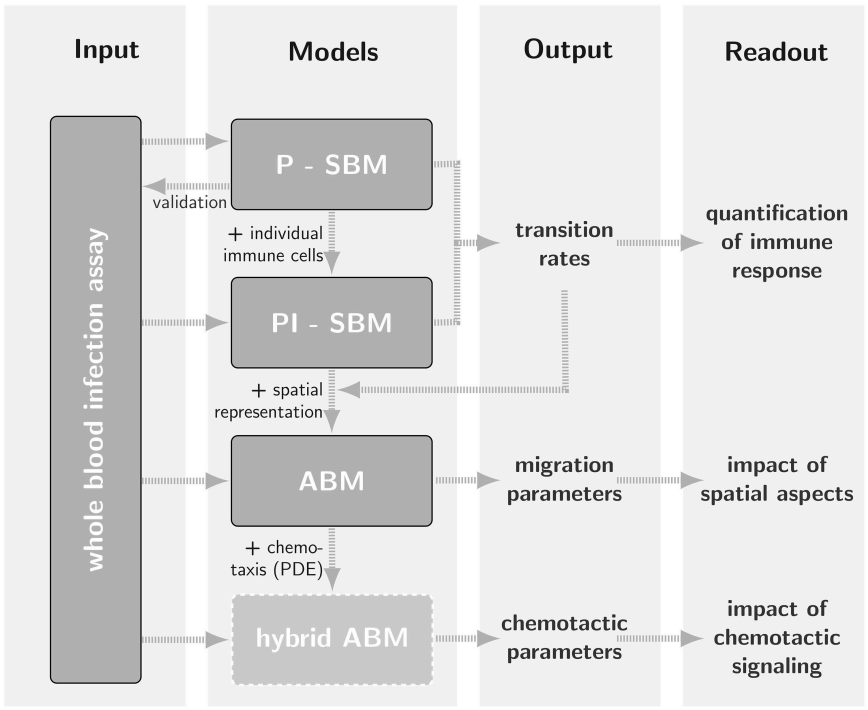

FIGURE 1 | Schematic representation of the bottom-up modeling approach as a strategy for parameter estimation where different mathematical models with increasing levels of complexity build on one another. Using model outputs at one level for calibration of models at a higher level is by way of example demonstrated for *Candida albicans* infection in a human whole-blood assay (Hünniger et al., 2014). The state-based model P-SBM, which focuses on the viewpoint of pathogens, was modified into the state-based model PI-SBM by accounting for actions of individual immune cells. After calibration of transition rates in the non-spatial state-based model, these were used to simulate the infection process in an agent-based model (ABM) that accounts for the spatial representation of the whole-blood infection assay. In the future, the calibration of migration parameters may for example serve as input for a hybrid ABM that captures the time-evolution of chemotactic signaling by solving reaction-diffusion equations.

cell to 18, i.e., $i, j < 10$, being much larger than observed in experiment (Hünniger et al., 2014). Furthermore, all killed *C. albicans* cells are given by the combined unit

$$C_K \equiv C_{KE} + C_{KR} + \sum_{i\geq 0}\sum_{j\geq 1}(M_{i,j} + G_{i,j})\, j\,, \tag{4}$$

and all alive *C. albicans* cells by the combined unit

$$C_A \equiv C_{AE} + C_{AR} + \sum_{i\geq 1}\sum_{j\geq 0}(M_{i,j} + G_{i,j})\, i\,. \tag{5}$$

It should be noted that only three of the five combined units are independent of each other, due to the conservation relations $C = C_E + C_G + C_M$ and $C = C_K + C_A$ for the total number of *C. albicans* cells C.

The simulation algorithm for the time-evolution of the PI-SBM is implemented in `C++` that is available upon request. In **Figure 2A**, the simulation algorithm is schematically depicted and can be compared to the simulation algorithm of the P-SBM in Supplementary Figure 1. We simulate a blood sample of 1 ml containing 5×10^5 monocytes, 5×10^6 PMN and 1×10^6 *C. albicans* cells that are initially extracellular and alive. In each time-step, which we set to $\Delta t_{PI-SBM} = 1$ min, the algorithm tests for each individual cell in the system whether or not it does undergo a state transition. To this end, a cell is first randomly selected by sampling its relative frequency of occurrence among all cell types in the system. Next, the state of this cell is updated using a random selection procedure for the one transition in this time-step that the cell can possibly make among all currently enabled transitions. Once the type of transition between states s and s' with rate $r_{s\to s'}$ is selected, it will be executed with probability $P_{s\to s'} = r_{s\to s'}\,\Delta t_{PI-SBM}$ and the system is updated accordingly. **Table 1** provides an overview of the transition rates for all possible state transitions of the model. After testing all individuals in the system for performing a state transition, the simulation time is advanced by one time-step and the whole procedure is repeated until the total simulation time is reached. Note that, since the ratio of the number of immune cells over the number of pathogenic cells is larger than five, the simulation run time of the PI-SBM is significantly increased compared with the P-SBM.

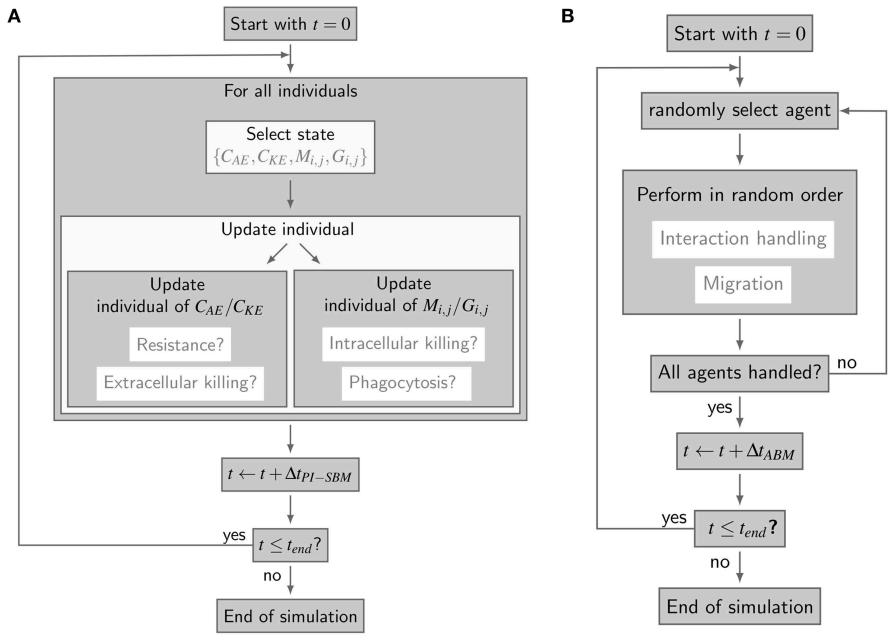

FIGURE 2 | Simulation algorithms of virtual infection models for whole-blood assays. (A) Flow-chart of the non-spatial PI-SBM simulation algorithm. In each time-step Δt_{PI-SBM}, all individuals are tested for possible state transitions. Individuals of extracellular alive and killed *C. albicans* states, i.e., C_{AE} and C_{KE}, respectively, are tested for becoming resistant and for extracellular killing. Individuals of immune cell states ($M_{i,j}$ or $G_{i,j}$) are tested for phagocytosis of *C. albicans* and for intracellular killing. **(B)** Flow chart of the spatial ABM simulation algorithm. In each time-step Δt_{ABM}, the migration and interaction handling is performed in random order for every randomly chosen agent.

2.2. Spatial Agent-based Model

The spatial virtual infection model for *C. albicans* in human blood is realized using an ABM approach. This model is implemented in C++ based on a previously established framework of Pollmächer and Figge (2014) and is the spatial counterpart of the non-spatial PI-SBM introduced in Section 2.1. The C++ source code of the ABM simulation algorithm is available upon request. In the ABM, the two types of immune cells—monocytes and PMN—as well as the pathogenic *C. albicans* cells are incorporated as virtual objects. These virtual objects are agents that are characterized by a spherical morphology with the physiological diameters of $d_M = 16\,\mu$m for monocytes, $d_G = 13.5\,\mu$m for PMN (Mak and Saunders, 2011) and $d_C = 7\,\mu$m for *C. albicans* (Mendling, 2006) (see **Figure 3A**) and that can migrate and interact with each other on encounter in the three-dimensional spatial environment (see **Figure 3B**). We impose a cuboid environment with an edge length of $1000\,\mu$m representing $1\,\mu$l blood and use *random periodic* boundary conditions for the cuboid, i.e., an agent which leaves the environment at some boundary point is deleted from the system and a new agent with identical properties re-enters the environment at some other randomly chosen boundary point. The cuboid environment is represented as a continuous space, i.e., allowing agents to move in a manner that is more realistic than could be captured by a lattice-based approach. This advantage is accompanied by the drawback that well-defined neighborhood relations as naturally existing between neighboring sites on a lattice are not present in continuous space representations. However, in order to efficiently determine cell–cell encounters, we use a neighborhood list method, which reduces the computational complexity to a close-to linear dependency on the number of agents in the system (Rapaport, 1996). At time point $t = 0$, agents are initialized with all *C. albicans* cells being in the state alive-and-extracellular. The time-evolution of the system is simulated by the random selection method (Skvoretz, 2002; Figge, 2005) that handles the migration and interaction of agents per time-step Δt in a random fashion (see **Figure 2B**).

We use ratios in cell numbers that are equivalent to those in the PI-SBM, where $1\,\mu$l of blood contains 5×10^3 PMN, 5×10^2 monocytes and 1×10^3 *C. albicans* cells, i.e., in total 6.5×10^3 cells. Viewing cells as interacting point particles, an average volume of $v \approx \frac{1}{6.5}\times10^6\,\mu\text{m}^3$ can be attributed to each cell, implying an average distance of $l \approx v^{1/3} \approx 55\,\mu$m between immune cells and *C. albicans* cells. Even though this distance is clearly larger than the diameters of these cells, $l \gg d_M, d_G, d_C$, we assume that the migration behavior of immune cells and *C. albicans* cells in blood resembles a random walk of agents without directional persistence. This assumption is based on the fact that the total number of erythrocytes in human blood ranges from $4\times10^6 - 6\times10^6$ cells/μl (McClatchey, 2003). Estimating the total number of cells in $1\,\mu$l of blood to be about six millions, an average volume

TABLE 1 | Rates of state transitions in the non-spatial PI-SBM.

Transition rate	Description	State transition
ϕ_M	Phagocytosis by monocytes	$M_{i,j} + C_{AE} \rightarrow M_{i+1,j}$ $M_{i,j} + C_{KE} \rightarrow M_{i,j+1}$
κ_M	Intracellular killing by monocytes	$M_{i,j} \rightarrow M_{i-1,j+1}$
ϕ_G	Phagocytosis by PMN for first-time phagocytosis event	$G_{0,0} + C_{AE} \rightarrow G_{1,0}$ $G_{0,0} + C_{KE} \rightarrow G_{0,1}$
$\phi_{G^\star}$	Phagocytosis by PMN for repeated phagocytosis events	$G_{i,j} + C_{AE} \rightarrow G_{i+1,j}$ $G_{i,j} + C_{KE} \rightarrow G_{i,j+1}$
κ_G	Intracellular killing by PMN	$G_{i,j} \rightarrow G_{i-1,j+1}$
$\kappa_{EK}(t)$	Extracellular killing by antimicrobial peptides released by first-time PMN phagocytosis with decreasing activity Rate depends on the activity of antimicrobial peptides ($\bar{\kappa}_{EK}$) and the decay of their antimicrobial activity (γ) as defined in Hünniger et al. (2014)	$C_{AE} \rightarrow C_{KE}$
ρ	Resistance against phagocytosis and/or killing	$C_{AE} \rightarrow C_{AR}$, $C_{KE} \rightarrow C_{KR}$

For details see (Hünniger et al., 2014).

of $v_c \approx \frac{1}{6}\times 10^3\,\mu\text{m}^3$ can be attributed to each cell, implying a mean free path of $l_{fp} \approx v_c^{1/3} \approx 5\,\mu$m between point particles. This distance is not only clearly smaller than the distance between immune cells and *C. albicans* cells, $l_{fp} \ll l$, but also smaller than the diameters of erythrocytes, *C. albicans* cells as well as of the immune cells under consideration. It can be concluded that cells are not migrating with directional persistence in blood, because frequent collisions with the overwhelming number of erythrocytes will induce diffusive migration of cells with diffusion coefficients in whole-blood that can be very different for the different cell types. This is a consequence of the fact that monocytes and PMN perform active migration, whereas *C. albicans* cells are immotile due to the complete lack of cellular organelles for motility (Margulies and Schwartz, 1998) and its movement in whole blood is only passive.

Even though blood is a non-Newtonian fluid, i.e., showing pseudoplastic properties with variable viscosity depending on the exerted shear stress in capillaries of different sizes (Fahraus and Lindqvist, 1931), the experimental setup of the whole-blood infection assay is such that the viscosity as well as the temperature in the mildly stirred test tube remain constant (Hünniger et al., 2014). Therefore, the Stokes-Einstein equation (Einstein, 1905) can be applied to infer the diffusion coefficient D_C for the passive movement of *C. albicans* cells. Based on a whole-blood viscosity of about $\eta \approx 4\,mPa\,s$ (Rosenson et al., 1996), Boltzmann constant k_B and temperature $T = 37°$C (Hünniger et al., 2014), this yields the relatively small diffusion coefficient $D_C = k_B T/(3\pi\eta d_C) \approx 1\,\mu\text{m}^2/\text{min}$. In contrast, the active migration of monocytes and PMN requires to estimate their diffusion coefficients numerically.

The time-step Δt_{ABM} for simulations in the ABM has to be chosen such that a smooth migration of cells is sampled in time. In order to ensure this, we require that during one time-step Δt_{ABM} cells do not migrate further than a certain distance, which we set to equal the mean free path $l_{fp} = 5\,\mu$m:

$$\Delta t_{ABM} = \frac{l_{fp}^2}{6\,D_{max}}\,. \tag{6}$$

Here, $D_{max} \equiv \max\{D_C, D_M, D_G\}$ denotes the largest out of the three diffusion coefficients for *C. albicans* cells (D_C), monocytes (D_M), and PMN (D_G). Since it can be expected that the active migration of immune cells is associated with diffusion coefficients D_M and D_G with $D_M, D_G \gg 1\,\mu\text{m}^2/\text{min}$ in the whole-blood infection assay, it follows from Equation (6) that the time-step in the ABM will be much smaller than in the state-based model PI-SBM: $\Delta t_{ABM} \ll \Delta t_{PI-SBM} = 1$ min. Moreover, stochasticity in the ABM requires that each simulation has to be repeated multiple times, resulting into relatively high computational costs compared with the PI-SBM, in particular, if we would have envisaged to estimate each model parameter instead of following the strategy of a bottom-up modeling approach.

Computational costs associated with parameter estimation in the ABM can be significantly reduced by making use of the previously estimated rates of state transitions in the state-based model PI-SBM (see Section 2.1 and **Table 1**). In the course of a simulation, migrating cells in the ABM may either spontaneously undergo state transitions or interact with each other upon spatial contact. In **Figure 3C**, we present a schematic overview of processes that occur according to defined rules associated with certain probabilities. It is important to note that, due to the spatial aspects that are captured by the ABM but not the PI-SBM, we have to distinguish between processes that are *contact-dependent* and *contact-independent*.

For *contact-independent* processes—such as intracellular and extracellular killing as well as the occurrence of *C. albicans* resistance against phagocytosis and/or killing—the conversion of rates from the PI-SBM to the ABM is straightforward. Since these processes are not determined by any spatial requirements, a simple re-scaling is performed. For example, *C. albicans* cells become resistant in the PI-SBM with probability $P_{PI-SBM}(\rho) = \rho\,\Delta t_{PI-SBM}$. In the ABM, where the resolution of time is set by the time-step $\Delta t_{ABM} \ll \Delta t_{PI-SBM}$, we check in each time-step with probability

$$P_{ABM}(\rho) = P_{PI-SBM}(\rho)\frac{\Delta t_{ABM}}{\Delta t_{PI-SBM}} \tag{7}$$

whether this process occurs.

In contrast, *contact-dependent* processes in the ABM are characterized by the requirement that two cells have to get into spatial contact first, before such a process—for example, a phagocytosis event of a *C. albicans* cell by a monocyte with transition rate ϕ_M—can take place. In the PI-SBM, spatial contact is not explicitly modeled; rather, the interaction partner for each monocyte is randomly chosen once per time-step Δt_{PI-SBM}. The associated probability is determined by the time-dependent ratio of non-resistant fungal cells over the sum of extracellular fungal cells and immune cells. Once an interaction partner was chosen, the phagocytosis event itself occurs with probability

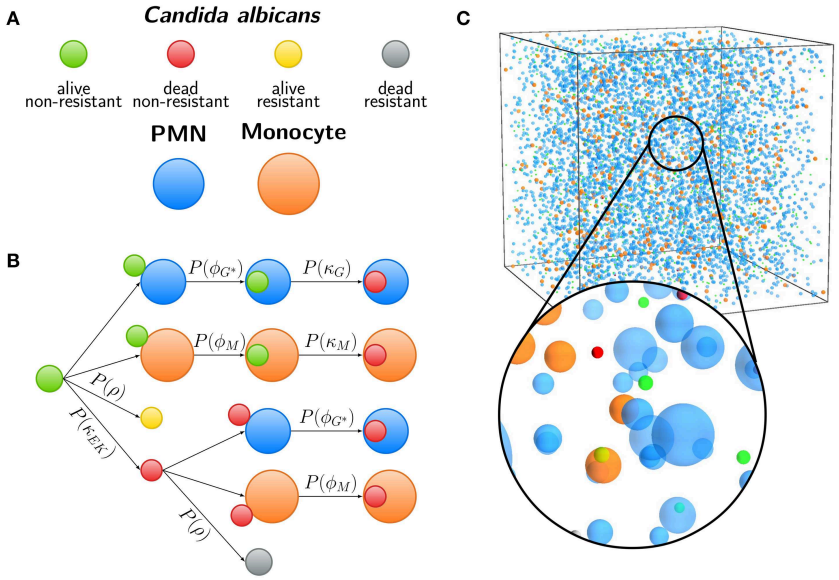

FIGURE 3 | Agent-based model (ABM) of the human whole-blood infection assay. (A) Agents used in the ABM are *Candida albicans* cells in the four states (i) alive and non-resistant (green), (ii) dead and non-resistant (red), (iii) alive and resistant (yellow), and (iv) dead and resistant (gray). Furthermore, granulocytes (polymorphonuclear neutrophils, PMN) and monocytes are shown in blue and orange, respectively. **(B)** Schematic overview of examples for interactions in the ABM. Each arrow indicates the execution of an interaction event, either depending on spatial contact between different cells or by a contact-independent process. *C. albicans* cells that are in extracellular space and alive (C_{AE}) or killed (C_{KE}) can become resistant with probability $P(\rho)$. After spatial contact, alive or killed *C. albicans* cells can be phagocytosed by PMN or monocytes with probabilities $P(\phi_G|\phi_{G^*})$ or $P(\phi_M)$, respectively. Intracellular alive *C. albicans* cells are killed with probabilities $P(\kappa_G)$ or $P(\kappa_M)$ depending on the type of phagocyte. **(C)** Visualization of the three-dimensional cuboid environment of the ABM that corresponds to 1 μl of the whole-blood infection assay, containing 5000 PMN, 500 monocytes, and 1000 *C. albicans* cells. The time-evolution of the simulated infection scenario can be viewed in Supplementary Video 1.

$P_{PI-SBM}(\phi_M) = \phi_M \, \Delta t_{PI-SBM}$ in the PI-SBM. Correspondingly, in the ABM, we request that this process takes place with the same probability,

$$P_{ABM}(\phi_M) = P_{PI-SBM}(\phi_M)\,, \tag{8}$$

on every encounter between a monocyte and a *C. albicans* cell. This correspondence of event probabilities for the two modeling approaches imposes a condition on the spatial dynamics of cells, i.e., on the values of the diffusion coefficients in the ABM and by that on the time-step Δt_{ABM} (see Equation 6). For optimal migration parameters, i.e., parameters that result in good agreement with the experimental data, it is expected that measurement of the associated phagocytosis rate in the ABM coincides with the corresponding rate from the PI-SBM.

2.3. Parameter Estimation

2.3.1. Simulated Annealing

The *a priori* unknown transition rates of the PI-SBM are determined by the method of Simulated Annealing based on the Metropolis Monte Carlo scheme (SA-MMC) that is depicted in **Figure 4A**. This optimization method randomly explores the parameter space of transition rates to find the global minimum of the fitting error, i.e., the most suitable parameter set that produces the best fit of the simulation to the experimental data obtained from the whole-blood infection assay.

The parameter estimation algorithm starts with a randomly chosen set of parameter values within the interval of $[0, 1]$ per minute, represented by the vector $\vec{p}$, and calculates the resulting time-evolution of state occupations from the simulation algorithm of the PI-SBM (see Section 2.1). To score the simulation result for a particular set of parameters, we combined different kinetics of the PI-SBM, referred to as *combined units*, which are identical with the experimental kinetics measured in the whole-blood infection assay (see Section 2.1). In this way, the experimental kinetics can be directly compared with the combined units c obtained from the model simulation, which is then scored by calculating the least-squares error (LSE) at experimental data points k as the weighted sum over c:

$$E[\vec{p}] = \sum_c \epsilon_c \, \frac{1}{2} \sum_k (x^{dat}_{k,c} - x^{sim}_{k,c}[\vec{p}])^2 \,. \tag{9}$$

Here, ϵ_c is adjusted as to fit each combined unit comparably well to the experimental data. The same values for ϵ_c were used in the PI-SBM and the ABM and are given in Supplementary Table 1. Next, the parameter set $\vec{p}$ is randomly varied within a pre-defined neighborhood of 10% variation, leading to a new

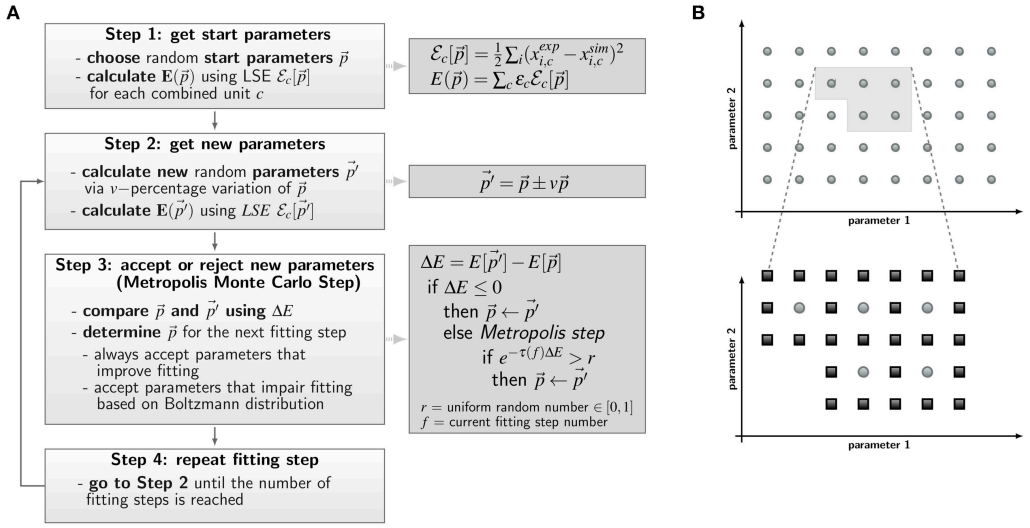

FIGURE 4 | Concepts of parameter estimation algorithms for non-spatial state-based models (SBM) and spatial agent-based models (ABM). (A) Flow chart of parameter estimation by the global optimization method Simulated Annealing based on the Metropolis Monte Carlo (SA-MMC). Light gray boxes describe Steps 1–4 of the algorithm; equations and pseudo code applied in these steps are provided in the dark gray boxes. **(B)** Schematic overview of the local optimization method *adaptive grid search algorithm* used for estimation of ABM migration parameters. Simulations are performed for sets of parameters on a regular grid in a predefined area of the search space and are evaluated by the *least squares error* (LSE). The initial grid (upper panel) contains sets of parameters with smallest LSE (light gray area) and this area is refined for a more accurate identification of the optimal parameter set (lower panel). Here, light gray dots represent parameter configurations from the first refinement level and dark gray squares represent parameter configurations of the subsequent refinement level.

set of parameter values, $\vec{p}\,'$, as indicated in **Figure 4A**, Step 2. Subsequently, the simulation of the PI-SBM is performed again for parameter values $\vec{p}\,'$ and the corresponding score $E[\vec{p}\,']$ is calculated. Whether the new simulated data will be accepted or rejected is decided by applying the MMC scheme that is depicted in **Figure 4A**, Step 3. The probability to accept worse parameter values is influenced by $\tau(f)$, representing the "inverse system temperature" in a SA process. The simulation of the annealing process involves a gradual decrease of the system temperature with progressed fitting, i.e., $\tau(f)$ is increased with the number of performed fitting steps f (see Supplementary Information 2.1).

After performing a total number of fitting steps, the fitting algorithm is repeated starting from a newly chosen random parameter set. This is done for a certain number of runs and the set of parameters with the minimal fitting error ($\vec{p}_{min}$) is saved from each fitting process. The mean values of the parameter values and their standard deviations are computed over all runs to determine the robustness of the estimated parameters.

We repeatedly perform the parameter estimation procedure for different system sizes in terms of the total number of individual cells. In doing so, the system size is stepwise increased by factors of ten, which is associated with increasing computing time for the model simulation but is partly compensated by a decrease in the number of fitting steps to avoid computational overload (see Supplementary Table 2). We start the estimation algorithm with a low number of individuals and a large number of fitting steps. The resulting parameter values are subsequently used as start parameter values for the system with next-higher number of individuals, i.e., for a 10-fold larger system. This procedure is repeated until a system size is reached where the number of individuals correspond to the measured numbers of PMN (about 5×10^6) and monocytes (about 5×10^5).

2.3.2. Adaptive Regular Grid Search

As described in Section 2.2, probabilities for state transitions in the ABM of the whole-blood infection assay can be derived from the interaction rates of the PI-SBM. This reduces the space of parameters that has to be searched in the process of parameter estimation, leaving only two migration parameters—i.e., the diffusion coefficients D_M and D_G, respectively, for monocytes and PMN—to be calibrated. However, even for a reduced parameter search space, there still is need for a calibration strategy that keeps the number of ABM simulations within limits, because simulating stochastic processes requires sufficient numbers of repetitions in order to obtain numerical results that are statistically sound.

We apply the *adaptive regular grid search algorithm* (Powell, 1998) to search iteratively for a local optimum in the parameter space (see **Figure 4B**). Motivated by biological constraints this is done for a pre-defined region of the parameter space. This region is represented on a regular grid and for each grid point the ABM is simulated with the corresponding set of parameter

values. Afterwards, simulations are evaluated with the least-squares error (LSE), scoring deviations between the simulation results and the experimental data for all combined units $c = \{C_K, C_A, C_E, C_M, C_G\}$ (see Section 2.1 and Equation 9). The values for the LSE are used to determine the adaptive refinement of the grid before the next iteration step, where intermediate grid points are calculated by bisection of the grid constant for the sets of parameters with lowest LSE. This imposes a grid refinement that ensures a more detailed scanning of the parameter space in relevant regions and defines the refinement level. The initial grid constant and the number of refinement steps determine how fine-grained the parameter space is represented by grid points and their values have to be chosen depending on the LSE landscape.

We further decrease computational costs associated with parameter estimation in the ABM by system scaling. Thus, similar to the procedure applied for the state-based model PI-SBM, we first scan the parameter space with a small system of 1/5 μl blood and subsequently re-scan the relevant parameter region with the system of 1 μl blood as defined in Section 2.2.

3. Results

3.1. Quantification of the Immune Response by the State-based Model

We quantified innate immune mechanisms in human whole-blood assays of infection with the pathogenic fungus *C. albicans* using a SBM. To this end, we modified a previously introduced SBM, referred to as P-SBM. This model was derived with the focus on state transitions of the pathogen (P) that may be induced by immune cells. However, immune cells in the P-SBM were only effectively modeled and not explicitly account for as individual cells (Hünniger et al., 2014). In the present work, we modified the P-SBM to model the interaction with individual immune cells—monocytes and granulocytes (PMN)—in detail. Since the focus of this model is on state transitions of both pathogen (P) and immune cells (I), we term this model PI-SBM. For reasons of comparison with the P-SBM, we used the same experimental data as in Hünniger et al. (2014) to quantify innate immune mechanisms by estimating the transition rates that yield the best fit to the data. Specific combinations of *C. albicans* states, referred to as *combined units*, were introduced that are directly related to different *C. albicans* populations measured over 4 h post-infection in experiment. As explained in detail in the Materials and Methods Section, the combined units include all extracellular *C. albicans* cells (C_E), *C. albicans* cells that are phagocytosed, respectively, by monocytes (C_M) or by granulocytes (C_G). Furthermore, all killed and alive *C. albicans* cells are given by the combined units C_K and C_A, respectively. The manually adjusted scores ϵ_c of combined units c are given in Supplementary Table 1. We simulate a blood sample of 1 ml containing 5×10^5 monocytes, 5×10^6 PMN and 1×10^6 *C. albicans* cells that are initially extracellular and alive.

To estimate the values of transition rates in the PI-SBM that yield the best fit to experimental data, i.e., the fit with the smallest least squares error (LSE), we applied the method of SA-MMC scheme (for details see Section 2.3.1). In **Figure 5**, the resulting transition rates of the PI-SBM are compared with those previously obtained within the P-SBM (for a quantitative comparison see also Supplementary Tables 3, 4). The direct comparison between the P-SBM and PI-SBM revealed that most transition rates are quantitatively similar in the two models.

The largest deviations in the values of transition rates between the two models were observed for the phagocytosis rate of monocytes (ϕ_M) and the killing rate of monocytes (κ_M). This was further investigated by performing the parameter estimation for the PI-SBM again, where only ϕ_M and κ_M were randomly varied while all other rates were kept fixed. We performed 50 runs and obtained very different standard deviations for these transition rates: while the standard deviation of ϕ_M was only 4%, this was 16% in the case of κ_M. We conclude that the PI-SBM is generally robust in all transition rates, except for κ_M that is also not directly determined by the data, because alive and killed *C. albicans* cells in phagocytes were not distinguished in these experiments. Similar observations were made for the P-SBM, where it was shown that variations in κ_M did not lead to significant differences in the fitting error (Hünniger et al., 2014).

To determine the impact of variations in the transition rates on the kinetics of the combined units in the PI-SBM, we performed 50 simulations with transition rates that were randomly sampled within their respective standard deviations. The kinetics of individual sub-populations are plotted in Supplementary Figure 2 while the results for the combined units are given in **Figure 6**. It can be seen that the simulated combined units agree well with the corresponding experimental data. In

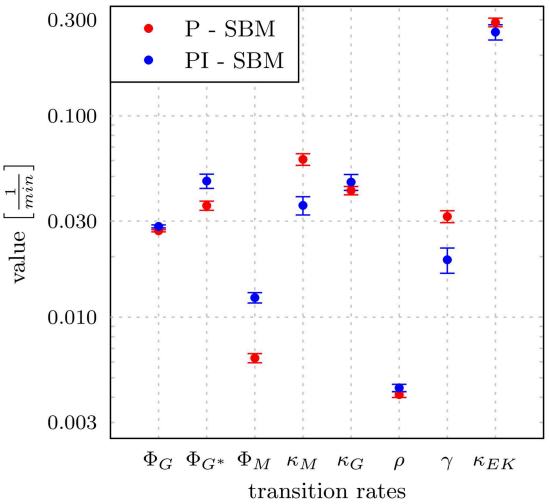

FIGURE 5 | Transition rates obtained from the model calibration to experimental data of the whole-blood infection assay. The results for the modified state-based model PI-SBM are compared to the P-SBM (Hünniger et al., 2014). The values are compared for the rate of phagocytosis by monocytes (ϕ_M), and by PMN on initial and subsequent events (ϕ_G,ϕ_{G^*}), rate of killing by monocytes (κ_M) and PMN (κ_G), rate of acquiring resistance against phagocytsis and/or killing (ρ) as well as the values of parameters for extracellular killing (γ, $\bar{\kappa}_{EK}$). Error bars correspond to standard deviations.

particular, the resulting kinetics of the PI-SBM revealed that 4 h post-infection 82% *C. albicans* cells were phagocytosed by PMN, whereas only 4% *C. albicans* cells were phagocytosed by monocytes. Furthermore, PMN play a major role in the immune response, because these phagocytes are associated with 97% of all killed *C. albicans* cells (see Supplementary Figure 2A). This is achieved either directly, via phagocytosis and intracellular killing (66.5%) of the pathogen, or indirectly by the release of antimicrobial peptides on a pathogen's first event of phagocytosis (30.5%) (see Supplementary Figure 2H). Four hours post-infection, most *C. albicans* cells were killed (89%) while a minority of 11% cells were extracellular and became resistant against killing and phagocytosis. These results are in quantitative agreement with those obtained previously for the P-SBM (Hünniger et al., 2014).

3.2. Predictions on Monocytopenia and Neutropenia from PI-SBM

The state-based model PI-SBM opens the possibility to study the dependence of the immune response against *C. albicans* on the number of PMN and monocytes in blood. Simulating the virtual infection scenario with the previously estimated parameters (see Supplementary Table 3), we considered various cases of immune cell deficiencies. The model predictions at 4 h post-infection and for gradual decreases in the immune cell numbers are presented in **Figure 7** for the cases of monocytopenia and neutropenia separately.

We found, as expected from the above quantification of the immune response, that monocytopenia is not a critical condition with regard to *C. albicans* infections: deficiency of monocytes and even their complete absence was fully compensated by PMN-mediated killing. In fact, patients with monocytopenia have not been reported to develop systemic candidiasis to date (Lionakis, 2014). The situation is extremely different in the case of neutropenia. In the absence of PMN, the number of killed *C. albicans* cells is predicted to decrease from about 89% under physiological conditions down to 45%, i.e., $C_K = 89\%$ for 5×10^6 PMN and $C_K = 45\%$ for $\leq 5 \times 10^3$ PMN (see **Figure 7B**). Monocytes compensated PMN deficiency by phagocytosis of *C. albicans* cells only partly, where the fraction increased from 3% under physiological conditions up to 48%. However, 42% of the *C. albicans* cells acquired resistance against killing and/or phagocytosis, resulting from the combined effect of absent PMN phagocytosis and extracellular killing that is normally mediated by PMN release of antimicrobial peptides.

For a decrease in PMN number by one order of magnitude from physiological conditions, we found that monocytes can sustain the immune response fairly well. In this case, the fraction of killed *C. albicans* cells was still 79% and the phagocytosis by monocytes and PMN reached, respectively, 20% and 55% of *C. albicans* cells. A significant deterioration of the immune response was observed for PMN concentrations below 5×10^5 cells/ml (see **Figure 7**). Interestingly, this concentration was reported to mark the transition from moderate to severe neutropenia (Munshi and Montgomery, 2000), which is a

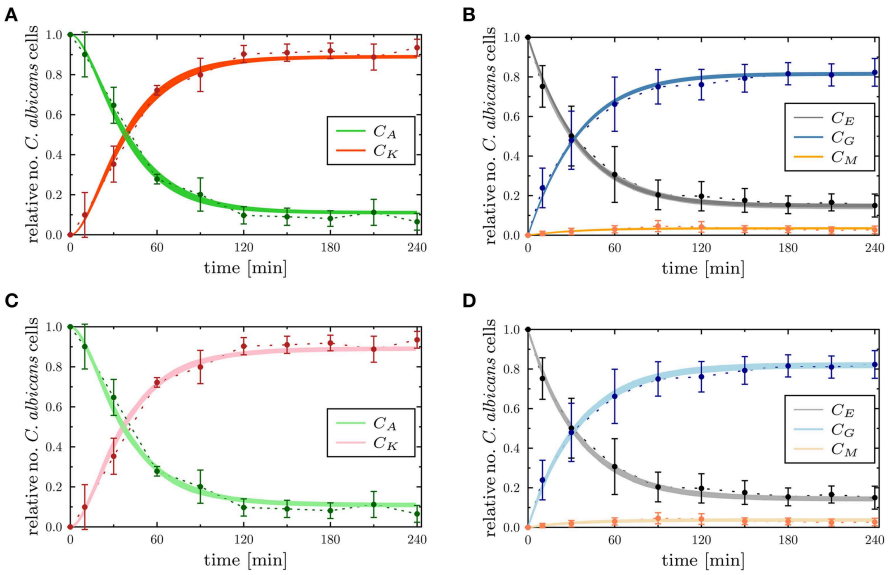

FIGURE 6 | Comparison of the time-evolution for the combined units from the experimental whole-blood infection assay (dotted lines as a guide for the eye) with the PI-SBM in (A,B), and the ABM in (C,D). In **(A,B)**, the thickness of the solid lines represents the standard deviation of the PI-SBM simulation results as obtained from 50 simulations for normally distributed transition rates as given in Supplementary Table 3. The thickness of the solid lines in **(C,D)** represents the standard deviation obtained by 30 simulations of the stochastic ABM. Time-evolution of killed (C_K) and alive (C_A) *C. albicans* cells are depicted in **(A,C)**, and the dynamics of *C. albicans* cells that are in extracellular space (C_E), phagocytosed by monocytes (C_M) and PMN (C_G) are shown in **(B,D)**.

condition that is known to be associated with high risks for candidemia in cancer patients (Lunel et al., 1999; Alangaden, 2011).

3.3. Agent-based Model Captures Immune Response in Time and Space

State-based models (SBM) do not account for any spatial aspects. For example, cells in the PI-SBM do not actually migrate during the immune response and, therefore, do not have to get into contact before a phagocytosis event can take place. In contrast, agent-based models (ABM) do capture spatial aspects in a defined environment. Applying a bottom-up modeling approach, we implemented an ABM that is—apart from its spatial aspects—the exact analog of the non-spatial PI-SBM. As depicted in **Figure 1**, all transition rates that were previously estimated for the PI-SBM were fed into the ABM (see Section 2.2 for details). The only parameters left to estimate were those related to cell migration, which in the dense cell system of the whole-blood assay resembles a random walk. In particular, while the diffusion coefficient associated with the passive movement of *C. albicans* cells could be inferred from the Stokes-Einstein equation to be $D_C \approx 1\,\mu\text{m}^2/\text{min}$, the active migration behavior of immune cells requires a rigorous parameter estimation of the diffusion coefficients D_M and D_G for monocytes and PMN, respectively.

It should be noted that, even in the case of low-dimensional parameter spaces, the estimation of parameters for ABM generally turn out to be computationally intensive. This is a consequence of the fact that ABM simulate the interactions between thousands of agents in continuous space as stochastic processes. To simultaneously facilitate an increase in model complexity and a decrease in computational expense for parameter estimation, we applied the local optimization algorithm *adaptive regular grid search*. This algorithm compares ABM simulations by evaluating the least squares error (LSE) regarding the experimental data of the whole-blood infection assay. Stochastic effects of the ABM were investigated by comparing simulation results for a fixed set of parameter values with varying number of *in silico* replicates. Using 100 *in silico* replicates as a reference for the mean value of the LSE, we generally observed for relevant parameter sets, i.e., parameter sets that yield reasonable agreement with the experimental data, that relative variations in the mean LSE were already well below 10% for 30 *in silico* replicates. Therefore, we set the number of *in silico* replicates to 30 throughout the whole parameter space.

The *adaptive regular grid search* algorithm searches the space of D_M and D_G on a pre-defined grid of diffusion coefficients, $0 < D_M, D_G < 800\,\mu\text{m}^2/\text{min}$. This range for the diffusion coefficients implies that the time step Δt_{ABM} varies between $5.2 \times 10^{-3}\,\text{min} \leq \Delta t_{\text{ABM}} \leq 4.2\,\text{min}$ (see Equation 6). As described in Section 2.3.2, we started with a relatively coarse grid of step size $100\,\mu\text{m}^2/\text{min}$ and computed at each grid point the LSE by comparing the experimental data with a small ABM system, i.e., representing $1/5\,\mu\text{l}$ of blood (see Supplementary Figure 3). These results were used to determine the regime of parameters in which the parameter estimation was continued for the large ABM system simulating $1\,\mu\text{l}$ of blood. The parameter regime was determined by the rectangle that contains all pairs of diffusion coefficients (D_G, D_M) for which the LSE values were found to be minimal from separately varying each parameter. The corner points of this rectangle were $(D_G, D_M) = (100, 0)\,\mu\text{m}^2/\text{min}$ and $(D_G, D_M) = (600, 800)\,\mu\text{m}^2/\text{min}$ (see gray region in Supplementary Figure 3). Subsequently, the grid was refined based on simulations of the large ABM by determining the path of minimal LSE values and adding grid points around this path by adaptive bisection. After simulation of the ABM for parameter sets corresponding to the added grid points, the procedure of grid refinement was repeated. This can be seen in **Figure 8**, where we plot a map of the LSE landscape together with the paths of minimal LSE values for each level of refinement. It was observed that the course of these paths covers a relatively broad range of diffusion coefficients for monocytes, D_M, whereas this is a fairly narrow range of D_G-values for PMN.

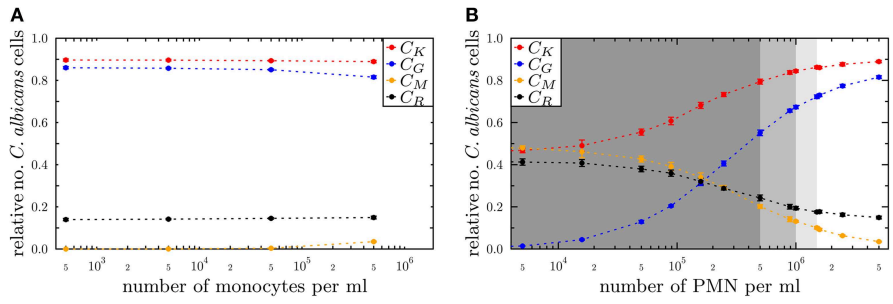

FIGURE 7 | Simulation results of the PI-SBM with different immune cell numbers at 4 h post-infection for the conditions (A) monocytopenia and (B) neutropenia. The relative numbers of *C. albicans* cells of killed cells (C_K), phagocytosed cells in monocytes (C_M) and in PMN (C_G) as well as cells that became resistant (C_R) against killing and/or phagocytosis are depicted for different numbers of monocytes and PMN. The number of **(A)** monocytes and **(B)** PMN in the simulations are reduced separately, starting from physiological concentrations of $5{\times}10^5$ /ml monocytes and $5{\times}10^6$ /ml PMN down to vanishing concentrations. In **(B)**, the light gray region represents the range of light neutropenia ($< 1.5 \times 10^6$ PMN per ml), medium gray region represents the range of moderate neutropenia ($< 1 \times 10^6$ PMN per ml) and dark gray region represents the range of severe neutropenia ($< 5 \times 10^5$ PMN per ml).

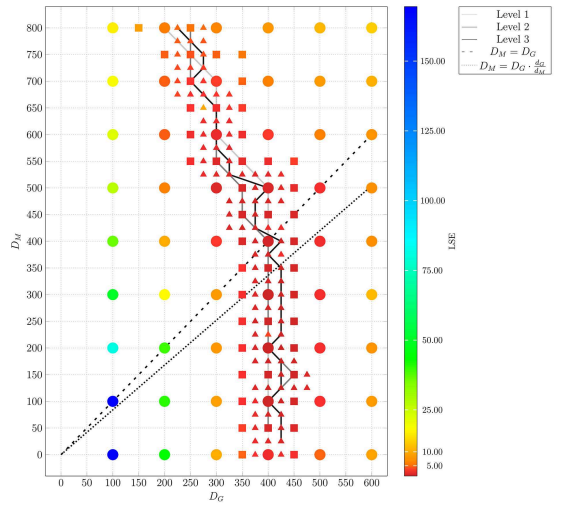

FIGURE 8 | Result of ABM parameter estimation by *adaptive regular grid search*. The diffusion coefficients for monocytes, D_M, and PMN, D_G, were scanned within the regime that was determined by parameter scanning for the small ABM (1/5 μl blood). At each grid point, 30 ABM simulations were performed for the large system (1 μl blood) and the mean least squares error (LSE) is depicted. By determining the path of minimal LSE values and adding grid points around this path by adaptive bisection, three refinement levels are considered. Dots represent grid points of the first refinement level, squares represent grid points of the second refinement level, and triangles represent grid points of the third refinement level. The paths of minimal LSE values for the first, second and third refinement level are traced by light gray, medium gray, and dark gray lines, respectively.

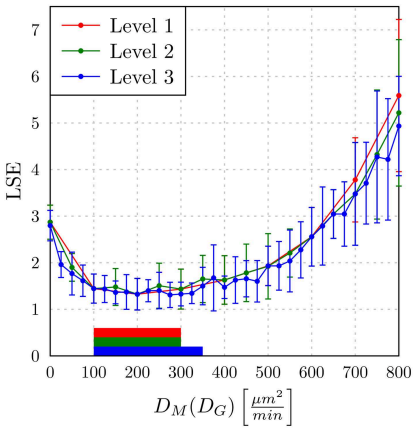

FIGURE 9 | The least squares error (LSE) of the paths of grid points along the diffusion coefficients for monocytes (D_M) as a function of the minimal diffusion coefficient for PMN (D_G): $D_M(D_G)$. Mean values and standard deviations were obtained from averaging over 30 ABM simulations. The paths of the first, second, and third refinement level are shown, respectively, as red, green, and blue lines (guide for the eyes). The horizontal bars indicate regions of diffusion coefficients with values comparable to the absolute LSE minimum of each refinement level. All values outside these regions are significantly different from the absolute LSE minimum (Wilcoxon rank sum test with $p < 0.05$).

In **Figure 9**, we present the LSE values as a function of $D_M(D_G)$ along the paths of minimal LSE values for the three levels of refinement. From the third level of refinement we inferred the point of absolute LSE minimum to be located at $(D_G^{min}, D_M^{min}) = (425, 275)\,\mu\text{m}^2/\text{min}$. However, since the landscape of $D_M(D_G)$ resembled an extended valley across neighboring data points, we performed a statistical analysis by applying the Wilcoxon rank sum test between the absolute LSE minimum and its neighboring points to check for significant differences between them. Imposing a p-value of $p < 0.05$ for significant difference, we obtained points with similar values of the LSE ranging in the interval $D_M = 100\,\mu\text{m}^2/\text{min}$ to $D_M = 350\,\mu\text{m}^2/\text{min}$ for monocytes and $D_G = 400\,\mu\text{m}^2/\text{min}$ to $D_G = 425\,\mu\text{m}^2/\text{min}$ for PMN (see **Figure 8**). These findings imply that the immune response in the whole-blood infection assay was much more sensitive to variations in the diffusion coefficients of PMN than of monocytes, emphasizing the dominant role of PMN over monocytes from the viewpoint of cell migration.

Our results are consistent with the absolute LSE minima of refinement level one and two, which were both at $(D_G^{min}, D_M^{min}) = (400, 200)\,\mu\text{m}^2/\text{min}$ and that also belong to this interval (see **Figure 9**). Interestingly, while we expected that monocytes are less migratory active than PMN, i.e., restricting the relevant parameter regime in **Figure 8** to the region below the dashed line, we also found that the interval around the absolute LSE minimum contains the parameter set $(D_G, D_M) = (425, 350)\,\mu\text{m}^2/\text{min}$. The ratio of these diffusion coefficients, $D_M/D_G \approx 0.82$, resembles the value expected from the Stokes-Einstein equation (Einstein, 1905) implying $D_M/D_G = d_G/d_M$ (dotted line in **Figure 8**). Taken together, we consider the diffusion coefficients $(D_G^{min}, D_M^{min}) = (425, 275)\,\mu\text{m}^2/\text{min}$ to represent the immune cell dynamics reasonably well and use these values in our further analyses below.

Next, we compared the ABM simulation results for the absolute LSE minimum with those of the PI-SBM. These are plotted together with the experimental data of the whole-blood infection assay in **Figure 6** and in Supplementary Figure 4 for the time evolution of *C. albicans* sub-populations. Thus, we found that both modeling approaches, the non-spatial SBM and the spatial ABM, yielded excellent agreement with the experimental data. Furthermore, we found that our simulation results obtained from the stochastic ABM were robust, which can be seen from the line thicknesses in **Figures 6C,D** representing the standard deviations obtained from 30 ABM simulations.

3.4. Predictions on Hyper- and Hypo-inflammation from ABM

To investigate the impact of hyper- and hypo-inflammation associated with the dynamics of immune cells, we varied the diffusion coefficients of monocytes and PMN separately around the absolute LSE minimum $(D_G^{min}, D_M^{min}) = (425, 275)\,\mu\text{m}^2/\text{min}$. Keeping the diffusion coefficient D_G fixed and varying the D_M for monocytes between $100\,\mu\text{m}^2/\text{min}$ and $600\,\mu\text{m}^2/\text{min}$, we

observed at 4 h post-infection no substantial changes in the populations of killed, resistant and phagocytosed *C. albicans* cells (see **Figure 10A**). At extreme values $D_M > D_G$, a slight increase (decrease) in the number of killed (resistant) *C. albicans* cells was observed accompanied by a slight increase in the phagocytosis by both monocytes and PMN. This may be attributed to a stronger mixing of the cell system for high diffusion coefficients D_M. In general, however, the immune response does not appear to be sensitive to this parameter, which is in agreement with the finding for monocytopenia that did not have a substantial impact on infection clearance (see **Figure 7A**).

In the opposite case, where D_M was fixed and D_G was varied between $100\,\mu m^2/min$ and $600\,\mu\text{m}^2/\text{min}$, it was again observed that for increased values $D_G > 425\,\mu\text{m}^2/\text{min}$ the impact on the immune response against *C. albicans* is only weak. In contrast, for decreased values $D_G < 400\,\mu\text{m}^2/\text{min}$ the immune response was strongly affected by the reduced migratory activity of PMN. This could be observed by a substantial increase (decrease) in the number of resistant (killed) *C. albicans* cells (see **Figure 10B**). In particular, for $D_G = 100\,\mu\text{m}^2/\text{min}$ the phagocytosis of *C. albicans* cells by PMN was reduced by more than 20% and the relative number of resistant *C. albicans* cells reached the value of 28%. Comparing this scenario with the condition of PMN deficiency (see **Figure 7B**), we found that this PMN paralysis resembles moderate to severe neutropenia associated with a relative number of about 20% and 30% of resistant *C. albicans* cells, respectively.

4. Discussion

In this study, we applied a bottom-up modeling approach to simulate an experimental infection assay for *C. albicans* in human blood. As illustrated in **Figure 1**, this approach combines different mathematical models with increasing complexity that build on one another. We started from a previously developed state based model (SBM), here referred to as P-SBM (Hünniger et al., 2014), that neglects all spatial aspects and describes the time-evolution of pathogens in different states—e.g., alive, phagocytosed and killed—during the early response of the innate immune system. To include the immune response mediated by monocytes and granulocytes (PMN), in this work we modified the P-SBM into a SBM that does as well-explicitly account for the immune cell states and is therefore referred to as PI-SBM. The rates of state transitions in the PI-SBM were estimated by comparison with experimental data (Hünniger et al., 2014) using the global optimization method *simulated annealing* based on the Metropolis Monte Carlo scheme (SA-MMC).

The resulting model kinetics of both SBM were found to be in quantitative agreement with experimental data and confirmed that PMN play the major role in the immune defense against *C. albicans* in human blood. This is indicative for the general validity of both models, despite the structural difference of the simulation algorithms regarding the level of detail at which immune cells are modeled. Furthermore, the PI-SBM allows making predictions on infection scenarios in patients with immune cell deficiencies, i.e., neutropenia and monocytopenia. Performing *in silico* experiments with varying numbers of either monocytes or PMN, revealed that loss of monocytes was mainly compensated by PMN. In contrast, decreasing PMN number lead to a strongly reduced immune response against *C. albicans* for PMN numbers below 5×10^5 /ml (see **Figure 7**). Our quantitative prediction is substantiated by published data that account this PMN concentration as severe neutropenia (Munshi and Montgomery, 2000). It is also reported that neutropenia impairs the outcome of candidemia and is a risk factor, in particular, for cancer patients developing candidemia (Guiot et al., 1994; Bow et al., 1995; Lunel et al., 1999). From the quantitative agreement between predictions of the PI-SBM and reported findings for *C. albicans* infection, we attribute a high predictive potential to this virtual infection model that may be exploited in future studies, e.g., focusing on conditions of immune dysregulation and/or comparing the impact of different pathogens. The possibility to quantify functional alteration of immune cells rather than pure numerical aberrations is of particular interest in this regard.

In order to account for spatial aspects of the immune response, we extended the SBM to an agent-based model (ABM), where cells are simulated as agents that can migrate in continuous

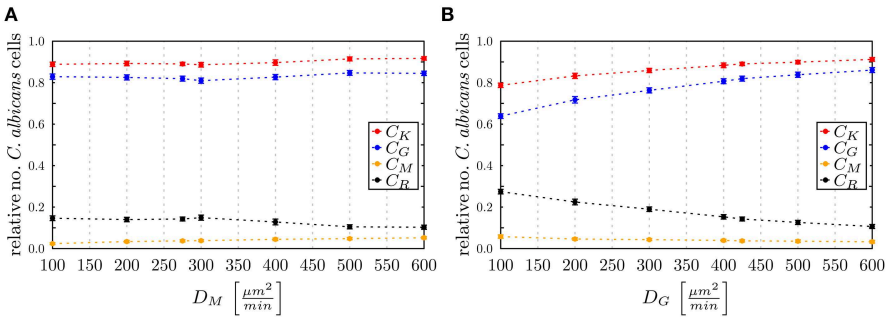

FIGURE 10 | Simulation results of the ABM at 4 h post-infection for varied diffusion coefficients around the absolute least squares error (LSE) minimum with $(D_G^{min}, D_M^{min}) = (425, 275)\,\mu\text{m}^2/\text{min}$ for (A) monocytes keeping D_G fixed and (B) PMN keeping D_M fixed. The relative numbers of *C. ablicans* cells of killed cells (C_K), phagocytosed cells in monocytes (C_M) and in PMN (C_G) as well as cells that became resistant (C_R) against killing and/or phagocytosis are depicted.

three-dimensional space and can interact with each other on encounter in space. Applying the bottom-up modeling approach, we made use of the rates that were determined by fitting the PI-SBM to the experimental data and estimated the diffusion coefficients of immune cells in blood (see **Figure 1**). Due to high computational costs of ABM simulations, applying the global optimization method SA-MMC was no realistic option and we chose the computationally affordable local optimization method *adaptive regular grid search*. This method searches for the optimum within a pre-defined parameter space, which in the present case was a two-dimensional space spanned by the diffusion coefficients for monocytes and PMN. In contrast, applying SA-MMC was beneficial in the case of PI-SBM for three reasons: (i) the parameter space was eight-dimensional, (ii) limitations of the parameter space would have been difficult to motivate biologically, and (iii) computational costs for repeated simulations were still acceptable due to the neglect of spatial aspects.

As live cell imaging in whole-blood assays cannot yet be performed today, computer simulations are the only tool to predict diffusion coefficients of immune cells. Parameter estimation of the ABM predicted intervals for the diffusion coefficients that yielded quantitatively comparable results. For monocytes this interval, $D_M = 100\,\mu\text{m}^2/\text{min}$ to $D_M = 350\,\mu\text{m}^2/\text{min}$, was substantially broader than for PMN with $D_G = 400\,\mu\text{m}^2/\text{min}$ to $D_G = 425\,\mu\text{m}^2/\text{min}$, indicating the importance of fine-tuned PMN motility.

Furthermore, by varying the diffusion coefficients of the immune cells, we demonstrated the impact of hyper- and hypo-inflammation in immune dysregulation. In general, reducing (increasing) immune cell motilities around optimal values reduced (increased) the number of interaction events between cells and by that the phagocytosis of *C. albicans* cells. In the case of PMN, reduction of cell motility and phagocytosis events was additionally associated with a decrease in the release of antimicrobial peptides contributing to the decrease in killing of *C. albicans* cells. This in turn lead to an increase in the number of resistant *C. albicans* cells reaching levels that were well-beyond those observed for paralytic monocytes (see **Figure 10**). Comparing the hypo-inflammatory condition with PMN deficiency, we found that diffusion coefficients around $D_G = 100\,\mu\text{m}^2/\text{min}$ resembled the outcome of moderate to severe neutropenia.

The bottom-up modeling approach presented here may be extended in various ways. For example, the implementation of a hybrid ABM could be envisaged where molecular interactions, e.g., as mediated by antimicrobial peptides, are not simulated in a rule-based fashion but in an explicit way by a molecular diffusion solver. Other directions of future research include (i) focusing on conditions of immune dysregulation, (ii) comparing the impact of different pathogens, and (iii) including other types of innate immune cells. Furthermore, it is conceivable to combine modeling approaches with microscopy experiments of infection scenarios *in vitro* in an image-based systems biology approach (Mech et al., 2014; Figge and Murphy, 2015; Medyukhina et al., 2015). First steps into this direction have recently been made, e.g., by establishing algorithms for the automated image analysis of phagocytosis assays (Mech et al., 2011; Kraibooj et al., 2014) and for the automated tracking and classification of PMN from time-lapse microscopy (Mokhtari et al., 2013; Brandes et al., 2015) that was applied in the context of comparing *C. albicans* and *C. glabrata* infection (Duggan et al., 2015a). In the future, we expect that a systems medicine approach exploiting the predictive power of virtual infection models will play an important role in the context of infectious disease diagnosis.

Author Contributions

TL, ST, MTF: Conception and design of the investigation and work. MTF: Contribution of materials and computational resources. TL, ST, JP, MTF: Data processing, implementation and application of the computational algorithm. TL, ST, JP, KH, OK, MTF: Evaluation and analysis of the results. TL, ST, JP, KH, OK, MTF: Drafting the manuscript and revising it critically for important intellectual content and final approval of the version to be published. TL, ST, JP, KH, OK, MTF: Agreement to be accountable for all aspects of the work in ensuring that questions related to the accuracy or integrity of any part of the work are appropriately investigated and resolved.

Funding

This work was financially supported by the Deutsche Forschungsgemeinschaft (DFG) through the excellence graduate school Jena School for Microbial Communication (JSMC) and the CRC/TR124 FungiNet (project B4 to MTF and project C3 to OK).

Acknowledgment

We thank C. M. Svensson for valuable discussions on the statistical analysis of the agent-based model simulations.

Supplementary Material

The Supplementary Material for this article can be found online at: http://journal.frontiersin.org/article/10.3389/fmicb.2015.00608/abstract

References

Alangaden, G. J. (2011). Nosocomial fungal infections: epidemiology, infection control, and prevention. *Infect. Dis. Clin. North Am.* 25, 201–225. doi: 10.1016/j.idc.2010.11.003

Ashyraliyev, M., Fomekong-Nanfack, Y., Kaandorp, J. A., and Blom, J. G. (2009). Systems biology: parameter estimation for biochemical models. *FEBS J.* 276, 886–902. doi: 10.1111/j.1742-4658.2008.06844.x

Bittig, A. T., and Uhrmacher, A. M. (2010). "Spatial modeling in cell biology at multiple levels," in *Simulation Conference (WSC),*

Proceedings of the 2010 Winter, Number 2005 (Baltimore, MD: IEEE), 608–619.

Bow, E. J., Loewen, R., Cheang, M. S., and Schacter, B. (1995). Invasive fungal disease in adults undergoing remission-induction therapy for acute myeloid leukemia: the pathogenetic role of the antileukemic regimen. *Clin. Infect. Dis.* 21, 361–369.

Brandes, S., Mokhtari, Z., Essig, F., Hünniger, K., Kurzai, O., and Figge, M. T. (2015). Automated segmentation and tracking of non-rigid objects in time-lapse microscopy videos of polymorphonuclear neutrophils. *Med. Image Anal.* 20, 34–51. doi: 10.1016/j.media.2014.10.002

Cunha, C., Kurzai, O., Löffler, J., Aversa, F., Romani, L., and Carvalho, A. (2014). Neutrophil responses to aspergillosis: new roles for old players. *Mycopathologia* 178, 387–393. doi: 10.1007/s11046-014-9796-7

Dueck, G. (1993). New optimization heuristics. *J. Comput. Phys.* 104, 86–92.

Duggan, S., Essig, F., Hünniger, K., Mokhtari, Z., Bauer, L., Lehnert, T., et al. (2015a). Neutrophil activation by *Candida glabrata* but not *Candida albicans* promotes fungal uptake by monocytes. *Cell. Microbiol.* doi: 10.1111/cmi.12443. [Epub ahead of print].

Duggan, S., Leonhardt, I., Hünniger, K., and Kurzai, O. (2015b). Host response to *Candida albicans* bloodstream infection and sepsis. *Virulence*. doi: 10.4161/21505594.2014.988096. [Epub ahead of print].

Einstein, A. (1905). Über die von der molekularkinetischen theorie der Wärme geforderte Bewegung von in ruhenden Flüssigkeiten suspendierten Teilchen. *Ann. Phys.* 322, 549–560.

Fahraus, R., and Lindqvist, T. (1931). The viscosity of the blood in narrow capillary tubes. *Am. J. Physiol.* 96, 562–568.

Figge, M. T., and Murphy, R. (eds.). (2015). Image-based systems biology. *Cytometry A*. 87, 459–461. doi: 10.1002/cyto.a.22638

Figge, M. T. (2005). Stochastic discrete event simulation of germinal center reactions. *Phys. Rev. E* 71:051907. doi: 10.1103/PhysRevE.71.051907

Gonzalez, O. R., Kueper, C., Jung, K., Naval, P. C., and Mendoza, E. (2007). Parameter estimation using simulated annealing for S-system models of biochemical networks. *Bioinformatics* 23, 480–486. doi: 10.1093/bioinformatics/btl522

Guiot, H., Fibbe, W., and Van't Wout, J. (1994). Risk factors for fungal infection in patients with malignant hematologic disorders: implications for empirical therapy and prophylaxis. *Clin. Infect. Dis.* 18, 525–532.

Hünniger, K., Lehnert, T., Bieber, K., Martin, R., Figge, M. T., and Kurzai, O. (2014). A virtual infection model quantifies innate effector mechanisms and *Candida albicans* immune escape in human blood. *PLoS Comput. Biol.* 10:e1003479. doi: 10.1371/journal.pcbi.1003479

Hünniger, K., Bieber, K., Martin, R., Lehnert, T., Figge, M. T., Löffler, J., et al. (2015). A second stimulus required for enhanced antifungal activity of human neutrophils in blood is provided by Anaphylatoxin C5a. *J. Immunol.* 194, 1199–1210. doi: 10.4049/jimmunol.1401845

Hernandez-Vargas, E. A., Wilk, E., Canini, L., Toapanta, F. R., Binder, S. C., Uvarovskii, A., et al. (2014). The effects of aging on influenza virus infection dynamics. *J. Virol.* 88, 4123–4131. doi: 10.1128/JVI.03644-13

Horn, F., Heinekamp, T., Kniemeyer, O., Pollmächer, J., Valiante, V., and Brakhage, A. A. (2012). Systems biology of fungal infection. *Front. Microbiol.* 3:108. doi: 10.3389/fmicb.2012.00108

Kirkpatrick, S., Gelatt, C. D., and Vecchi, M. P. (1983). Optimization by simulated annealing. *Science* 220, 671–680.

Kraibooj, K., Park, H.-R., Dahse, H.-M., Skerka, C., Voigt, K., and Figge, M. T. (2014). Virulent strain of lichtheimia corymbifera shows increased phagocytosis by macrophages as revealed by automated microscopy image analysis. *Mycoses* 57, 56–66. doi: 10.1111/myc.12237

Lionakis, M. S. (2014). New insights into innate immune control of systemic candidiasis. *Med. Mycol.* 52, 555–564. doi: 10.1093/mmy/myu029

Lunel, F. M. V., Meis, J. F., and Voss, A. (1999). Nosocomial fungal infections: candidemia. *Diagn. Microbiol. Infect. Dis.* 34, 213–220.

Luo, S., Skerka, C., Kurzai, O., and Zipfel, P. F. (2013). Complement and innate immune evasion strategies of the human pathogenic fungus *Candida albicans*. *Mol. Immunol.* 56, 161–169. doi: 10.1016/j.molimm.2013.05.218

Mak, T. W., and Saunders, M. E. (2011). *Primer to the Immune Response: Academic Cell Update Edition*. Burlington; San Diego; London: Academic Press.

Margulies, L., and Schwartz, K. V. (1998). *Five Kingdoms - An Illustrated Guide to the Phyla of Life on Earth, 3rd Edn.* New York, NY: W. H. Freeman and Company.

McClatchey, K. D. (2003). Clinical laboratory medicine. *Clin. Chem.* 49, 344–345. doi: 10.1373/49.2.344

Mech, F., Thywißen, A., Guthke, R., Brakhage, A. A., and Figge, M. T. (2011). Automated image analysis of the host-pathogen interaction between phagocytes and *Aspergillus fumigatus*. *PLoS ONE* 6:e19591. doi: 10.1371/journal.pone.0019591

Mech, F., Wilson, D., Lehnert, T., Hube, B., and Thilo Figge, M. (2014). Epithelial invasion outcompetes hypha development during *Candida albicans* infection as revealed by an image-based systems biology approach. *Cytometry A* 85, 126–139. doi: 10.1002/cyto.a.22418

Medyukhina, A., Timme, S., Mokhtari, Z., and Figge, M. T. (2015). Image-based systems biology of infection. *Cytometry A* 87, 462–470. doi: 10.1002/cyto.a.22638

Mendling, W. (2006). *Vaginose, Vaginitis und Zervizitis*. Heidelberg: Springer Science & Business Media.

Metropolis, N., Rosenbluth, A. W., Rosenbluth, M. N., Teller, A. H., and Teller, E. (1953). Equation of state calculations by fast computing machines. *J. Chem. Phys.* 21, 1087.

Mokhtari, Z., Mech, F., Zitzmann, C., Hasenberg, M., Gunzer, M., and Figge, M. T. (2013). Automated characterization and parameter-free classification of cell tracks based on local migration behavior. *PLoS ONE* 8:e80808. doi: 10.1371/journal.pone.0080808

Moles, C. G., Mendes, P., and Banga, J. R. (2003). Parameter estimation in biochemical pathways: a comparison of global optimization methods. *Genome Res.* 13, 2467–2474. doi: 10.1101/gr.1262503

Munshi, H. G., and Montgomery, R. B. (2000). Evidence-based case review: severe neutropenia: a diagnostic approach. *West. J. Med.* 172, 248–252. doi: 10.1136/ewjm.172.4.248

Pollmächer, J., and Figge, M. T. (2014). Agent-based model of human alveoli predicts chemotactic signaling by epithelial cells during early *Aspergillus fumigatus* infection. *PLoS ONE* 9:e111630. doi: 10.1371/journal.pone.0111630

Powell, M. (1998). Direct search algorithms for optimization calculations. *Acta Numerica* 7, 287–336.

Rapaport, D. C. (1996). *The Art of Molecular Dynamics Simulation*. New York, NY: Cambridge University Press.

Rosenson, R., McCormick, A., and Uretz, E. (1996). Distribution of blood viscosity values and biochemical correlates in healthy adults. *Clin. Chem.* 42, 1189–1195.

Skvoretz, J. (2002). Complexity theory and models for social networks. *Complexity* 8, 47–55. doi: 10.1002/cplx.10062

Storn, R., and Price, K. (1997). Differential evolution – a simple and efficient heuristic for global optimization over continuous spaces. *J. Glob. Opt.* 11, 341–359.

Tokarski, C., Hummert, S., Mech, F., Figge, M. T., Germerodt, S., Schroeter, A., et al. (2012). Agent-based modeling approach of immune defense against spores of opportunistic human pathogenic fungi. *Front. Microbiol.* 3:129. doi: 10.3389/fmicb.2012.00129

Von Neumann, J. (1951). The general and logical theory of automata. *Cereb. Mech. Behav.* 1, 41.

Conflict of Interest Statement: The authors declare that the research was conducted in the absence of any commercial or financial relationships that could be construed as a potential conflict of interest.

Copyright © 2015 Lehnert, Timme, Pollmächer, Hünniger, Kurzai and Figge. This is an open-access article distributed under the terms of the Creative Commons Attribution License (CC BY). The use, distribution or reproduction in other forums is permitted, provided the original author(s) or licensor are credited and that the original publication in this journal is cited, in accordance with accepted academic practice. No use, distribution or reproduction is permitted which does not comply with these terms.

Frontiers

Supplementary Material
9 June 2015

Supplementary Material: Bottom-up modeling approach for the quantitative estimation of parameters in pathogen-host interactions

Teresa Lehnert [1,2,+], **Sandra Timme** [1,2+], **Johannes Pollmächer** [1,2], **Kerstin Hünniger** [3], **Oliver Kurzai** [3,2] **and Marc Thilo Figge** [1,2*]

[1] *Applied Systems Biology, Leibniz Institute for Natural Product Research and Infection Biology Hans-Knöll-Institute (HKI), Jena, Germany*
[2] *Faculty of Biology and Pharmacy, Friedrich Schiller University Jena, Jena, Germany*
[3] *Fungal Septomics, Septomics Research Center, Friedrich Schiller University and Leibniz Institute for Natural Product Research and Infection Biology Hans-Knöll-Institute (HKI), Jena, Germany*
[+] *Authors contributed equally*

Correspondence*:
Marc Thilo Figge
Applied Systems Biology, Leibniz Institute for Natural Product Research and Infection Biology - Hans Knöll Institute (HKI), Adolf-Reichwein-Straße 23, Jena, 07745, Germany, thilo.figge@hki-jena.de

1 SUPPLEMENTARY DATA

Supplementary Video 1. Typical time evolution of the virtual infection scenario in the spatial ABM. The three-dimensional environment corresponds to 1 μl of blood containing 500 monocytes, 5000 PMN and 1000 *C. albicans* cells. The cells are represented as spherical agents that migrate depending on their respective diffusion coefficients and interact depending on rules as depicted in Figure 3 (B). *C. albicans* cells occur in the four states (i) alive and non-resistant (green), (ii) dead and non-resistant (red), (iii) alive and resistant (yellow) and (iv) dead and resistant (gray). Furthermore, granulocytes (polymorphonuclear neutrophils, PMN) and monocytes are shown in blue and orange, respectively. The video comprises the immune response during four hours post infection. In the beginning of the video, most *C. albicans* cells are non-phagocytosed and are frequently found to be alive and non-resistant (green). Towards the end of the video, non-phagocytosed *C. albicans* cells are mostly resistant (*i.e.*, yellow and gray) while most of *C. albicans* cells have been phagocytosed.

2 SUPPLEMENTARY INFORMATION

2.1 ANNEALING FUNCTION τ

The function $\tau(f)$ determines the acceptance of worse parameters during the applied fitting procedure Metropolis Monte Carlo based on Simulated Annealing. This function of fitting steps f is defined in form of the Hill equation, *i.e.*

$$\tau(f) = \tau_0 + \frac{f^n}{(P^n + f^n)} \left(\tau_\infty - \tau_0\right), \tag{1}$$

that ranges between τ_0 and τ_∞ (see Supplementary Table 1 for applied values) and is characterized by the coefficient $n = 3$ describing the slope of the function as well as the point of inflection $P = 0.5\, f_{total}$ (with f_{total} the total number of fitting steps). We determined the value for n and P by manual adjustment.

3 SUPPLEMENTARY TABLES AND FIGURES

Supplementary Table 1. Score values ϵ_c for combined units c.

combined unit c	score value ϵ_c
C_A	45
C_K	20
C_E	70
C_M	200
C_G	30

Manually adjusted score values ϵ_c of the combined units c that are used for comparison with experimental data from whole-blood infection assay. All states of the PI-SBM that represent alive (killed) *C. albicans* cells are summarized to the combined unit C_A (C_K). States of *C. albicans* cells in extracellular space, in monocytes or in PMN are represented by the combined units C_E, C_M or C_G, respectively.

Supplementary Table 2. Individual start conditions of the fitting algorithm.

$C_{AE}(0)$	$M_{0,0}(0)$	$G_{0,0}(0)$	number of runs	number of fitting steps	τ
100	50	500	100	3 000	[0.05,5.0]
1 000	500	5 000	50	1 000	[5.0;30.0]
10 000	5 000	50 000	20	250	[5.0;80.0]
100 000	50 000	500 000	10	50	[50.0;80.0]

Start conditions for the parameter fitting algorithm. The number of individuals of alive *C. albicans* cells in extracellular space ($C_{AE}(0)$), monocytes ($M_{0,0}(0)$) and PMN ($G_{0,0}(0)$) at time $t = 0$ min was stepwise increased by keeping their ratio constant. For each step, the number of runs with corresponding number of fitting steps per run and the range of τ was adjusted.

Supplementary Table 3. Transition rates for PI-SBM.

	rate $[min^{-1}]$	standard deviation $[min^{-1}]$	standard deviation $[\%]$
ϕ_G	$2.83 \cdot 10^{-2}$	$0.49 \cdot 10^{-3}$	1.7
ϕ_{G*}	$4.75 \cdot 10^{-2}$	$3.86 \cdot 10^{-3}$	8.13
ϕ_M	$1.25 \cdot 10^{-2}$	$0.74 \cdot 10^{-3}$	5.9
κ_M	$3.59 \cdot 10^{-2}$	$3.74 \cdot 10^{-3}$	10.4
κ_G	$4.69 \cdot 10^{-2}$	$4.25 \cdot 10^{-3}$	9.1
ρ	$0.45 \cdot 10^{-2}$	$0.19 \cdot 10^{-3}$	4.2
γ	$1.93 \cdot 10^{-2}$	$2.76 \cdot 10^{-3}$	14.3
$\bar{\kappa}_{EK}$	$26.07 \cdot 10^{-2}$	$22.65 \cdot 10^{-3}$	8.7

The transition rates of the P-SBM are given by the phagocytosis rate ϕ_G of PMN that phagocytose for their first time, the phagocytosis rate $\phi_{G^\star}$ of PMN that phagocytose for at least the second time, the phagocytosis rate ϕ_M of monocytes, the intracellular killing rate κ_M of monocytes, the intracellular killing rate κ_G of PMN, the resistance rate ρ and the rates that determine the extracellular killing κ_{EK} and γ.

Supplementary Table 4. Transition rates for P-SBM.

	rate $[min^{-1}]$	standard deviation $[min^{-1}]$	standard deviation $[\%]$
ϕ_G	$2.69 \cdot 10^{-2}$	$0.33 \cdot 10^{-3}$	1.24
$\phi_{G^\star}$	$3.58 \cdot 10^{-2}$	$1.88 \cdot 10^{-3}$	5.24
ϕ_M	$0.63 \cdot 10^{-2}$	$0.33 \cdot 10^{-3}$	5.25
κ_M	$6.08 \cdot 10^{-2}$	$4.04 \cdot 10^{-3}$	6.64
κ_G	$4.26 \cdot 10^{-2}$	$2.03 \cdot 10^{-3}$	4.76
ρ	$0.41 \cdot 10^{-2}$	$0.13 \cdot 10^{-3}$	3.25
γ	$3.16 \cdot 10^{-2}$	$2.15 \cdot 10^{-3}$	6.8
$\kappa_{\bar{E}K}$	$29.13 \cdot 10^{-2}$	$14.35 \cdot 10^{-3}$	4.93

The transition rates of the PI-SBM are given by the phagocytosis rate ϕ_G of PMN that phagocytose for their first time, the phagocytosis rate $\phi_{G^\star}$ of PMN that phagocytose for at least the second time, the phagocytosis rate ϕ_M of monocytes, the intracellular killing rate κ_M of monocytes, the intracellular killing rate κ_G of PMN, the resistance rate ρ and the rates that determine the extracellular killing κ_{EK} and γ.

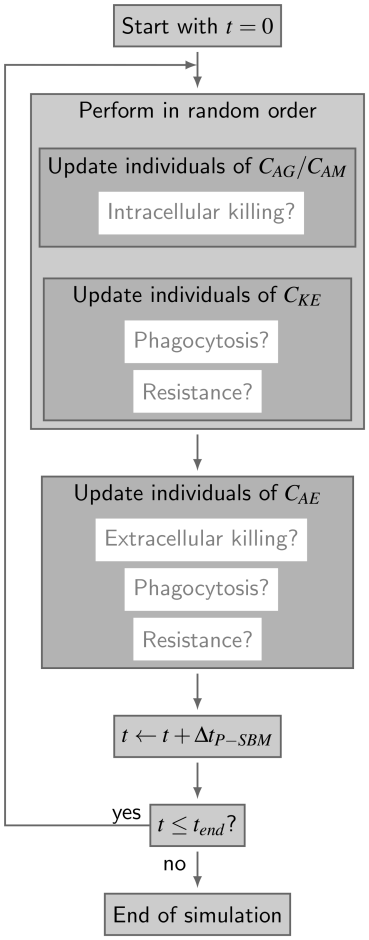

Supplementary Figure 1. Flow-chart of the non-spatial P-SBM simulation algorithm. In each time-step Δt_{P-SBM}, all individuals of *C. albicans* cell states are tested for possible state transitions. Individuals of alive *C. albicans* cells in monocytes (C_{AM}) or PMN (C_{AG}) are tested for intracellular killing. Individuals of the state killed-and-extracellular *C. albicans* cells (C_{KE}) are tested for phagocytosis and for becoming resistant. The individuals of the state alive-and-extracellular *C. albicans* cells (C_{AE}) are tested for phagocytosis, for extracellular killing and for becoming resistant.

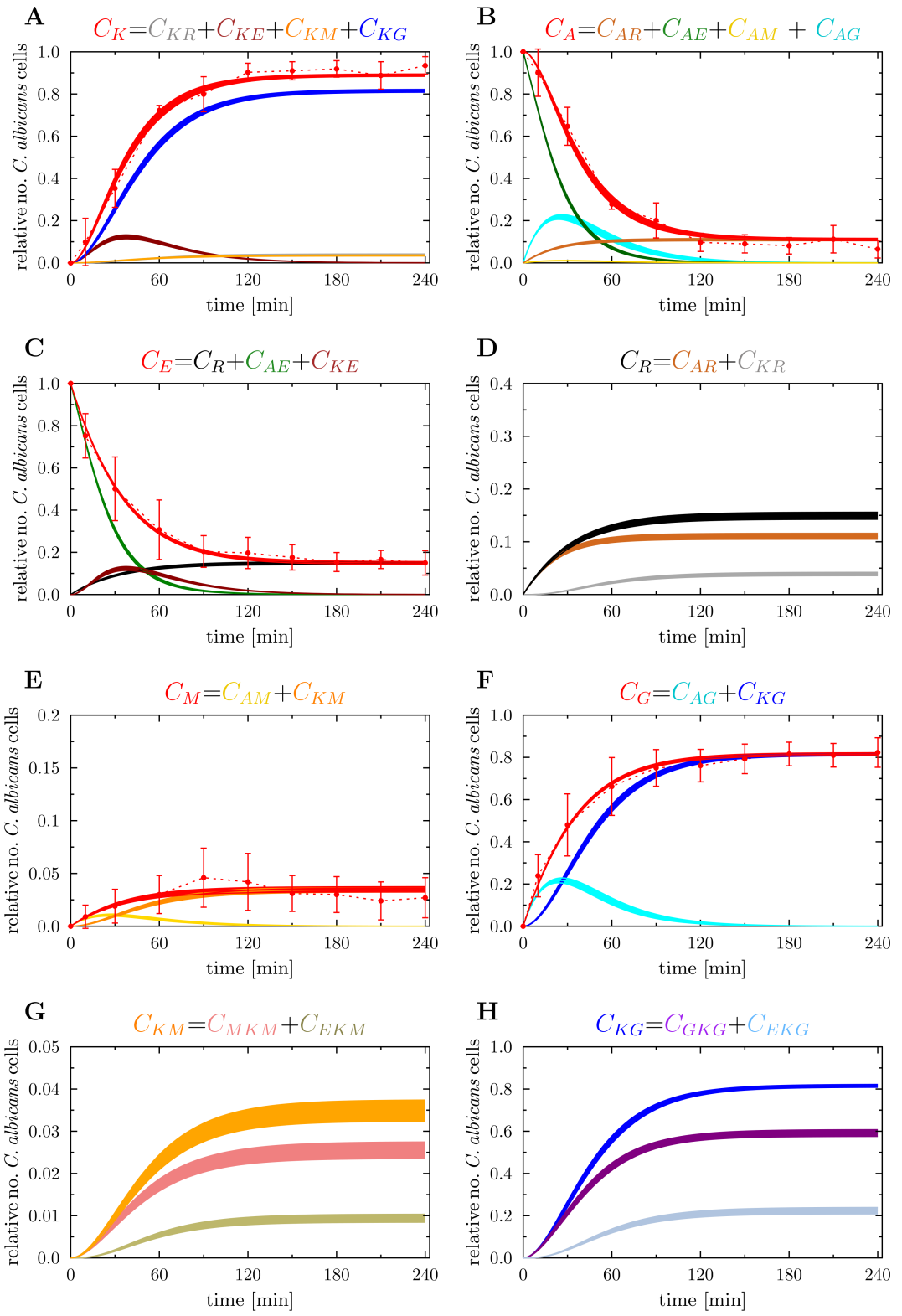
A
C_K=C_{KR}+C_{KE}+C_{KM}+C_{KG}
B
C_A=C_{AR}+C_{AE}+C_{AM} + C_{AG}
C
C_E=C_R+C_{AE}+C_{KE}
D
C_R=C_{AR}+C_{KR}
E
C_M=C_{AM}+C_{KM}
F
C_G=C_{AG}+C_{KG}
G
C_{KM}=C_{MKM}+C_{EKM}
H
C_{KG}=C_{GKG}+C_{EKG}
relative no. *C. albicans* cells
time [min]

Supplementary Figure 2. Kinetics of PI-SBM simulations (red solid lines) for the minimal least squares error (LSE) relative to the experimental data from whole-blood infection assays (red dotted lines as guide for the eye). The error bars correspond to the standard deviations of five independent experiments. The thickness of the solid lines represents the standard deviation of the simulation results as obtained from 50 simulations for normally distributed transition rates as given in Supplementary Table 2. Colored symbols refer to different *C. albicans* states, where their time courses are indicated by continuous lines with the same color. (A) Time-dependent relative number of killed *C. albicans* cells (C_K) that were experimentally measured by survival plates. The experimental results were compared with the combination of simulated data representing all killed *C. albicans* of the model, *i.e.* extracellularly killed *C. albicans* (C_{KE}), killed resistant *C. albicans* (C_{KR}), killed *C. albicans* that are in monocytes (C_{KM}) or PMN (C_{KG}). (B) Alive *C. albicans* (C_A) that were measured by survival plates and simulated by the combination of alive *C. albicans* that are in extracellular space (C_{AE}), in monocytes (C_{AM}), in PMN (C_{AG}) or became resistant against phagocytosis (C_{AR}). (C) Time course of *C. albicans* cells that are in extracellular space of blood (C_E). Experimental data was obtained by FACS analysis and simulated data is represented by the combination of *C. albicans* cells that are extracellular alive (C_{AE}), extracellularly killed (C_{KE}) and resistant against phagocytosis (C_R). (D) The simulated resistant *C. albicans* (C_R) are the sum of alive and dead resistant *C. albicans* cells at each time point of the simulation time. (E) Time course of *C. albicans* cells that were phagocytosed by monocytes (C_M). This is defined as sum of alive and killed *C. albicans* cells in monocytes, *i.e.* C_{AM} and C_{KM}, respectively. The corresponding experimental data was obtained by FACS analysis. (F) Relative number of *C. albicans* cells in PMN (C_G) during the whole-blood infection, where internalized *C. albicans* cells can be alive (C_{AG}) or dead (C_{KG}). (G) Simulation result of killed *C. albicans* cells within monocytes (C_{KM}), that is defined as the sum of internalized *C. albicans* that were intracellularly killed(C_{MKM}) and those who were extracellularly killed (C_{EKM}). (H) Simulated time course of killed *C. albicans* cells in PMN (C_{KG}), that is composed of intracellularly killed *C. albicans* cells (C_{GKG}) and extracellularly killed *C. albicans* cells (C_{EKG}) in PMN.

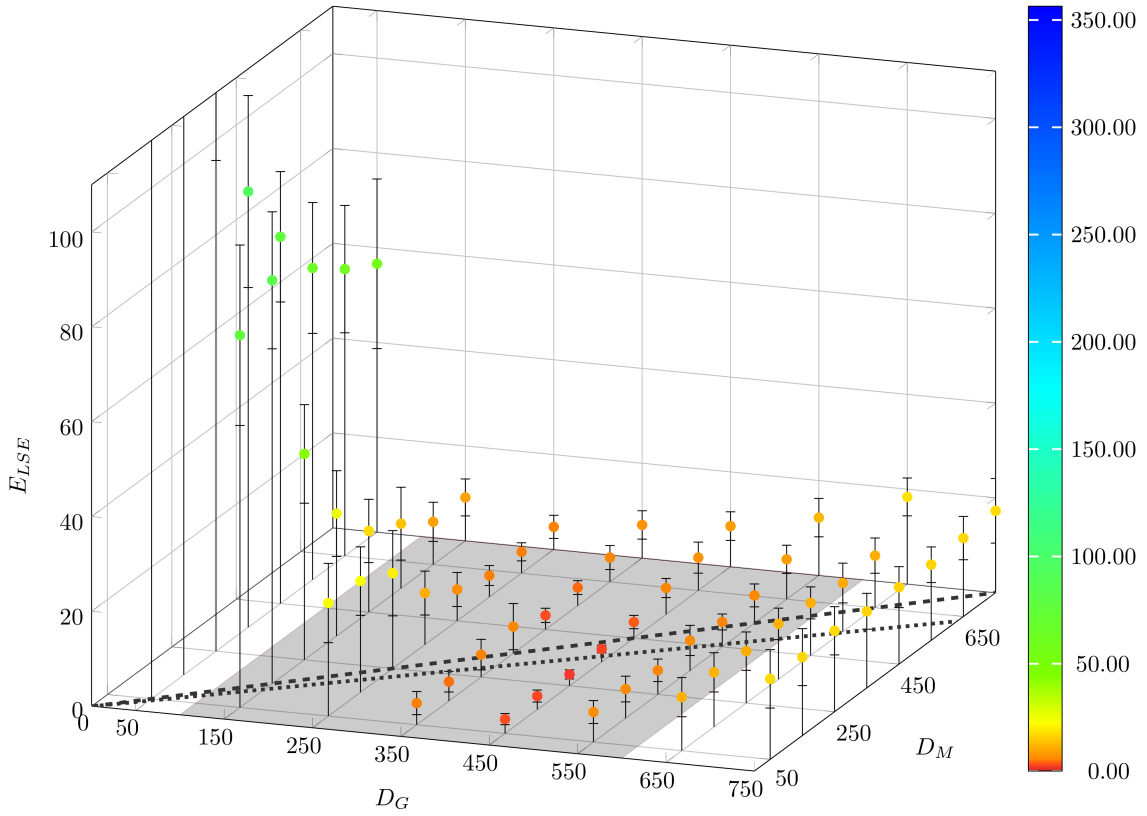

Supplementary Figure 3. Result of ABM parameter estimation by *adaptive regular grid search* applied to the small ABM representing $1/5\,\mu l$ blood. The space of diffusion coefficients of monocytes (D_M) and PMN (D_G) was scanned at the grid points in the pre-defined area. At each grid point the mean value of the least squares error (LSE) and the standard deviation over 30 simulations are shown. The gray region represents the rectangle that contains all pairs of diffusion coefficients for which the LSE values were found to be minimal from separately varying each diffusion coefficient. The dashed line corresponds to $D_M = D_G$ and the dotted line corresponds to diffusion coefficients that follow the Stokes-Einstein equation for monocytes and PMN, *i.e.* $D_G/D_M = d_M/d_G$ with monocyte diameter $d_M = 16\,\mu m$ and PMN diameter $d_G = 13.5\,\mu m$.

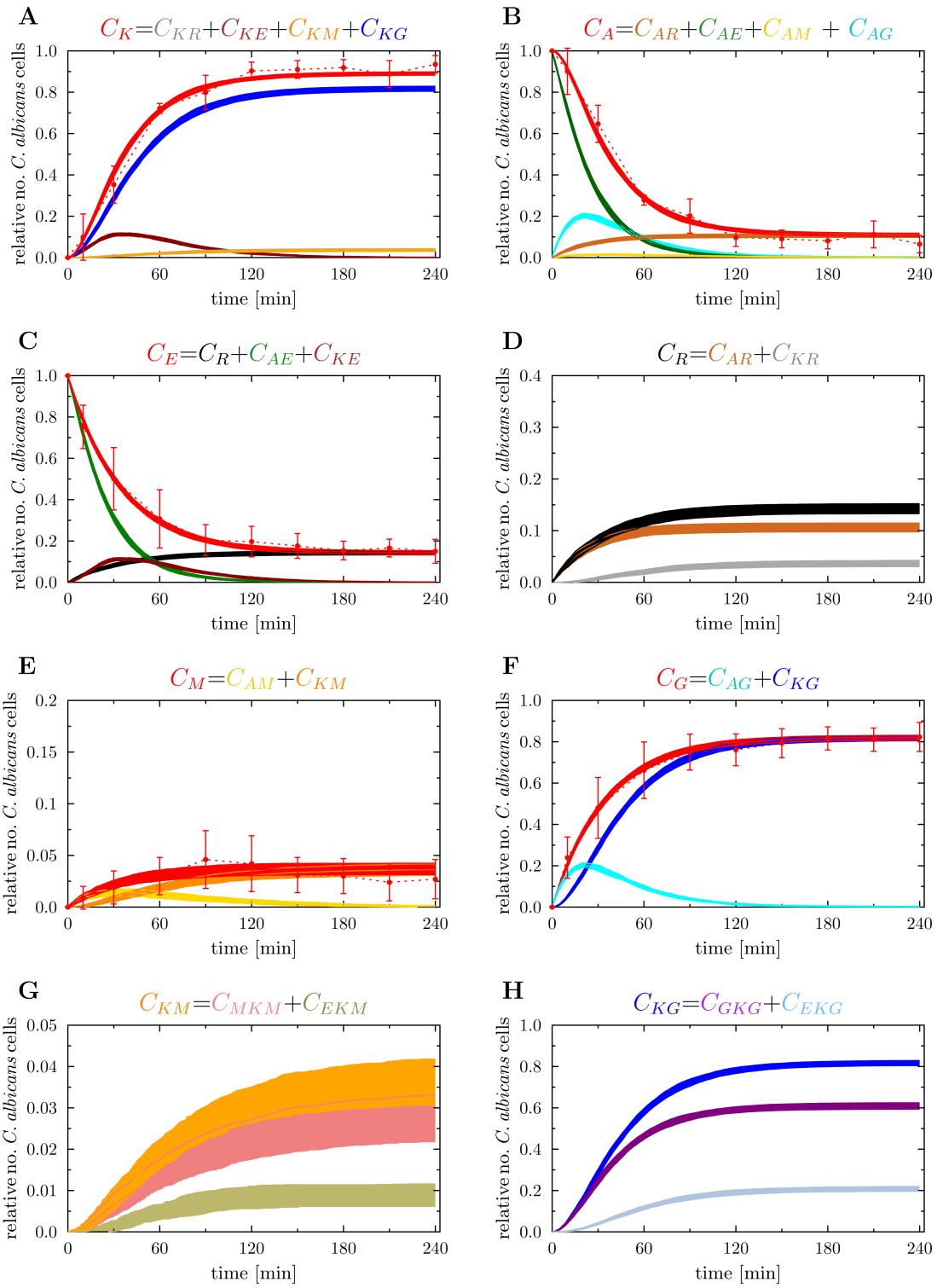
A
C_K=C_{KR}+C_{KE}+C_{KM}+C_{KG}
B
C_A=C_{AR}+C_{AE}+C_{AM} + C_{AG}
C
C_E=C_R+C_{AE}+C_{KE}
D
C_R=C_{AR}+C_{KR}
E
C_M=C_{AM}+C_{KM}
F
C_G=C_{AG}+C_{KG}
G
C_{KM}=C_{MKM}+C_{EKM}
H
C_{KG}=C_{GKG}+C_{EKG}
relative no. *C. albicans* cells
time [min]

Supplementary Figure 4. Kinetics of ABM simulations with $(D_G^{min}, D_M^{min}) = (425, 275)\,\mu m^2/min$ (red solid lines) for the minimal least squares error (LSE) relative to the experimental data from whole-blood infection assays (red dotted lines as guide for the eye). The error bars correspond to the standard deviations of five independent experiments. The thickness of the solid lines represents the standard deviation of the simulation results as obtained from 30 simulations. Colored symbols refer to different *C. albicans* states, where their time courses are indicated by continuous lines with the same color. (A) Time-dependent relative number of killed *C. albicans* cells (C_K) that were experimentally measured by survival plates. The experimental results were compared with the combination of simulated data representing all killed *C. albicans* of the model, *i.e.* extracellularly killed *C. albicans* (C_{KE}), killed resistant *C. albicans* (C_{KR}), killed *C. albicans* that are in monocytes (C_{KM}) or PMN (C_{KG}). (B) Alive *C. albicans* (C_A) that were measured by survival plates and simulated by the combination of alive *C. albicans* that are in extracellular space (C_{AE}), in monocytes (C_{AM}), in PMN (C_{AG}) or became resistant against phagocytosis (C_{AR}). (C) Time course of *C. albicans* cells that are in extracellular space of blood (C_E). Experimental data was obtained by FACS analysis and simulated data is represented by the combination of *C. albicans* cells that are extracellular alive (C_{AE}), extracellularly killed (C_{KE}) and resistant against phagocytosis (C_R). (D) The simulated resistant *C. albicans* (C_R) are the sum of alive and dead resistant *C. albicans* cells at each time point of the simulation time. (E) Time course of *C. albicans* cells that were phagocytosed by monocytes (C_M). This is defined as sum of alive and killed *C. albicans* cells in monocytes, *i.e.* C_{AM} and C_{KM}, respectively. The corresponding experimental data was obtained by FACS analysis. (F) Relative number of *C. albicans* cells in PMN (C_G) during the whole-blood infection, where internalized *C. albicans* cells can be alive (C_{AG}) or dead (C_{KG}). (G) Simulation result of killed *C. albicans* cells within monocytes (C_{KM}), that is defined as the sum of internalized *C. albicans* that were intracellularly killed(C_{MKM}) and those who were extracellularly killed (C_{EKM}). (H) Simulated time course of killed *C. albicans* cells in PMN (C_{KG}), that is composed of intracellularly killed *C. albicans* cells (C_{GKG}) and extracellularly killed *C. albicans* cells (C_{EKG}) in PMN.

4.5 Deciphering the counterplay of *Aspergillus fumigatus* infection and host inflammation by evolutionary games on graphs

SCIENTIFIC REPORTS

OPEN

Received: 16 March 2016
Accepted: 20 May 2016
Published: 13 June 2016

Deciphering the Counterplay of *Aspergillus fumigatus* Infection and Host Inflammation by Evolutionary Games on Graphs

Johannes Pollmächer[1,2], Sandra Timme[1,2], Stefan Schuster[3], Axel A. Brakhage[2,4], Peter F. Zipfel[2,5] & Marc Thilo Figge[1,2]

www.nature.com/scientificreports

SCIENTIFIC REPORTS

OPEN

Deciphering the Counterplay of *Aspergillus fumigatus* Infection and Host Inflammation by Evolutionary Games on Graphs

Received: 16 March 2016
Accepted: 20 May 2016
Published: 13 June 2016

Johannes Pollmächer[1,2], Sandra Timme[1,2], Stefan Schuster[3], Axel A. Brakhage[2,4], Peter F. Zipfel[2,5] & Marc Thilo Figge[1,2]

Microbial invaders are ubiquitously present and pose the constant risk of infections that are opposed by various defence mechanisms of the human immune system. A tight regulation of the immune response ensures clearance of microbial invaders and concomitantly limits host damage that is crucial for host viability. To investigate the counterplay of infection and inflammation, we simulated the invasion of the human-pathogenic fungus *Aspergillus fumigatus* in lung alveoli by *evolutionary games on graphs*. The layered structure of the innate immune system is represented by a sequence of games in the virtual model. We show that the inflammatory cascade of the immune response is essential for microbial clearance and that the inflammation level correlates with the infection-dose. At low infection-doses, corresponding to daily inhalation of conidia, the resident alveolar macrophages may be sufficient to clear infections, however, at higher infection-doses their primary task shifts towards recruitment of neutrophils to infection sites.

The great efficiency of the human immune system with regard to the recognition and elimination of infectious microbes is due to its layered and redundant structure and its well-orchestrated response across elevating levels. For example, the complex immune system is divided into the two main interacting levels of innate and adaptive immunity. Many infectious microbes are cleared already by the innate immune response that is immediately active but only grossly specific[1]. However, if the infectious microbe cannot be cleared in this way, inflammatory signals elevate the response from the level of innate immunity to the level of adaptive immunity. Activation of an adaptive response, *e.g.* involving affinity maturation of antibodies by B-cells in germinal centres, takes days to weeks, however, at the benefit of being highly specific for the invader[2].

The layered structure of the immune system is also recognised within the levels of innate and adaptive immunity itself. For example, adaptive immunity does not necessarily require to mount the tedious process of antibody affinity maturation, if the infectious microbe was encountered before and can be defeated by the activation of previously generated memory cells that directly go into production of the highly specific antibodies[2]. Similarly, innate immunity comprises the immediate response of humoral immunity, like the complement system, that may eliminate the infectious microbes by opsonisation associated with inflammatory signalling to recruit and activate phagocytic cells within a few hours and/or the formation of membrane attack complexes[3]. Furthermore, one can distinguish phagocytic cells that are resident in organs from those that are recruited in support from the bloodstream to the site of infection within tens of hours[1].

Apart from the fact that the layered structure of the immune system is beneficial for the strength and efficiency of the response, it is obvious that an elevating regulation between infection and inflammation is beneficial in being protective for the host itself. The danger for the human host due to dysregulation of the immune response

[1]Research Group Applied Systems Biology, Leibniz Institute for Natural Product Research and Infection Biology – Hans Knöll Institute, Jena, Germany. [2]Faculty of Biology and Pharmacy, Friedrich Schiller University Jena, Germany. [3]Department of Bioinformatics, Faculty of Biology and Pharmacy, Friedrich Schiller University Jena, Germany. [4]Department of Molecular and Applied Microbiology, Leibniz Institute for Natural Product Research and Infection Biology – Hans Knöll Institute, Jena, Germany. [5]Department of Infection Biology, Leibniz Institute for Natural Product Research and Infection Biology – Hans Knöll Institute, Jena, Germany. Correspondence and requests for materials should be addressed to M.T.F. (email: thilo.figge@leibniz-hki.de)

becomes impressively evident in the case of sepsis, *i.e.* a whole-body inflammatory response to an infection that may induce multi organ failure[4]. Thus, as important as it is that the human host responds with inflammation against infection, it is mandatory for the protection of the host against its own immune system to avoid unnecessary overshoots and to ensure a proper shut down of the response after infection clearance[5]. In what follows, we refer to the pathogen-induced infection and the host-driven inflammation, which are opposing actions from positions of defence, as *counterplay*.

Virtual infection-inflammation models can be constructed by different modelling techniques like for example by *ordinary differential equation models* (ODE), *state-based models* (SBM), *agent-based models* (ABM) and game theory. The purpose of a theoretical study and the complexity of a biological system determine how suitable a certain approach is.

ODE allow for straightforward modelling and have previously been applied in the context of bacterial infections[6–9] as well as for *A. fumigatus* infection[10]. However, ODE assume spatially homogeneous environments, where the constituents occur in high concentrations, making them inappropriate for a realistic simulation of the infection-inflammation scenarios of *A. fumigatus* conidia in the lung. SBM and ABM allow for the stochastic simulation of biological systems at the level of single events[11,12]. While SBM neglect spatial resolution, ABM simulate single individuals within a real spatial structure that may be represented on a grid or in continuous space. For example, a virtual infection-inflammation model of the human-pathogenic fungus *Candida albicans* in human blood was recently formulated in terms of a bottom-up modelling approach using SBM and ABM for quantitative parameter estimation[13,14]. Another ABM was developed for investigation of spatio-temporal dynamics of *A. fumigatus* infection of *in vitro* experiments[15] and in a virtual human alveolus with regard to inflammation-induced chemotaxis of AM[16]. The latter model was extended to a hybrid ABM that enabled investigation of molecular diffusion using *partial differential equations* to decipher quantitative properties of candidate chemokines[17].

The aforementioned modelling techniques simulate the time course of an underlying biological system by means of mechanistic processes. As a consequence, the dimensions of the parameter space are rapidly increasing and, since many of these parameters are unknown to date, a rigorous parameter estimation may render these approaches infeasible[14]. Therefore, to investigate the innate immune response against *A. fumigatus* in the human lung at the humoral and cellular level, we here pursue a game-theoretical approach that resolves the counterplay of infection and inflammation at the different levels.

Game theory is a mathematical concept of optimisation and the main advantage of this approach is that different effector mechanisms can be elegantly condensed into a reduced number of combined parameters. This renders computational simulations tractable and still allows for the identification of the key parameters that deserve particular attention in future experimental investigations. *Classical game theory* (CGT) was originally developed as decision support[18] in interactive situation in which the aims, goals and preferences of individual actors, *i.e.* the players of a game, are in conflict with each other[19]. The decisions available to the players correspond to strategies from which they can choose. Based on its own strategy and the strategies of the other players with which interactions are carried out players receive a benefit – also termed *payoff*[20]. However, each player in CGT was assumed to act perfectly rationally, to have the complete set of information about all possible outcomes of the game and their related payoffs as well as the cognitive capabilities to deduce from this information the optimal strategy[19]. To represent phenomena observed in interactions between living organisms, the paradigm of CGT turned out to be too restrictive.

The restrictions were softened by the concept of *evolutionary game theory* (EGT)[21]. This concept allowed for more flexibility and – inspired by evolution theory – implemented irrational behaviour, *e.g.* in terms of mutation. Thus, players do not simply optimise their payoff with regard to their strategic alternatives; rather, they replicate, survive or die based on the fitness associated with their respective strategy[22]. As a consequence, the dynamics of strategies involves a series of iterative evolutionary steps, a feature completely missing in CGT[19]. Moreover, the field of *evolutionary games on graphs* emerged, where not all players interact with each other, but the number of interactions is reduced to the ones that can be reasoned for by neighbourship relations between individuals, *e.g.* based on spatial proximity, social connections or genetic relationships[19]. There have been several contributions to the field of fungal infections using game-theoretic approaches in the recent past[23]: Hummert *et al.* investigated the cooperative behaviour between *Candida albicans* cells that were phagocytosed by macrophages[24]. In another study on *C. albicans* infection, the dynamics of the yeast-to-hyphal transition in response to various actions of the host was investigated by EGT[25]. It was found that the host requires a differentiated response to the distinct morphological states of *C. albicans* in order to keep the fungus in the least pathogenic state. Other examples, going beyond the context of fungal infections, have been reviewed by Hummert *et al.* regarding cellular interactions[20] and by Bohl *et al.* regarding molecular interactions[26].

In this study, we theoretically investigate the counterplay of infection and inflammation during the innate immune response against invading microbes by applying EGT. The main advantages of this stochastic modelling approach are that (i) systems with a small number of constituents are adequately captured, (ii) model parameters are reduced by a relative representation of processes, and (iii) spatial system resolution can be realized on a graph. While such a modelling approach is generally applicable to infection-inflammation scenarios caused by any kind of infectious microbe, for illustrative purposes we here focus on the concrete example of the saprophytic human-pathogenic fungus *Aspergillus fumigatus*[27]. This fungus represents a prime example, because humans inhale several thousands of its ubiquitously present airborne conidia every day[28]. Thus, while this fungus constitutes a common challenge to the human host, its potential threat can obviously be permanently managed under physiological immune conditions. This implies that an innate immune response against this infectious agent is generally sufficient, involving moderate inflammatory conditions that are usually mounted unnoticed in immunocompetent individuals. However, the situation is different for immunocompromised individuals and/or when high fungal doses are inhaled, in which case the pathogen can become a major cause of life-threatening

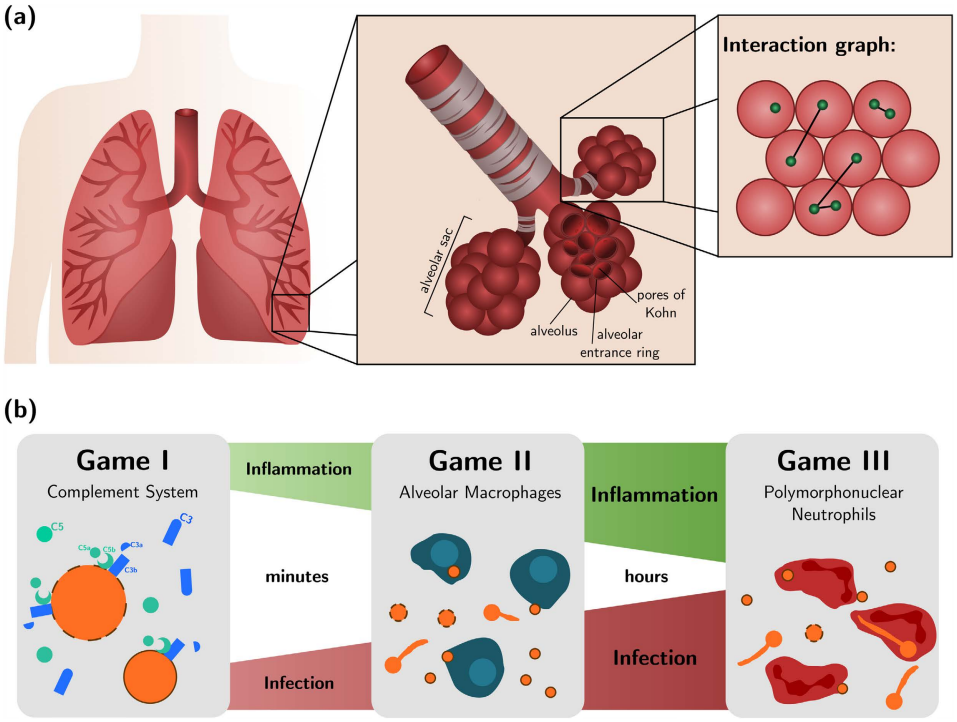

Figure 1. Lung architecture and design of evolutionary games. (**a**) Organisation of densely packed alveoli in alveolar sacs in the lower respiratory tract of the lung. An example distribution of eight fungal cells (shown in *green*) over a cross-sectioned alveolar sac and their proximity-based interactions (*black* connections). (**b**) Model design of the consecutive sequence of evolutionary games on graphs for the innate immune response against *A. fumigatus* infection in the lung.

infections[29]. The immune system of immunocompromised individuals may not be able to clear the lung from *A. fumigatus* conidia in due time, before the onset of conidial germination that may be followed by invasive growth[30]. Inhaled conidia typically are in a resting state, covered by a rodlet layer that renders them immunologically inert[31]. However, taking advantage of nutrient-rich conditions in the lung alveoli, resting conidia may swell and germinate, ultimately leading to the formation of hyphae and the ability of the fungus to penetrate tissue and eventually enter the bloodstream, disseminating through the whole body. As a consequence, invasive pulmonary aspergillosis is associated with high mortality rates ranging from 30–90%[32].

On invading the human organism, fungal cells are partly intercepted by mucosal epithelial cells, however, due to their small size of about 2–3 μm, significant amounts of the conidia can enter the lower respiratory tract of the lung (see Fig. 1(a)). They end up in so-called *alveolar sacs* (AS)[33] that consist of alveoli, which are the smallest units of the human lung[27]. Alveoli exist in various polyhedral shapes with a surface to volume ratio that optimises the gas exchange through their thin epithelial layers[34]. Once conidia enter the alveoli, they are embedded within the nutrient-rich and highly viscous alveolar lining layer, also called pulmonary surfactant, where they are faced with several defence mechanisms of the host[27,35]. During the innate immune response different sequential phases can be involved. Depending on how successful the pathogen can be cleared from the human host in one phase, the next phase, which is associated with a higher level of inflammation, may be initiated. As depicted in Fig. 1(b), the innate immune response against *A. fumigatus* conidia comprises humoral factors, like the complement system that is subject of Game I, and phagocytic cells, such as *alveolar macrophages* (AM) and *polymorphonuclear neutrophils* (PMN) being subjects of Game II and III, respectively.

As soon as conidia get into contact with the surfactant, complement is activated and proteins start to opsonise their surfaces, with amounts of bound complement proteins being proportional to the surface area of the fungal cell[36]. Opsonisation by complement proteins induces inflammation at the site of infection and the release of chemoattractants, *e.g.* C3a and C5a[3]. In addition to that, opsonisation of the fungal surface increases phagocytosis and the production of reactive oxygen intermediates (ROI) by AM and PMN enhancing phagocyte activation on direct physical contact with the pathogen[30]. Taken together, while the complement system drives the innate immune response against *A. fumigatus* by inflammatory signals, the formation of terminal membrane attack complexes are expected to be prohibited by the thickness of the cell wall[37].

Upon contact of *A. fumigatus* conidia with type II *alveolar epithelial cells* (AEC), these cells secrete inflammatory molecules, such as IL-6 and TNF-α as well as the chemoattractant IL-8[38]. AM are resident phagocytes in lung alveoli and are the first immune cells that get into contact with inhaled pathogens like *A. fumigatus* conidia[34,39].

They are able to phagocytose both resting and swollen conidia, but only swollen conidia are effectively killed intracellularly[39]. AM lack the ability to phagocytose the hyphal morphotype of *A. fumigatus*, but are critical for hyphal recognition because this leads to the chemotactic recruitment of circulating phagocytes, like PMN, from the bloodstream to the site of infection[29,40].

PMN phagocytose and kill conidia but also hyphal structures. If hyphal structures are too large for being phagocytosed, PMN may release the content of their granules into extracellular space[30]. These extracellular factors are involved in killing hyphae, but also cause damage to the surrounding host tissue[27]. Furthermore, PMN may commit an altruistic suicide as a final act of defence against hyphae, thereby releasing DNA fibers into the environment that may trap the fungus[41]. These so-called *neutrophilic extracellular traps* (NETs) were shown to have fungistatic rather than fungicidal effects[41]. AM and PMN are thought to be key players in the defence against *A. fumigatus* and an impairment of either phagocyte type is commonly associated with a relatively high susceptibility for severe infections by this fungus[42].

As is clear from the example of the human-pathogenic fungus *A. fumigatus*, investigating the counterplay of infection and inflammation is highly important in order to gain insights into the complex host-pathogen interactions that may ultimately reveal possibilities for therapeutic interventions. However, since it is virtually impossible to investigate these processes in alveoli of the human lung *in vivo* and under physiological conditions[16], we here pursue a systems biology approach starting with theoretical modelling. We apply EGT on graphs to investigate the counterplay of pathogen-induced infection and increasing levels of host inflammation during *A. fumigatus* infection in AS of the human lung according to the time course depicted in Fig. 1(b). The model is constructed on the firm basis of experimental data available today (see Methods section) and is applied to generate new hypothesis that can direct future experimental investigations (see Discussion section).

The present study, using infections by the human-pathogenic fungus *A. fumigatus* as an example, reveals the importance of the immune response to be tightly regulated and that this regulation is realised by the layered structure of the immune system. In particular, our simulations reconcile the contradictory view on the role of AM in the immune response[43,44]: We observe that AM have a key role in the regulation of the first steps of the immune response and that this regulation depends on the strength of the infection-dose. While the phagocytic activity of AM is sufficient to limit low infection-doses – corresponding to values of daily inhalation – inflammatory signalling by AM for recruitment of PMN becomes their primary task at higher infection-doses.

Results

In this section, we first analyse the degree of proximity between conidia of *A. fumigatus* in AS of the human lung. Based on the derived interaction graphs between fungal cells, we then consider the results of three evolutionary games representing distinct stages of the innate immune response against this human-pathogenic fungus (see Fig. 1(b)). These stages comprise the humoral response by the complement system (Game I), the cellular immune response by AM (Game II) and PMN (Game III). Finally, by linking these three individual games in a time-ordered fashion, we present the results of infection-inflammation scenarios in the human host. To quantify the infection-inflammation scenarios, we defined the infection score (see Eq. 6) and normalised inflammations that mediate between Game I and II (see Eq. (7)) and Game II and III (see Eq. (8)).

Virtual infection-inflammation model reveals degree of fungal interactions in alveolar sacs. We performed *in silico* experiments to simulate the counterplay of *A. fumigatus* infection and host inflammatory response by evolutionary games on graphs. A graph defines the proximity-based interactions between fungal cells in AS of the human lung (see Fig. 1(a)). Each game of the infection-inflammation scenario represented a consecutive sequence of three stages of innate immunity (see Fig. 1(b)). Within each AS, consisting on average of 21 densely packed alveoli, the drawn number of conidia n_{fc} were uniformly distributed over its alveoli. As shown in Fig. 2(a), we found that irrespective of the fungal dose, most likely there will be no conidium at all in a randomly chosen AS. However, of all the AS that contained fungal cells, their number clearly depended on the fungal dose and was associated with quite different upper limits of conidia that could be expected in the AS. For a fungal dose that corresponds to daily inhalation ($6.3 \cdot 10^3$ conidia), two conidia per AS are conceivable, whereas for extremely high doses (10^7 conidia) up to eight conidia may be encountered in a single AS.

Fungal individuals in the same AS may become engaged in a game among each other under the influence of the immune response at a certain stage. As described in the Methods section, the graph-based approach defines interactions between fungal cells, where the number of interactions per fungal cell depends on their number in the corresponding AS. As shown in Fig. 2(b), this analysis revealed that two fungal cells in an AS most likely stay solitary, whereas three to eight individuals in an AS typically lead to one expected interaction per conidium.

Complement activity drives emergence of fungal morphotypes. In Game I, different morphotypes emerge from the interaction of fungal cells with the complement system that are shown in Fig. 3 for different parameter combinations and for low ($n_{fc} = 2$) and high ($n_{fc} = 8$) infection-doses. As could be expected, with rising nutrient availability E_S for swollen conidia or diminishing complement effects c_S against swollen conidia, their fraction increases over that of resting conidia, $f_S > f_R$. Regions with comparable fractions of resting and swollen conidia, $f_R \approx f_S$, were found for both infection-doses, however, these regions were more extended for the lower infection-dose. At high infection-doses, where conidia had on average more interaction partners per alveolus, it was frequently observed that one of the two populations dominated over the other one with a fraction above 80 %. This effect could be attributed to the dose-dependent impact of adaptation and mutation events in each simulation time-step. For low relative to high infection-doses, mutations occur more often than adaptation events due to a lack of interaction neighbours among the widely separated fungal cells.

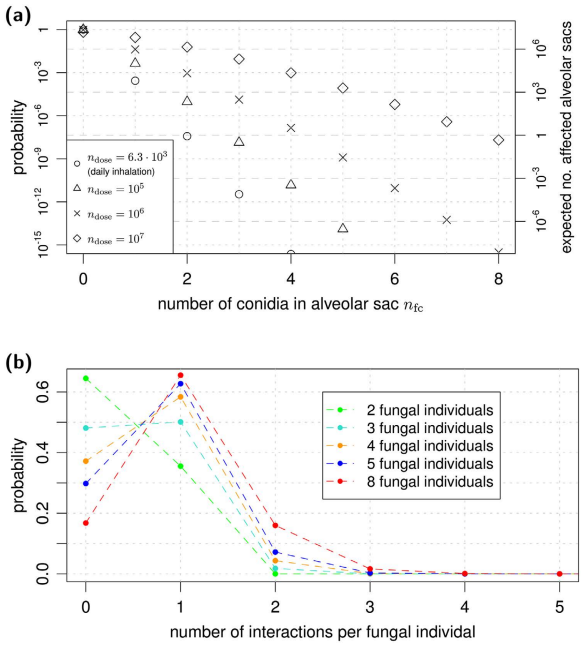

Figure 2. Number of conidia and their interactions per alveolar sac. (**a**) Dose-dependent probability distribution for the number of conidia entering the alveolar sac. Rescaling of the probability values were used to determine the expected number of affected alveolar sacs in the human lung, as shown by the scale on the right hand side. (**b**) Probability distribution for the number of interactions per fungal individual depending on the number of conidia inserted into the alveolar sac. Distributions were obtained from 10^6 interaction graphs.

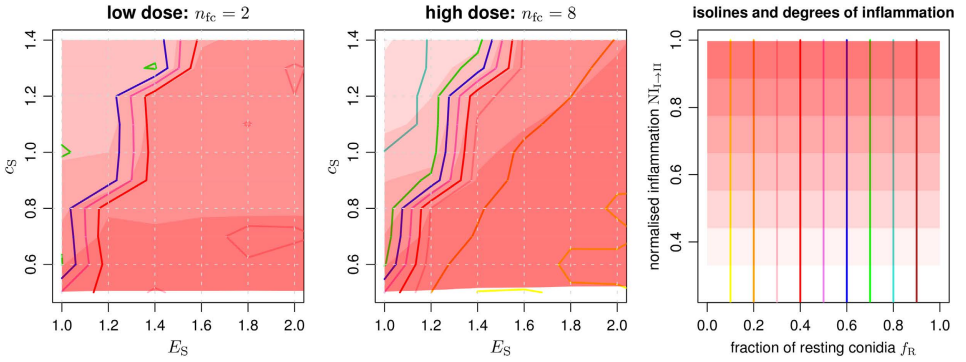

Figure 3. Fractions of *A. fumigatus* morphotypes and degrees of inflammation in response to the complement system. Equilibrium fractions of conidia in the resting state were determined from averaging over 100 repetitions per parameter configuration. Parameters were scanned in a lattice-based fashion at distinct points of the parameter space. Isolines (*colored lines*) for fractions of conidia in the resting state and isobands (*red shaded areas*) for different degrees of inflammation were generated using a modified version of the marching-squares algorithm for bilinear interpolation over rectangular grids. Parameters $E_R = 1$, $c_R = 0.5$ were kept fixed.

Alveolar macrophages reach phagocytic limits for high fungal doses. We performed simulations of Game II to identify the most relevant parameters under the impact of the immune response by AM. Using the concept of mutual information, as explained in the Methods section, we found that the activity of AM was of central importance regarding the infection score IS_{II} (see Eq. (6) and Table S2). Our investigations revealed that AM were in the position to keep the fungal cells in check for low infection-doses of fungal cells and for sufficiently high phagocytosis activity of AM. However, as shown in Fig. 4, AM were not able to remove the infectious agents in high-dose scenarios due to their inability to counteract hyphal cells appropriately. It can be expected that their function regarding elevation of the immune response via inflammatory and chemoattracting signals plays an important role in this case.

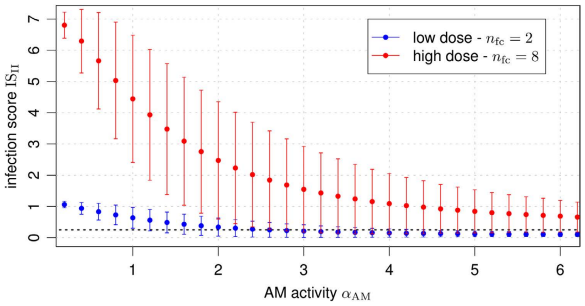

Figure 4. Dose-dependent infection scores according to simulations of Game II. The average infection score IS_{II} over all parameter combinations shown as a function of AM activity. Error bars denote one standard deviation. The *black short-dashed line* marks the infection score threshold IS = 0.25 below which clearance of infection is achieved.

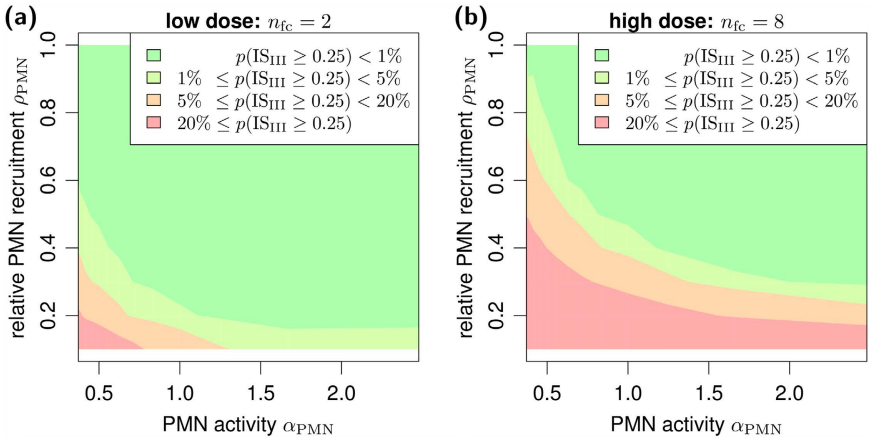

Figure 5. Dose-dependent connection between infection score and PMN parameters. Landscape of the persistent infection probability for different fungal doses in scenarios with (**a**) low and (**b**) high infection-doses. Isobands (*colored areas*) for different probability ranges were generated using a modified version of the marching-squares algorithm for bilinear interpolation over rectangular grids.

Recruitment of neutrophils can be essential for successful clearance. In Game III, *A. fumigatus* conidia were faced with the professional phagocytes PMN. First, we identified the most relevant parameters by computing the mutual information between each of the game's parameters and the infection score (see Eq. 6). The PMN recruitment ρ_{PMN} and phagocytosis activity α_{PMN} against live fungal cells were found to be most relevant for the outcome of the infection (see Table S2). We further analysed these parameters for low and high infection-doses and the results are shown in Fig. 5. It should be noted that the infection score $IS_{III} = 0.25$ represented the special case of one resting conidium in the AS that survived the immune response of the host. Consequently, infection scores $IS_{III} < 0.25$ and $IS_{III} \geq 0.25$ represent, respectively, clearance and persistence of the *A. fumigatus* infection. The measure $p(IS_{III} \geq 0.25)$, plotted in Fig. 5, denotes the fraction of parameter combinations over all performed simulations for which the fungal infection persisted in the host. We identified the most important parameters for infection clearance and found that, for a low number of infectious agents, PMN were able to clear the infection in most of the cases, whereas reduced recruitment and activity of PMN eventually led to the persistence of infection. In the limit of high infection-dose, PMN activity and a sufficiently high recruitment were pivotal to remove *A. fumigatus*. We further found that a reduced PMN activity could be partly compensated by an increase in the PMN recruitment. Moreover, independent of the precise value of PMN activity, sufficient PMN recruitment was generally found to be an essential prerequisite for successful infection clearance.

Infection-inflammation scenarios reveal regulatory role of alveolar macrophages. Going beyond the separated analysis of evolutionary games for the three distinct stages of the innate immune response against the human-pathogenic fungus *A. fumigatus*, we linked the games in a time-ordered fashion to simulate infection-inflammation scenarios in the human host. Thus, starting with Game I, we determined the infection score IS_I (see Eq. 6) due to the immune response by the complement system. Next, we linked Game I to Game II by computing the normalised inflammation $NI_{I \to II}$ (see Eq. (7)), which determined AM activity in the second stage of the immune response. The infection-inflammation scenario at this stage was evaluated by the infection

www.nature.com/scientificreports/

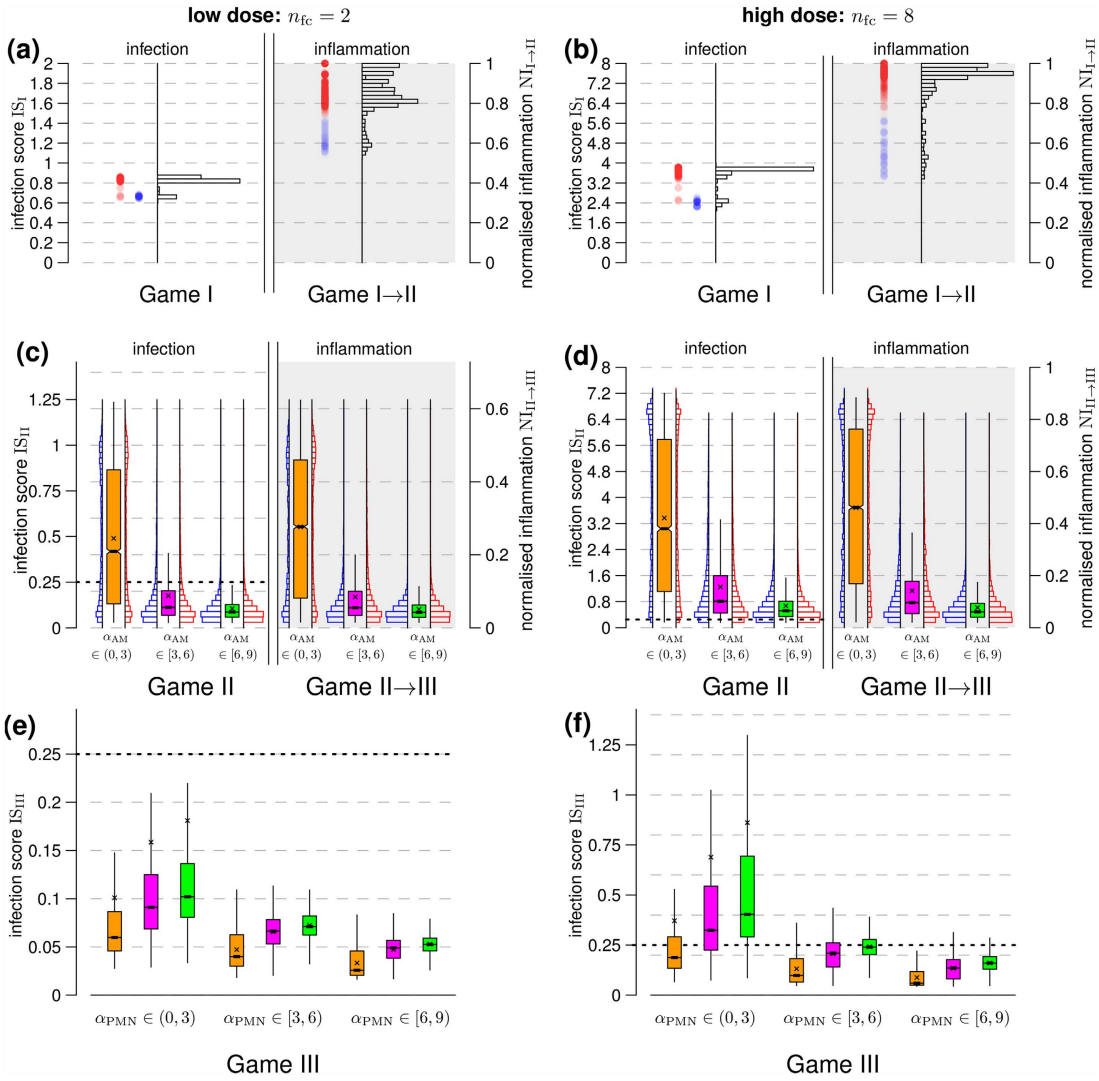

Figure 6. Dose-dependent relation between infection and inflammation across the consecutive sequence of evolutionary games. Two infection-inflammation scenarios were simulated: low infection-dose in (**a**,**c**,**e**) and high infection-dose in (**b**,**d**,**f**). In (**a**,**b**) the distribution of infection scores and corresponding values for the normalised inflammation are shown as *black histograms*. The distribution of higher (lower) values for the normalised inflammation with $NI_{I\to II} \geq 0.75$ ($NI_{I\to II} < 0.75$) are shown by circles colored in *red* (*blue*). The inflammatory signal $NI_{I\to II}$ was fed into Game II scaling AM activity. The effects of high and low values for the normalised inflammation are shown in (**c**,**d**) using *red* and *blue* inline histograms grouped by different levels of AM activity. The *red* and *blue* inline histograms were combined in the *notched box plots* and shown in *orange*, *violet* and *green* color, respectively, for low, medium and high AM activity with average values marked by (×). (**e**,**f**) Connection between Game II and Game III was set by the recruitment parameter $\rho_{PMN} = NI_{II\to III}$. Distributions for the different AM activities are presented in the same colors as in (**d**,**e**) grouped by PMN activities. The *black short-dashed lines* in (**c**–**f**) mark the infection score threshold IS = 0.25 below which clearance of infection is achieved.

score IS_{II} (see Eq. 6) and linking to Game III was realised by the normalised inflammation $NI_{II\to III}$ (see Eq. (8)), which determined PMN recruitment in the third stage of the immune response and gave rise to the infection score IS_{III} (see Eq. 6 and Fig. 1(b)).

The simulation results for low and high infection-doses as well as for varying AM and PMN activities are presented in Fig. 6. The counterplay between *A. fumigatus* infection and the complement system (Game I) yielded values for the infection score and the normalised inflammation that are shown in Fig. 6 for (a) low ($n_{fc} = 2$) and (b) high ($n_{fc} = 8$) infection-doses. The infection score IS_I resulting from Game I is depicted on the left-hand side in the black histograms in Fig. 6(a,b), while the corresponding normalised inflammation $NI_{I\to II}$ is shown on the

right-hand side. The normalised inflammation revealed a bimodal distribution that subdivides all simulations into infection-inflammation scenarios with low (blue) and high (red) NI-values. Interestingly, a comparison with the corresponding classes for the infection score did not show this clear separation. This result was observed for both low and high infection-doses and an in-depth analysis revealed that, while low (blue) inflammation values were associated with lower infection scores, higher (red) inflammation values were not only associated with higher infection scores but, quite unexpectedly, also with lower infection scores. It turned out that the reason for this behavior is in the effect that the complement system exerted on resting and swollen conidia. As can be observed in Fig. 3, high inflammation (dark red areas) exist for $f_R > 0.5$ and corresponds indeed to lower infection scores where the fraction of resting conidia is larger than that of swollen conidia. Furthermore, it could be observed that these cases were associated with approximately equal complement activity against resting and swollen conidia ($c_R \approx c_S$) in combination with only small differences between the nutrient contributions E_R and E_S.

The normalised inflammation $NI_{I\to II}$ that was induced by the response of the complement system (Game I) had direct impact on AM activity in Game II. The corresponding results are depicted in Fig. 6 for (c) low and (d) high infection-doses. In both cases, the highest impact on the infection scores could be attributed to the AM activity α_{AM}, where higher AM activity was associated with more strongly reduced infection and vice versa. Interestingly, only marginal differences were induced by low (blue) and high (red) infection-inflammation scenarios from the complement response with regard to the resulting distributions of infection scores after AM response in Game II (see Fig. 6(c,d), blue and red inline histograms). Of note, we generally observe that the level of infection is reflected by the level of inflammation (see Fig. 6(c,d)). In scenarios with low infection-dose, as shown in Fig. 6(c), AM with high activity were in the position to clear the infection in most of the cases ($p(IS_{II} < 0.25) = 95\%$), in contrast to scenarios with high infection-dose (see Fig. 6(d)), where even high AM activity could only reduce but not entirely clear the infection in most of the cases ($p(IS_{II} < 0.25) = 10\%$). In both infection scenarios and irrespective of AM activity, a statistically relevant number of different parameter configurations resulted in the PMN recruitment by AM to support in the elimination of the infectious agents. Interestingly, distributions of infection scores in Game II (IS_{II}) generally induced qualitatively comparable distributions for the normalised inflammation ($NI_{II\to III}$).

Linking Game II and Game III by the normalised inflammation $NI_{II\to III}$, we found that, since AM with lower activity induced on average higher infection scores, they gave rise to increased levels of inflammation associated with increased PMN recruitment. In general, low infection-doses were found to be cleared for a wide range of PMN activities as indicated by infection score $IS_{III} < 0.25$ in Fig. 6(e). This implies, in agreement with our earlier observations (see Fig. 5(a)), that the amount of recruited PMN was always sufficient and could even compensate lower PMN activities. The situation is different for the case of high infection-doses, where a minimum-activity of PMN was required to ensure statistically firm clearance of infection (see Fig. 6(f)). Interestingly, we observed an advantageous effect for fungal clearance by PMN for AM with reduced activity in counteracting the fungal pathogens and consequently higher production of inflammatory signals increasing PMN recruitment. As can for example be seen for high PMN activity and high infection-dose, the probability for a persistent infection rose from $p(IS_{III} \geq 0.25) = 0.7\%$ in cases with low AM activity to $p(IS_{III} \geq 0.25) = 2.5\%$ in cases with high AM activity. This stresses once again the pivotal role of AM with regard to PMN recruitment. For low and medium PMN activity, the probability for a persistent infection $p(IS_{III} \geq 0.25)$ was ranging, respectively, from 32% to 86% and from 12% to 43%. For pathogen removal, high PMN activity was required the higher the infection-dose and the lower the AM induced inflammatory signal produced for PMN recruitment.

Discussion

In this study, we applied EGT on graphs to investigate the dynamic counterplay between pathogens and the human immune system in various infection-inflammation scenarios. For illustrative purposes we focused on the concrete example of *A. fumigatus* infection, because even though this human-pathogenic fungus constitutes a common challenge, its potential threat can obviously be permanently managed under physiological immune conditions. Our virtual infection-inflammation model combined the three temporally distinct stages of the innate immune response against this fungal pathogen, *i.e.* the direct and immediate response by the complement system (Game I), followed by the phagocytic activity of AM (Game II) and the subsequent recruitment and immune response by PMN (Game III). Thus, going beyond separate *in silico* experiments of the three stages, we linked the three individual games in a time-ordered fashion. This is achieved by accounting for the quantitative elevation in the host inflammation, depending on the evolution of the various morphotypes that *A. fumigatus* can exhibit in the course of an infection. We performed stochastic computer simulations of various infection-inflammation scenarios scanning the parameter space of the model to identify and predict the relative importance of specific mechanisms in the innate immune response against *A. fumigatus*.

The activity of the complement system and the availability of nutrients determine the evolution of the fungal morphotypes, *i.e.* how the population of fungal cells is composed of resting and swollen conidia. In line with earlier experiments in mice, where a major inflammatory complement component (C5a) was depleted inducing a higher virulence of the pathogen[45], it was observed in the model that conidia did shift from the resting state to the swollen state associated with a higher infection potential. It can be concluded, that in this case the pressure of the complement system became so low that the uptake of nutrients made this state transition beneficial. We also found this effect to be increased in the limit of high infection-doses.

While the complement system is believed not to contribute to direct killing of this fungus, in agreement with previous experimental investigations[29,30,46], our simulations predicted a substantial contribution of the complement system to AM activity in AS via inflammatory signalling. Interestingly, on the one hand, it is well-known that AM comprise the largest population of resident cells in the respiratory tract[47] and that impairment of their function is one of the risk factors for invasive mycoses[43]. On the other hand, based on experiments with mice, Mircescu *et al.* claimed that PMN but not AM play the essential role in the immune response against

A. fumigatus[44]. Our simulations revealed that these seemingly contradictory view points could be reconciled by accounting for the impact of the infection-dose on the time course of the infection-inflammation scenario. In particular, we observed in the *in silico* experiments that AM have a key role in the regulation of the immune response and that this regulatory effect depended on the strength of the infection-dose. As a matter of fact, infections could generally be cleared by AM alone and without considerable PMN recruitment in the limit of low infection-doses corresponding to the typical dose of daily inhalation, where AM were mainly confronted with conidia in the resting and swollen state. In contrast, higher infection-doses were associated with higher inflammation and, consequently, inflammation-dependent PMN recruitment by AM was pronounced, such that PMN but not AM were ultimately playing the essential role in the phagocytosis of the fungal cells. This simulation-derived interpretation is in agreement with the fact that the study by Mircescu *et al.* was indeed performed with infection-doses that were orders of magnitude above the dosis of daily inhalation[44].

The regulatory function of AM was of paramount importance in the simulations, due to the quantitative and qualitative limitations of AM to phagocytose and kill *A. fumigatus* in the hyphal state[39]. However, apart from AM activities directed against the pathogen itself, these immune cells do also play an important role in shutting down inflammation and in initiating tissue recovery at sites of damage in later stages[48–50]. PMN are essential and highly skilled phagocytes that are equipped with various antifungal capabilities that can be fungicidal and/or fungistatic[30,34,39]. Our simulation results confirmed the importance of PMN, however, their recruitment and defensive function were most important in the limit of high infection-doses. Interestingly, impairment of PMN function in the scenarios with low infection-doses was compensated by an increased recruitment of these cells, however, this could consequently imply an increase in self-damage of tissue, *e.g.* by neutrophilic respiratory burst, which constitutes a threat for the host itself[51]. Nevertheless, PMN recruitment was found to play an important factor across all possible infection-doses, because lack of PMN function was associated with increased probabilities for pathogen persistence, as could be expected from findings in previous experimental studies[52]. Even though beyond the scope of the current modelling approach, it is very well conceivable that PMN recruitment by AM-induced inflammation occurs more quickly in the limit of high infection-doses.

Systems biology relies on the cross-fertilisation between theory and experiment. While uncertain or even unknown biological parameters can only be determined in wet-lab experiments, theoretical approaches can direct this exploration by generating concrete hypotheses. Obviously, parameters in the payoff matrices of EGT relate to the abstract concept of reproductive fitness in terms of nutrient uptake and immune response and, therefore, may be difficult and/or impossible to be separately measured in experiment. However, our study suggests that quantitative insights about the metabolic activities of different *A. fumigatus* morphotypes would narrow down the range of relevant nutrient contributions in the model and by that render scanning of several parameters obsolete. In turn, the model could be refined, extended and reviewed to focus investigations on particular aspects in the reduced parameter space with higher attention to details. Furthermore, guided by the outcome of our simulations, we suggest experimental investigations that may clarify the dependence between the infection-dose and the inflammatory signalling, *e.g.* by determining the cytokine profile secreted from AM and/or PMN. Similarly, *A. fumigatus* infection in mice with fully and/or partly impaired AM and/or PMN populations could as well be systematically investigated as a function of the infection-dose to specify the model dynamics of infection-inflammation scenarios. These investigations could be performed using different microscopy techniques: light-sheet microscopy could reveal cellular distributions, i.e. of conidia, AM and PMN, in the lung, whereas multi-photon microscopy could even allow monitoring dynamical aspects of cells in the lung. Furthermore, processes like phagocytosis of fungal cells by AM and PMN as well as recruitment of PMN could be quantified using fluorescence-activated cell sorting (FACS) at different time points and as a function of the infection-dose. Spatial-temporal insights from imaging experiments will support realistic mathematical modeling within the image-based systems biology approach[11].

The current version of the virtual infection-inflammation model captures the most relevant aspects of the innate immune response against *A. fumigatus*, but could be extended by other mechanisms, even including aspects of adaptive immunity, to more comprehensively resemble the full complexity of the infection process. For example, the first cells getting into physical contact with inhaled conidia are AEC of type I and type II, where type II cells were reported to internalise conidia and to generate inflammatory signals[38]. In this study, we intentionally omitted responses by AEC due to considerable gaps in our knowledge about type I AEC[53] that, in fact, make up the alveolar surface almost entirely[54]. Dendritic cells were also shown to contribute to fungal clearance[55] and a dysregulation in Th1/Th2 responses lead to invasive pulmonary aspergillosis despite a non-neutropenic status of the host[56], thus, revealing substantial evidence for the importance of adaptive immune responses in *A. fumigatus* infection. In future work, extensions of the virtual model might include responses mediated by adaptive immunity to study the relative contributions from innate and adaptive immune effectors and functions. This could be realised by a network of evolutionary games, where the immune response of the host is adapting regarding the activity against pathogenic attacks. The charming aspects of EGT lie, on the one hand, in the elegant reduction of model parameters to the ratios of parameters and, on the other hand, in the inherent extensibility that allows to realistically capture the characteristic features of complex host-pathogen interactions.

Methods

Modelling the dynamics of host-pathogen interactions by EGT on graphs. The game-theoretical description of the infection-inflammation scenario considered in this study is constructed as a consecutive sequence of three evolutionary games (see Fig. 1(b)). These games comprise the time course of the innate immune response and are played on graphs in order to perform *in silico* experiments of *A. fumigatus* infection using a pseudo-spatial representation of AS. Here, each fungal cell represents an infectious individual that interacts with other proximal fungal cells under the elevating inflammatory response of the host. In what follows, we present

a detailed description of the interaction graph construction, the distribution of different cell types in an AS, the design of the sequentially organised games and the evolutionary dynamics algorithm.

Environmental setting: alveolar sacs. Evolutionary dynamics take place in a typical AS. AS are organisational structures in the lower respiratory tract of the lung and are composed of 21 alveoli on average[33,57]. Alveoli in an AS are inter-connected via alveolar entrance rings and pores of Kohn[53,58], whereas different AS are considered as fairly independent units. In order to reflect connectivity properties between alveoli in a cylindrically shaped AS, we represent them by densely packed spheres as shown in Fig. 1(a). A relationship between any two neighbouring alveoli is assumed if their spheres touch each other.

Distribution of cells in alveolar sacs. Each alveolus represents a virtual site in which typical numbers of fungal and immune cells are placed. The number of fungal cells present in one AS emerges from a dose-dependent distribution over all AS upon inhalation or upon administration. The fungal dosis ranges from $n_{dose} = 6.3 \cdot 10^3$ conidia (daily inhalation for humans) to $n_{dose} = 10^7$ conidia (administration in experiments with mice). First, the number of fungal cells per AS, n_{fc}, is drawn from the Binomial distribution:

$$B_{fc/AS}(n_{dose}, p, n_{fc}) = \binom{n_{dose}}{n_{fc}} p^{n_{fc}} (1 - p)^{n_{dose} - n_{fc}}, \tag{1}$$

where $p = 1/n_{AS}$ denotes the probability to choose the AS under consideration and the total number of AS is about $n_{AS} = 2.3 \cdot 10^7$ in humans[33,57]. Second, the number of fungal cells per AS, n_{fc}, is uniformly distributed over the alveoli of the AS. Similarly, the number of resident AM (n_{AM}) and recruited PMN (n_{PMN}) follow the same distribution process over AS. In this case, n_{dose} in Eq. 1 is replaced by the total number of $2.1 \cdot 10^9$ macrophages in humans, whereas for PMN this number can be up to eight times higher depending on the strength of PMN recruitment[40].

Construction of the interaction graph. The interaction graph is based on the spatial proximity between *A. fumigatus* conidia in the AS. Interactions between the fungal cells of an AS are generated in a rule-based fashion: Two fungal cells interact,

1. If they are located in the same alveolus or
2. If they are randomly selected from two neighbouring alveoli and do not yet have another inter-alveolar interaction.

These rules give rise to a proximity-based interaction graph between all fungal cells in the same alveolus or fungal cells that are nearby in neighbouring alveoli, *e.g.* reflecting intra-alveolar localisation close to one of the pores of Kohn or the alveolar entrance ring. An example for a fungal interaction graph is shown in Fig. 1(a).

Sequential design of host-pathogen games. Fungal cells are viewed as infectious agents that play against each other for survival under the inflammatory pressure of the immune system. The different morphotypes that conidia of *A. fumigatus* can develop with time correspond to the strategies that the fungal cells may adopt in each game and are summarised in Table S1. We consider three different stages of innate immunity that are reflected by three distinct evolutionary games and that are played on the interaction graph of fungal individuals as depicted in Fig. 1(b).

In each of the three games, beneficial effects like the consumption of nutrients as well as the pressure of the immune system are aggregated in an utility function per individual, which contains quantitative information about the reproductive fitness of the fungal cell. This utility function has the general structure

$$U_i = (\text{nutrients})_i + (\text{immune response})_i, \tag{2}$$

where i denotes the i-th fungal individual. Nutrients generally increase the reproductive fitness and their contributions enter the expression with a positive sign, in contrast to payoffs associated with the immune response that have values below zero. The amount of nutrient uptake by fungal individuals depends on the strategy adopted by the cell, where E_D, E_R, E_S and E_H denote the nutrient contributions for fungal cells in the state "dead", "resting", "swollen" and "hyphal", respectively. Since the reproductive fitness of hyphae is higher than for swollen conidia and swollen conidia outperform resting conidia, we set the relation between the nutrient contributions to $E_D < E_R \leq E_S \leq E_H$ with $E_D = 0$ for dead cells. Reduction of reproductive fitness induced by immune responses either acts on single fungal individuals or on pairs of individuals that are interacting with each other in a game-specific context.

Game I–Complement system. The proteins of the complement system are always present in the alveolar lining layer (surfactant) and immediately surround each fungal cell starting from its entry into the AS. Opsonisation of conidia induces inflammation and phagocyte attraction to the site of infection. This is the predominant immune response in the first minutes. At this stage, conidia of *A. fumigatus* may either stay in the "resting" state or initiate radial growth and switch to the "swollen" state. This game is restricted to these two states, because, during the first hour after entry into the lower respiratory tract, conidia do not germinate. Opsonisation and chemoattraction are represented by morphotype-specific negative payoffs as a function of the complement responses c_R and c_S that are associated with resting and swollen conidia, respectively. These effects are taken into account for each fungal individual irrespective of alveolar localisation and interaction partners. Both, resting and swollen conidia, can not evade opsonisation by the complement, but swollen conidia do activate the complement system more intensively, implying that $c_S \geq c_R$[36]. In addition, proximal fungal individuals interfere with each other due

$P_1^G(s_1, s_2)$		s_2			
		R	**S**	**H**	**D**
Game I					
s_1	R	$-c_R/2$	$-c_S/2$	–	–
	S	$-c_R/2$	$-c_S/2$	–	–
	H	–	–	–	–
	D	–	–	–	–
Game II					
s_1	R	$-1/2 \times m_R$	$-\frac{m_R}{m_R+m_S} \times m_R$	$-\frac{m_R}{m_R+m_H} \times m_R$	$-m_R$
	S	$-\frac{m_S}{m_S+m_R} \times m_S$	$-1/2 \times m_S$	$-\frac{m_S}{m_S+m_H} \times m_S$	$-m_S$
	H	$-\frac{m_H}{m_H+m_R} \times m_H$	$-\frac{m_H}{m_H+m_S} \times m_H$	$-1/2 \times m_H$	$-m_H$
	D	0	0	0	0
Game III					
s_1	R	$-1/2 \times g_R$	$-\frac{g_R}{g_R+g_S} \times g_R$	$-\frac{g_R}{g_R+g_H} \times g_R$	$-g_R$
	S	$-\frac{g_S}{g_S+g_R} \times g_S$	$-1/2 \times g_S$	$-\frac{g_S}{g_S+g_H} \times g_S$	$-g_S$
	H	$-\frac{g_H}{g_H+g_R} \times g_H$	$-\frac{g_H}{g_H+g_S} \times g_H$	$-1/2 \times g_H$	$-g_H$
	D	0	0	0	0

Table 1. Payoff matrices for Game I, II and III. Payoffs $P_1^I(s_1, s_2)$, $P_1^{II}(s_1, s_2)$ and $P_1^{III}(s_1, s_2)$ of Game I, Game II and Game III are shown for fungus 1 interacting with fungus 2. R, S, H and D denote resting, swollen, hyphal and dead fungal cells, respectively. The complement response for resting and swollen fungal cells in the Game I are represented by c_R and c_S, respectively. m_H, m_R, m_S and g_R, g_S, g_H are the responses by AM or PMN on encounter of resting condia, swollen conidia or hyphae. The complement responses satisfy the condition $c_R \leq c_S$ as well as the AM responses $m_H \leq m_R \leq m_S$ and the PMN responses $g_R \leq g_S \leq g_H$, which determine the payoffs.

to superimposed inflammatory and chemoattracting complement signals and by that induce further negative payoffs P^I that depend on the number of interaction partners.

The utility function of fungal cell i in this game is described as

$$U_i^I = E_{s_i} - c_{s_i} + \sum_{j \in \mathcal{N}_i} P_i^I(s_i, s_j), \tag{3}$$

where $s_i \in \{R, S\}$ is the morphotypic strategy of fungal individual i, c_{s_i} is the complement response associated with strategy s_i, $\mathcal{N}_i$ are the interaction partners of fungal cell i and $P_i^I(s_i, s_j)$ the payoffs as defined by the payoff matrix for Game I in Table 1. The utility function indicates that the more interaction partners a fungal individual has, the more it will be under pressure by complement activity.

Game II–Alveolar macrophages. The second game refers to the time scale of a few hours after entrance of conidia in the AS, which is the phase where germination of conidia becomes possible. In this phase, *A. fumigatus* conidia get into contact with professional phagocytes, *i.e.* AM being resident in alveoli. They are able to phagocytose conidia and have the potential to kill swollen conidia, while they fail to phagocyte fungal cells that filamented and have hyphae. The AM activity α_{AM} measures the ability to phagocytose and kill the fungal cells. At this stage of the immune response, conidia are enabled to adopt the four strategies "resting", "swollen", "hyphal" and "dead", where the latter strategy is preferred in the case of a strong immune response that is not compensated by a nutrient contribution ($E_D = 0$). The number of AM present in an alveolus is drawn from a Binomial distribution, as was done previously in our agent-based virtual *A. fumigatus* infection models[16,17] and as described before.

In this game, pairs of fungal cells are interacting under the pressure of the immune response mediated by AM. Each fungal cell of a pair aims to adopt a strategy that improves its reproductive fitness, at the risk of increasing the pressure by the immune system for both fungal cells. Fungal cells with no interaction partner receive the full immune exertion by AM, as if they would interact with a dead fungal cell. Thus, in the simulation algorithm a solitary fungal cell was virtually connected with a fungal cell in the state "dead".

AM respond with morphotype-specific activities, including phagocytosis, killing, inflammation and recruitment, which are summarised in the immune responses m_R, m_S, m_H against resting, swollen and hyphal fungal cells, respectively. Dead fungal cells receive a zero payoff from immune activities by AM (AM response $m_D = 0$). The response of AM against swollen conidia m_S is set to be strongest, followed by resting conidia m_R and the hyphal morphotype m_H, *i.e.*, the relation between the AM responses is given by $m_D < m_H \leq m_R \leq m_S$, which is in line with experimental observations[39].

The utility function of fungal cell i is defined as follows:

$$U_i^{\mathrm{II}} = E_{s_i} + \sum_{j \in \mathcal{R}_i^{\mathrm{AM}}} P_i^{\mathrm{II}}(s_i, s_j), \tag{4}$$

where $\mathcal{R}_i^{\mathrm{AM}} \subset \mathcal{N}_i$ denotes the set of interactors for which the fungal pair (i, j) with $j \in \mathcal{R}_i^{\mathrm{AM}}$ is randomly selected for AM–*A. fumigatus* interaction. The payoffs related to the AM immune response, $P_i^{\mathrm{II}}(s_i, s_j)$, are defined in the payoff matrix shown in Table 1.

Game III–Polymorphonuclear neutrophils. AM have important immune regulatory functions for the recruitment of cells from the bloodstream. For example, once recruited to the site of infection, PMN have an armory of weapons to attack pathogens. They can kill the fungus intracellularly after successful phagocytosis or extracellularly by the secretion of reactive oxygen species. Furthermore, they can undergo NETosis by committing an altruistic suicide in which they release their DNA and by that trap the fungus to prevent it from further spreading. After the recruitment of PMN to lung alveoli, these phagocytes govern the immune response and their overall activity is measured by the parameter α_{PMN}.

We introduce the parameter ρ_{PMN} to control the relative number of recruited PMN to the site of infection, where we impose – in agreement with observations in wet-lab experiments[40] – an upper PMN recruitment limit of eight times the number of present AM. As in Game II, pairs of conidia interact with PMN in a randomised fashion and can adopt the four strategies "resting", "swollen", "hyphal" and "dead" in this game. However, in contrast to Game II, the various defence mechanisms of PMN give rise to different relations in their specific responses. The relations between the PMN responses g_{R}, g_{S} and g_{H} against fungal cells in the resting, swollen and hyphal state are given by $g_{\mathrm{R}} \leq g_{\mathrm{S}} \leq g_{\mathrm{H}}$[29]. The utility function of fungal cell i in Game III is given by

$$U_i^{\mathrm{III}} = E_{s_i} + \sum_{j \in \mathcal{R}_i^{\mathrm{PMN}}} P_i^{\mathrm{III}}(s_i, s_j), \tag{5}$$

where $j \in \mathcal{R}_i^{\mathrm{PMN}}$ defines the interaction pairs (i, j), which randomly interact with a PMN. $P_i^{\mathrm{III}}(s_i, s_j)$ is the payoff imposed by interaction with a PMN as defined in Table 1.

The three games are linked in sequential order – Game I → Game II → Game III – to investigate the counterplay of *A. fumigatus* infection and host inflammation. Game linking is associated with the inflammatory signalling in response to the infectious agent, initiating the next higher instance along the cascade of the innate immune response. To this end, we introduce measures that enable quantifying the degree of infection and inflammation.

Quantification of infection and inflammation for game linking. To quantify the degree of infection induced by the human-pathogenic fungus *A. fumigatus* we define the infection score (IS) that is computed after execution of game G:

$$\mathrm{IS}_G = n_{\mathrm{fc}}\left(\frac{f_{\mathrm{R}} + 2f_{\mathrm{S}} + 4f_{\mathrm{H}}}{4}\right). \tag{6}$$

Here n_{fc} denotes the number of fungal cells in the AS and $f_{\mathrm{R}}, f_{\mathrm{S}}, f_{\mathrm{H}}$ and f_{D} with $f_{\mathrm{R}} + f_{\mathrm{S}} + f_{\mathrm{H}} + f_{\mathrm{D}} = 1$ refer to the fractions of fungal cells in the resting, swollen, hyphal and dead state, respectively. By construction, the infection score assumes increasing values $\mathrm{IS}_G = n_{\mathrm{fc}}/4$, $\mathrm{IS}_G = n_{\mathrm{fc}}/2$ and $\mathrm{IS}_G = n_{\mathrm{fc}}$ for populations consisting of increasingly challenging morphotypes $f_{\mathrm{R}} = 1$, $f_{\mathrm{S}} = 1$ and $f_{\mathrm{H}} = 1$, respectively. Furthermore, particular infection scores IS_G correspond to specific numbers of persisting fungal cells, irrespective of the infection-dose. For example, $\mathrm{IS}_G = 0.5$ either corresponds to one fungal cell in the swollen state or to two conidia in the resting state, whereas $\mathrm{IS}_G = 0.25$ represents one remaining fungal cell that is in the resting state. This threshold, $\mathrm{IS}_G = 0.25$, is set in the further analysis to distinguish between persistent ($\mathrm{IS}_G \geq 0.25$) and cleared ($\mathrm{IS}_G < 0.25$) infections.

Game linking is associated with the inflammatory signalling in response to the infectious agent. In particular, we link the complement system (Game I) with AM response (Game II) by the normalised inflammation (NI) measure that is defined as

$$\mathrm{NI}_{\mathrm{I}\to\mathrm{II}} = f_{\mathrm{S}} + \frac{c_{\mathrm{R}}}{c_{\mathrm{S}}} f_{\mathrm{R}} \in \left[\frac{c_{\mathrm{R}}}{c_{\mathrm{S}}}, 1\right]. \tag{7}$$

Based on literature data[36], this measure accounts for the relative difference in the complement response against the fractions of resting (f_{R}) and swollen (f_{S}) conidia. Furthermore, $\mathrm{NI}_{\mathrm{I}\to\mathrm{II}}$ accounts for relative differences in the complement response against resting and swollen conidia by the scaling factor $c_{\mathrm{R}}/c_{\mathrm{S}}$. The normalised infection value $\mathrm{NI}_{\mathrm{I}\to\mathrm{II}}$ regulates the response of AM in Game II by scaling the AM activity α_{AM}: $\widetilde{\alpha}_{\mathrm{AM}} = \mathrm{NI}_{\mathrm{I}\to\mathrm{II}} \times \alpha_{\mathrm{AM}}$. Similarly, we link Game II to Game III by modelling PMN recruitment to depend on AM-secretion of the PMN-chemoattractant MIP-1. The secretion of MIP-1 is known to depend on the different *A. fumigatus* morphotypes[40]. Thus, we consider the relative recruitment number $\rho_{\mathrm{PMN}} = \mathrm{NI}_{\mathrm{II}\to\mathrm{III}}$, with the normalised inflammation:

$$\mathrm{NI}_{\mathrm{II}\to\mathrm{III}} = f_{\mathrm{H}} + \frac{11}{18} f_{\mathrm{S}} + \frac{1}{6} f_{\mathrm{R}} \in [0, 1], \tag{8}$$

where the coefficients conserve the relative responses of AM to MIP-1 for the different *A. fumigatus* morphotypes, as deduced from Ref. 40. Note that, in case the *A. fumigatus* infection can be cleared by AM, *i.e.* all fungal cells are dead $f_{\mathrm{D}} = 1$ and $f_{\mathrm{R}} = f_{\mathrm{S}} = f_{\mathrm{H}} = 0$ after Game II was played, no PMN-chemoattractant would be secreted and no PMN would be recruited.

Evolutionary dynamics. In each game, iterations over repetitive evolutionary steps t_{evo} are performed as depicted in Fig. S1. To ensure equilibration of the evolutionary dynamics, we set the number of iterations to 10^4. In each iteration step fungal cells receive nutrients and are confronted with the respective immune response. Each individual fungal cell evaluates its utility function in every time step t_{evo} containing the information on its reproductive fitness. Mutation and adaptation are evolutionary mechanisms performed in response to differences in the utility functions of individuals in the following way.

Mutation. Random change between strategies with probability $p = 0.01$.

Adaptation. Probabilistic change of an individual's current strategy s_i into a strategy s' applied by at least one fungal individual in the neighbourhood with higher reproductive fitness. Proportional imitation is applied as microscopic update rule and a distinction is drawn between the strategy "dead" (s_{dead}) and strategies related to individuals that are alive:

Case $s' \neq s_{dead}$: if strategy s' is played in the neighbourhood $\mathcal{N}_i$ of individual i, it adopts strategy s' with probability:

$$p(s_i \to s') = \frac{1}{\lambda |\mathcal{N}_i \cap \mathcal{I}(s')|} \sum_{j \in \mathcal{N}_i \cap \mathcal{I}(s')} \max(U_j^G - U_i^G, 0) \tag{9}$$

where $\mathcal{I}(s')$ is the set of all individuals playing strategy s' and λ a normalisation factor to ensure $p(s_i \to s') \in [0, 1]$.

Case $s' = s_{dead}$:

$$p(s_i \to s_{dead}) = \frac{1}{\lambda} \max(-U_i^G, 0). \tag{10}$$

Statistical measures. In order to distinguish parameters of the games by their relevance for the outcome of the infection-inflammation scenarios, we compute the mutual information (MI) as follows:

$$\mathrm{MI}(X, Y) = \sum_{x \in X} \sum_{y \in Y} p(x, y) \log_2 \left(\frac{p(x, y)}{p(x) p(y)} \right). \tag{11}$$

Here, X is the set of values related to one unknown parameter and Y the corresponding set of infection scores IS_G of game G. Furthermore, $p(x, y)$ denotes the joint probability function, $p(x)$ and $p(y)$ are marginal probability distributions of X and Y, respectively[59]. Since IS_G is a continuous measure, Y is discretised using different bin sizes for the calculation of MI(X, Y). We checked that the dependence of the mutual information MI(X, Y) on the binning of the infection score IS_G does not affect the ranking of the most important parameters. These are the AM activity α_{AM} in Game II (see Table S2 and Fig. S2 (a)) and both PMN activity α_{PMN} and PMN recruitment ρ_{PMN} in Game III (see Table S2 and Fig. S2 (b)).

Implementation and Simulation. All parameters used in the evolutionary games are scanned in reasonable ranges to capture their influence on the outcome of each game and the ultimate outcome of the infection. The evolutionary game-theoretical algorithm is implemented in the object-oriented programming language `C++` and simulations are performed by the simulation algorithm depicted in Fig. S1. Statistical analyses are carried out using `R`. To reduce effective runtime, the algorithm is parallelised and is executed on a SUSE Linux Enterprise Server version 11 based on a x86-64 architecture with 512 GB RAM and 48 AMD Opteron processors, each running on 1781 MHz.

Virtual infection-inflammation scenarios were performed for different fungal doses and varied parameter configurations. To account for the stochastic nature of the *in silico* experiments, 100 repetitions were executed and from each simulation long-term density distributions of resting and swollen conidial fractions with their related averages and standard deviations were extracted.

References

1. Murphy, K. P., Janeway, C., Travers, P. & Walport, M. *Janeway's Immunobiology* (Garland Science, New York and London, 2008), 7 edn.
2. McLennan, I. C. M. Germinal centers. *Annual Review of Immunology* **12,** 117–139 (1994).
3. Zipfel, P. F. & Skerka, C. Complement regulators and inhibitory proteins. *Nature Reviews Immunology* **9,** 729–40 (2009).
4. Angus, D. C. & van der Poll, T. Severe sepsis and septic shock. *New England Journal of Medicine* **369,** 840–51 (2013).
5. Chi, H. *et al.* Dynamic regulation of pro- and anti-inflammatory cytokines by MAPK phosphatase 1 (MKP-1) in innate immune responses. *Proceedings of the National Academy of Sciences of the United States of America* **103,** 2274–2279 (2006).
6. Clermont, G. *et al. In silico* design of clinical trials: a method coming of age. *Critical Care Medicine* **32,** 2061–2070 (2004).
7. Kumar, R., Clermont, G., Vodovotz, Y. & Chow, C. C. The dynamics of acute inflammation. *Journal of Theoretical Biology* **230,** 145–55 (2004).
8. Day, J. *et al.* A reduced mathematical model of the acute inflammatory response II. Capturing scenarios of repeated endotoxin administration. *Journal of Theoretical Biology* **242,** 237–56 (2006).
9. Kumar, R., Chow, C. C., Bartels, J. D., Clermont, G. & Vodovotz, Y. A mathematical simulation of the inflammatory response to anthrax infection. *Shock (Augusta, Ga.)* **29,** 104–11 (2008).
10. Tanaka, R. J. *et al. In silico* modelling of spore inhalation reveals fungal persistence following low dose exposure. *Scientific Reports* **I,** 13958 (2015).
11. Medyukhina, A., Timme, S., Mokhtari, Z. & Figge, M. T. Image-based systems biology of infection. *Cytometry Part A* **87,** 462–70 (2015).

12. An, G. *In silico* experiments of existing and hypothetical cytokine-directed clinical trials using agent-based modeling. *Critical Care Medicine* **32,** 2050–60 (2004).
13. Hünniger, K., Lehnert, T., Bieber, K., Martin, R., Figge, M. T. & Kurzai, O. A Virtual Infection Model Quantifies Innate Effector Mechanisms and *Candida albicans* Immune Escape in Human Blood. *PLOS Computational Biology* **10,** e1003479 (2014).
14. Lehnert, T. *et al.* Bottom-up modeling approach for the quantitative estimation of parameters in pathogen-host interactions. *Frontiers in Microbiology* **6,** 1–15 (2015).
15. Tokarski, C. *et al.* Agent-Based Modeling Approach of Immune Defense Against Spores of Opportunistic Human Pathogenic Fungi. *Frontiers in Microbiology* **3,** 129 (2012).
16. Pollmächer, J. & Figge, M. T. Agent-based model of human alveoli predicts chemotactic signaling by epithelial cells during early *Aspergillus fumigatus* infection. *PLOS ONE* **9,** e111630 (2014).
17. Pollmächer, J. & Figge, M. T. Deciphering chemokine properties by a hybrid agent-based model of *Aspergillus fumigatus* infection in human alveoli. *Frontiers in Microbiology* **6,** 503 (2015).
18. von Neumann, J. & Morgenstern, O. *Theory of Games and Economic Behavior* (Princeton University Press, Princeton, 1944), 2nd edn.
19. Szabó, G. & Fáth, G. Evolutionary games on graphs. *Physics Reports* **446,** 97–216 (2007).
20. Hummert, S. *et al.* Evolutionary game theory: cells as players. *Molecular BioSystems* **10,** 3044–3065 (2014).
21. Nowak, M. A. *Evolutionary Dynamics* (Harvard University Press, 2006).
22. Epstein, J. M. Prisoner's dilemma and public goods games in different geometries: Compulsory versus voluntary interactions. *Complexity* **8,** 31–38 (2003).
23. Renaud, F. & de Meeüs, T. A simple model of host-parasite evolutionary relationships. Parasitism: compromise or conflict? *Journal of theoretical biology* **152,** 319–27 (1991).
24. Hummert, S., Hummert, C., Schröter, A., Hube, B. & Schuster, S. Game theoretical modelling of survival strategies of *Candida albicans* inside macrophages. *Journal of Theoretical Biology* **264,** 312–8 (2010).
25. Tyc, K. M., Kühn, C., Wilson, D. & Klipp, E. Assessing the advantage of morphological changes in *Candida albicans*: A game theoretical study. *Frontiers in Microbiology* **5,** 1–11 (2014).
26. Bohl, K. *et al.* Evolutionary game theory: molecules as players. *Molecular BioSystems* **10,** 3066–74 (2014).
27. Latgé, J.-P. *Aspergillus fumigatus* and Aspergillosis. *Clinical Microbiology Reviews* **12,** 310–350 (1999).
28. Codina, R., Fox, R. W., Lockey, R. F., DeMarco, P. & Bagg, A. Typical levels of airborne fungal spores in houses without obvious moisture problems during a rainy season in Florida, USA. *Journal of Investigational Allergology and Clinical Immunology* **18,** 156–162 (2008).
29. Brakhage, A. A., Bruns, S., Thywissen, A., Zipfel, P. F. & Behnsen, J. Interaction of phagocytes with filamentous fungi. *Current Opinion in Microbiology* **13,** 409–415 (2010).
30. Heinekamp, T. *et al.* Interference of *Aspergillus fumigatus* with the immune response. *Seminars in immunopathology* **37,** 141–52 (2015).
31. Aimanianda, V. *et al.* Surface hydrophobin prevents immune recognition of airborne fungal spores. *Nature* **460,** 1117–1121 (2009).
32. Brakhage, A. A. & Langfelder, K. Menacing Mold: The Molecular Biology of *Aspergillus fumigatus*. *Annual Review of Microbiology* **56,** 433–455 (2002).
33. Weibel, E. R. *Morphometry of the Human Lung* (Springer Berlin Heidelberg, 1963).
34. Hasenberg, M., Stegemann-Koniszewski, S. & Gunzer, M. Cellular immune reactions in the lung. *Immunological Reviews* **251,** 189–214 (2013).
35. Alonso, C., Waring, A. & Zasadzinski, J. A. Keeping lung surfactant where it belongs: protein regulation of two-dimensional viscosity. *Biophysical Journal* **89,** 266–73 (2005).
36. Kozel, T. R., Wilson, M. A., Farrell, T. P. & Levitz, S. M. Activation of C3 and binding to *Aspergillus fumigatus* conidia and hyphae. *Infection and Immunity* **57,** 3412–7 (1989).
37. Levitz, S. M. Overview of host defenses in fungal infections. *Clinical Infectious Diseases* **14,** S37–S42 (1992).
38. Osherov, N. Interaction of the pathogenic mold *Aspergillus fumigatus* with lung epithelial cells. *Frontiers in Microbiology* **3,** 1–9 (2012).
39. Margalit, A. & Kavanagh, K. The innate immune response to *Aspergillus fumigatus* at the alveolar surface. *FEMS Microbiology Reviews* **11,** 1–18 (2015).
40. Steele, C. *et al.* The Beta-Glucan Receptor Dectin-1 Recognizes Specific Morphologies of *Aspergillus fumigatus*. *PLOS Pathogens* **1,** e42 (2005).
41. Bruns, S. *et al.* Production of extracellular traps against *Aspergillus fumigatus in vitro* and in infected lung tissue is dependent on invading neutrophils and influenced by hydrophobin RodA. *PLOS Pathogens* **6,** e1000873 (2010).
42. Hillmann, F. *et al.* Virulence determinants of the human pathogenic fungus *Aspergillus fumigatus* protect against soil amoeba predation. *Environmental Microbiology* **17,** 2858–2869 (2015).
43. Roilides, E., Katsifa, H. & Walsh, T. J. Pulmonary host defences against *Aspergillus fumigatus*. *Research in Immunology* **149,** 454–65; discussion 523–4 (1998).
44. Mircescu, M. M., Lipuma, L., van Rooijen, N., Pamer, E. G. & Hohl, T. M. Essential Role for Neutrophils but not Alveolar Macrophages at Early Time Points following *Aspergillus fumigatus* Infection. *The Journal of Infectious Diseases* **200,** 647–656 (2009).
45. Hector, R. F., Yee, E. & Collins, S. Use of DBA/2N Mice in Models of Systemic Candidiasis and Pulmonary and Systemic Aspergillosis. *Infection and Immunity* **58,** 1476–1478 (1990).
46. Speth, C., Rambach, G., Lass-Flörl, C., Dierich, M. P. & Würzner, R. The role of complement in invasive fungal infections. *Mycoses* **47,** 93–103 (2004).
47. Philippe, B. *et al.* Killing of *Aspergillus fumigatus* by alveolar macrophages is mediated by reactive oxidant intermediates. *Infection and Immunity* **71,** 3034–3042 (2003).
48. Lambrecht, B. N. Alveolar Macrophage in the Driver's Seat. *Immunity* **24,** 366–368 (2006).
49. Segal, B. H. Role of macrophages in host defense against aspergillosis and strategies for immune augmentation. *The Oncologist* **12,** 7–13 (2007).
50. Bowden, D. H. The alveolar macrophage. *Environmental Health Perspectives* **55,** 327–341 (1984).
51. Butterfield, T. A., Best, T. M. & Merrick, M. A. The Dual Roles of Neutrophils and Macrophages in Inflammation: A Damage and Repair. *Journal of Athletic Training* **41,** 457–465 (2006).
52. Meier, A. *et al.* Toll-like receptor (TLR) 2 and TLR4 are essential for *Aspergillus*-induced activation of murine macrophages. *Cellular Microbiology* **5,** 561–570 (2003).
53. Herzog, E. L., Brody, A. R., Colby, T. V., Mason, R. & Williams, M. C. Knowns and unknowns of the alveolus. *Proceedings of the American Thoracic Society* **5,** 778–782 (2008).
54. McCormick, A., Loeffler, J. & Ebel, F. *Aspergillus fumigatus*: Contours of an opportunistic human pathogen. *Cellular Microbiology* **12,** 1535–1543 (2010).
55. Bozza, S. *et al.* Dendritic cells transport conidia and hyphae of *Aspergillus fumigatus* from the airways to the draining lymph nodes and initiate disparate Th responses to the fungus. *Journal of Immunology (Baltimore, Md.: 1950)* **168,** 1362–1371 (2002).
56. Roilides, E., Sein, T., Roden, M., Schaufele, R. L. & Walsh, T. J. Elevated serum concentrations of interleukin-10 in nonneutropenic patients with invasive aspergillosis. *The Journal of Infectious Diseases* **183,** 518–20 (2001).

57. Parker, H., Horsfield, K. & Cumming, G. Morphology of distal airways in the human lung. *Journal of Applied Physiology (Bethesda, Md.: 1985)* **31,** 386–391 (1971).
58. Bastacky, J. & Goerke, J. Pores of Kohn are filled in normal lungs: low-temperature scanning electron microscopy. *Journal of Applied Physiology (Bethesda, Md.: 1985)* **73,** 88–95 (1992).
59. MacKay, D. J. C. *Information theory, inference, and learning algorithms* vol. 7 (Cambridge University Press, Cambridge, 2003), 4th edn.

Acknowledgements
We thank Carl-Magnus Svensson for valuable discussions regarding the statistical evaluation of the results. This work was financially supported by the excellence graduate school Jena School for Microbial Communication (JSMC) and the CRC/TR124 FungiNet (Projects A1, B1, B4 and C6) that are both funded by the Deutsche Forschungsgemeinschaft (DFG).

Author Contributions
J.P., P.F.Z. and M.T.F. conceived and designed the study. M.T.F. contributed materials and computational resources. J.P. processed the data, implemented and applied the computational algorithm. J.P., S.T., S.S., A.A.B., P.F.Z. and M.T.F. evaluated and analysed the results. J.P., S.T., S.S., A.A.B., P.F.Z. and M.T.F. wrote the manuscript and revised it critically.

Additional Information
Supplementary information accompanies this paper at http://www.nature.com/srep

Competing financial interests: The authors declare no competing financial interests.

How to cite this article: Pollmächer, J. *et al.* Deciphering the Counterplay of *Aspergillus fumigatus* Infection and Host Inflammation by Evolutionary Games on Graphs. *Sci. Rep.* **6**, 27807; doi: 10.1038/srep27807 (2016).

This work is licensed under a Creative Commons Attribution 4.0 International License. The images or other third party material in this article are included in the article's Creative Commons license, unless indicated otherwise in the credit line; if the material is not included under the Creative Commons license, users will need to obtain permission from the license holder to reproduce the material. To view a copy of this license, visit http://creativecommons.org/licenses/by/4.0/

Supplementary Information

Deciphering the Counterplay of *Aspergillus fumigatus* Infection and Host Inflammation by Evolutionary Games on Graphs

Johannes Pollmächer[1,2], Sandra Timme[1,2], Stefan Schuster[3], Axel A. Brakhage[2,4], Peter F. Zipfel[2,5], and Marc Thilo Figge[1,2,*]

[1]Research Group Applied Systems Biology, Leibniz Institute for Natural Product Research and Infection Biology – Hans Knöll Institute, Jena, Germany
[2]Faculty of Biology and Pharmacy, Friedrich Schiller University Jena, Germany
[3]Department of Bioinformatics, Faculty of Biology and Pharmacy, Friedrich Schiller University Jena, Germany
[4]Department of Molecular and Applied Microbiology, Leibniz Institute for Natural Product Research and Infection Biology – Hans Knöll Institute, Jena, Germany
[5]Department of Infection Biology, Leibniz Institute for Natural Product Research and Infection Biology – Hans Knöll Institute, Jena, Germany
[*]E-mail: thilo.figge@leibniz-hki.de

Table S1: Game-dependent morphotype options of *A. fumigatus*.

permitted morphotype (yes/no)	*A. fumigatus* strategy/morphotype resting (R)	swollen (S)	hyphal (H)	dead (D)
Game I: complement system	yes	yes	no	no
Game II: AM	yes	yes	yes	yes
Game III: PMN	yes	yes	yes	yes

Possible strategies for fungal cells in the three different games. In Game I only resting and swollen conidia occur, while in Game II and Game III all four strategies are possible.

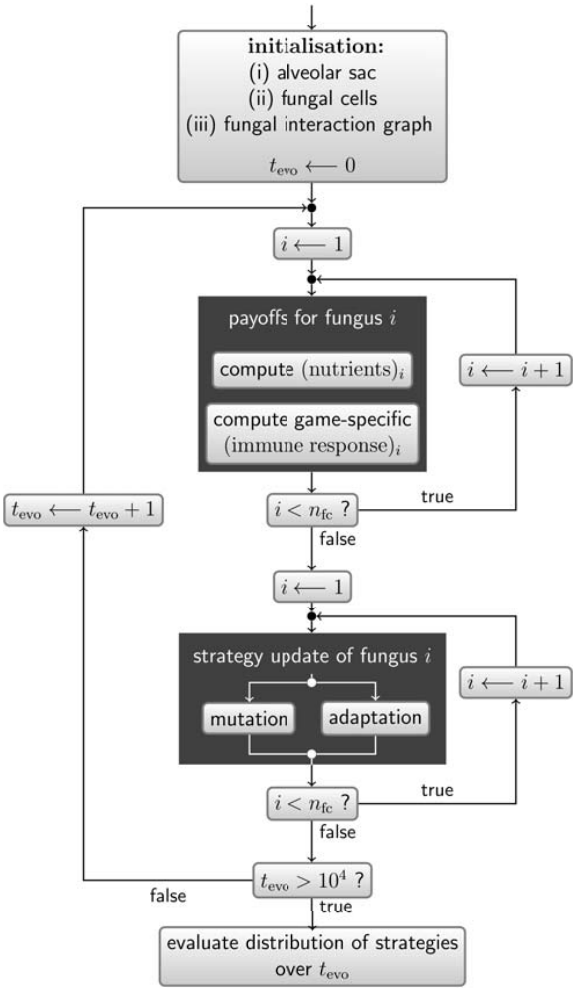

Figure S1: Simulation algorithm of each evolutionary game. Schematic overview of the simulation algorithm as applied for each evolutionary games on the fungal interaction graphs in alveolar sacs. Iterations over evolutionary steps t_{evo} include the computation of payoffs per fungus and microscopic strategy updates based on the concepts of mutation and adaptation. The number of fungal cells for which simulations are performed in the alveolar sac is denoted by n_{fc}.

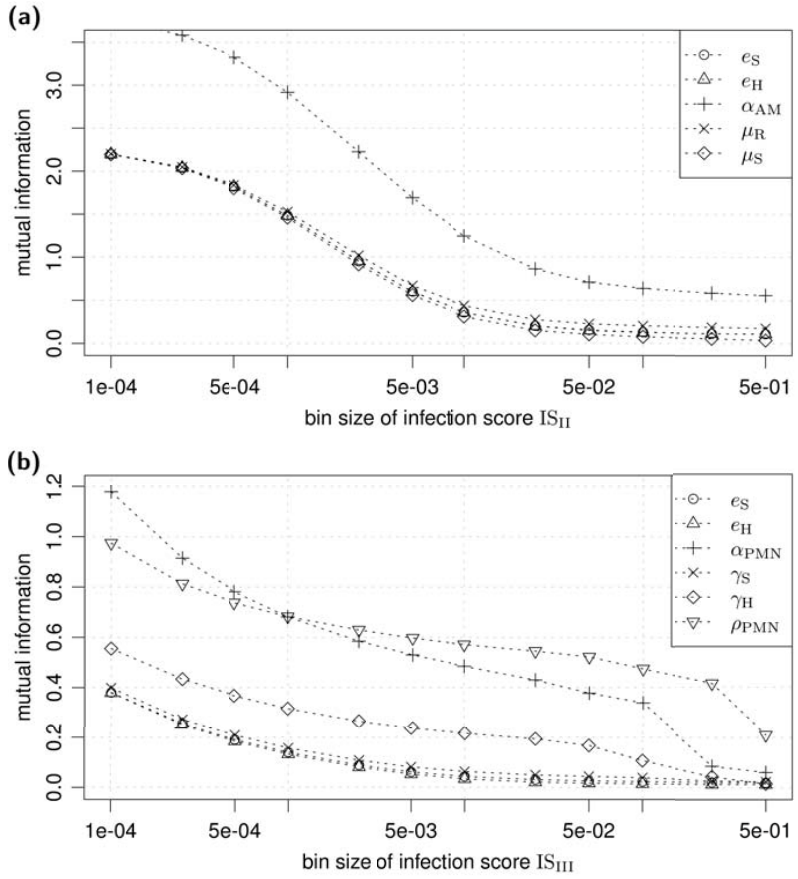

Figure S2: Dependence of mutual information on the bin size. Mutual information for the parameters of (a) Game II and (b) Game III as a function of the bin size of the infection score.

Table S2: Mutual information between infection score and parameters of Game II and Game III.

parameter	condition	MI (Game II)	MI (Game III)
$e_S = E_S/E_R$	$e_S \geq 1$	0.3679	0.0434
$e_H = E_H/E_S$	$e_H \geq 1$	0.3463	0.0338
$\alpha_{AM} = m_R/E_R$		**1.1439**	–
$\mu_R = m_R/m_H$	$\mu_R \geq 1$	0.3220	–
$\mu_S = m_S/m_R$	$\mu_S \geq 1$	0.3324	–
$\alpha_{PMN} = g_R/E_R$		–	**0.4847**
ρ_{PMN}	$\rho_{PMN} \in [0, 1]$	–	**0.5708**
$\gamma_S = g_S/g_R$	$\gamma_S \geq 1$	–	0.0632
$\gamma_H = g_H/g_S$	$\gamma_H \geq 1$	–	0.2161

The mutual information (MI) as a function of the infection score (IS) was computed for bin size 0.01 and for each of the games parameters. E_R, E_S, E_H describe the nutrient contributions for resting, swollen and hyphal fungal cells, respectively. μ_R, μ_S and γ_R, γ_S are fractions of response variables for the encounter of resting and swollen conidia and hyphae by either AM or PMN. *Bold* numbers denote the most relevant parameters of the respective evolutionary game, which are the AM activity α_{AM} in Game II and both PMN activity α_{PMN} and PMN recruitment ρ_{PMN} in Game III.

4.6 Unpublished material

4.6.1 Grid-based monitoring of agents in off-grid agent-based models

A central task in spatially-resolved agent-based models comprises the identification of agent pairs that are interacting with each other. Models in which the spatial locations of agents are restricted to pre-defined lattice points these interactions can easily be obtained by successive exploration of the neighboring grid-points to the one occupied by one of the interaction partners. In off-lattice approaches agents can take positions in continuous space which automatically detaches the neighborhood relationship between agents compared to the lattice-based approach. Agents with postions in continuous space require a condition for which interactions are initiated and executed. Since the interaction of biological cells is based upon physical contact a distance-dependent interaction condition can be applied. If cells with spherical morphologies in three-dimensional space are considered, the following interaction condition can be applied:

$$d(\vec{s}_i, \vec{s}_j) \leq r_i + r_j \ , \tag{4.1}$$

where $\vec{s}_i = (x_i, y_i, z_i)^{\mathrm{T}}$, $\vec{s}_j = (x_j, y_j, z_j)^{\mathrm{T}}$ are the positions and r_i, r_j are the radii of agent i and agent j, respectively (Fig. 4.1(a)). $d(\vec{s}_i, \vec{s}_j)$ denotes the Euclidean distance in three-dimensional space:

$$d(\vec{s}_i, \vec{s}_j) = \sqrt{(x_j - x_i)^2 + (y_j - y_i)^2 + (z_j - z_i)^2} \ . \tag{4.2}$$

For the determination of interaction pairs one could consider to check each of the agent pairs for the condition (4.1). This brute force method then would lead to $n(n-1)/2$ interaction checks per iteration step, where n is the number of agents. This would imply high computational costs due to a related time complexity of $\mathcal{O}(n^2)$.

To reduce the time-complexity associated to the brute force approach a grid-based monitoring of agents was developed. For this aim a regular grid $\mathcal{G}$ with grid constant $a \in \mathbb{R}$ coupled to the continuous space was implemented. Each grid point maps a position in continuous space and is described by an index vector:

$$f_{\mathrm{p}} : \ \mathbb{Z}^3 \longrightarrow \mathbb{R}^3 \ , \quad \begin{pmatrix} k \\ \ell \\ m \end{pmatrix} \mapsto a \begin{pmatrix} k \\ \ell \\ m \end{pmatrix} \ . \tag{4.3}$$

Furthermore, each grid point is associated to a cubic volume of the size a^3 in the following way:

$$f_{\mathrm{v}} : \ \mathbb{Z}^3 \longrightarrow \mathbb{R}^3 \ , \quad \begin{pmatrix} k \\ \ell \\ m \end{pmatrix} \mapsto \left[ak - \frac{a}{2} \ , \ ak + \frac{a}{2}\right) \times \left[a\ell - \frac{a}{2} \ , \ a\ell + \frac{a}{2}\right) \times \left[am - \frac{a}{2} \ , \ am + \frac{a}{2}\right) \ . \tag{4.4}$$

If $\mathcal{S} \subset \mathbb{R}^3$ denotes the spatial volume covered by the system under consideration then $\mathcal{G}$ is defined as follows:

$$\mathcal{G} := \left\{ \vec{g} \in \mathbb{Z}^3 | f_{\mathrm{v}}(\vec{g}) \cap \mathcal{S} \neq \emptyset \right\} \ . \tag{4.5}$$

This grid is used as a kind of spatial orientation for the agents as follows: Each agent is associated with the grid point that is closest to its current position. The grid point associated to the agent can be found by simple mercantile roundings of its spatial coordinates. Agent i with position $(x_i, y_i, z_i)^{\mathrm{T}}$ would be associated with grid point

$$\begin{pmatrix} k_i \\ \ell_i \\ m_i \end{pmatrix} = \begin{pmatrix} \lceil x_i/a \rfloor \\ \lceil y_i/a \rfloor \\ \lceil z_i/a \rfloor \end{pmatrix} \in \mathbb{Z}^3 \ , \tag{4.6}$$

where $\lceil \cdot \rfloor$ denotes the mercantile rounding operator (see also Fig. 4.1(b)). In a reverse conclusion this means that each grid point holds a set of agents. To obtain the interaction partners in this grid-based monitoring approach only the agents associated to neighboring grid points and the grid point associated to the agent under consideration have to be checked for interaction. Depending on the choice of the grid constant a and the size of the agents, neighboring grid points of higher order than only the Moore-neighborhood may have to be considered as well (see Fig. 4.1(c,d)).

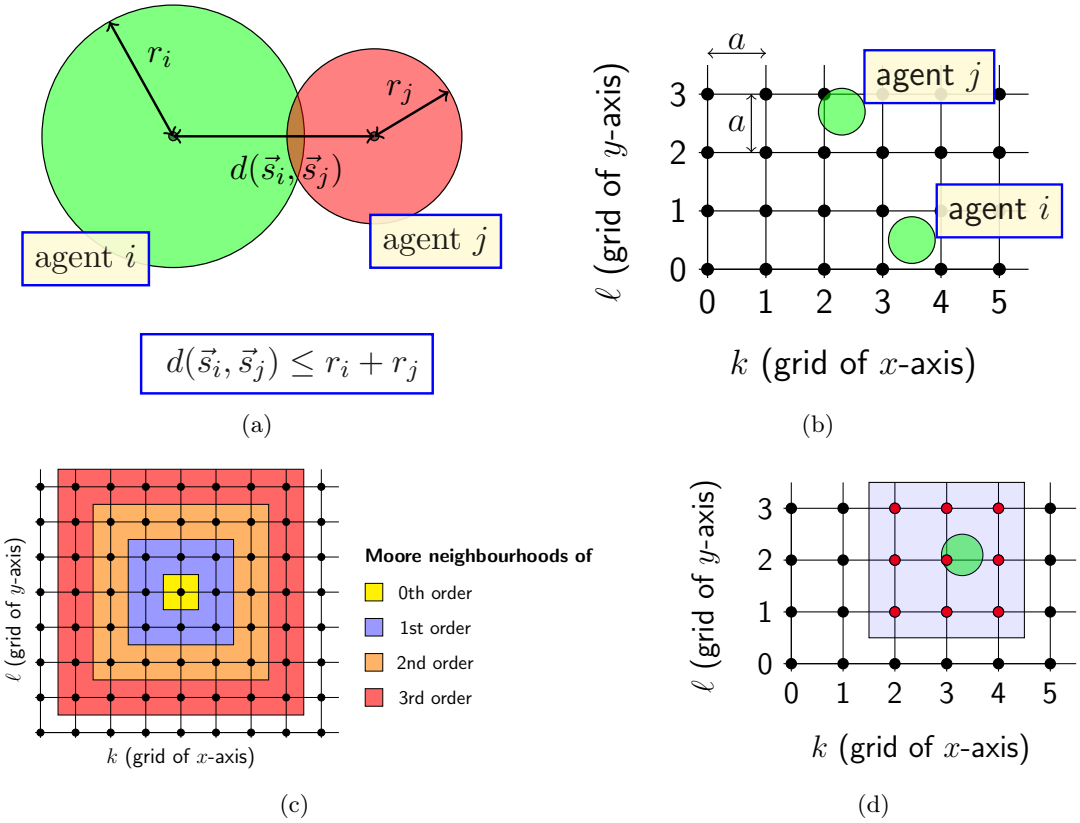

Figure 4.1: Basic concepts for the grid-based monitoring of agents in off-grid spatial environments. (a) Interaction condition in agent-based models at the scale of cells assuming spherical cell symmetry. (b) Mapping of continuously placed agents to grid-points. Here, agent j associates to the point $(2, 3)^{\mathrm{T}}$ and agent i would get grid point $(4, 1)^{\mathrm{T}}$ assigned. (c) The Moore neighborhood relationship for the grid point surrounded by *yellow* color with different orders. (d) The identification of interactions for the agent (shown in *green*) that is assigned to grid point $(3, 2)^{\mathrm{T}}$ follows the traversal of grid points of the Moore neighborhood up to the first order.

A benchmark of the method was performed in order to obtain the computing time and the consumed memory of both, the grid-based monitoring as introduced before and the brute force approach (see Fig. 4.2). In Fig. 4.2(a) it can be seen that the computing time per simulation increases relatively strong for the brute force approach with increasing numbers of agents, whereas grid-based monitoring is able to stay well below one hour computing time for 10^4 agents and 10^3 iterations. This effect can be attributed to the different time-scaling of the two approaches, which was further investigated in Fig. 4.2(b). The brute force methods time complexity scales quadratically in the number of agents as it shows a slope of approximately two in the log-log plot of Fig. 4.2(b). In contrast to that the grid-based monitoring approach scales approximately linear in time for different grid constants over the number of agents.

In addition to that the dependence of the computing time on the grid constant a could be resolved in Fig. 4.2(c). From these results it can be deduced that there exists an optimal grid constant a_{opt} in terms of computing time. As shown in Fig. 4.2(c), a_{opt} is independent of the

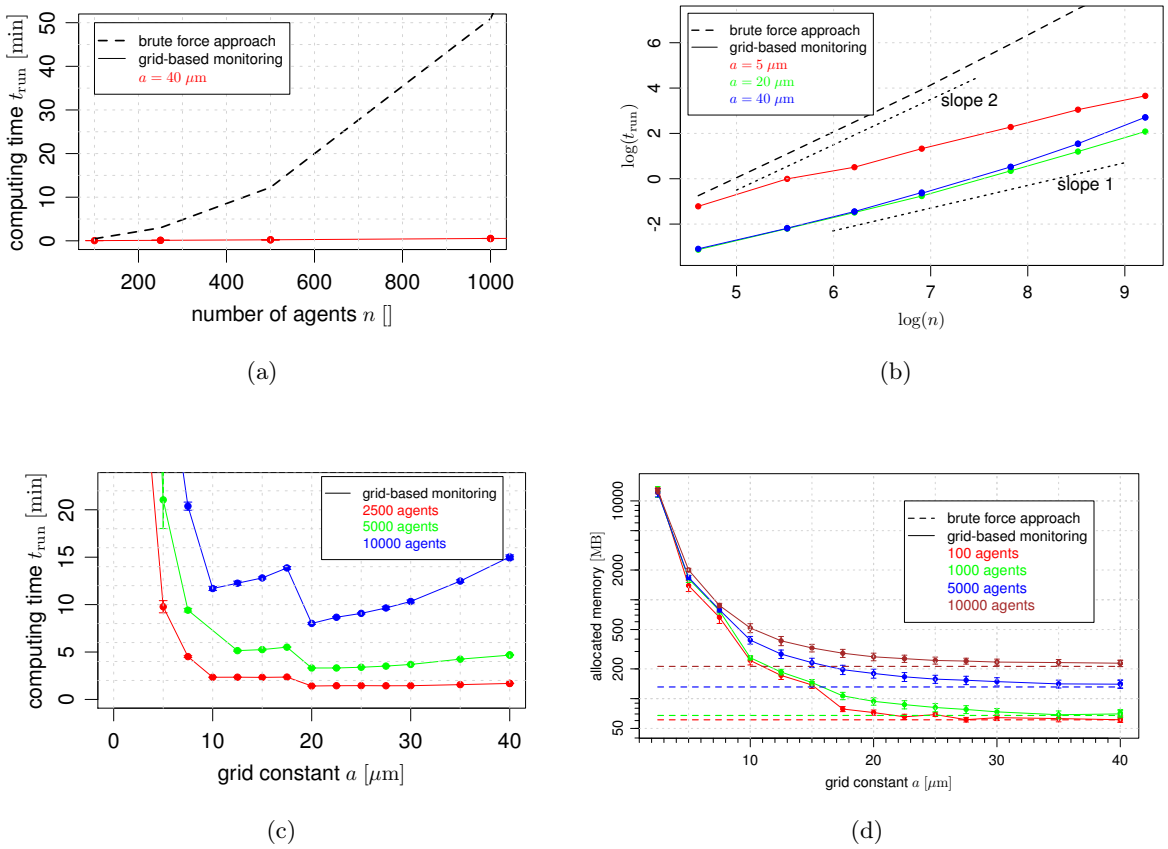

Figure 4.2: Benchmarking of the grid-based monitoring approach and comparison with brute force interaction detection. A test cubic environment of $1\,\text{mm}^3$ volume with reflecting boundary conditions was used. Number of agents and grid constants were varied in order to determine the computing time and the amount of memory allocated during the execution of the simulation. Per simulation run 10^3 iterations were performed and agents had a radius of $10\,\mu$m. To account for stochasticity of the results 100 simulations per parameter configuration were executed. In each plot error bars denote one standard deviation. (a) The average computing time per simulation is shown for the grid-based monitoring and the brute force approach. (b) A log-log plot is used for the identification of the intrinsic time-scaling associated to each of the methods. (c) The dependence of the computing time on the value of the grid constant a for different agent densities are resolved. (d) Comparison of the average memory consumption over the course of simulation for both approaches including the relation to the value of the grid constant a.

number of agents in the system. In order to capture all interactions of one agent accurately for lower grid constants Moore neighborhoods of higher order have to be considered, too. The benchmark system requires to check the Moore neighborhood of 0th and 1st order for grid constants $a \geq 20\,\mu$m. If the grid constant is below $20\,\mu$m it is not guaranteed to successfully find all interaction partners of one agent due to its radius of $10\,\mu$m. Thus, if a is in the range of $[10\,\mu\text{m}, 20\,\mu\text{m})$ the Moore neighborhoods from the 0th up to the 2nd order have to be traversed, for $\frac{20}{3}\,\mu\text{m} \leq a < 10\,\mu$m the ones from the 0th up to the 3rd order have to be considered and so forth. In general: If $k = \lceil 2r_{\text{agent}}/a \rceil$, where r_{agent} is the radius of each agent in the system, the Moore neighborhoods from the 0th to the kth order have to be traversed for accurate interaction detection. From the perspective of computing time it is favorable to traverse as less as possible grid points as the check of every grid point for agent interactions causes some computing cost. This characteristic of grid-based monitoring is reflected in Fig. 4.2(c) for all $a < 20\,\mu$m, where computation time rises stepwise with increased grid resolutions due to additional orders of Moore

neighborhoods that have to be taken into account. Furthermore, it can be seen that computing time rises also for increasing grid constants $a > 20\,\mu$m, with an augmentation of this effect for higher agent densities. Considering two identical systems, but with different grid constants $a_1 < a_2$ for grid-based monitoring, higher numbers of agents are associated with one grid point on average in the system with grid constant a_2. Since for accurate interaction detection at least the 0th and 1st Moore neighborhood have to be checked, the number of agent-agent checks is higher in the system with grid constant a_2 relative to the one with a_1. This difference is intensified the higher the agent density in the system due to increased differences of grid point occupation by agents between the two systems. In reverse this means that a proper choice of a is the more important the higher the agent density of the system under consideration. Optimality is reached for the situation where the Moore neighborhoods of 0th and 1st are just about enough to capture all interactions accurately. Here, the number of grid points that come into consideration for interaction detection are minimized as well as the grid point occupancy by agents. In the benchmark optimality is achieved for $a = 20\,\mu$m, which is exactly the lower limit for which $k = 1$. In general computing time gets minimal for $a_{\text{opt}} = 2r_{\text{agent}}$ assuming all agents having the same size. If heterogenous sizes have to be considered, then the maximum radius $r_{\text{agent,max}}$ determines optimality in the following way: $a_{\text{opt}} = 2r_{\text{agent,max}}$.

In terms of computer memory the brute force approach generally requires less amounts compared to grid-based monitoring as it is not taking advantage of any additional data structure (see Fig. 4.2(d)). Naturally, both approaches allocate more memory for higher numbers of agents. The amount of memory required for grid-based monitoring over the course of simulation execution depends on the resolution of the grid and increases with diminished grid constants. Furthermore, it can be seen that the memory used by brute force always marks a lower limit for grid-based monitoring. Considering the optimal grid constant a_{opt} for the system that was benchmarked the required memory increased compared to brute force by factors from 1.2 to 1.4.

In summary, grid-based monitoring outperforms brute force interaction detection in terms of computing time at the price of some additional computer memory. The approach is most worthwhile for systems with high numbers of agents and/or high agent densities in which relatively high numbers of interactions have to be checked for. It takes full advantage of the facilitating features behind cellular automata and grid-based space representations, but it still maintains continuous agent placing. The main advantage of grid-based monitoring over brute force lies in a reduction of the number of interactions to be checked over the course of time-integration. This is achieved by defining a spatial neighborhood relation based on a regular lattice on which the agents are associated in a location-dependent fashion. In grid-based monitoring for interaction detection each agent uses its associated grid-point as a basis for efficient spatial orientation.

4.6.2 An agent-based framework to model and simulate host-pathogen interaction

During the origination of this thesis a flexible and extensible framework for the purpose of multi-scale agent-based modeling and simulation was developed. The implementation is written in the object-oriented programming language `C++` and takes full advantage of modern software architecture, *i.e.* modularisation as well as usage of UML and object-oriented design patterns, which enhances technical exchange and transfer between different developers. The framework was successfully applied in the simulations that were part of already published papers presented in the sections 4.2, 4.3 and 4.4.

Structural considerations for spatio-temporal modeling

The framework and relations between classes are on the one hand hierarchically organized to account for structural connections like containedness between components and on the other hand cross-connections exist that map relationships that are not organized in strict hierarchical fashion.

The root of the tree-like hierarchical structure is given by the *environment* node. Here, the whole world of the model is represented. The environment subdivides into spatial compartments, so-called *sites* each representing a specific bounded volume. Simulations of one, two and three-dimensional spatial systems can be executed. A site may represent a regular shape like a cuboid or a spherical structure, but is totally flexible for particular requirements of the biological system under consideration. In the framework spatially extended entities like agents are placed at continuous positions in space, which demands for a fast method to determine the agent-agent interactions. For this purpose a grid-based monitoring of agents in off-grid agent-based models was developed that was already introduced in subsection 4.6.1.

Agents are embedded in the sites and represent the cells of the biological system. Each agent is associated to one site. Properties related to the spatial structure, size and color are encoded in a *morphology* object. The program accounts exclusively for spherically shaped agents and compositions of a set of spheres per agent, which simplifies interaction detection enormously. Each agent implements its mode of *migration*. Random migration with or without directional persistence time as well as migration modes with directional bias are selectable. It is also possible to handle non-constant values for speed and turning angles in order to account for probability distributions of these measures that may got obtained from experimental studies. In general, position shifts as caused by migration are handled via displacement vectors, which are scaled to the chosen timestep. Agents also contain a pre-defined scheme for the execution of *interactions* with other agents. On the one hand a finite state machine handles rate-based probabilistic state transitions that are contextually coupled to physical operations in space like the internalisation of a pathogen by a phagocyte or a touching without enclosure in the case of interaction avoidance. Agent-specific degrees of differentiation are mapped in the *cell-state* object, which is implemented as finite state machine with rate-dependent state transitions.

The framework is able to perform multi-scale simulations if the *molecular layer* is used to model diffusion or reaction-diffusion processes (see Fig. 4.3 for a brief overview). Finite difference solvers on regular grids of arbitrary dimension and on triangulated two-dimensional lattices are available to integrate discretized partial differential equations in space and time. Cross-connections between molecular layer and the agents are used in the case of receptor-ligand interactions on the cellular surface.

Modularisation and workflow of the framework

The agent-based modeling and simulation framework is decomposed into modules which represent the working chain or data-pipeline of the executable program. In Fig. 4.4 the modules are shown in the context of the implemented workflow. For data-exchange between the different modules and for the purpose of initial parametrisation `XML` and `CSV` formats are used. For consistency reasons a specific `XML` node-structure that maps the object-oriented relationships according to the UML diagram of the framework was generated for each module. In the following a brief description of each module is given:

input: The input module recieves the configuration of the system by the user in form of `XML` files. In these files, the environment, agents and their interactions, molecules and their reactions, numerical solvers, approaches to reduce computational costs and simulation dy-

namics are defined. In this module the quantitative values for the processes considered in the simulation are set and stored.

simulation: The input of the first module is forwarded to the simulation module in which the system to be simulated is initialized. Furthermore, the time-integration based on random selection dynamics is executed. Throughout the whole simulation readouts of agents, molecules, states, interactions and/or events can be defined and are captured, which then get passed to the output module. To account for the stochasticity of randomized processes or events over the simulation, replicates can be generated. In this module runtime is effectively reduced by executing a number of simulations in parallel, which favors the execution of large-scale simulations on multi-core servers and computer clusters.

output: The data that was generated in the simulations is stored in the output module in structured multi-dimensional arrays. For the purpose of data-exchange with other modules `CSV` files are used. To store and forward the information about the dynamics of the system over time a `XML`-format that maps the configuration of the system for each timepoint is at hand (*time-oriented configuration output*). A `CSV` or `XML` output representing the evolution of single agents with their positions, states, interactions and further events is also available (*agent-oriented configuration output*). Methods for graphical output of two-dimensional data in scatterplots and lineplots as well as of one-dimensional data in histograms is directly possible.

analyzer: This module takes advantage of the structured outputs and formats that were generated by the output module. Automatized methods to calculate standard statistical measures like mean or standard deviation can be applied to the data. In addition to that there exist interfaces to include scripts from other powerful statistical programming languages like `R` to include automatic evaluation procedures with particular purposes. The analyser also aggregates the time-step oriented configuration output to give general overviews about the dynamics of subpopulations, cell states and cell-cell interactions.

visualizer: Here, the spatio-temporal system is rendered in three-dimensional space using the open source software `POV-Ray`. First, each `XML` file of the time-oriented configuration output is used to render single images representing snapshots of the system. Second, from these snapshots videos can be generated with the open source video tool `ffmpeg` which then capture the dynamics of the system.

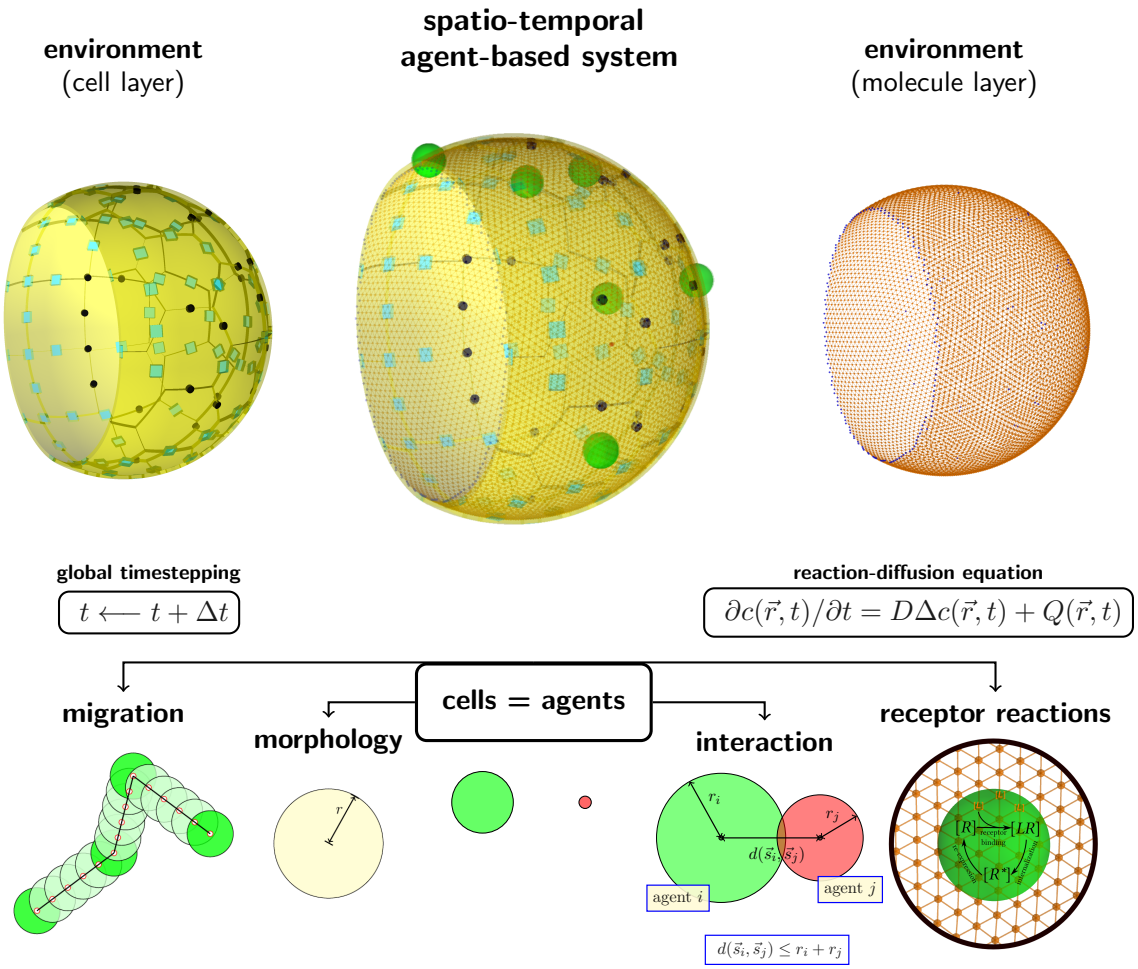

Figure 4.3: Overview of structural relationships between different components of the agent-based modeling and simulation framework. As example for an application the hybrid agent-based model of the three-quarter human alveolus from [106] was chosen. The system is composed of an environment, which has a molecule layer for the diffusion and reaction of molecules and a cell layer representing the epithelium that bounds the biological environment. Biological cells of the host and the pathogen are also termed agents in this agent-based framework and receive definitions for their inherent properties: migration, morphology, interaction and reactions of surface receptors.

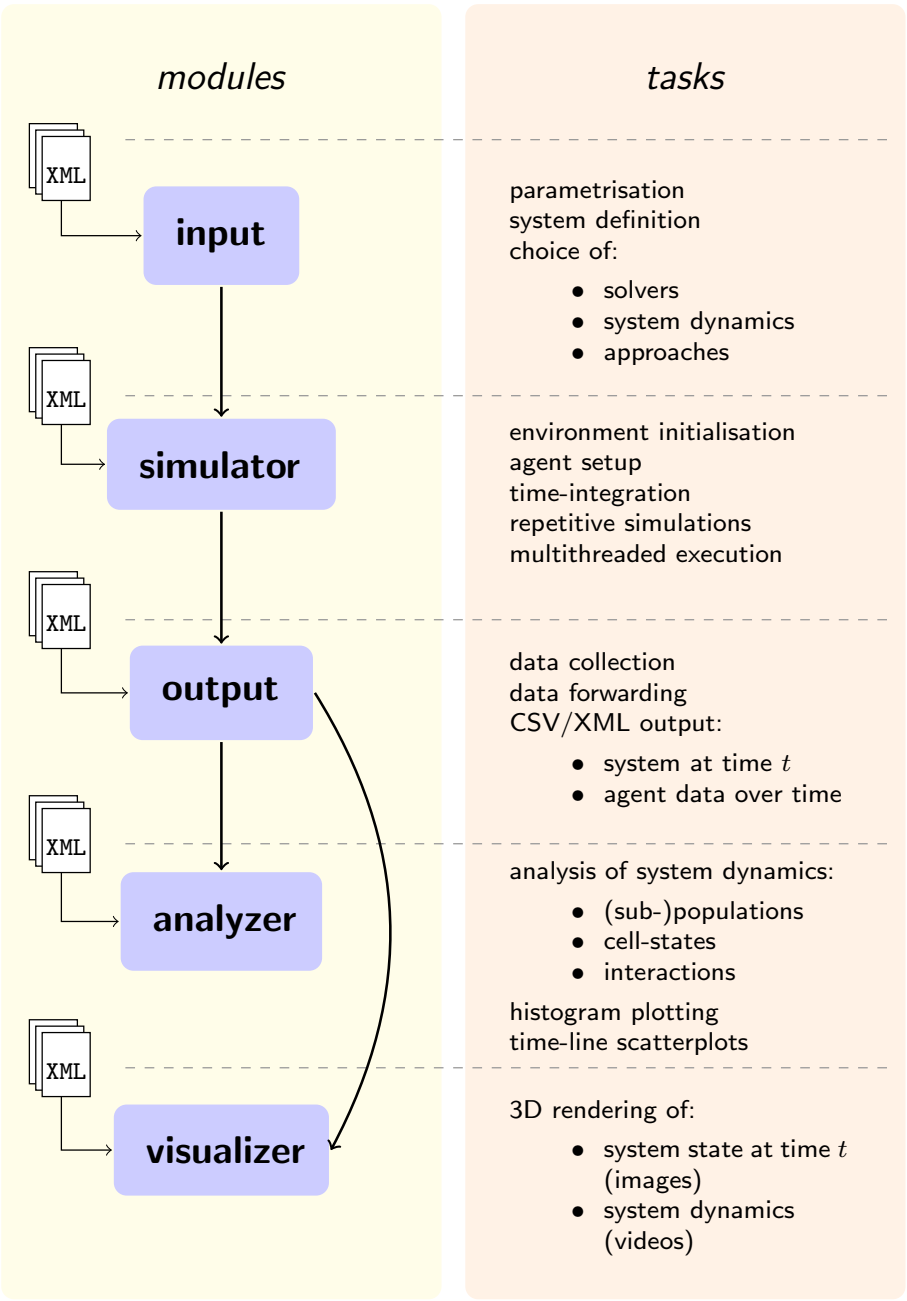

Figure 4.4: Modularized structure and workflow of the agent-based modeling and simulation framework. The algorithm of the software follows a chain of framework modules, with each module being responsible for the execution of specific tasks.

Chapter 5

Discussion

Over the past two decades the cases of fungal infections steadily increased and have become a major threat to immunocompromised individuals [107]. Only about 100 of a current number of 10^5 known fungal species are considered pathogenic [1, 6]. In this work the most important airborne human-pathogenic fungus *A. fumigatus* was investigated using mathematical modeling and computer simulations. Since individuals experience permanent conidial exposure due to inhalation of several hundreds to thousands infectious agents of *A. fumigatus* on a daily basis [7, 11, 17], a central aim of this thesis was the generation of experimentally verifyable predictions regarding the interaction of the host with *A. fumigatus* in the lower respiratory tract. Theoretical investigations as carried out in this work comprise model engineering and their execution by means of computer simulations in which everything is entirely controllable [61, 99]. Experimental investigations are typically limited by ethical concerns, the availability and costs of methodological tools as well as the ability of the investigator to prepare the scenario to be studied. The experimental observation of the lower respiratory tract under physiological conditions including *in vivo* imaging can be hard to realize due to the vital function of the lung. Its peculiar morphology introduces difficulties for the experimentalist to investigate the interplay with the fungus without compromising the host by experimental preparations. Furthermore, under physiological conditions, associated with only hundreds to thousands of inhaled conidia, the limits of detectability can be reached due to low intensities of the inflammatory signals under consideration. Thus, computational approaches to unravel obscured details are highly valuable to overcome limitations of wet-lab approaches and to widen our understanding of life-threatening infection processes.

This chapter is organized as follows: First, the computational methods and tools that were used and applied are reflected with respect to their efficiency, feasibility and realism. Section 5.2 summarizes and discusses the main results of the first-author publications [104,106] and also those of the submitted paper on the relation between *A. fumigatus* infection and host inflammation by evolutionary games on graphs (see Section 4.5). In the last section an outlook for possible model extensions is given. Furthermore, ideas for future work directions and beneficial readouts from laboratory experiments are presented. Finally, the thesis comes to a conclusion.

5.1 Methodoligical considerations

The foundation of this work was set by the implementation of a flexible, extensible and reusable spatio-temporal agent-based modeling and simulation framework. This tool was purposely de-

signed and developed with the goal to adequatly map the features of innate immunity in response to different fungal species. This modularized framework enables modeling at the scale of cells and molecules and furthermore accounts for the spatial aspects of the biological environment. These spatial aspects include the site of infection, its morphology and cellular composition as well as of the different cells like phagocytes and fungal cells that are involved in the host-pathogen interaction. Additionally, spatio-temporal features as the migration and interaction of cells and their responses to external cues like cytokines were included. Since agent-based computer simulations are cost intensive in terms of computing time [62], the framework takes advantage of state-of-the-art software design principles, efficient algorithms and was written in the object-oriented programming language `C++`.

Entities like cells, boundaries and epithelial or fluidic layers were allowed to occupy arbitrary positions in continuous space, which disposes artificial spatial grids and their resolutions as used in other approaches [75, 80]. As a consquence of modeling space continuously the interaction detection between cells exaggerates the issue of fast computations. Consequently, a grid-based monitoring method to compute the interaction partners of a cell, having approximately linear time complexity in the number of agents, was engineered (see Section 4.6.1). Since cell morphologies were considered spherical or compositions of several connected spheres in the agent-based framework the interaction detection method took full advantage of their spherical symmetry. The archetype of this method stems from the field of molecular dynamics in which neighbor lists as such are commonly used [108] to reduce the number of interacting pairs to be checked. Its high efficiency and success in multi-cell systems arises from the fact that physical contact is required to initiate an interaction between a pair of cells. Thus, in the present case a fixed cutoff for interactions is set by the sum of cell radii related to the interacting pair, in contrast to molecular dynamics in which the range of a force dictates this threshold [108]. The runtime efficiency comes at the price of some additional memory compared to a brute force interaction detection. There exist methods like Verlet-lists, which perform comparable in terms of time complexity [109, 110], but the implementation of these methods is not as straight-forward as the one chosen in the present framework. Still our approach could get improved by parallelized interaction identification or by the application of adaptive resolution cell lists to account for space-dependent interaction cutoffs as was recently published by Awile *et al.* [110].

In the present implementation time evolves iteratively with a pre-defined timestep Δt of fixed size and in each timestep we updated all agents in a random order [111]. This is also termed random selection dynamics and explained in Appendix A in more detail. Asynchronous updates as applied in the self-written framework proved to be more realistic with respect to the simulation of biological systems [85,112]. However, simulation algorithms with discrete timesteps of fixed stepsize, on the one hand, ensure a robust integration of the dynamics, but are, on the other hand, computationally demanding [113]. Reductions in the number of elementary update procedures, *i.e.* in computation time, can be achieved by adaptive stepsize algorithms as used in Kempf *et al.* [70] or by the implementation of a global event-scheduler in which each update of an agent relates to a process mathematically described by a pre-defined rate [85].

The utility of spatio-temporal modeling in the field of fungal infections was first discussed in [6] (see Section 4.1). The demand for computational *A. fumigatus* infection models was accomodated by Tokarski *et al.* with an agent-based model in which hunting strategies of neutrophils were studied [80]. Since neutrophils are considered to be of central importance in counteracting *A. fumigatus* [47, 53], this aspect is of high relevance. In the first application of the self-written agent-based modeling and simulation framework, the early immune response to conidia of *A. fumigatus* in alveoli of the human lung was investigated [104] (see Section 4.2). A three-dimensional to-scale model of a typical human alveolus was generated, on which the host-pathogen interaction under physiological conditions was studied. We took advantage of the first-passage event, which, in the present model, denoted the minimal duration it takes an arbitrary alveolar macrophage to establish physical contact with an *A. fumigatus* conidium in the alveolus. Performing computer

simulations on first-passage-times under various parameter combinations, we were in the positon to unravel the migration mode of alveolar macrophages. Precursor studies on abstract cell-target encounters showed the relative importance of biased migration in the direction of the target to reduce first-passage times [114,115]. Our study showed an essential role of chemotactic migration in the direction of the pathogen *A. fumigatus* for removal by alveolar macrophages before its onset of germination and invasive growth. In a next study [106] (see Section 4.3), the alveolus model was refined and extended to explicitly account for the, as yet experimentally unidentified, chemokine. For this aim, the diffusion equation was numerically solved on the alveolar surface and a chemotaxis model was integrated. To numerically simulate molecular motion and reactions in the fluidic pulmonary surfactant a discretization with 10^4 close-to-regular Delaunay-triangulated grid points over the curved alveolar surface was generated (see Appendix A.1.2 for explanations). We implemented a state-of-the-art finite-difference approach on Voronoi cells with a forward-Euler method to integrate the reaction-diffusion equation in space over time [63]. The method is first order accurate in time and second order accurate in space. The number of grid-points chosen to simulate the molecular dynamics constituted a trade-off between numerical accuracy and computation time as more grid-points would increase accuracy as well as computation time. As a result of chemokine secretion by AEC, the formation of chemokine gradients over time could be observed at every spatial position of the surface and in turn the mechanistic reaction between chemokines and receptors of AM was modeled in an explicit fashion as well. A modified version of the receptor-kinetics model of Guo *et al.*, suitable to the properties of the grid and the spherical morphology of AM, found application [83]. Modeling molecular dynamics and cellular migration in a hybrid agent-based approach allowed for the identification of chemokine parameter ranges including secretion rates, diffusion constants as well as degradation rates.

Spatio-temporal agent-based modeling of *A. fumigatus* infection in human alveoli provided detailed insights into elementary processes of the early infection dynamics, but it proved also to increase heavily in computational load if higher model detail was considered. To monitor high-dose infection processes at the scale of tens of hours including PMN would render hybrid agent-based modeling intractable due to tremendous amounts of unknown parameters. In consequence the modeling strategy was altered to individual-based evolutionary game theory, in which spatial proximity between fungal cells was represented by an undirected graph. Most advantagous, game theory abstracts from mechanistic interactions and condenses information in so-called payoffs. Here, the relations between the payoffs are more important than particular quantities. Thus, evolutionary game theory on graphs allowed for an enormous parameter reduction and enabled studying stage-specific *A. fumigatus* behavior against the complement system, AM and PMN. Additionally, combining the different stages in consecutive fashion enabled studying *A. fumigatus* infection dynamics for different immune-statuses of the host. Application of (evolutionary) game theory to fungal infection is not novel *per se* [97, 98], but combining evolutionary games in a consecutive fashion to simulate the infection over time constitutes an innovative approach with potential applicability in other fields, in which the temporal evolution of a system is of relevance.

5.2 Discussion of the main results

Agent-based model of human alveoli enables studying *A. fumigatus* infection under physiological condition

The respiratory tract, with the alveoli as its smalles units, constitutes a major portal of entry for foreign substances and microorganisms into the body of mammals due to a delicate epithelial barrier separating between the bloodstream and inhaled air [26, 35]. The fight against inhaled conidia of the pathogen *A. fumigatus* is a daily challenge for the immune system [47]. Based on literature data we engineered a realistic three-dimensional to-scale representation of a typical human alveolus [116] including alveolar epithelial cells of type I and type II, pores of Kohn and

AM. We considered a three-quarter spherical structure, which is the most frequently observed alveolar shape in the human lung [116]. The dynamics of respiration were captured by periodic inflation and deflation of the alveolar volume with pre-defined respiration conditions, *e.g.* resting state and heavy exercise, which differed from each other in respiration frequency and in alveolar volume increase. Respiration parameters were translated into changes of the alveolar radius, which was accompanied with a periodic increase and decrease of the alveolar surface. Migrating AM were in the position to enter or leave the three-quarter alveolus through pores of Kohn or the alveolar entrance ring. The concept of waiting times allowed for a dynamic equilibrium, in which the number of AM in the alveolus fitted a Binomial distribution with 4.4 ± 2.1 AM over time. Furthermore, the presence and behavior of immunologically active proteins in the highly viscous alveolar lining layer [117] was explicitly integrated by a Delaunay-triangulated close-to-regular grid representing the fluid. This allowed for the explicit integration of the molecular scale, which in turn enabled us to consider particular cytokines that link and direct the different components of innate immunity.

The present alveolus model allows for the localisation of epithelial cells in space and is in the position to represent the steady state dynamics of resident AM in alveoli over time. To keep simulations computationally tractable a spherical alveolar representation was chosen despite the polyhedral nature of alveolar structures, which generate a relatively high surface-to-volume ratio [26, 116]. Previous *in silico* models, *e.g.* for aerosol transport [118], successfully applied the spherical approximation and took advantage of a mathematically convenient description of the alveolar surface using spherical coordinates. Our model enables studying the early immune response to arbitrary foreign microorganisms under controllable conditions, which offers opportunities *in silico* that are refused in wet-lab investigations. Investigations on the innate immune response to *A. fumigatus* conidia in lung alveoli are of particular interest for the study of temporal dynamics due to the ability of this pathogen to rapidly adapt and to quickly become invasive under nutrient rich conditions [119]. Thus, *A. fumigatus* sets a tight time-scale for removal by the host and only timely discovery of the fungus puts the host in favor for clearance.

Alveolar macrophages require chemotactic cues to detect *A. fumigatus* before the onset of germination

AM are professional phagocytes resident in lung alveoli and constitute the first cells, which may eliminate inhaled conidia of *A. fumigatus* [26,47,50]. In addition to that they initiate and regulate pro- and anti-inflammatory responses and the recruitment of cells from the bloodstream [39,120–122]. To date it is not known how AM patrol in alveoli to maintain a pathogen-free alveolar surface. Experimental studies on *A. fumigatus* infection in mice and *in vitro* attest relatively low mobility or even sessile behavior to AM [26, 123, 124]. Other *in vitro* studies proved the motile response of AM in chemokine gradients with speeds up to 8 μm/min [125, 126]. However, AM are thought to substantially contribute to phagocytosis and direct killing of *A. fumigatus* [127], but the way AM get in contact with conidia entering alveoli is an open issue. Thus, we studied this process *in silico* performing computer simulations on first-passage-times of AM to invading conidia of *A. fumigatus*. Here, the time measurement started from randomly positioned AM and one conidium over the alveolar surface and ended at the event of first cell-contact between an arbitrary AM and the conidium. Since the migration mode of AM is not known *in vivo*, we initially simulated AM performing a persistent random walk, which was defined by quantitative values for speed and directional persistence time. Scanning random migration parameters in experimentally relevant ranges confirmed the intuitive notion that increased speeds and/or directional persistence times reduce the time of first passage. Nevertheless, independent of the speed and persistence time, a remarkable fraction of first-passage-times for persistent random walk migration of AM showed values well above six hours, which is the time *A. fumigatus* conidia require to environmentally adapt and to initiate germination and invasive growth. Thus, persistent random walk was ruled out due to the inability of AM to avoid damage to the host.

In consequence a second migration mode, biased persistent random walk, with bias in the direction of the conidium was implemented assuming that the motile response of AM was driven by chemotactic signals produced by the alveolar epithelial cell in contact with the fungus. The intensity of the distance-dependent directional bias was linked to the steady-state gradient of a permanently secreting point source with constant secretion rate on a two-dimensional plane. Performing computer simulations with chemotaxis tremendously reduced first-passage-times by one order of magnitude compared to randomly migrating AM. For speed values of 4 μm/min and above AM were able to find the conidium within six hours in at least 95 % of the cases. In chemotaxis studies with AM an average speed of 3.8 μm/min was observed [126], which is in good agreement with the required speed estimate emerging from our study.

Next to alveolar epithelial cells as chemokine producers, a potential source of the required chemokine might also arise from the interaction of conidia with the complement system. The complement proteins C3b and C5b opsonize conidia [46] and enhance phagocytosis by AM, but importantly the byproducts C3a and C5a are candidate chemoattractants for AM [45, 126].

Hybrid agent-based model deciphers properties of an alveolar macrophage chemoattractant

The as yet experimentally unidentified AM chemoattractant, which was required to put AM in favor for fungal detection under physiological conditions, was the central aspect in a follow-up study [106] (see Section 4.3). The implicit and time-independent model of the chemokine profile of the first model [104] was replaced by an explicit spatio-temporal representation including rate-based chemokine secretion by either type I or type II AEC, diffusive molecular motion, degradation of the chemokine and reaction of the chemokine ligands with receptors on the surface of AM. Here, each AM was in the position to sense local gradients of the chemoattractant by a receptor-kinetics model, which was composed of consecutively arranged receptor-ligand binding, receptor internalization and receptor re-expression. The model extension to the scale of molecules enabled studying the response of AM in terms of first-passage times to single conidia under different combinations of chemokine parameters. The integration of the chemokine increased complexity and introduced further unknown parameters like the diffusion coefficient as well as secretion- and degradation rate of the chemokine. Since respiration had relatively low impact on the outcome of the first-passage scenario in the first study [104], the respiratory conditions were fixed to make computations tractable.

To account for chemokine parameter variations, *i.e.* in the diffusion coefficient and in the secretion rate by AEC, parameters were scanned logarithmically in repetitive first-passage time scenarios. Parameter combinations for which more than five percent of the first-passage-times resulted in values above six hours were ruled out as candidates as we assumed that the potential AM chemoattractant would successfully guide AM to the spot of infection in order to eliminate the pathogen. In this study, the ratio of the AEC secretion rate to the chemokine diffusion coefficient separated between parameter combinations associated with fungal detection in time and parameter combinations that were not sufficient for this task. A threshold for this ratio was determined for different combinations of AM speed and directional persistence times. Interestingly, even an AM speed of 2 μm/min was sufficient for cases in which relatively high chemokine secretion rates were combined with low diffusion coefficients. A minor role could be attributed to the degradation rate of the AM chemoattractant as variations in the experimentally relevant regime induced only relatively small changes to the distribution of first-passage-times.

Still, there exist a number of potential chemokines that would attract AM towards *A. fumigatus* like IL-8, which was produced by A549 type II AEC in contact with *A. fumigatus* conidia [9,128] and was shown to bind to the G-protein coupled AM chemokine receptor CXCR2 [129]. Since complement proteins are present in the pulmonary surfactant and interact with the surface of *A. fumigatus* conidia the cleavage products C3a and C5a remain candidate AM chemoattrac-

tors [45]. In addition to the experimentally unidentified AM chemoattractant the cascade that leads to the production of this molecule is also not known to date. That AEC of either type I or type II are involved in the early stages of pathogen recognition seems highly likely due to their physical contact to conidia from their entry into alveoli. The repertoire of inflammatory cytokines and chemokines secreted by type II AEC in response to *A. fumigatus* conidia underpins that notion [31]. The pulmonary surfactant was introduced earlier as a surface-coating fluid that is associated with a reduction of surface tension to avoid alveolar collapse. Next to this vital role its viscosity is directly linked to the diffusion coefficient of the chemokine with increased viscosity associated to a reduced diffusion coefficient. Thus, the surfactant is able to decelerate the dissipation of chemokine gradients and in turn can compensate for lower production rates of the AM chemoattractant.

Evolutionary game theory on graphs identifies key immune mechanisms in response to high- and low-dose exposure to *A. fumigatus*

It is very well-known that AM and PMN constitute most valuable innate immune effectors in the fight against fungal pathogens [24,127]. In laboratory experiments studying an *A. fumigatus* infection is typically associated with the administration of several hundreds of thousands to millions of infectious agents in one shot, which is an extreme compared to the inhalation dose on a daily basis associated with a few thousand conidia [130]. Different dosages may introduce some bias to the assessment of relevant and irrelevant innate immune mechanisms. For example, impairment of AM function was identified as a major risk factor for invasive mycoses [131], but, on the other hand, Mircescu *et al.* found that AM were dispensible for fungal clearance in an *A. fumigatus* infection model in mice [53]. This contradictory view on the role of AM may arise from the dosage dependence of the eventual effect by particular innate immune mechanism. To delineate the relative contributions and the relative importance of different innate immune mechanisms with respect to the dosage of administered conidia, an *A. fumigatus* infection model of evolutionary games on graphs was developed. For each of the major components of innate immunity, *i.e.* the complement system, AM and PMN, one evolutionary game was created to simulate the host-pathogen interaction in alveolar sacs *in silico*.

In each evolutionary game fungal cells of *A. fumigatus* were viewed as infectious agents that play against each other under the pressure of the immune system. The extent of the immune response against a fungal cell was linked to the morphological state of *A. fumigatus*, *i.e.* resting, swollen or hyphal, and also to the interferences between the immune responses of fungal cells that were in spatial proximity. In terms of game-theory the three morphological states resting, swollen and hyphal were considered strategies, which the fungal cells could adopt. Immune responses were associated with a decrease in reproductive fitness, the quantitative measure of fungal viability. An increase in reproductive fitness was achieved by nutrient uptake that was generally consumed by fungal cells in a strategy-dependent fashion. If the pressure of the immune system exerted to the fungal cell outbalanced nutrient uptake and resulted in negative reproductive fitness, then a dead strategy, denoting non viable fungal cells, was adopted. Each game was executed iteratively over evolutionary steps, in which each fungal cell evaluated its reproductive fitness and updated its strategy by either strategy-mutation or strategy-adaptation to the strategy of a proximal fungal cell with higher fitness, with the objective to increase the own reproductive fitness. The innate immune responses were configured with different parameter combinations to investigate uncertainties in exact parameter values and to allow for studying the effect of the hosts' immune status to the outcome of the infection. Furthermore, the study took high- and low-dose exposure to *A. fumigatus* into account and the corresponding requests to the different components of the innate immune system.

The complement system was shown to set an initial emergence of resting or swollen conidia depending on the complement activity against either morphotype. The relative fraction of swollen to resting conidia increased if higher doses and relatively equal complement responses

to resting and swollen conidia were present. Thus, in agreement with former experimental studies [132], impaired complement responses against morphotypes associated with higher infectious potential, *i.e.* swollen conidia, were shown to increase the virulence of the fungus. Studying the response of AM revealed substantial differences in their role over the course of infection in high- and low-dose scenarios. While non-impaired AM were able to clear the infection in low-dose infections with *A. fumigatus* they were shown to reach their phagocytic limits for high-dose fungal exposure. This could be attributed to qualitative and quantitative limitations of AM to phagocytose and kill the overwhelming amount of fungal cells in the hyphal state, which was the most virulent strategy in this evolutionary game. From these results the infectious dose seemed to disentangle contradictory viewpoints on AM in the literature. AM are able to successfully remove all infectious agents of *A. fumigatus* in low-dose scenarios, but they have to rely on further innate immune components in high-dose scenarios. Screening the literature gives evidence that PMN are key effectors against fungal pathogens [7,17,26,47]. We were able to confirm that non-impaired neutrophils could cope with all morphotypes of *A. fumigatus*. An even more important parameter in order to succeed over the pathogen was found in the number of recruited PMN from the blood stream. We showed that an increased number of recruited PMN could compensate for slight impairments in neutrophil function, but that a minimum number of recruited PMN was required to put the host in the position to clear the infection. In turn, this demanded for a model in which the regulation of the recruitment was included. Since the orchestration between different players of the immune system is mediated by the release of inflammatory molecules, we introduced particular inflammatory signals to combine the individual evolutionary games in order to generate one virtual infection model.

Combination of evolutionary games reveals the relation between *A. fumigatus* infection and host inflammation

An immune response can be thought of as a finely tuned cascade of signal receptions, reactions and signal emissions by different components of the immune system. Each immune effector has its own receptors, emittors and features on how to counteract depending on the combination of received signals and their respective intensities. We combined the three evolutionary games consecutively to model and simulate an elevating sequence of infection and inflammation in alveolar sacs. Starting from the evolutionary game related to the complement system the initial encounter of *A. fumigatus* conidia resulted in inflammatory activation of AM by complement molecules. In a next step AM were able to recruit PMN, if AM were not able to clear the infection themselves. The quantitative values for AM activation and PMN recruitment were generated from specific complement and AM responses against the resulting *A. fumigatus* morphotypes encountered in the games, respectively.

As in the single evolutionary games a distinction was drawn between high- and low-dose exposure to *A. fumigatus*. The complement system encountered inhaled conidia of *A. fumigatus* first. Interestingly, a partly impaired inflammatory response by the complement system against swollen conidia could be compensated in the evolutionary game associated with AM. Irrespective of the fungal dose AM induced similar responses to compositions of fungal morphologies associated with higher or lower complement inflammation. But, as previously seen in the evolutionary game with AM, in low-dose scenarios the status of AM determined whether PMN recruitment was required or not. While impaired AM were not able to remove the infectious agents entirely highly active AM were able to clear the infection for low fungal doses themselves. In the high-dose case AM had to rely on fungal clearance by recruited PMN stressing the importance of the regulatory function of AM by inflammatory signaling in the early immune response. Since without AM, recruitment of PMN would be hampered severely, the regulatory role of AM over the course of infection should recieve intensified considerations in future experimental research. For PMN we found that the higher the infectious dose the more important a proper activity was required to set the host in the position to finally succeed over the pathogen. In particular, for

high numbers of fungal cells in alveolar sacs the likelihood of fungal clearance increased with an increased number of recruited PMN by AM . Thus, in those cases it was more important for the host that AM rather trigger enough PMN recruitment than actively participate in removal of fungal pathogens. In summary, studying *A. fumigatus* infection and host inflammation in a sequence of evolutionary games on graphs demonstrated the relative importances of immune effectors for different-doses and that inflammatory mediation between immune cells was required to ensure host viability and variations in inflammatory signals were connected with different probabilities for fungal clearance.

5.3 Open issues, perspectives and future work

The current mainstream of investigations in fungal microbiology focuses on the identification of particular genes or proteins, of their functions and relationships with other genes and proteins. These 'omics'-approaches at the scale of molecules enhance our understanding of particular mechanisms at the level of a single cell. However, these informations can only be exploited if they are properly integrated in the next higher organizational structure, which comprises cellular interplay in organs or compartments of organs. With hybrid agent-based modeling at the scale of cells and molecules in one approach an initial integration of combined knowledge from both scales succeeded and primal predictions could be generated. These predictions can only be verified experimentally to drive future modeling approaches on the early immune response in lung alveoli. Examples for experimentally required verifications are proofs for AM chemoattraction in response to conidia covering AEC of either type I or type II and the identification of the AM chemoattrant. Since the hybrid agent-based simulations were at the limits of computational tractability due to a relatively high number of unknown parameters it would be highly valuable to obtain a fraction of them in laboratory experiments. Estimations of AM speed and directional persistence time, surfactant viscosity, the mass of the AM chemoattractant or its production- and secretion rate would reduce scanning of broad parameter ranges, *i.e.* reduce computational load, and would also open opportunities to further model extension and refinement to make it more realistic. Currently, the hybrid agent-based model contains the interactions and reactions of the chemokine responsible for directing AM to *A. fumigatus*, but it is known that proteins of the complement cascade like C3 and C5 contribute substantially to immunity against fungal pathogens [17, 45, 47]. In addition, AM and PMN secrete fungicidal reactive intermediates into the extracellular space to enhance their attacks against *A. fumigatus* [47]. On the other hand *A. fumigatus* is in the position to actively downregulate the immune response by secretion of proteases and the cytotoxin gliotoxin [33].

Another option to increase realism could be the analysis of different morphological representations of lung alveoli. It is well-known that alveolar surfaces take up polyhedral shapes to optimize the surface to volume ratio [26], thus an investigation of the influence of more flexible alveolar shapes could open new perspectives. The studies of this thesis considered the most frequently observed three-quarter spherical approximation of human alveoli. As a starting point for future research in alveolar shape analysis with respect to fungal infections a truncated cone representation as well as one-quarter spheroids could be studied as these, taken together, make up about 44% of all human alveoli [116]. It should be noted that idealized mathematical shapes like spheres or regular cubic grids enormously reduce computational costs of the simulations and it would be hard to estimate how strong increased levels of morphological detail would increase the run-time of the model execution. At the moment, the framework is in the position to execute multiple simulations in parallel, which reduces the time of program execution depending on the availability of multiple cores. If the distinct tasks within one simulation can be executed in parallel, then it would be conceivable to als distribute the work load over the cores of the machine on which the program is executed. Such distributed processing would presumably be applicable to a number of connected alveoli in an alveolar sac or an alveolar duct, which would lead the

investigations in the direction of studying fungal infection dynamics at the organ level.

Individual cells like AM and *A. fumigatus* conidia were mathematically modeled using spheric morphology, which is quite close to their average shape. But as soon as conidia of *A. fumigatus* begin to germinate they appear elongated as combined spherical and cylindrical objects, which would render the current morphology of cells not useful with respect to accuracy in spatial occupation. Foresightful, the agent-based modeling and simulation framework features object representation by a series of connected spheres, which in turn maintains the opportunity of using the grid-based monitoring of agents as engineered in this thesis (see Sec. 4.6). Moreover chemotactic cells like AM generate membrane extensions, so-called filopodia, preferentially at the front of the cell to sense chemokine gradients and protrude at the rear to crawl in the preferred direction [133, 134]. This includes also dynamic variations in the shape of the cell membrane in response to the environment over short time spans, which can be challenging to realize from a modeling perspective. The art of modeling includes choosing from a number of system features the ones that are most meaningful for the outcome of a particular simulation result. Therefore, future extensions to the current set-up of the hybrid agent-based model for studying fungal infection dynamics in human alveoli strongly depend on the insights the simulation should give and the questions to be answered by the model [61, 99].

The application of game theory to the most important aspects of immunity to *A. fumigatus* infection in the lung could confirm that the regulatory role of AM and the recruitment of PMN and their activity are of central importance. Elegantly, the first stages of the immune response including the complement system, AM and PMN were combined by consecutive execution of evolutionary games on graphs that were linked to each other by inflammatory signals in response to the amount of pathogenic fungal cells and their morphological state. Still this model can be extended with other immune cells of the adaptive immune system like dendritic cells or T-cells to map other players, which are known to cause disbalanced or insufficient immune responses to infectious agents of *A. fumigatus* [135]. To draw a picture with increased detail one could consider to organize the relations between distinct games rather as a highly connected network of signals and responses than as a consecutively organized sequence. However, with respect to the focus on the relation between infection and inflammation over the course of the early immune response a reasonable level of abstraction was chosen. The current approach assumed that *A. fumigatus* adapted to the host with the most beneficial morphological state, *i.e.* resting, swollen or hyphal state, for its reproductive success. It is well-known that *A. fumigatus* employs different passive or active mechanisms to shield itself from immune recognition or to counteract particular immune responses [17,47], thus, considering both sides, *i.e.* the host and the pathogen, as players with respect to game theory could further delineate between processes of minor and processes of major importance for either the host or the pathogen.

In two *in silico* studies of *A. fumigatus* infection in human alveoli the agent-based modeling and simulation framework was applied and set-up an extendable foundation of the early innate immune response against this fungal pathogen. The present computational approach is in the position to segment the immune response into experimentally verifyable pieces in order to arrive at reasonable conclusions for the process as a whole. Furthermore, the framework proved its flexibility and was applied to an experimental human whole-blood infection assay for *Candida albicans* [81] (see Section 4.4). Here, a bottom-up modeling approach was exploited to refine the level of model detail in an iterative fashion. Since each refinement was associated with an increased number of unknown parameters, the refined models took advantage of estimated parameters from the previous levels of model detail. Thus, only newly introduced parameters were scanned for their impact in experimentally reasonable ranges and were estimated by comparison of their respective population dynamics with experimental data in repetitive stochastic simulations. In particular the framework shed light into the migration parameters of monocytes and neutrophils in human whole-blood, which can be considered highly valuable from an experimental perspective as the high density of erythrocytes hinders direct imaging of immune cell

migration. Ultimately, a final objective of the series of bottom-up models is a highly detailed hybrid agent-based model including secretion of reactive intermediates by activated neutrophils and chemoattraction of innate immune cells to hot spots of *Candida* infection.

A central goal of computational modeling approaches in theoretical biology is the generation of realistic representations including the relevant entities and processes of a particular system in order to draw verifyable predictions of its behavior under pre-defined initial conditions. The modeller typically encounters two basic limitations with respect to model complexity and model detail :

1. the computer resources in terms of memory, the number of processors and their repsective clock frequencies,
2. the availability of data from experiments or from the literature.

Finally both of them have to be tackled using efficient state-of-the-art algorithms and by initiation of cooperations with experimental partners in the field of study. In this thesis a simulation tool was engineered that met the challenge to tackle primarily issue 1. The *in silico* models of this thesis paved the way for future research in the early immune response to fungal infection in lung alveoli and can serve as a basis for future research. The present theoretical approach would strongly benefit from experimental verification of the predictions generated in this thesis. Furthermore, a systems biology approach with extensive exchange between experimentalists and theoreticians could drastically accelerate the acquisition of knowledge about *A. fumigatus* infection in lung alveoli and would aid to finally arrive at reasonable therapies and drugs that reduce the risk of fatal fungal infections in immunocompromised patients.

Bibliography

[1] Blackwell M: **The Fungi: 1, 2, 3 ... 5.1 million species?** *American Journal of Botany* 2011, **98**(3):426–438.

[2] Mavor A, Thewes S, Hube B: **Systemic Fungal Infections Caused by Candida Species: Epidemiology, Infection Process and Virulence Attributes**. *Current Drug Targets* 2005, **6**(8):863–874.

[3] Krijgsheld P, Bleichrodt R, van Veluw GJ, Wang F, Müller WH, Dijksterhuis J, Wösten HAB: **Development in Aspergillus.** *Studies in Mycology* 2013, **74**:1–29.

[4] Lin SJ, Schranz J, Teutsch SM: **Aspergillosis Case-Fatality Rate: Systematic Review of the Literature**. *Clinical Infectious Diseases* 2001, **32**(3):358–366.

[5] Kitano H: **Systems Biology: A Brief Overview**. *Science* 2002, **295**(5560):1662–1664.

[6] Horn F, Heinekamp T, Kniemeyer O, Pollmächer J, Valiante V, Brakhage AA: **Systems biology of fungal infection**. *Frontiers in Microbiology* 2012, **3**(APR):1–20.

[7] Latgé JP: **Aspergillus fumigatus and Aspergillosis**. *Clinical Microbiology Reviews* 1999, **12**(2):310–350.

[8] Rhodes JC: **Aspergillus fumigatus : Growth and virulence**. *Medical Mycology* 2006, **44**(s1):77–81.

[9] McCormick A, Loeffler J, Ebel F: **Aspergillus fumigatus: Contours of an opportunistic human pathogen**. *Cellular Microbiology* 2010, **12**(11):1535–1543.

[10] Brakhage AA, Liebmann B: **Aspergillus fumigatus conidial pigment and cAMP signal transduction: significance for virulence.** *Medical Mycology* 2005, **43 Suppl 1**(s1):S75–82.

[11] Codina R, Fox RW, Lockey RF, DeMarco P, Bagg A: **Typical levels of airborne fungal spores in houses without obvious moisture problems during a rainy season in Florida, USA**. *Journal of Investigational Allergology and Clinical Immunology* 2008, **18**(3):156–162.

[12] Hospenthal DR, Kwon-Chung KJ, Bennett JE: **Concentrations of airborne Aspergillus compared to the incidence of invasive aspergillosis: Lack of correlation**. *Medical Mycology* 1998, **36**(3):165–168.

[13] Proctor BE, Parker BW: **Microbiology of the Upper Air: III. An Improved Apparatus and Technique for Upper Air Investigations.** *Journal of Bacteriology* 1938, **36**(2):175–185.

[14] Aimanianda V, Bayry J, Bozza S, Kniemeyer O, Perruccio K, Elluru SR, Clavaud C, Paris S, Brakhage AA, Kaveri SV, Romani L, Latgé JP: **Surface hydrophobin prevents immune recognition of airborne fungal spores**. *Nature* 2009, **460**(7259):1117–1121.

[15] Behnsen J, Hartmann A, Schmaler J, Gehrke A, Brakhage AA, Zipfel PF: **The opportunistic human pathogenic fungus aspergillus fumigatus evades the host complement system**. *Infection and Immunity* 2008, **76**(2):820–827.

[16] Dagenais TRT, Keller NP: **Pathogenesis of Aspergillus fumigatus in Invasive Aspergillosis**. *Clinical Microbiology Reviews* 2009, **22**(3):447–465.

[17] Brakhage AA, Bruns S, Thywissen A, Zipfel PF, Behnsen J: **Interaction of phagocytes with filamentous fungi**. *Current Opinion in Microbiology* 2010, **13**(4):409–415.

[18] Latgé JP: **The pathobiology of Aspergillus fumigatus**. *Trends in Microbiology* 2001, **9**(8):382–389.

[19] Hohl TM, Feldmesser M: **Aspergillus fumigatus: Principles of Pathogenesis and Host Defense**. *Eukaryotic Cell* 2007, **6**(11):1953–1963.

[20] Segal BH, Romani LR: **Invasive aspergillosis in chronic granulomatous disease.** *Medical Mycology* 2009, **47**(Suppl 1):S282–90.

[21] Tillie-Leblond, Tonnel AB: **Allergic bronchopulmonary aspergillosis**. *Allergy* 2005, **60**:1004–1013.

[22] Thompson G, Patterson T: **Pulmonary Aspergillosis**. *Seminars in Respiratory and Critical Care Medicine* 2008, **29**(2):103–110.

[23] Balloy V, Si-Tahar M, Takeuchi O, Philippe B, Nahori MA, Tanguy M, Huerre M, Akira S, Latge JP, Chignard M: **Involvement of Toll-Like Receptor 2 in Experimental Invasive Pulmonary Aspergillosis**. *Infection and Immunity* 2005, **73**(9):5420–5425.

[24] Hillmann F, Novohradská S, Mattern DJ, Forberger T, Heinekamp T, Westermann M, Winckler T, Brakhage AA: **Virulence determinants of the human pathogenic fungus Aspergillus fumigatus protect against soil amoeba predation**. *Environmental Microbiology* 2015, **17**(8):2858–2869.

[25] Jahn B, Koch A, Schmidt A, Wanner G, Gehringer H, Bhakdi S, Brakhage AA: **Isolation and characterization of a pigmentless-conidium mutant of Aspergillus fumigatus with altered conidial surface and reduced virulence**. *Infection and Immunity* 1997, **65**(12):5110–5117.

[26] Hasenberg M, Stegemann-Koniszewski S, Gunzer M: **Cellular immune reactions in the lung**. *Immunological Reviews* 2013, **251**:189–214.

[27] Fortwendel JR, Panepinto JC, Seitz AE, Askew DS, Rhodes JC: **Aspergillus fumigatus rasA and rasB regulate the timing and morphology of asexual development.** *Fungal Genetics and Biology* 2004, **41**(2):129–39.

[28] Latgé JP, Steinbach W: *Aspergillus fumigatus and Aspergillosis*. Washington: ASM Press, 1st edition 2009.

[29] Brakhage AA, Langfelder K: **Menacing Mold: The Molecular Biology of Aspergillus fumigatus**. *Annual Review of Microbiology* 2002, **56**:433–455.

[30] Slesiona S, Gressler M, Mihlan M, Zaehle C, Schaller M, Barz D, Hube B, Jacobsen ID, Brock M: **Persistence versus Escape: Aspergillus terreus and Aspergillus fumigatus Employ Different Strategies during Interactions with Macrophages**. *PLOS ONE* 2012, **7**(2):e31223.

[31] Osherov N: **Interaction of the pathogenic mold Aspergillus fumigatus with lung epithelial cells**. *Frontiers in Microbiology* 2012, **3**(September):1–9.

[32] Behnsen J, Lessing F, Schindler S, Wartenberg D, Jacobsen ID, Thoen M, Zipfel PF, Brakhage AA: **Secreted Aspergillus fumigatus protease Alp1 degrades human complement proteins C3, C4, and C5**. *Infection and Immunity* 2010, **78**(8):3585–3594.

[33] Kupfahl C, Heinekamp T, Geginat G, Ruppert T, Härtl A, Hof H, Brakhage AA: **Deletion of the gliP gene of Aspergillus fumigatus results in loss of gliotoxin production but has no effect on virulence of the fungus in a low-dose mouse infection model**. *Molecular Microbiology* 2006, **62**:292–302.

[34] Murphy KP, Travers P, Walport M: *Janeway's Immunobiology*. New York and London: Garland Science, 7th edition 2007.

[35] Herzog EL, Brody AR, Colby TV, Mason R, Williams MC: **Knowns and unknowns of the alveolus.** In *Proceedings of the American Thoracic Society, Volume 5* 2008:778–782.

[36] Castranova V, Rabovsky J, Tucker JH, Miles PR: **The alveolar type II epithelial cell: a multifunctional pneumocyte.** *Toxicology and Applied Pharmacology* 1988, **93**(3):472–483.

[37] Daniels CB, Orgeig S: **Pulmonary Surfactant: The Key to the Evolution of Air Breathing**. *Physiology* 2003, **18**(4):151–157.

[38] Bastacky J, Lee CY, Goerke J, Koushafar H, Yager D, Kenaga L, Speed TP, Chen Y, Clements JA: **Alveolar lining layer is thin and continuous: low-temperature scanning electron microscopy of rat lung.** *Journal of Applied Physiology (Bethesda, Md. : 1985)* 1995, **79**(5):1615–1628.

[39] Fels A, Cohn ZA: **The alveolar macrophage**. *Society* 1986, **60**(2):353–369.

[40] Krombach F, Münzing S, Allmeling AM, Gerlach JT, Behr J, Dörger M: **Cell size of alveolar macrophages: an interspecies comparison.** *Environmental Health Perspectives* 1997, **105 Suppl**(September):1261–1263.

[41] Hussell T, Bell TJ: **Alveolar macrophages: plasticity in a tissue-specific context.** *Nature Reviews Immunology* 2014, **14**(2):81–93.

[42] Bastacky J, Goerke J: **Pores of Kohn are filled in normal lungs: low-temperature scanning electron microscopy.** *Journal of Applied Physiology (Bethesda, Md. : 1985)* 1992, **73**:88–95.

[43] Amitani R, Murayama T, Nawada R, Lee W, Niimi A, Suzuki K, Tanaka E, Kuze F: **Aspergillus culture filtrates and sputum sols from patients with pulmonary aspergillosis cause damage to human respiratory ciliated epithelium in vitro**. *European Respiratory Journal* 1995, **8**(10):1681–1687.

[44] Paris S, Boisvieux-Ulrich E, Crestani B, Houcine O, Taramelli D, Lombardi L, Latgé JP: **Internalization of Aspergillus fumigatus conidia by epithelial and endothelial cells.** *Infection and Immunity* 1997, **65**(4):1510–4.

[45] Zipfel PF, Skerka C: **Complement regulators and inhibitory proteins**. *Nature Reviews Immunology* 2009, **9**(10):729–40.

[46] Kozel TR, Wilson Ma, Farrell TP, Levitz SM: **Activation of C3 and binding to Aspergillus fumigatus conidia and hyphae.** *Infection and Immunity* 1989, **57**(11):3412–7.

[47] Heinekamp T, Schmidt H, Lapp K, Pähtz V, Shopova I, Köster-Eiserfunke N, Krüger T, Kniemeyer O, Brakhage AA: **Interference of Aspergillus fumigatus with the immune response.** *Seminars in Immunopathology* 2015, **37**(2):141–52.

[48] Speth C, Rambach G, Lass-Flörl C, Dierich MP, Würzner R: **The role of complement in invasive fungal infections**. *Mycoses* 2004, **47**(August 2003):93–103.

[49] Levitz SM: **Overview of host defenses in fungal infections.** *Clinical Infectious Diseases* 1992, **14 Suppl 1**:S37–S42.

[50] Balloy V, Chignard M: **The innate immune response to Aspergillus fumigatus.** *Microbes and Infection / Institut Pasteur* 2009, **11**(12):919–27.

[51] Philippe B, Ibrahim-Granet O, Prévost MC, Gougerot-Pocidalo Ma, Perez MS, Van der Meeren a, Latgé JP: **Killing of Aspergillus fumigatus by alveolar macrophages is mediated by reactive oxidant intermediates**. *Infection and Immunity* 2003, **71**(6):3034–3042.

[52] Steele C, Rapaka RR, Metz A, Pop SM, Williams DL, Gordon S, Kolls JK, Brown GD: **The Beta-Glucan Receptor Dectin-1 Recognizes Specific Morphologies of Aspergillus fumigatus**. *PLOS Pathogens* 2005, **1**(4):e42.

[53] Mircescu MM, Lipuma L, van Rooijen N, Pamer EG, Hohl TM: **Essential Role for Neutrophils but not Alveolar Macrophages at Early Time Points following Aspergillus fumigatus Infection**. *The Journal of Infectious Diseases* 2009, **200**(4):647–656.

[54] Bruns S, Kniemeyer O, Hasenberg M, Aimanianda V, Nietzsche S, Thywissen A, Jeron A, Latgé JP, Brakhage AA, Gunzer M: **Production of extracellular traps against Aspergillus fumigatus in vitro and in infected lung tissue is dependent on invading neutrophils and influenced by hydrophobin RodA.** *PLOS Pathogens* 2010, **6**(4):e1000873.

[55] Fuller SH, Millett LI: **Computing Performance: Game Over or Next Level?** *Computer* 2011, **44**:31–38.

[56] Bossel H: *Modellbildung und Simulation - Konzepte, Verfahren und Modelle zum Verhalten dynamischer Systeme*. Braunschweig/Wiesbaden: Vieweg Verlagsgesellschaft 1994.

[57] Monsef Y: **Modelling and simulation of complex systems: Methods, Techniques and Tools**. *Simulation* 1998, **70**(2):127.

[58] Fishwick PA: *Simulation model design and execution: building digital worlds*. Prentice Hall 1995.

[59] Wilkinson DJ: **Stochastic modelling for quantitative description of heterogeneous biological systems.** *Nature Reviews Genetics* 2009, **10**(2):122–133.

[60] Guo Z, Tay J: **Granularity and the validation of agent-based models**. In *Proceedings of the 2008 Spring Simulation* 2008:153–161.

[61] Medyukhina A, Timme S, Mokhtari Z, Figge MT: **Image-based systems biology of infection.** *Cytometry Part A* 2015, **87**(6):462–470.

[62] Chavali AK, Gianchandani EP, Tung KS, Lawrence MB, Peirce SM, Papin JA: **Characterizing emergent properties of immunological systems with multi-cellular rule-based computational modeling**. *Trends in Immunology* 2008, **29**(12):589–599.

[63] Sukumar SR, Nutaro JJ: **Agent-Based vs. Equation-Based Epidemiological Models: A Model Selection Case Study**. In *2012 ASE/IEEE International Conference on BioMedical Computing*, SocialInformatics 2012:74–79.

[64] Bauer AL, Beauchemin CA, Perelson AS: **Agent-based modeling of host–pathogen systems: The successes and challenges**. *Information Sciences* 2009, **179**(10):1379–1389.

[65] Fachada N, Lopes V, Rosa A: **Agent-based modelling and simulation of the immune system: a review**. In *Epia 2007 Lncs*, *Volume 4874* 2007:300–315.

[66] Railsback SF, Lytinen SL, Jackson SK: **Agent-based Simulation Platforms: Review and Development Recommendations**. *Simulation* 2006, **82**(9):609–623.

[67] Hucka M, Finney A, Sauro HM, Bolouri H, Doyle JC, Kitano H, Arkin AP, Bornstein BJ, Bray D, Cornish-Bowden A, Cuellar AA, Dronov S, Gilles ED, Ginkel M, Gor V, Goryanin II, Hedley WJ, Hodgman TC, Hofmeyr JH, Hunter PJ, Juty NS, Kasberger JL, Kremling A, Kummer U, Le Novère N, Loew LM, Lucio D, Mendes P, Minch E, Mjolsness ED, Nakayama Y, Nelson MR, Nielsen PF, Sakurada T, Schaff JC, Shapiro BE, Shimizu TS, Spence HD, Stelling J, Takahashi K, Tomita M, Wagner J, Wang J: **The systems biology markup language (SBML): A medium for representation and exchange of biochemical network models**. *Bioinformatics* 2003, **19**(4):524–531.

[68] Richmond P, Walker D, Coakley S, Romano D: **High performance cellular level agent-based simulation with {FLAME} for the {GPU}**. *Briefings in Bioinformatics* 2010, **11**(3):334–347.

[69] Hwang M, Garbey M, Berceli SA, Tran-Son-Tay R: **Rule-Based Simulation of Multi-Cellular Biological Systems-A Review of Modeling Techniques.** *Cellular and Molecular Bioengineering* 2009, **2**(3):285–294.

[70] Kempf H, Bleicher M, Meyer-Hermann M: **Spatio-temporal cell dynamics in tumour spheroid irradiation**. *The European Physical Journal D* 2010, **60**:177–193.

[71] Byrne H, Drasdo D: **Individual-based and continuum models of growing cell populations: a comparison**. *Journal of Mathematical Biology* 2009, **58**(4-5):657–687.

[72] Figge MT: **Stochastic discrete event simulation of germinal center reactions**. *Physical Review E, Statistical, Nonlinear, and Soft Matter Physics* 2005, **71**(5 Pt 1):51907.

[73] Figge MT, Garin A, Gunzer M, Kosco-Vilbois M, Toellner KM, Meyer-Hermann M: **Deriving a germinal center lymphocyte migration model from two-photon data.** *The Journal of Experimental Medicine* 2008, **205**(13):3019–29.

[74] Meyer-Hermann M, Figge MT, Toellner KM: **Germinal centres seen through the mathematical eye: B-cell models on the catwalk**. *Trends in Immunology* 2009, **30**(4):157–164.

[75] Bogle G, Dunbar PR: **Simulating T-cell motility in the lymph node paracortex with a packed lattice geometry.** *Immunology and Cell Biology* 2008, **86**(8):676–687.

[76] Bogle G, Dunbar PR: **Agent-based simulation of T-cell activation and proliferation within a lymph node**. *Immunology and Cell Biology* 2010, **88**(2):172–179.

[77] Bogle G, Dunbar PR: **On-lattice simulation of T cell motility, chemotaxis, and trafficking in the lymph node paracortex.** *PLOS ONE* 2012, **7**(9):e45258.

[78] Figge MT, Meyer-Hermann M: **Geometrically repatterned immunological synapses uncover formation mechanisms**. *PLOS Computational Biology* 2006, **2**(11):1377–1384.

[79] Figge MT, Meyer-Hermann M: **Modeling receptor-ligand binding kinetics in immunological synapse formation**. *European Physical Journal D* 2009, **51**:153–160.

[80] Tokarski C, Hummert S, Mech F, Figge MT, Germerodt S, Schroeter A, Schuster S: **Agent-Based Modeling Approach of Immune Defense Against Spores of Opportunistic Human Pathogenic Fungi**. *Frontiers in Microbiology* 2012, **3**(April):129.

[81] Lehnert T, Timme S, Pollmächer J, Hünniger K, Kurzai O, Figge MT: **Bottom-up modeling approach for the quantitative estimation of parameters in pathogen-host interactions**. *Frontiers in Microbiology* 2015, **6**(June):1–15.

[82] Kirschner DE, Chang ST, Riggs TW, Perry N, Linderman JJ: **Toward a multiscale model of antigen presentation in immunity**. *Immunological Reviews* 2007, **216**:93–118.

[83] Guo Z, Sloot PM, Tay JC: **A hybrid agent-based approach for modeling microbiological systems**. *Journal of Theoretical Biology* 2008, **255**(2):163–175.

[84] Schaller G, Meyer-Hermann M: **A modelling approach towards epidermal homoeostasis control**. *Journal of Theoretical Biology* 2007, **247**(3):554–573.

[85] Guo Z, Tay JC: **Multi-timescale event-scheduling in multi-agent immune simulation models**. *Biosystems* 2008, **91**:126–145.

[86] Kempf H, Bleicher M, Meyer-Hermann M: **Spatio-Temporal Dynamics of Hypoxia during Radiotherapy**. *PLOS ONE* 2015, **10**(8):e0133357.

[87] Szabó G, Fáth G: **Evolutionary games on graphs**. *Physics Reports* 2007, **446**(4-6):97–216.

[88] Hummert S, Bohl K, Basanta D, Deutsch A, Werner S, Theißen G, Schröter A, Schuster S: **Evolutionary game theory: cells as players**. *Molecular BioSystems* 2014, :3044–3065.

[89] von Neumann J, Morgenstern O: *Theory of Games and Economic Behavior*. Princeton: Princeton University Press, 2nd edition 1944.

[90] Epstein JM: **Zones of cooperation in demographic prisoner's dilemma**. *Complexity* 1998, **4**:36–48.

[91] Smith JM, Price G: **The logic of animal conflict**. *Nature* 1973, **246**:15–18.

[92] Smith JM: **The theory of games and the evolution of animal conflicts.** *Journal of Theoretical Biology* 1974, **47**:209–221.

[93] Frey E: **Evolutionary game theory: Theoretical concepts and applications to microbial communities**. *Physica A: Statistical Mechanics and its Applications* 2010, **389**(20):4265–4298.

[94] Ohtsuki H, Nowak MA: **The replicator equation on graphs**. *Journal of Theoretical Biology* 2006, **243**:86–97.

[95] Lieberman E, Hauert C, Nowak MA: **Evolutionary dynamics on graphs.** *Nature* 2005, **433**(7023):312–316.

[96] Bohl K, Hummert S, Werner S: **Evolutionary game theory: molecules as players**. *Molecular BioSystems* 2014, :3066–3074.

[97] Hummert S, Hummert C, Schröter A, Hube B, Schuster S: **Game theoretical modelling of survival strategies of Candida albicans inside macrophages.** *Journal of Theoretical Biology* 2010, **264**(2):312–8.

[98] Tyc KM, Kühn C, Wilson D, Klipp E: **Assessing the advantage of morphological changes in Candida albicans: A game theoretical study**. *Frontiers in Microbiology* 2014, **5**(FEB):1–11.

[99] Sbalzarini IF: **Modeling and simulation of biological systems from image data**. *BioEssays* 2013, **35**(5):482–490.

[100] Ashyraliyev M, Fomekong-Nanfack Y, Kaandorp JA, Blom JG: **Systems biology: parameter estimation for biochemical models**. *FEBS Journal* 2009, **276**(4):886–902.

[101] Kirschner DE, Linderman JJ: **Mathematical and computational approaches can complement experimental studies of host-pathogen interactions**. *Cellular Microbiology* 2009, **11**(February):531–539.

[102] Kitano H: **Computational systems biology**. *Nature* 2002, **420**(6912):206–210.

[103] Whitsett J, Alenghat T: **Respiratory epithelial cells orchestrate pulmonary innate immunity**. *Nature Immunology* 2015, **16**:27–35.

[104] Pollmächer J, Figge MT: **Agent-based model of human alveoli predicts chemotactic signaling by epithelial cells during early Aspergillus fumigatus infection.** *PLOS ONE* 2014, **9**(10):e111630.

[105] Hünniger K, Lehnert T, Bieber K, Martin R, Figge MT, Kurzai O: **A Virtual Infection Model Quantifies Innate Effector Mechanisms and Candida albicans Immune Escape in Human Blood.** *PLOS Computational Biology* 2014, **10**(2):e1003479.

[106] Pollmächer J, Figge MT: **Deciphering chemokine properties by a hybrid agent-based model of Aspergillus fumigatus infection in human alveoli.** *Frontiers in Microbiology* 2015, **6**(May):503.

[107] Martin GS, Mannino DM, Eaton S, Moss M: **The epidemiology of sepsis in the United States from 1979 through 2000.** *The New England Journal of Medicine* 2003, **348**(16):1546–1554.

[108] Hockney R, Eastwood J: *Computer simulation using particles*. CRC Press, 1st edition 1989.

[109] Verlet L: **Computer" experiments" on classical fluids. I. Thermodynamical properties of Lennard-Jones molecules**. *Physical Review* 1967, **159**:98–103.

[110] Awile O, Büyükkeçeci F, Reboux S, Sbalzarini IF: **Fast neighbor lists for adaptive-resolution particle simulations**. *Computer Physics Communications* 2012, **183**(5):1073–1081.

[111] Cornforth D, Green DG, Newth D: **Ordered asynchronous processes in multi-agent systems**. *Physica D: Nonlinear Phenomena* 2005, **204**(1-2):70–82.

[112] Caron-Lormier G, Humphry RW, Bohan Da, Hawes C, Thorbek P: **Asynchronous and synchronous updating in individual-based models**. *Ecological Modelling* 2008, **212**(3-4):522–527.

[113] Chan WKV, Son YJ, Macal CM: **Agent-based simulation tutorial - Simulation of emergent behavior and differences between agent-based simulation and discrete-event simulation**. *Proceedings - Winter Simulation Conference* 2010, :135–150.

[114] Charnick SB, Lauffenburger DA: **Mathematical analysis of cell-target encounter rates in three dimensions. Effect of chemotaxis.** *Biophysical Journal* 1990, **57**(5):1009–23.

[115] Charnick SB, Fisher ES, Lauffenburger DA: **Computer simulations of cell-target encounter including biased cell motion toward targets: single and multiple cell-target simulations in two dimensions.** *Bulletin of Mathematical Biology* 1991, **53**(4):591–621.

[116] Hansen JE, Ampaya EP: **Human air space shapes, sizes, areas, and volumes.** *Journal of Applied Physiology* 1975, **38**(6):990–5.

[117] Alonso C, Waring A, Zasadzinski JA: **Keeping lung surfactant where it belongs: protein regulation of two-dimensional viscosity.** *Biophysical Journal* 2005, **89**:266–273.

[118] Balásházy I, Hofmann W, Farkas A, Madas BG: **Three-dimensional model for aerosol transport and deposition in expanding and contracting alveoli.** *Inhalation Toxicology* 2008, **20**(6):611–21.

[119] Hasenberg M, Behnsen J, Krappmann S, Brakhage A, Gunzer M: **Phagocyte responses towards Aspergillus fumigatus**. *International Journal of Medical Microbiology* 2011, **301**(5):436–444.

[120] Segal BH: **Role of macrophages in host defense against aspergillosis and strategies for immune augmentation.** *The Oncologist* 2007, **12 Suppl 2**:7–13.

[121] Warner LA, Holt PG, Margaret P, Hospital PM: **Alveolar macrophages**. *Immunology* 1981, **42**:134–147.

[122] Lambrecht BN: **Alveolar macrophage in the driver's seat.** *Immunity* 2006, **24**(4):366–8.

[123] Behnsen J, Narang P, Hasenberg M, Gunzer F, Bilitewski U, Klippel N, Rohde M, Brock M, Brakhage AA, Gunzer M: **Environmental dimensionality controls the interaction of phagocytes with the pathogenic fungi Aspergillus fumigatus and Candida albicans.** *PLOS Pathogens* 2007, **3**(2):e13.

[124] Westphalen K, Gusarova G: **Sessile alveolar macrophages communicate with alveolar epithelium to modulate immunity**. *Nature* 2014, **506**(7489):503–506.

[125] Glasgow JE, Farrell BE, Fisher ES, Lauffenburger DA, Daniele RP: **The motile response of alveolar macrophages. An experimental study using single-cell and cell population approaches.** *The American Review of Respiratory Disease* 1989, **139**(2):320–329.

[126] Farrell BE, Daniele RP, Lauffenburger Da: **Quantitative relationships between single-cell and cell-population model parameters for chemosensory migration responses of alveolar macrophages to C5a.** *Cell Motility and the Cytoskeleton* 1990, **16**(4):279–93.

[127] Romani L: **Immunity to fungal infections**. *Nature Reviews Immunology* 2011, **11**(4):275–288.

[128] Zhang Z, Liu R, Noordhoek JA, Kauffman HF: **Interaction of airway epithelial cells (A549) with spores and mycelium of Aspergillus fumigatus.** *The Journal of Infection* 2005, **51**(5):375–82.

[129] Miller AL, Strieter RM, Gruber AD, Ho SB, Lukacs NW: **CXCR2 Regulates Respiratory Syncytial Virus-Induced Airway Hyperreactivity and Mucus Overproduction**. *The Journal of Immunology* 2003, **170**(6):3348–3356.

[130] O'Gorman CM, Fuller HT: **Prevalence of culturable airborne spores of selected allergenic and pathogenic fungi in outdoor air**. *Atmospheric Environment* 2008, **42**:4355–4368.

[131] Roilides E, Katsifa H, Walsh TJ: **Pulmonary host defences against Aspergillus fumigatus.** *Research in Immunology* 1998, **149**(4-5):454–65; discussion 523–4.

[132] Hector RF, Yee E, Collins S: **Use of DBA/2N Mice in Models of Systemic Candidiasis and Pulmonary and Systemic Aspergillosis**. *Infetion and Immunity* 1990, **58**(5):1476–1478.

[133] Lauffenburger Da, Horwitz aF: **Cell migration: a physically integrated molecular process.** *Cell* 1996, **84**(3):359–69.

[134] Iglesias PA, Devreotes PN: **Navigating through models of chemotaxis.** *Current Opinion in Cell Biology* 2008, **20**:35–40.

[135] Roilides E, Sein T, Roden M, Schaufele RL, Walsh TJ: **Elevated serum concentrations of interleukin-10 in nonneutropenic patients with invasive aspergillosis.** *The Journal of Infectious Diseases* 2001, **183**(3):518–20.

[136] de Berg M, Cheong O, van Kreveld M, Overmars M: *Computational Geometry*. New York, Heidelberg: Springer, 3rd edition 2008.

[137] Press W, Teukolsky S, Vetterling W, Flannery B: *Numerical Recipies: The Art of Scientific Computing*. New York: Cambridge University Press, 3rd edition 2007.

Appendix A

Numerical approaches

A.1 Computational geometry

Computational geometry considers the design and analysis of algorithms and data structures dedicated to solve geometric problems [136]. It originated as own field of research in the late 1970s. In this section brief explanations of two concepts, the Voronoi tesselation and the Delaunay triangulation, are given. These concepts are related to the published paper presented in section 4.3 [106].

A.1.1 Voronoi tesselation

The Voronoi tesselation is linked to the post office problem: The positions of a finite number of post offices are available on a two-dimensional plane, but based on the current position of a letter sender the post-office closest to him is sought after [136]. In more abstract terms the goal of the Voronoi tesselation is to subdivide the two-dimensional plane into facets with each of them representing an area related to one post office in which this post office is the closest over all other post-offices.

The Voronoi tesselation can be reformulated mathematically: Using Euclidian metrics in two-dimensional Euclidean space the distance d between two points $\vec{r}_i = (x_i, y_i)^{\mathrm{T}}$ and $\vec{r}_j = (x_j, y_j)^{\mathrm{T}}$ is given by

$$d(\vec{r}_i, \vec{r}_j) = \sqrt{(x_j - x_i)^2 + (y_j - y_i)^2}\,. \tag{A.1}$$

Let $\mathcal{P} = \{\vec{r}_1, \vec{r}_2, ..., \vec{r}_n\}$ be a set of n different points. A planar subdivision of the plane into facets $V(\vec{r}_i)$ with

$$\vec{q} \in V(\vec{r}_i) \quad \Longleftrightarrow \quad d(\vec{q}, \vec{r}_i) < d(\vec{q}, \vec{r}_j)\ \forall\ i \neq j \tag{A.2}$$

is called Voronoi tesselation $V(\mathcal{P})$ [136] (see Fig. A.1(a)).

A.1.2 Delaunay triangulation

Triangulations are important instruments to solve differential equations on irregular structured surfaces with finite element methods and also for visualisation purposes. Triangulations use triangles to subdivide a surface from a set of points and are not unique in terms of construction (see Fig. A.1(b)). In triangulation applications typically measures are taken at the locations

of the points, *e.g.* the temperature or humidity in case of weather estimations or the height above sealevel in the case of a terrain interpolation. To predict the measures in between the set of locations where these measures are taken interpolation is widely used. Errors due to interpolation get reduced if the triangles used for the calculation are not too thin, with the best case being a regular triangle. Interpolations put Delaunay triangulations in favor due to its attribute to maximize the smallest angle over all triangles [136]. As another consequence the aggregated edge length over all triangles is minimized in Delaunay triangulations over other triangulations.

Mathematically a triangulation on a plane surface is considered a Delaunay triangulation if it fulfills the following condition: The circumscribed circle of each triangle does only contain the points defining this triangle (see Fig. A.1(d)). This condition is also termed Delaunay criterion [136].

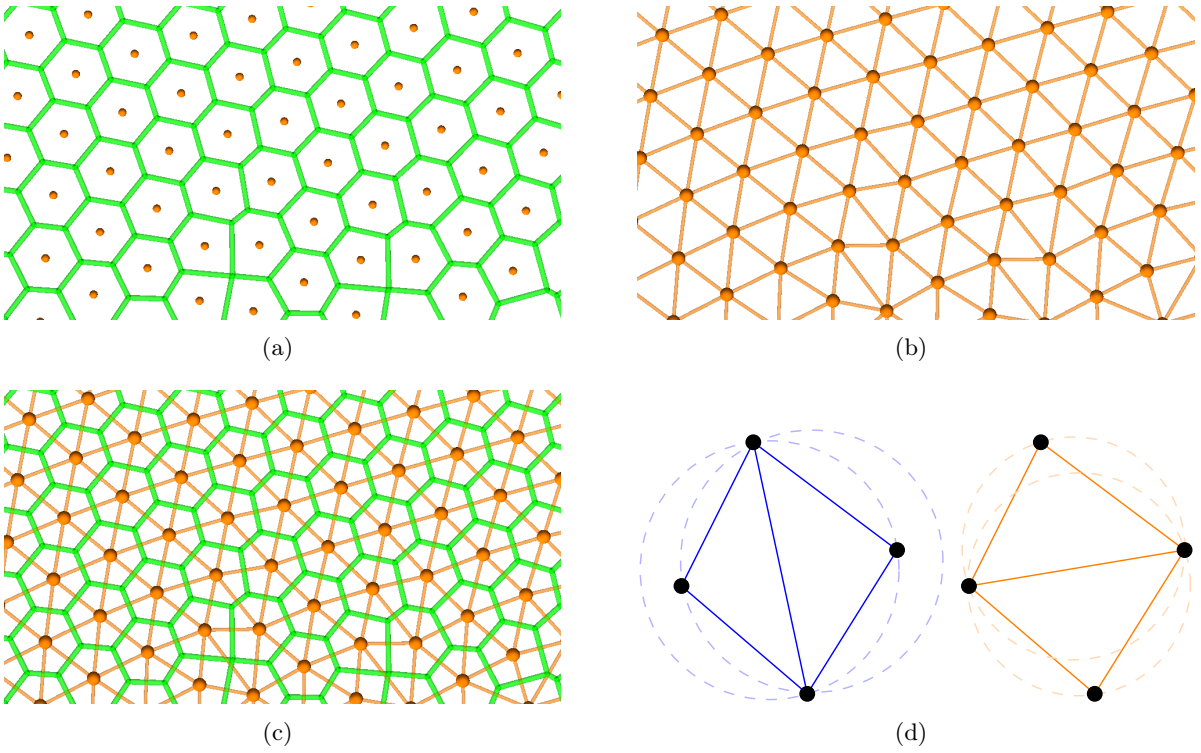

Figure A.1: Resulting data structures after the application of planar computational geometry algorithms. (a) Voronoi tesselation with its edges (*green lines*) separating between the faces. *Orange* points served as seeds for the construction of the Voronoi tesselation. (b) Delaunay triangulation of a finite number of points (shown in *orange*). (c) Overlay of the Delaunay triangulation and the Voronoi tesselation. The Delaunay triangulation is the dual graph of the Voronoi tesselation and vice versa. (d) Visualisation of the Delaunay criterion for a set of four points. There exist two different ways for triangulation of the same set of four points shown on the left and on the right hand side. The *blue* triangles are not Delaunay triangulated as the circumscribed circles of the triangles contain more than the three points related to the respective triangle. Both *orange* triangles fulfill the Delaunay criterion and would render this triangulation a valid Delaunay triangulation.

A.2 Computational stochastics

A.2.1 Random sampling from probability distributions

The agent-based modeling and simulation framework, which was engineered over the origination of this thesis handles various input data. Among these data are experimentally determined distributions of cell migration speed or their directional changes in terms of turning angles. These discrete distributions are required to be reflected in the simulations, such that statistically equivalent distributions of the corresponding measures appear in the readout of the computational simulations. For this purpose a Monte Carlo acceptance-rejection method is implemented, which can reproduce different continuous and discrete density distributions [137] (see Alg. 1).

Algorithm 1 Monte Carlo acceptance-rejection method to generate a random variate x with density distribution $f(x)$ in the interval $[a, b]$.

function RandomVariateAcceptanceRejection(f,a,b)
    define $f_{\max} = \max_{[a,b]}(f)$
    repeat
        $x \leftarrow$ uniform random variate $\in [a, b]$
        $p \leftarrow$ uniform random variate $\in [0, f_{\max}]$
    until $p < f(x)$
return x

A.2.2 Generation of random permutations

Permutations consider the ordering of a finite number of elements in combinatorics. The agent-based simulations in this work execute updates of agents over one timestep in a random order, *i.e.* each agent performs exactly one update per timestep. This subtask refers to the generation of random permutations without repetition. To enhance computational performance, advantage was taken of the Fisher-Yates shuffle (see Alg. 2), which shows linear time complexity in the number of elements to be shuffled.

Algorithm 2 Fisher-Yates shuffle for the generation of random permutations with time complexity $\mathcal{O}(n)$ in the number of elements n.

function GenerateRandomPermutation(n)
    for $i = 1$ to n **do**
        $a[i] \leftarrow i$ ▷ initializing the array
    for $i = 1$ to $n - 1$ **do**
        $j \leftarrow$ uniform random variate $\in [i, n]$
        $temp \leftarrow a[i]$ ▷ swap array elements i and j
        $a[i] \leftarrow a[j]$
        $a[j] \leftarrow temp$
return a

A.2.3 Random selection method

The random selection method is an asynchronous updating scheme applied in each iteration step, *i.e.* agents are not updated in parallel as commonly applied in cellular automata [62]. To more realistically capture the nature of living organisms, like biological cells, random selection performs agent updates in a random order per timestep such that in each step a random permutation over

all agents is generated [111]. In this work, random selection is applied in the works related to the agent-based modeling and simulation framework and wraps around the agent update procedure as can be seen in Alg. 3.

Algorithm 3 Random selection method integrating agent dynamics from time t_{start} to t_{end} by timestep dt for n_{agents} with indexes $\in [1, n_{\text{agents}}]$.

```
1: function RandomSelectionMethod(t_start, t_end, dt, n_agents)
2:     t ← t_start
3:     while t < t_end do
4:         a[] ← GenerateRandomPermutation(n_agents)
5:         for i = 1 to n_agents do
6:             update agent with index a[i]
7:         t ← t + dt
8: return
```

Danksagung

Diese Arbeit ist mit vielen schönen Erinnerungen, aber auch mit dem anstrengenden Schlußspurt bis zur Ziellinie verbunden. Die Beteiligten, die in besonderer Weise zum Gelingen dieser Dissertation beigetragen haben, möchte ich an dieser Stelle wertschätzend erwähnen.

Meinem Doktorvater, Prof. Dr. Marc Thilo Figge, gilt mein ganz besonderer Dank, denn es ist ihm besonders gut gelungen ein ausgewogenes Maß zwischen Anleitung und selbständigem Schaffen und Wirken durch mich zu finden. Für inhaltliche Schwierigkeiten und Engpässe hatte er stets ein offenes Ohr und einer gemeinsamen Entwicklung von Lösungsideen räumte er die nötige Zeit ein. Ich gehöre zu dem Kreis der Doktoranden, die am Entstehen der Forschungsgruppe Angewandte Systembiologie am Hans-Knöll-Institut mitgewirkt haben und ich freue mich sehr ein Teil der spannenden und erfolgreichen Entwicklung dieser Arbeitsgruppe gewesen zu sein. Das Erfolgsrezept der Arbeitsgruppe rührt meines Erachtens aus einem hohen Maß an Engagement, gegenseitiger Hilfe und Wertschätzung her, die stets von Prof. Figge gelebt und den Mitarbeitenden kommuniziert wurde.

Den aktuellen und ehemaligen Mitarbeitenden der Arbeitsgruppen Angewandte Systembiologie und Systembiologie/ Bioinformatik sei an dieser Stelle für die ausgezeichnete Arbeitsathmosphäre, die vielen positiven Gespräche auf dem Weg zur Mensa und in den legendären Kaffeepausen gedankt. Diese halfen maßgeblich bei der Lösung von schwierigen Problemen, indem ich mich durch Belange abseits der Arbeit oder unnützes Wissen gezielt defokussieren konnte, um später dann wieder neu Anlauf zu nehmen. Meiner Büronachbarin Teresa Lehnert danke ich für die schönen Jahre, die gegenseitigen Inspirationen bei der mathematischen Modellierung von Pilzinfektionen und dem kreativen Austausch von Ideen für das nächste Geburtstagsgeschenk in der Arbeitsgruppe. Sandra Timme übernimmt den riesigen Berg Programmcode von mir der zum agentenbasierten Framework gehört, was ich nicht als leichtes Unterfangen einschätze. Vielen Dank für deine Übersicht und Gelassenheit, wenn es um ärgerliche Fehler und Programmabstürze ging, die aus meinem Code herrührten, und natürlich auch für das gemeinsame und konstruktive Entwickeln am Quellcode über die Jahre. Der gesamten Arbeitsgruppe Angewandte Systembiologie möchte ich für ihre angenehme Verabschiedung im August 2015 danken, da sie mir durch viele kleine Überraschungen den Abschied nicht so schwer haben fallen lassen. Für die inhaltliche und sprachliche Kontrolle der vorliegenden Doktorarbeit möchte ich mich bei Teresa Lehnert und Sandra Timme bedanken.

Als Stipendiat der Graduiertenschule Jena School for Microbial Communication (JSMC) standen mir stets die Türen zu universitären und außeruniversitären Weiterbildungen, internationalen Konferenzen und Workshops offen. Das gut gestrickte Netzwerk aus Promovierenden, Betreuenden und dem Manager lieferte mir viele Ansprechpartner, wenn es um arbeits- und projektbezogene Fragestellungen und Probleme ging. Ich habe im besonderen Maße von der Mitorganisation der 3rd International Student Conference of Microbial Communication (MiCom 2012), den Kursen der Jenaer Gradiertenakademie (JGA), dem wissenschaftlichen Austausch auf JSMC internen Symposia und der Beihilfe von Stipendiaten mit Kind profitieren können.

Abschließend möchte ich mich bei meinem familiären Umfeld bedanken, welches mir die nötige Ruhe, Kraft und viel Ausgleich zur täglichen Arbeit vor dem Monitor gab. Meiner Frau

Anne habe ich den nötigen Freiraum zu verdanken, den ich von Zeit zu Zeit wieder benötigte, wenn etwas mehr Arbeit oder Veranstaltungen anstanden, die außerhalb der üblichen Arbeitszeiten stattfanden. Außerdem hatte sie stets ein offenes Ohr für aktuelle Ereignisse, konnte gut darauf eingehen, sich hineindenken und verhalf mir zur gezielten Entspannung. Da auch sie einer Vollzeitstelle während der Entstehung dieser Arbeit nachging, war es manchmal schwierig die Betreuung für unsere gemeinsame Tochter Raphaela zu garantieren. Hier gilt ein großer Dank meiner Schwiegermutter, die teils wochenweise die Betreuung sicherstellen konnte und uns somit den Rücken freihielt. Auch Raphaela selbst sei an dieser Stelle durch ihre Fröhlichkeit, Unbeschwertheit und enorme Agilität gedankt, welche mich an so mancher Stelle aus der Reserve locken konnte und sich somit so mancher Knoten im Gehirn löste. An letzter Stelle sei meinen Eltern gedankt, die mir das Handwerkszeug und den nötigen Rückhalt auf den Lebensweg gaben. Außerdem unterstützten sie mich nach Kräften und haben mir ermöglicht den Weg zu gehen, den ich an verschiedenen Stellen in meiner universitären Ausbildung für richtig hielt.

Ehrenwörtliche Erklärung

Hiermit erkläre ich, dass mir die geltende Promotionsordnung der biologisch-pharmazeutischen Fakultät bekannt ist und ich mich mit bestem Wissen an diese Ordnung gehalten habe. Die vorliegende Dissertation habe ich selbständig und nur unter Verwendung der angegebenen Hilfsmittel, Daten und Quellen angefertigt. Unterstützung während meiner wissenschaftlichen Arbeit und zur Erstellung des vorliegenden Dissertationstextes habe ich nur von den genannten Co-Autoren und in der Danksagung genannten Personen erhalten. Ich habe keine Hilfe von externen Vermittlungs- oder Beratungsdiensten in Anspruch genommen. Niemand hat mittelbare oder unmittelbare geldwerte Leistungen erhalten, für Arbeiten die im Zusammenhang mit dem Inhalt der vorgelegten Dissertation stehen.

Die vorgelegte Dissertation wurde bisher nicht als Prüfungsarbeit für eine andere wissenschaftliche Prüfung eingereicht. Im Speziellen habe ich sie an keiner anderen Hochschule eingereicht, um einen akademischen Grad zu erhalten.

Jena, den 22.12.2016

Johannes Pollmächer

Johannes Pollmächer

Curriculum Vitae

✉ *johannes.pollmaecher@web.de*

Education

2011–2015 **PhD Student**, *Research Group: Applied Systems Biology, Leibniz Institute for Natural Product Research and Infection Biology - Hans-Knöll-Institute*, Jena (Germany).
Topic: Individual-based modeling and predictive simulation of fungal infection dynamics.
Supervisor: Prof. Dr. Marc Thilo Figge

2008–2011 **Academic Studies of Computer Science**, *University of Leipzig*, Leipzig (Germany).

2003–2009 **Academic Studies of Mathematics and Physics**, *University of Leipzig*, Leipzig (Germany).

2003 **Abitur**, *Martin-Rinckart-Gymnasium*, Eilenburg (Germany).

Theses

2011 **BSc Thesis**, *University of Leipzig*, Group of Natural Language Processing, Faculty of Computer Science and Mathematics.

Title *Separation of crawled FindLinks documents into languages*

Supervisors Prof. Dr. Uwe Quasthoff, Dipl.-Inf. Dirk Goldhahn

2009 **State Examination Thesis**, *University of Leipzig*, Didactics of Physics, Faculty of Physics and Geography, University of Leipzig.

Title *Cellular automata in the context of multidisciplinarity*

Supervisors Prof. Dr. Wolfgang Oehme, Prof. Dr. Ulrich Behn

Grant

Stipend **JSMC Fellowship**, *Graduate School Jena School for Microbial Communication, since October 2011.*

Publications

Papers

[1] Pollmächer J, Timme S, Schuster S, Brakhage AA, Zipfel PF, Figge MT: **Deciphering the Counterplay of Aspergillus fumigatus Infection and Host Inflammation by Evolutionary Games on Graphs.** *Sci. Rep.* 2016, 6:27807. doi:10.1038/srep27807

[2] Pollmächer J, Figge MT: **Deciphering chemokine properties by a hybrid agent-based model of Aspergillus fumigatus infection in human alveoli.** *Front. Microbio.* 2015, 6:503. doi:10.3389/fmicb.2015.00503

[3] Lehnert T, Timme S, Pollmächer J, Hünniger K, Kurzai O, Figge MT: **Bottom-up modeling approach for the quantitative estimation of parameters in pathogen-host interactions.** *Front. Microbio.* 2015, 6:608. doi:10.3389/fmicb.2015.00608

[4] Pollmächer J, Figge MT: **Agent-based model of human alveoli predicts chemotactic signaling by epithelial cells during early Aspergillus fumigatus infection.** *PLOS ONE* 2014, 9(10), e111630. doi:10.1371/journal.pone.0111630

[5] Horn F, Heinekamp T, Kniemeyer O, Pollmächer J, Valiante V, Brakhage AA: **Systems biology of fungal infection**. *Front. Microbio.* 2012, 3:108. doi:10.3389/fmicb.2012.00108

Talks

[6] Pollmächer J, Figge MT: **Unraveling the early immune response in Aspergillus fumigatus infection using hybrid agent-based modeling.** *Conference: 49th Scientific Conference of the German speaking Mycological Society (DMykG) e. V. and 1st International Symposium of the CRC/Transregio FungiNet*, Jena (Germany) 2015

[7] Pollmächer J, Figge MT: **Hybrid agent-based model of Aspergillus fumigatus infection in human alveoli predicts chemoattraction of alveolar macrophages and parameter-regimes of chemokine properties.** *Conference: International Congress on Systems Immunology, Immunoinformatics and Immune-computation (ICSI$^{\beta}$)*, Taormina (Italy) 2015

[8] Pollmächer J, Timme S, Figge MT: **Unraveling fungal-host interactions with spatio-temporal agent-based models.** *Conference: 4th International Student Conference on Microbial Communication (MiCom 2014)*, Jena (Germany) 2014

[9] Pollmächer J, Figge MT: **On the first-passage-task of alveolar macrophages to detect *A. fumigatus* conidia** *Conference: 2nd International Workshop: Systems Biology of Micobial Infection*, Jena (Germany) 2013

Posters

[10] Pollmächer J, Figge MT: **Hybrid agent-based modeling of human alveoli reveals chemokine properties in *Aspergillus fumigatus* infection.** *Conference: 5th International Student Conference on Microbial Communication (MiCom 2015)*, Jena (Germany) 2015

[11] Timme S, Pollmächer J, Lehnert T, Medyukhina A, Totzauer S, Hünniger K, Buhlmann D, Skerka C, Kurzai O, and Figge MT: **Agent-based Modeling on Cellular and Molecular Scales.** *Conference: 4th International Student Conference on Microbial Communication (MiCom 2015)*, Jena (Germany) 2015

[12] Pollmächer J, Figge MT: **A hybrid agent-based modeling approach of Aspergillus fumigatus infection in the human alveolus.** *Conference: JSMC Symposium*, Jena (Germany) 2014

[13] Brandes S, Pollmächer J, and Figge MT: **Analysis of Dynamic Properties in Biological Systems from Image-Data.** *Conference: 3rd International Student Conference on Microbial Communication (MiCom 2012)*, Jena (Germany) 2012

[14] Pollmächer J, Figge MT: **A Spatio-Temporal Modeling Framework to Simulate Host-Pathogen Interactions.** *Conference: German Conference on Bioinformatics (GCB 2012)*, Jena (Germany) 2012

Jena, December 22, 2016

Johannes Pollmächer